UNIVERSIDAD DE LAS PALMAS DE GRAN CANARIA

DEPARTAMENTO DE FÍSICA

TESIS DOCTORAL

Long-term variability and effects on larval fish distribution of the Gulf of Mexico Loop Current and Rings

(Variabilidad a largo plazo de la Corriente de Lazo y Anillos, y efectos en la distribuciones de larvas de peces en el Golfo de México)

DAVID LINDO ATICHATI

ENERO DE 2012

LAS PALMAS DE GRAN CANARIA

47/2011-12

UNIVERSIDAD DE LAS PALMAS DE GRAN CANARIA
SUBDIRECCIÓN DE TERCER CICLO Y POSTGRADO

Reunido el día de la fecha, el Tribunal nombrado por el Excmo. Sr. Rector Magfco. de esta Universidad, el/a aspirante expuso esta TESIS DOCTORAL.

Terminada la lectura y contestadas por el/a Doctorando/a las objeciones formuladas por los señores miembros del Tribunal, éste calificó dicho trabajo con la nota de APTO CUM LAUDE

Las Palmas de Gran Canaria, a 27 de marzo de 2012

El/a Presidente/a: Dr/a. D/a., Santiago Hernández León,

El/a Secretario/a: Dr/a. D/a. Ángel Rodríguez Santana,

El/a Vocal: Dr/a. D/a. María Elsa Vázquez Otero,

El/a Vocal: Dr/a. D/a. José Luis Pelegrí Llopart,

El/a Vocal: Dr/a. D/a. Eugenio Fraile Nuez,

El Doctorando: David Lindo Atichati,

Anexo I

D/Dª.....SALVADOR GALVÁN HERRERA....SECRETARIO/A DEL DEPARTAMENTO DE.....FÍSICA..... DE LA UNIVERSIDAD DE LAS PALMAS DE GRAN CANARIA,

CERTIFICA,

Que el Consejo de Doctores del Departamento en su sesión de fecha.....tomó el acuerdo de dar el consentimiento para su tramitación, a la tesis doctoral titulada "*LONG-TERM VARIABILITY AND EFFECTS ON LARVAL FISH DISTRIBUTION OF THE GULF OF MEXICO LOOP CURRENT AND RINGS*" presentada por el/la doctorando/a D DAVID LINDO ATICHATI y dirigida por el Doctor D PABLO SANGRÀ INCIARTE.

Y para que así conste, y a efectos de lo previsto en el Artº 73.2 del Reglamento de Estudios de Doctorado de esta Universidad, firmo la presente en Las Palmas de Gran Canaria, a.....de.....de dos mil….doce.....

A Olívia o Quélén-Maurice...

Acknowledgements

This thesis was possible thanks to the funding provided by the Atlantic Oceanographic and Meteorological Laboratory (AOML) of the National Oceanic and Atmospheric Administration (NOAA) through the project Fish Stock Assessment From Satellite Observations. The grant awarded by "*Obra Social La Caixa*" gave me the opportunity to take PhD courses of the graduate program in Meteorology and Physical Oceanography at the University of Miami (RSMAS).

First and foremost, I would like to express my deepest gratitude to my dissertation advisor, Dr. Pablo Sangrà, for giving me the opportunity to conduct this dissertation under his supervision, encouragement, outstanding scientific support, and friendship. I am grateful to him for hosting me during my visit at UCLA, and for offering me his temper and know-how.

I would like to thank the co-advisor of mi dissertation Dr. Gustavo Goni, director of the physical oceanography division at NOAA/AOML, who has also been my supervisor there for the last years. He has taught me how to work with altimetry data and guided me during the meticulous process of becoming an author.

The co-advisor of my dissertation Dr. Barbara Muhling has played a key role in my dissertation. I would like to extend to her my deepest gratitude for introducing me to the fascinating world of larval-fish with so much patience and accuracy. Thanks Barb for showing me how to be succinct and precise. I am getting there!

I am very grateful to the Physics Department of the ULPGC, the administrative services of the *Facultad de Ciencias del Mar*, and the *Servicio de Investigación y Tercer Ciclo* for making all the PhD procedures easier. In particular, I would like to mention Dr. Alonso Hernández-Guerra for his wise advise when choosing my advisor, and María Dolores Morales Sosa for brilliantly managing my academic paperwork and defense proceedings.

I sincerely thank Dr. Silvia Garzoli for inviting me to collaborate with and learn from the PHOD team at NOAA/AOML, and for always having her door open to guide me. I also acknowledge Dr. Arthur Mariano for being my supervisor at University of Miami (RSMAS).

I warmly thank Dr. Nelson Melo-González (NOAA/AOML) for being always there "en la lucha" and for offering me the helpful poetry of José Martí.

I greatly appreciate the effort of Dr. Francis Bringas and Jay Harris (NOAA/AOML) for helping me with the programming, and Dr. Francisco Machín for his support during the last months. I sincerely thank Dr. Francisco Alemany of the *Instituto Español de Oceanografía* (IEO) for the productive discussion we had.

Dr. Frank Muller-Karger deserves a special mention for hosting me at the University of South Florida (USF), allowing me to teach graduate lectures, training me on how to write proposals, and above all for showing me that it is possible to be an excellent scientist, professor, and person.

A big THANK YOU! to my fellows at NOAA/AOML, NOAA/SEFSC, and USF/IMARS Dr. Ryan Smith, Dr. Elisabeth Jones, Dr. John Lamkin, Sennai Habtes, and Dr. Mitch Roffer.

Outside science I thank my sister Sonia and my mother for understanding me and supporting me wherever I am and have been. In all sincerity and conviction, I thank my father, for passing on me his courage, strength, and optimism. To Francisca, Tomeu, Abuela, Pedro, Cristina, and Uli, for sharing with me "the secret". To Miquel Àngel for his unconditional friendship all life long.

Last but not least, I would like to specially thank,

My wife, Queta, my Majorcan little girl. Thanks for being by my side during our PhD journey. One among the many other trips we will make, from now on with our baby.

Agradecimientos

Esta tesis ha sido posible gracias a la financiación del *Atlantic Oceanographic and Meteorological Laboratory* (AOML) de la *National Oceanic and Atmospheric Administration* (NOAA) a través del proyecto *Fish Stock Assessment From Satellite Observations*. La beca de postgrado de la "Obra Social La Caixa" me dio la oportunidad de poder tomar las asignaturas del doctorado en Meteorología y Oceanografía Física de la *University of Miami* (RSMAS).

En primer lugar, quisiera expresar mi más profunda gratitud a mi director de tesis, el Dr. Pablo Sangrà, por haberme dado la oportunidad de hacer la tesis bajo su supervisión, por la confianza en mi trabajo, su sobresaliente apoyo científico, y por su amistad. Por abrirme su casa en durante mi visita a UCLA, por brindarme su serenidad y su buen hacer.

Mi agradecimiento más sincero al co-director de mi tesis el Dr. Gustavo Goni, director de la división de oceanografía de AOML, quien también ha sido mi supervisor durante los últimos años. Gracias a él he aprendido a trabajar con altimetría satelital y he sido guiado a través del minucioso proceso de publicar.

La co-directora de mi tesis, la Dra. Barbara Muhling, ha sido y es una pieza clave para mí. Mi más profundo agradecimiento por descubrirme el fascinante mundo de las larvas, siempre con gran paciencia y precisión. Y por enseñarme a ser sucinto. *Thanks heaps Barb!*

Mi agradecimiento al Departamento de Física, a los servicios administrativos de la Facultad de Ciencias del Mar, y al Servicio de Investigación y Tercer Ciclo por facilitar con tanta agilidad todos los trámites. En especial al Dr. Hernandez-Guerra por su sabia recomendación para la elección de mi tutor, y a María Dolores Morales Sosa por gestionar a la perfección mi documentación académica y la lectura de mi tesis.

Tengo que agradecer enormemente a la Dra. Silvia Garzoli por invitarme a colaborar con el equipo de PHOD en Miami y por tener siempre sus puertas abiertas para orientarme. Al Dr. Arthur Mariano por ser mi supervisor en University of Miami (RSMAS).

Por supuesto al Dr. Nelson Melo-González de NOAA/AOML, por estar siempre a mi lado en la lucha y por darme ese toque poético de José Martí que tanto me ha ayudado.

Debo agradecer el esfuerzo al Dr. Francis Bringas y Jay Harris (NOAA/AOML) al ayudarme en la elaboración de programas y al Dr. Francisco Machín por su apoyo en los últimos meses. Al Dr. Francisco Alemany del Instituto Español de Oceanografía (IEO) un sincero agradecimiento por la fructífera discusión que tuvimos.

Especial mención al Dr. Frank Muller-Karger por facilitar mi estancia en University of South Florida (USF), por permitirme impartir clases de doctorado, por enseñarme a escribir propuestas, y sobretodo por mostrarme que se puede ser un excelente científico, profesor, y persona.

Un enorme ¡GRACIAS! a mis compañeros de NOAA/AOML, NOAA/SEFSC y USF/IMARS Dr. Ryan Smith, Dr. Elisabeth Jones, Jay Harris, Dr. John Lamkin, Sennai Habtes, y al Dr. Mitch Roffer.

Fuera de la ciencia, a mi hermana Sonia y a mi madre por comprenderme y apoyarme allá donde estuviese. A mi padre por regalarme su valentía, fuerza y optimismo. A Francisca, Tomeu, *s'*Abuela, *en* Pedro, Cristina y *n'*Uli, *per compartir es secret*. A *en* Miquel Àngel por su incondicional amistad desde siempre.

Y por último me gustaría agradecer especialmente,

A mi mujer Queta, *sa meva nina* mallorquina, por querer acompañarme con una sonrisa en nuestro viaje de doctorado. Uno de tantos muchos, en los que ahora seremos tres.

Abstract

The Gulf of Mexico (GOM) is an enclosed sea susceptible to climate change and anthropogenic pressures, as years of intense development and exploitation have resulted in significant change to the fisheries resources. It is the preferred spawning habitat for several commercially-important pelagic fish species (e.g. the Atlantic bluefin tuna). This basin is also characterized by a complex and highly variable system of currents and eddies, which affects the physical environment where fish spawn (Teo and Block 2010). The mesoscale circulation in the GOM is dominated by the Loop Current (LC) and rings shed by this major current. These powerful oceanic features carry anomalies in the physical, biological, and chemical properties of the region, and they affect -either directly or indirectly through their smaller-scale subsidiaries- just about every aspect of oceanography of the Gulf. For these reasons, the proposed investigation is focused on the satellite monitoring of the temporal and spatial variability of the LC and rings, and on the regulation of the larval fish distribution of some species by mesoscale oceanic features.

The overarching aim of this dissertation is to investigate, assess and analyze linkages between ocean circulation and the spatial and temporal distribution of larval fish in the Gulf of Mexico. This connection is explored in here through the use of satellite derived observations and *in situ* biological sampling.

The main goals of this research are to (1) monitor and describe the spatial and temporal variability of LC intrusions (northward), LC retreats (southward), and ring detachments; and (2) assess the influence of mesoscale ocean features on the distribution of larval fish spawned in the northern GOM in spring months from 1993 to 2007.

The data that will be used in this study include, but are not limited to, sea surface temperatures (*in situ* and from satellites), sea surface height from satellite altimetry, and ocean surface color. The biological data correspond to *in situ* samples collected in the GOM north of 24°N during spring (April to June) NOAA/NMFS surveys between 1993 and 2007. Larval fish data are available from the National

Marine Fisheries Service Southeast Area Monitoring and Assessment Program (SEAMAP) database.

This work provides a better description of the mesoscale dynamics in the LC and associated ring field, and will shed some light on the physical regulation of the distribution of early life stages of some fish species in the GOM. Research tools and results obtained in this work will be useful to make assessments and connectivity studies using similar methodologies and tools upstream in the Atlantic Ocean

The innovative character of this PhD dissertation is reflected in the close merging of oceanography and biology to study the changes, since 1993 to present, in the fisheries catches in the GOM. Results obtained from this work will allow making better assessments of the effect of long-term ocean changes and trends in ecosystems. An improved understanding of larvae assemblages in different water masses, characterized by circulation and sea surface height (SSH), will provides a benchmark for future coupled biophysical studies and habitat models in the region

Resumen

El Golfo de México (GDM) es un mar cerrado susceptible al cambio climático y a presiones antropogénicas, como demuestra el hecho que años de intenso desarrollo y explotación se han traducido en cambios significativos en los recursos pesqueros. Esta cuenca es el hábitat de reproducción preferido de varias especies de peces pelágicos comercialmente importantes (*e.g.*, el atún rojo atlántico), y se caracteriza por un sistema complejo y altamente variable de las corrientes y remolinos, lo cual afecta el entorno físico donde los peces desovan (Teo and Block 2010). La circulación de mesoescala en el GDM está dominada por la Corriente de Lazo (CL) y los anillos desprendidos por esta corriente principal. Estas energéticas estructuras oceánicas transportan anomalías en las propiedades físicas, biológicas y químicas de la región, y afectan –ya sea directa o indirectamente a través de estructuras dependientes de menor escala– a casi todos los aspectos de la oceanografía del GDM. Por estas razones, la investigación propuesta se centra en el control satelital de la variabilidad temporal y espacial de la CL y anillos, y en la regulación mediante estructuras oceánicas de mesoescala de la distribución de larvas de peces.

El propósito general de esta tesis es investigar, evaluar y analizar los vínculos entre la circulación oceánica y la distribución espacial y temporal de larvas en el GDM. Esta conexión se explora aquí a través del uso de satélites y observaciones derivadas de un muestreo biológico *in situ*.

Los principales objetivos de esta investigación son: (1) monitorizar y describir la variabilidad espacial y temporal de las intrusiones de la CL (hacia el norte), retiros de la CL (hacia el sur), y desprendimiento de anillos; y (2) evaluar la influencia de las estructuras oceánicas de mesoescala en la distribución de larvas desovadas en el norte del GDM (al norte de 24° N) durante los meses de primavera desde 1993 a 2007.

Los datos que se usan en este estudio incluyen, pero no se limitan a, las temperaturas superficiales del mar (*in situ* y de satélites), la altura de la superficie del mar (SSH) a partir de la altimetría satelital, e imágenes color de la superficie del océano. Los datos biológicos corresponden a las muestras recogidas *in situ* en el norte del GDM durante campañas de pesquerías llevadas a cabo en primavera (de abril a

junio) entre 1993 y 2007 por *National Marine Fisheries Service* (NMFS) de *National Oceanic and Atmospheric Administration* (NOAA). Los datos se obtienen de la base de datos del *National Marine Fisheries Service Southeast Area Monitoring and Assessment Program* (SEAMAP) facilitada por el *Southeast Fisheries Science Center* (SEFSC).

Este trabajo ofrece una actualizada descripción de la dinámica de mesoescala de la CL y campo de anillos asociado, y arroja luz sobre la regulación de la distribución física de las primeras etapas de vida de algunas especies de peces en el GDM. El carácter innovador de esta tesis doctoral radica en la estrecha unión de la oceanografía y la biología para estudiar los cambios, desde 1993 hasta el presente, en las capturas de larvas en el GDM. Los métodos y resultados obtenidos en este trabajo dan lugar a la posibilidad de realizar una mejor evaluación de los efectos de cambios en el océano a largo plazo y tendencias de algunos ecosistemas. Una mejor comprensión de las comunidades larvarias en diferentes masas de agua, caracterizadas por la circulación y altura superficial del mar (SSH), también ofrece un punto de referencia para futuros estudios biofísicos y modelos de hábitat en la región.

Dissertation preview

This dissertation, entitled "Long term ocean variability in marine ecosystems in the Gulf of Mexico", is a compilation of different studies that are based on satellite derived observations and *in situ* biological sampling carried out at the University of Miami and the Atlantic Oceanographic and Meteorological Laboratory (AOML) of the National Oceanic and Atmospheric Administration (NOAA), between the years 2009 and 2011. This research has been developed under the research lines of AOML, and it is also framed in the current investigation on the physical and biological coupling at the mesoscale and submesoscale level leaded by Dr. Pablo Sangrà from the Physics Department of the *Universidad de las Palmas de Gran Canaria*. The work has primarily been supported by the Physical Oceanography Department of AOML.

Dr. Pablo Sangrà has been the advisor of this dissertation work, together with the co-advisors Dr. Gustavo Goni of NOAA/AOML, and Dr. Barbara Muhling of the University of Miami.

The structure of the dissertation is as follows. A brief introductory chapter outlines the rationale and approach adopted in order to achieve the aims of the dissertation (Chapter I). An exhaustive description of the physical and biological oceanography of the Gulf of Mexico is given in the following chapter (Chapter II). The two subsequent chapters form the core of the dissertation and they are presented and discussed (Chapter III and Chapter IV). At the time of writing, these two chapters have been submitted for publication to two peer reviewed journals. Chapter V encloses the future research that arises from this dissertation, consisting of two works that are in preparation. The dissertation concludes with a discussion (Chapter VI) of the main findings from this investigation, as well as a summary of the conclussions.

At the end, a summary in Spanish is included, containing more than 50 pages (Chapter VII). This is a requirement from the PhD Thesis Regulations from the Universidad de Las Palmas de Gran Canaria (BOULPGC. Art.2 Chap.1, November 5th 2008).

Presentación de la tesis

Esta investigación se ha realizado en la Universidad de Miami y el *Atlantic Oceanographic and Atmospheric Laboratory* (AOML) de NOAA, entre los años 2009 y 2011. Ha sido desarrollada bajo las líneas de investigación de AOML, y a la vez se enmarca en la investigación actual del acoplamiento físico y biológico a nivel de mesoescala y sub-mesoescala liderado por el Dr. Pablo Sangrà del Departamento de Física de la Universidad de las Palmas de Gran Canaria.

El Dr. Pablo Sangrà ha sido el director de esta tesis, y los co-directores han sido el Dr. Gustavo Goni de NOAA/AOML y la Dra. Barbara Muhling de la University of Miami.

Esta tesis se organiza de la siguiente manera. Un breve capítulo introductorio inicial subraya los fundamentos y el enfoque adoptado para alcanzar los propósitos de este trabajo (Capítulo I). Las principales características de la oceanografía física y de los ecosistemas del Golfo de México (GDM) son descritas el siguiente capítulo (Capítulo II). Los dos capítulos siguientes forman el núcleo de la tesis, en ellos se muestran los principales resultados y se discuten (Capítulos III y IV). En estos momentos, dichos capítulos has sido enviados a dos revistas para ser considerados para publicación. El capítulo V muestra las futuras líneas de investigación que surgen de esta tesis, y que consisten en dos nuevos trabajos que están en preparación. Finalmente, el capítulo VI incluye una discusión general y las principales conclusiones.

Un requisito de la ULPGC (Reglamento para la elaboración, tribunal, defensa y evaluación de tesis doctorales, BOULPGC. Art. 2, cap. 1, 5 noviembre de 2008) es que se incluya un resumen en español al final de la tesis. Esta sección está debidamente incluida en el capítulo final (capítulo VII).

List of figures

List of tables

Contents

Chapter I: Introduction

1. Introduction

The overarching aim of this study is to investigate the link between early life stages of fishes and the variability of the mesoscale oceanic structures in the Gulf of Mexico (GOM). This connection is explored in here through the use of satellite-derived observations and *in situ* biological sampling. There are many examples in the literature of correlations between changes in physical oceanographic parameters and changes in fish resources (Ortner et al. 1984; Mann 1993; Bakun 2006). Commonly, these correlations hold for a few years, then break down. Although this does not necessarily mean that the correlation was invalid, it calls for a better understanding of the mechanism of interaction in the complex system between the physics and the biology before we can understand the time dependence of these correlations.

The GOM is a semi-enclosed sea bordered by the United States, Mexico and Cuba. The economic livelihoods of this international community depend on the many goods and services provided by the Gulf of Mexico; fisheries being one of the most important services. Considered to be a jewel among natural resources of the western hemisphere, the GOM wetlands are the source of an important seafood and shellfish industry, and its offshore waters support rich commercial and recreational fisheries, being the site for spawning and habitat of commercially relevant pelagic and benthic fish species (Shipp 1999; Rabalais et al. 1999). However, the GOM is susceptible to climate change and anthropogenic pressures, as years of intense development and exploitation have resulted in significant change to the fisheries resources. Major problems facing the Gulf, including habitat modification, pollution, and overexploitation, are generating uncertain impacts on this large marine ecosystem. Intensive fishing is the primary force driving biomass changes in the GOM, with climatic variability the secondary driving force (Sherman 2003). These two main pressures on the ecosystems may be addressed in part by having a synoptic comprehension of the physical-biological interactions in the GOM.

The region is characterized by a complex and highly variable circulation, in time and space, with an intense mesoscale activity that is dominated by two main features: the Loop Current (LC) and the rings shed by the LC. These powerful oceanic features carry anomalies in the physical, biological, and chemical properties of the region, and they affect -either directly or indirectly through their smaller-scale subsidiaries- just about every aspect of oceanography of the Gulf. For these reasons, the proposed investigation is focused on the

satellite monitoring of the temporal and spatial variability of the LC and rings, and on the regulation of the larval fish distribution of some species by mesoscale oceanic features.

Several studies show that physical and biological conditions for both larvae and adult fish in the GOM exhibit high spatial and temporal variability (Müller-Karger et al. 1991), which are likely linked to the patterns of spawning (Ortner et al. 1984; Bakun 2006). Variability in larval abundances of some pelagic species has been linked in more recent studies to environmental parameters -such as water temperature, salinity, water depth, and day length- and plankton distribution in the GOM region (Muhling et al. 2010; Richardson et al. 2010). Since some ecosystems are highly affected by changes in environmental conditions and plankton distribution (Teo and Block 2010), variability of ocean properties and mesoscale structures in the GOM is expected to have a direct effect on ecosystems in this region. In particular, recent studies show that a detailed knowledge of the temporal and spatial variability of mesoscale structures in the eastern GOM is fundamental for understanding the environmental conditions that influence distributions of the larvae of different fish species, spawning sites, larval growth and subsequent variability in larval and juvenile survival (Richards et al. 1993; Bakun 2006). However, there seems to be a lack of information in how the ecosystems respond to short and long-term variability patterns in the region, which could help in dealing with the climatic change pressures in the GOM.

All the previous aspects considered, the main goal of this dissertation is to investigate, assess and analyze the link between fisheries resources and the temporal and spatial variability in ocean properties and mesoscale activity in the GOM. On this regard, this work will provide a better description of the mesoscale dynamics in the LC and associated ring field, and will shed some light on the physical regulation of the distribution of early life stages of some fish species in the GOM. Research tools and results obtained in this work will be useful to make assessments and connectivity studies using similar methodologies and tools upstream in the Atlantic Ocean.

Essentially, then main 3 sections of this work are the following:

- The first section (Chapter II) describes the main characteristics of the Physical Oceanography and Ecosystems in the Gulf of Mexico. Firstly, the general and mesoscale circulation of the deep and coastal GOM is described, as well as the interconnectivity of the flow processes in the tropical Atlantic Ocean and Caribbean Sea. Then, the physical mechanisms driving the dynamics of the GOM are

investigated, described, and evaluated. On the other hand, the state of the art on the biological levels, primary production and nutrients in the GOM is reviewed. The population dynamics of pelagic larval fishes with relevant commercial importance in the GOM are presented, with emphasis on the dynamics of their early life stages. Then, the current comprehension on the environmental factors affecting ichthyoplankton distribution patterns and environmental conditions favorable for larval fish survival is investigated. Finally, a detailed description of the satellite derived data sources its relevance for biological end ecosystem studies is described.

- The second section (Chapter III and IV) is the longest in extension and make up the core of this work. Chapter III provides an extensive description of the long term variability of the Loop Current, associated ring field, and sea height anomaly in the GOM, and proposes a novel methodology to identify regions of circulation based on fields of sea surface height derived from satellite altimetry. On Chapter IV, spatial and temporal distributions of larval fishes are related to environmental conditions and mesoscale oceanographic structures. Using satellite altimetry and *in situ* larval fish densities, the novel methodology used in Chapter III to identify regions of different circulation is used in Chapter IV to estimate links between mesoscale features and larval distributions of some fish taxa in the GOM, during spring from 1993 to 2007. As a result, some light is shed on the spatial and temporal distributions of larval fishes and its correlations to mesoscale oceanographic structures

- Finally, the third section encloses a work that is in preparation that explores the effect of the atmospheric coupling on the migrations of the Loop Current, and the potential role that westward propagating eddies play on the Loop Current migrations. The innovative character of this latter work is reflected in using the footprint that cyclonic and anti-cyclonic eddies leave in sea surface height, temperature, and chlorophyll *a*, basically by applying Okubo-Weiss parameter. The discussion and conclusions obtained from this work will allow to make better assessments of the effect of long-term ocean changes and trends in the fisheries of the Gulf (Chapter VI), and stress the need for a sustained observing system able to resolve mesoscale features, which are important for the upper ocean temperature response to the changing climate, and continuous sampling of larvae of economically important species.

Chapter II: Physical oceanography and ecosystems in the Gulf of Mexico

1. Introduction

Although Europeans credited Christopher Columbus with the discovery of the Americas, the ships in his four voyages never reached the Gulf of Mexico (GOM). Instead, Columbus sailed into the Caribbean around Cuba and Hispaniola. The first European exploration of the GOM was by Amerigo Vespucci in 1497. He followed the coastal landmass of Central America before returning to the Atlantic Ocean via the Straits of Florida between Florida and Cuba. Vespucci described the voyage across the GOM in his letters, and it helped to produce the oldest known European cartographic representation of the New World. The first description of the ocean circulation in the GOM date from 1578, when William Bourne described a system in which the principal westward motion at the southern end of Africa merged with that of the central Atlantic, and some movement of water had to be diverted northward along the east coast of South America, into the Gulf of Mexico, and then eastward with the current between Florida and Cuba back to Europe (Peterson et al. 1996). Similarly to the first descriptions of the ocean circulation in the GOM, the study of the distribution of fishes in the region also started in the exploration of the Americas, when captain Bernard Romans developed a chart of East and West Florida native fishes (Romans and Concise 1775).

Today, the Gulf of Mexico is considered as one of the most productive marine ecosystems in the world, and an important global reservoir of biodiversity. Knowledge of marine biodiversity in the Gulf of Mexico varies by region and taxon. On a Gulf-wide basis and considering the whole marine life, 3,302 species are censed in the GOM (Galtsoff 1954), from which 986 are listed to be species of fish distributed in 197 families (Froese and Pauly, 2011). This biodiversity is supported on the physical oceanographic processes that modulate the physiology, metabolism, behavior, and early growth rates of marine life (Blaxter 1991), and therefore it is crucial to know the physical oceanographic processes that drive the region in order to explore the physical regulation of fisheries resources in the GOM.

The study area of this work is the enclosed region defined by 20°N to 31°N, and 80°W to 97°W. However, the GOM is a geographic region that together with the Caribbean Sea (CS), the Straits of Florida, and the adjacent western North Atlantic is comprised in a wider geographic region called the American Mediterranean Sea (Sverdrup et al. 1942) or Intra-Americas Sea (IAS) (Figure 2.1). A better understanding of the physical processes of the waters that flow in and through the IAS, especially its circulation variability, is important

because (1) it plays an important role as a conduit for mass, heat, salt and other tracers in the Atlantic circulation system (Schmitz and Richardson 1991); (2) the IAS contains the second largest body of very warm (≥ 28.5°) water on Earth: the western hemisphere warm pool (Wang and Enfield 2001), which is a significant heat source for the atmosphere; and (3) the waters of the IAS also support rich commercial fisheries and a major oil and gas industry (Tang et al. 2006). Even though the focus of this study is the GOM, recent studies have indicated that the GOM and the CS are dynamically inter-dependent; therefore certain aspects of the circulation in the Caribbean will also be discussed.

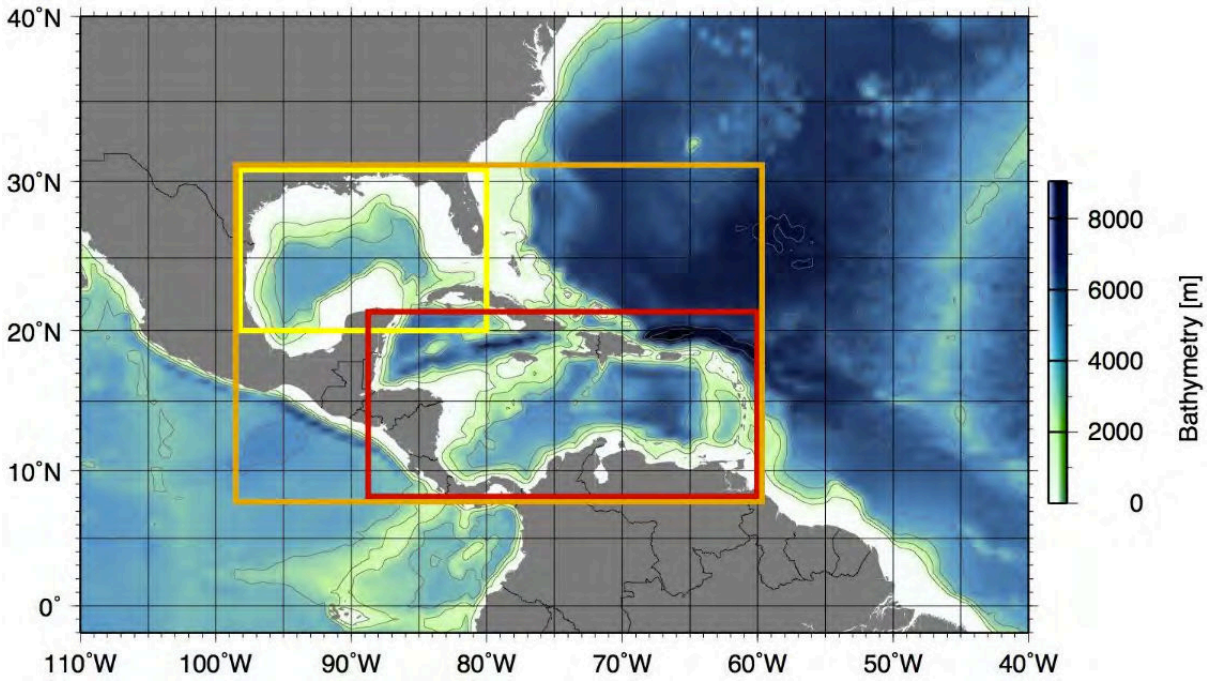

Figure 2.1. Intra-Americas Sea (IAS, orange rectangle) encompassing the Caribbean Sea (CS, red rectangle) and the Gulf of Mexico (GOM, yellow rectangle, and region of study). Bathymetric data was obtained from ETOPO1 (Amante et al. 2009), and contours in grey indicate isobaths from 500 to 8000 m with contours intervals of 1000 m.

Extensive physical oceanographic field and modeling studies have examined the GOM during the last 50 years (Amante et al. 2009). The main attractions have been the warm Loop Current and the large anticyclonic rings repeatedly shed by this current (Vukovich et al. 1979; Vukovich and Maul 1985; Yukovich 1986; Maul and Vukovich 1993; Elliott 1982; Lewis and Kirwan Jr 1987; Forristall et al. 1992; Sturges and Leben 2000; Nof 2005; Zavala-Hidalgo et al. 2006; Lugo-Fernández 2007; Alvera et al. 2009; Lugo-Fernández and Leben

2010). However, compared to the knowledge that has accumulated about physical processes in the GOM, very little is known about the biological oceanography of the region, and most biological oceanographic studies in the GOM have been geographically restricted (*e.g.*, Ortner et al. 1984; Biggs et al. 1984, 1988). Despite the importance of the region to fisheries, seasonal variability in larval fish assemblages in the GOM has been examined in relatively few studies, mainly focused on estuarine assemblages (Raynie and Shaw 1994; Tolan et al. 1997) or on relatively short-term interactions between assemblages and specific oceanographic features, such as the Mississippi River plume (Sogard et al. 1987; Govoni et al. 1989) or the Loop Current (Richards et al. 1993). Other studies have used ichthyoplankton survey data from the National Marine Fisheries Service's (NMFS's) gulf-wide Southeast Monitoring and Assessment Program (SEAMAP), but these studies are typically focused on a single species (Scott et al. 1993; Lyczkowski-Shultz and Ingram 2003; Lyczkowski-Shultz et al. 2007). Although these latter studies provided information on multiple species, no analyses were presented on the influence of mesoscale ocean features, whose associated energy tend to be higher than that of the main oceanic flow (Wunsch 1981), on the distribution patterns of fish larvae spawned in the GOM.

In the next three sections, a more detailed description of the circulation in the IAS and the GOM is presented. First, the circulation in the IAS is studied since it is critical for the understanding the GOM. Then the oceanography of the GOM is extensively presented, from its topography to the possible mechanisms to explain the Loop Current and ring field variability. The importance of mesoscale activity is stated and its variability is analyzed in order to conjecture the ocean processes that could influence some larval fish assemblages in the GOM. This gives us room to explore the grounds of marine biology and fisheries of the region, from the lowest biological levels to larval fish assemblages. Finally, the state of the art on satellite remote sensing is exposed and also its importance as a suitable tool to couple the physics and the biology of the oceans.

2. Circulation in the Intra-Americas Sea

To understand the circulation of the entire IAS (Figure 2.2) the primary focus here will be the CS, which is also critical for understanding the circulation in the GOM. The CS is characterized by a number of deep basins, complex bathymetry and geometry. To the south and west South and Central America bound it, to the north it is bounded by Cuba, Hispaniola, Puerto Rico and the Virgin Islands (the Greater Antilles), and to the east by the island chain of the Lesser Antilles. The Caribbean Sea is composed of numerous water masses of different origin that enter through the various island passages (Wüst and Gordon 1964; Metcalf 1976; Morrison and Nowlin Jr 1982). Some of these waters originate in the North Atlantic (*e.g.*, North Atlantic Deep Water), while others flow from the South Atlantic with origins further afield (*e.g.*, the Southern, Pacific, and Indian Oceans). The circulation is also influenced by freshwater inflow from the Amazon, Orinoco and Magdalena Rivers (Froelich et al. 1978; Restrepo and Kjerfve 2000; Hellweger and Gordon 2002; Muller-Karger and Castro February; Corredor et al. 2004).

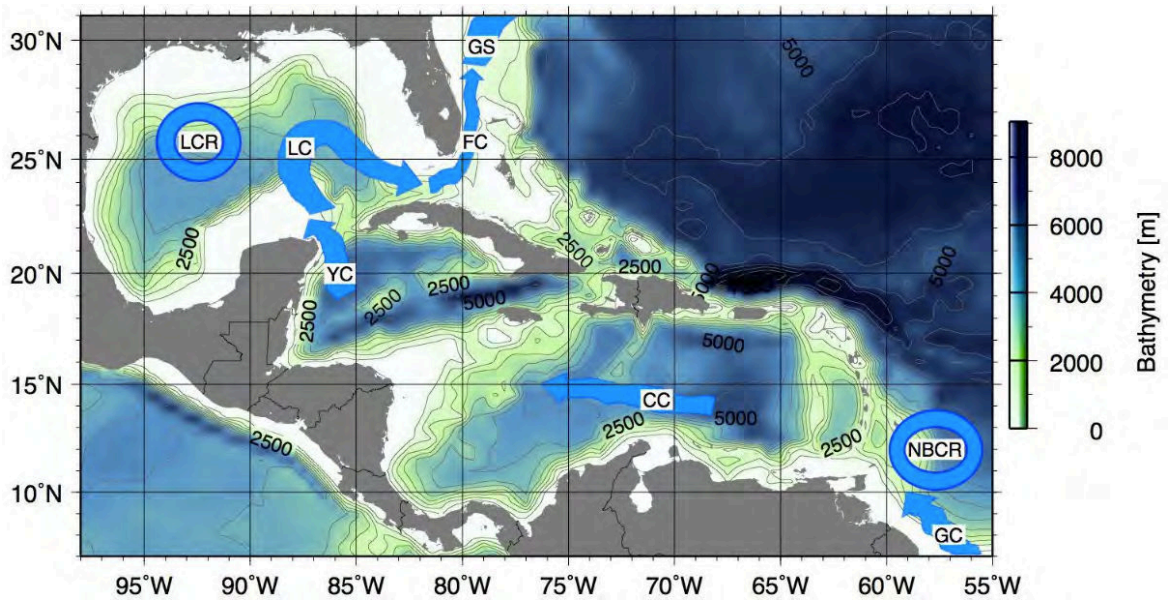

Figure 2.2. Principal oceanographic features of the Intra-Americas Sea (IAS), encompassing the Gulf of Mexico and the Caribbean Sea, with schematic cartoons showing the Guiana Current (GC), North Brazil Current Ring (NBCR), Caribbean Current (CC), Yucatan Current (YC), Loop Current (LC), Loop Current Ring (LCR), Florida Current (FC), and Gulf Stream (GS). Bathymetric data was obtained from ETOPO1 (Amante et al. 2009), and contours in grey indicate isobaths from 500 to 8000 m with contours intervals of 500 m.

As the North Brazil Current (NBC) flows north along the northeastern coast of South America, it reaches French Guiana, where part of the NBC separates from the coast and retroflects to join the North Equatorial Counter Current through a retroflection zone, where NBC rings (NBCR) are formed (Condie 1991; Schott et al. 1998; Mémery et al. 2000). The rest of the NBC continues flowing northwestward to form the Guiana (or Guyana) Current (GC) (Condie 1991). The section joining the NBC and the GC along the coast is marked by a relatively constant flow of 10 Sv (Johns et al. 1990). The GC has been previously referred to as the South Equatorial Current, the North Brazil Coastal Current, and the North Brazilian Current. The confusion surrounding its name is due partly to the seasonal change in flow of nearby currents (Flagg et al. 1986). The NBC retroflects between June and January each year according to some authors (Muller-Karger et al. 1988) and during boreal summer and fall according to others (Csanady 1990), while during the rest of the year it continues along the coast and becomes the GC with some leakage along the coast in the summer (Csanady 1990). When the Intertropical Convergence Zone (ITCZ) shifts north, the winds along the Guiana Coast weaken and shift from northeasterly to southeasterly (Borstad 1982). The change in flow and a reduction of Amazon River discharge after June are correlated with the weakening of the GC (Fuglister 1951) and a sharp reduction of the water supplied to the western tropical Atlantic and Caribbean (Borstad 1982). The GC surface water enters the Caribbean in the south eastern Caribbean, primarily between the southern Windward Islands (St. Vincent, St. Lucia, and Grenada) and between Grenada and the South American continent (Grade 1961). The total Caribbean inflow of 28 Sv is shown to be partitioned approximately equally between the Windward Islands Passages (~10 Sv), Leeward Islands Passages (~8 Sv, and the Greater Antilles Passages (~10 Sv) (Johns et al. 2002). The water then continues westward as the Caribbean Current (CC), the main surface circulation in the CS (Wüst and Gordon 1964; Hernández-Guerra and Joyce 2000).

The strongest flow in the Caribbean Sea is found across the southern third of the sea and belongs to the CC (Kinder 1983), where the highest surface velocities can reach 70 cm s^{-1} along the coasts of Venezuela. In the central Caribbean, the Caribbean Current appears to take the form of two jets centered near 13°N and 15°N, separated by a relatively weak eastward flow (Morrison and Nowlin Jr 1982). Hernandez-Guerra and Joyce (2000) sampled the water masses along 66°W from August to September 1997, finding different water masses in two sections: from Venezuela to about 13°N and from 14°N to Puerto Rico. From

Venezuela to 13°N they found a low-salinity water mass that originated in the tropics and South Atlantic. Within the southernmost portion of this area, they observed two different flow patterns. At the surface, there was an intensified westward jet with velocities of 130 cm s^{-1} in mid-basin. Underneath this flow, there was an eastward flow with a subsurface maximum near the coast of Venezuela. From 14°N to Puerto Rico, they found Caribbean surface water in the upper 50 m of the water column, showing salinity values of less than 35.5, and potential temperature of about 28°C. Below this flow, subtropial underwater -at about 150 m, salinity of 37.0 or higher, and temperature of 22-23°C. Caribbean surface water is probably a mixture of North Atlantic surface waters, Amazon River water, and local freshwater runoff from South America. Subtropical underwater is formed in the central tropical Atlantic, where evaporation exceeds precipitation. South of Hispaniola the two currents merge and flow northwestwards as the Yucatan Current (YC). This is also the region of largest sea surface height variability observed by satellite altimeters (Andrade et al. 2000; Bosch et al. 2002; Oey et al. 2003) which may be linked to the bathymetry, though the role of the local wind stress curl is less clear.

The YC flows through the Yucatan Channel, which connects the CS and the GOM, and forms the LC, which will be explained in detail in the following subsections. The LC exits the Gulf south of Florida to become the Florida Current (FC), which can be considered the "official" beginning of the Gulf Stream (GS) system and was first reported by the Spanish explorer Ponce de Leon in 1513 when he discovered Florida (Galtsoff 1954). The FC has been shown to have a mean transport of 31.5 Sv at 27°N in the straits of Florida (Lee et al. 1985; Molinari et al. 1985). A comprehensive description of the mean inflow distribution in the passages connecting the Atlantic Ocean with the CS, and the latter with the GOM is shown on Figure 2.3 (data from Johns et al. 2002).

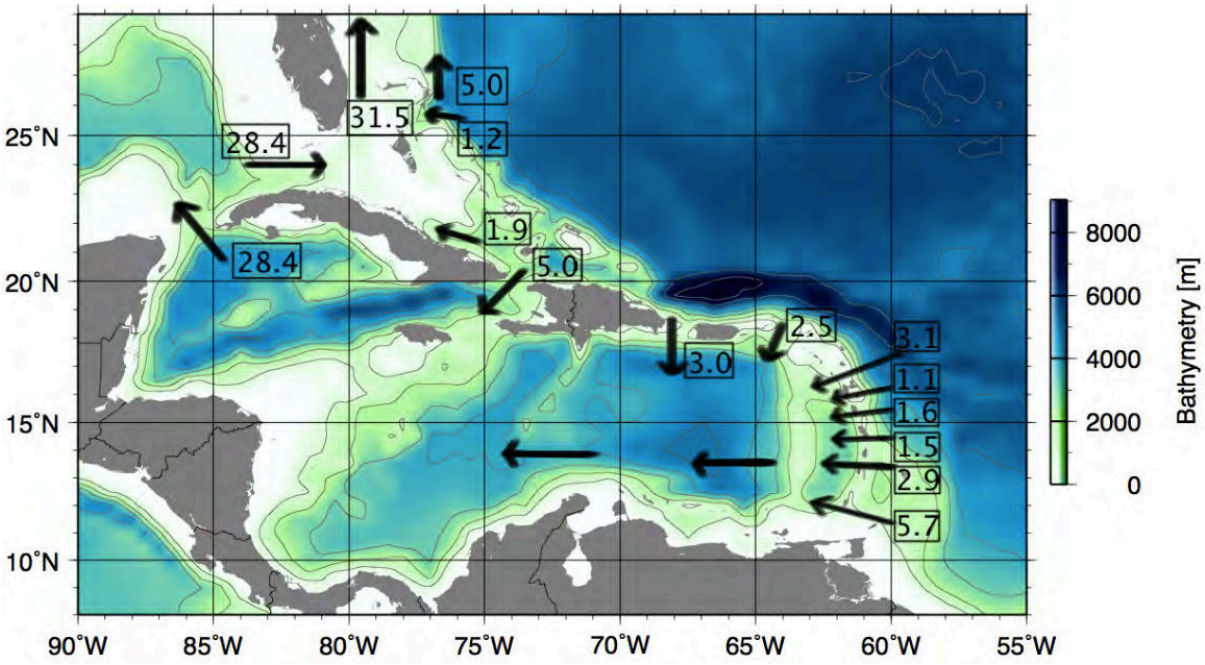

Figure 2.3. Mean transports (Sv) through main passages in the Intra-Americas Sea from combined wind/MOC (Meridional Overturning Circulation) forced model simulation with observed transports (Johns et al. 2002; Smith 2010) are presented. Bathymetric data was obtained from ETOPO1 (Amante et al. 2009), and contours in grey indicate isobaths every 1000 m.

Regarding its dynamics, the Caribbean circulation is under the constant influence of the tropical Atlantic trade winds, which vary owing to the northward migration of the ITCZ from its southernmost position in winter (approximately at the Equator) to its northernmost position in summer (approximately at 11°N), and therefore are typically stronger during boreal summer (Poveda et al. 2006; Muñoz et al. 2008). Transient atmospheric forcing in the form of easterly waves and hurricanes also plays a significant, yet not well understood, role in shaping the ocean circulation. With respect to the mesoscale circulation in the Caribbean, it experiences much variation in both space and time, some of it in the form of mesoscale eddies and meanders. The most recent explanation for the mesoscale variation found in the CS involves NBC rings (Goni and Johns 2001) related the mesoscale variability to "eddy waves", which occur when anticyclonic rings from the Brazil Current collide with the Lesser Antilles Passages (Andrade et al. 2000). Eddies propagate along the CC and then squeeze through the Yucatan Channel. In general, eddy activity is eroded after the Nicaraguan Rise through interaction with the bottom topography. Some eddies also enter the Cayman Sea from outside the Caribbean through the Windward Passage (Andrade et al. 2000). These Caribbean eddies can significantly affect the Loop Current's intrusion and shedding behavior

of warm-core rings, with anticyclonic eddies causing shedding at longer periods (14-16 months) (Oey et al. 2003). The potential explanation is that LC ring shedding exhibits correlation to the flux of potential vorticity through the Yucatan Channel (Candela et al. 2003). This potential vorticity flux is apparently driven by eddies and meanders in the Caribbean Sea. However, the effect of Caribbean eddies on the circulation variability in the Caribbean Sea and the GOM is not fully understood.

3. Oceanography of the Gulf of Mexico

This section is a synopsis of the state-of-the-art knowledge and understanding of 1) the local topography of the GOM 2) the general circulation in the deep GOM, 3) the coastal flow regimes on its continental margins, 4) the physical mechanisms that drive the LC excursions and trigger ring separations, and 5) the upstream conditions that define the large scale circulation of its surrounding waters. This synopsis has a descriptive nature, and its primary purpose is to review the ideas and results on the circulation in the GOM with a broader scope in mind; to provide the base ground for a long term monitoring of mesoscale ocean features in the GOM (chapter III) and to integrate the physical oceanographic knowledge to better understand what regulates the larval fish distribution in the region (chapter IV). Two peer-reviewed publications are derived from above mentioned chapters.

3.1 Topography

The Gulf of Mexico lies roughly within the limits of the western Florida coast in the east; Texas and eastern Mexican coasts in the west; and Louisiana, Alabama and Mississippi coasts in the north. The International Hydrographic Organization defines the southeast limit of the Gulf of Mexico as follows: a line joining Cape Catoche Light (21°37′N 87°04′W) with the Light on Cape San Antonio in Cuba (21°56′ 84°56′), through the northern Cuban coast to the meridian of 83°W and to the northward along this meridian to the latitude of the South point of the Dry Tortugas (24°35'N), along this parallel Eastward to Rebecca Shoal (82°35'W) then through the shoals and Florida Keys to the mainland at eastern end of Florida Bay, all the narrow waters between the Dry Tortugas and the mainland being considered to be within the Gulf.

The GOM occupies a Mediterranean-type basin that is connected to the Caribbean Sea by the Yucatan Strait where water flows in, describes a loop, and then flows out to the Atlantic Ocean via the Straits of Florida. The basin was formed by sea-floor spreading prior to the Cretaceous period between the Permian and early Jurassic periods (170-240 million

years before present). Bounded on the north by the United States, the south by Mexico and the east by Cuba, the surface area of the Gulf is 564,200 km^2 with a maximum east-west dimension of 1,575 Km and a maximum north-south dimension of about 900 Km.

The bottom topography of the GOM is illustrated in Figure 2.4. A narrow to moderately wide continental shelf (0-200 m depth) located along the boundaries of the Gulf constitutes about 35% of its area. Almost half of the basin is shallow continental shelf water, and about one-fourth of the Gulf is very deep (3,000 m). The deepest area, the Sigsbee Deep, is approximately 3,850 m deep.

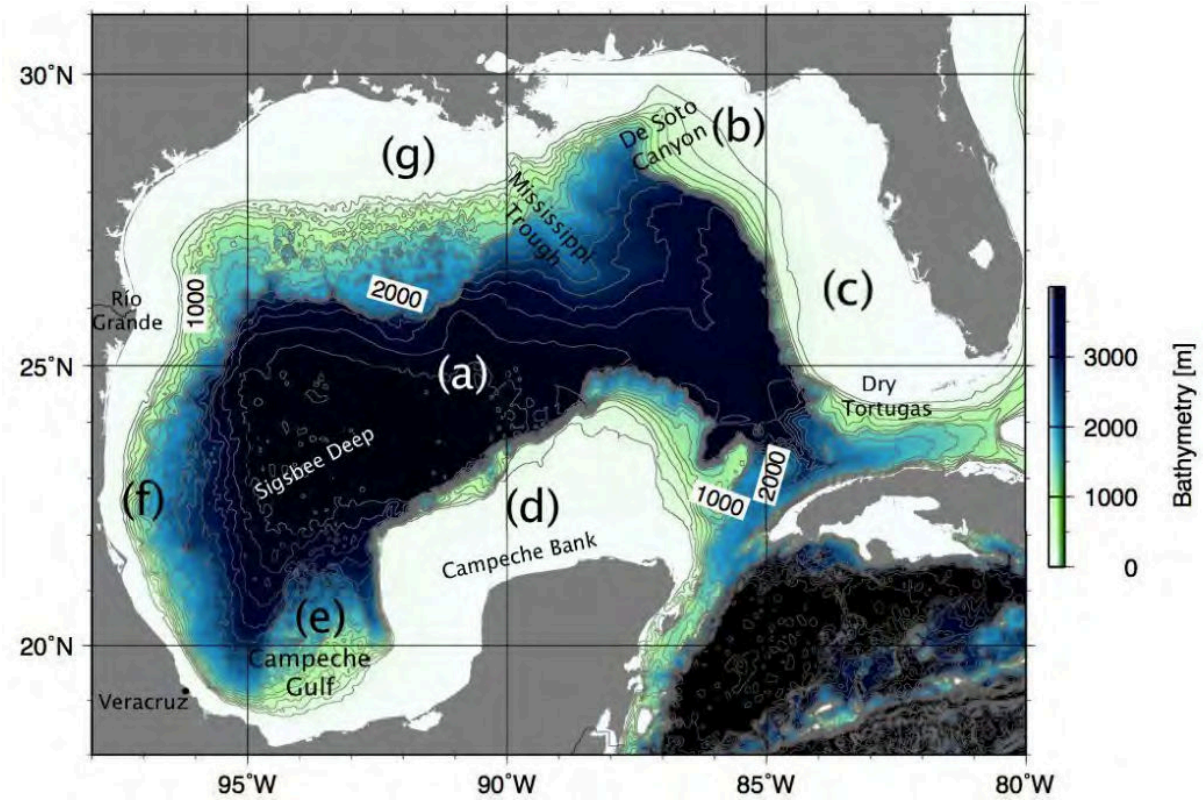

Figure 2.4. Bottom topography in the Gulf of Mexico (GOM), data retrieved from ETOPO1 1-minute Global Relief (Amante et al. 2009) and contours in grey indicate isobaths from 500 to 8000 m with contours intervals of 200 m. The map illustrates the seven distinct geographical regions in which the GOM is divided: (a) GOM Basin, (b) Northeast GOM, (c) South Florida Continental Shelf and Slope, (d) Campeche Bank, (e) Bay of Campeche, (f) Eastern Mexico Continental Shelf and Slope, and (g) Northern GOM.

The bathymetry has strong influence on the circulation in the GOM, as the Gulf's entrances are constricted by two wide and shallow continental shelves (Campache Bank, located North of Yucatan Peninsula, and the West Florida Shelf), with steep escarpments on

their seaward edge. The GOM is usually divided into seven distinct geographical provinces (Antoine 1972):

a) Gulf of Mexico Basin

This portion of the Gulf of Mexico contains the Sigsbee Deep and can be further divided into the continental rise, the Sigsbee Abyssal Plain, and the Mississippi Cone. The Sigsbee Abyssal Plain is a deep, flat portion of the Gulf bottom located northwest of Campeche Bank. In this relatively uniform area of the Gulf bottom, the Sigsbee Knolls and other small salt domes represent the only major topographical features. The DeSoto Canyon borders the Mississippi Cone to the east, and the Mississippi Trough bounds it to the west (Ewing et al. 1958).

b) Northeast Gulf of Mexico

This region of the Gulf bottom extends from just east of the Mississippi Delta near Biloxi to the eastern side of Apalachee Bay. The Florida Escarpment separates the Florida Platform from the Gulf Basin and also forms the southeastern side of the DeSoto Canyon. Some theories suggest that the canyon is the result of erosion caused by oceanic currents, possibly the Loop Current (Nowlin 1971).

c) West Florida Continental Shelf and Slope

A submerged portion of the larger emergent Florida Peninsula, this region of the Gulf of Mexico extends along the coast from Apalachee Bay to the Straits of Florida and includes the Florida Keys and Dry Tortugas. The pressure imposed upon the West Florida Shelf by the Loop Current is found to give rise to a southward flowing jet along the shelf edge (Hetland et al. 1999). Evidence suggests that this basin was at one time enclosed by a barrier reef system (Antoine and Ewing 1963; Ewing et al. 1966; Sheridan et al. 1966). In the Straits of Florida the Jordan Knoll appears to be composed of remnants from this ancient reef system. Evidence suggests that this reef may have once extended across the straits, adjoining the Florida reefs with those of northern Cuba.

d) Campeche Bank

Campeche Bank is located to the north of the Yucatan Peninsula (Ordonez 1936). The bank extends from the Yucatan Straits in the east to the Tabasco-Campeche Basin in the west and includes Arrecife Alacran. The region shows many similarities to the south Florida platform and some evidence suggests that the two ancient reef systems may have been continuous (Antoine and Ewing 1963).

e) Bay of Campeche

The Bay of Campeche is an isthmian embayment extending from the western edge of Campeche Bank to the offshore regions just east of Veracruz (~96° W). The Sierra Madre Oriental forms the southwestern border, and the associated coastal plain is similar to the Texas-Louisiana coast in the northern Gulf. The bottom topography is characterized by long ridges parallel to the exterior of the basin. Cyclonic eddies form near the western edge of the Loop Current, at the northeast shelf break of the Campeche Bank (Zavala-Hidalgo et al. 2003a). Similar to the northern Gulf, large quantities of oil are produced here.

f) Eastern Mexico Continental Shelf and Slope

Located between Veracruz to the south and the Rio Grande to the north, this geological province spans the entire eastern shore of Mexico. The relative complexity of the bottom structure increases from south to north (Bryant et al. 1968).

g) Northern Gulf of Mexico

The northern Gulf of Mexico extends from Alabama to the U.S.-Mexico border. North to south, the province extends from 200 miles inland of the present day shoreline to the Sigsbee escarpment. Emergent topographic features on the continental slope are the Flower Garden Banks off the Texas/Louisiana coast, and the pinnacles region offshore of the Mississippi/Alabama coast (Halbouty 1979).

3.2 General circulation

The most prominent and energetic components of the general circulation of the GOM are the Loop Current (LC), mesoscale eddies, and rings that are shed from the current (Figure 2.5). These powerful oceanic features affect, either directly or indirectly through their smaller-scale subsidiaries, just about every aspect of oceanography of the Gulf.

The LC in the Gulf is part of the Gulf Stream System, the very energetic western boundary current regime in the North Atlantic Ocean. The current is highly variable in position and strength with time, and can intrude northward into the northeastern GOM, forming an intense clockwise flow even as far northward as the Mississippi river delta or the Florida continental shelf (Huh et al. 1981; Wiseman and Dinnel 1988). The LC can retreat to have an almost direct path to the Straits of Florida – which is usually called port-to-port configuration - after shedding a LC ring. The LC ring is an anti-cyclonic warm-core ring, which is formed and pinched off from the LC, and then propagates westward (Elliott 1982). Water exits the IAS through the Straits of Florida as the FC between Florida and the Bahamas.

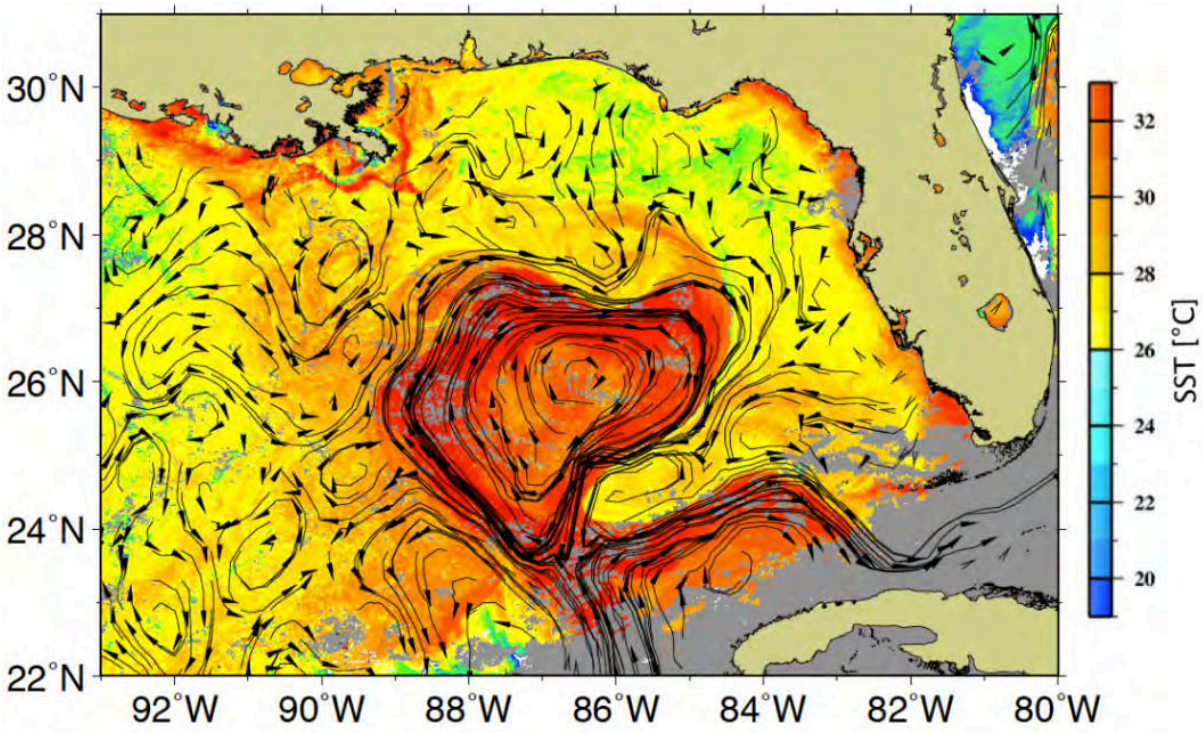

Figure 2.5. Sea surface temperature (SST) on April 25 2011, showing the Loop Current extended into the Gulf, and a warm ring forming from the strangulation of the current. Note the appearance of cyclonic eddies along the edges of the Loop Current, in particular two cyclones located in the 'bottle neck' of the current (approximately centred at 23°N, 88°W and 24.5°N, 85.5°W). Data was obtained from the Advanced Very High Resolution Radiometer (AVHRR), available with a resolution of 2 days on an 18 km grid. Black arrows in the background represent satellite-derived geostrophic currents.

Anticyclonic rings are shed from the LC in the eastern Gulf at irregular intervals (Vukovich 1988a; Sturges and Leben 2000; Leben 2005), which has been reported to range from 4 to 18 months (Sturges and Leben 2000). At this point it must be spelled out the difference between mesoscale eddies and rings. Although it is usually found in the literature that LC rings are designated indistinctively as rings or eddies, it must be clear here that eddies and rings are quite different structures. Shortly after formation they are rings, with little or no relative vorticity in its central core, while later on the core has gained enough angular velocity (through radial diffusion from the ring) to properly talk of an eddy (Auladell et al. 2010). For example, the LC ring represents a wrapped-up piece of the major current that describes a loop, and that is why during its initial stages –before that diffusion takes place- the ring is composed by a frontal region that retains the intense current of the loop on its edge, and a central core region where waters are roughly stagnant. On the other hand, whereas mesoscale eddies show radii comparable to the Rossby radius of deformation (~40

km, (Chelton et al. 1998)), the radius of the ring is much larger (~150 km, (Oey et al. 2005)). A simple diffusion-advection model with an effective diffusion coefficient (Sangrà et al. 2007) is appropriate to grossly simulate the temporal evolution of angular velocity of eddies that start in solid-body type rotation (Auladell et al. 2010). The diffusion-advection equation to study the angular velocity evolution, which is derived from cross-differentiation of the momentum isopycnic equations in cylindrical coordinates under the f-plane and axial-symmetry approximations, is the following:

$$\frac{\partial \omega}{\partial t} + u_r \frac{\partial \omega}{\partial t} = \frac{1}{r} \frac{\partial^2 (Kr\omega)}{\partial r^2} \quad (1)$$

where ω is angular velocity, u_r is radial velocity, K is an effective horizontal diffusion coefficient, t is time, and r radial position.

On the basis of all the explained above and the nature of its generation, rotation, robustness, and long-lived features (Fuglister 1971; Olson 1991), LC Anticyclonic rings will be named rings hereafter along this dissertation. Here it suffices to define rings as intense eddies or vortices that represent a wrapped-up piece of a major ocean current. These large rings shed by the LC have radii of approximately 150 km, swirl speeds of 1.8-2 m s^{-1}, around 800 m depth (similarly to the LC), translate westward into the GOM over space scales of hundreds to thousands of kilometers and exist for periods lasting from months to years (Oey et al. 2005). Rings move through the GOM carrying anomalies similar to the contrasts in physical, biological, and chemical properties observed across the major ocean currents. As a matter of fact, the ring field associated with the LC affects almost every aspect of the circulation in the entire GOM, being considered as the most energetic events in the circulation of the GOM (Sturges and Leben 2000). Once the rings are propagating into the western Gulf, cyclonic features may occasionally cleave these anticyclonic rings into smaller eddies (Biggs et al. 1996).

The shedding process can take several days to a few weeks, and often, after a ring has separated, it reattaches to the LC (Sturges et al. 1993). The frequency of LC ring shedding has been studied by many authors (Maul and Vukovich 1993; Sturges and Leben 2000; Leben 2005), stating that the interval between Loop Current ring shedding varies in the range of 6 to 17 months (Molinari 1980), with primary periods of 6 and 11 months (Sturges and Leben 2000).

A diverse group of complex processes variably participate in the composite mechanism of ring shedding. For a generalized mechanism of first detachment, either partial or complete, cyclone pairs, one on each side of the LC, play a key role. Detachment may occur after an extended LC is pinched-down or necked-down by cyclones, but not every necking-down is followed by detachment (Schmitz et al. 2005). The formation of these cyclones in the vicinity of the LC ring during the separation stage has also been studied (*e.g.*, Vukovich and Maul 1985; Cherubin et al. 2005). Westward propagation is also involved. The initial observational description of first detachment was published approximately 40 years ago (Cochrane 1972) when peripheral cyclones on the boundary of the LC were observed. It was called *first mode of detachment*. Another prototypical view of detachment is observed to occur when the LC has an east-west orientation on its tip (Schmitz et al. 2005). This tends to occur after a first detachment or near-detachment is followed by subsequent reattachment(s), and it is usually called *second mode of detachment*. Pulling apart by westward propagation is the principal initial source for this second mode of detachment, with cyclones slipping in behind the embryonic ring separation to bring about final visual detachment. In these cases, peripheral cyclones on the northern side of the LC often participate in the detachment process, normally in conjunction with a cyclone on the western side of the LC. Mixtures of these two modes of detachment may also occur, involving both cyclonic intrusion and westward propagation in roughly equal proportion (Schmitz 2005). The mechanisms of ring separation will be described in further on a separate section. However, one well-known component process, the penetration (sometimes referred to as an intrusion or northern excursion) of the LC approximately northwest into the GOM, is a basic requirement for the future separation of rings.

LC rings can be strongly reattached, involving the recapture of a previously detached ring by the LC. In addition, it is observed that reattachments can be made by neck filling after near detachments, along with weak reattachments by a touching-like contact between the LC and other anticyclonic features. An exhaustive list of previous studies of interest with respect to elements of the composite ring shedding process and reattachment can be found on the references (Cochrane 1972; Elliott 1982; Fratantoni et al. 1998; Molinari et al. 1978; Sturges and Leben 2000; Sturges et al. 1993; Vukovich 1988; Vukovich and Maul 1985; Zavala-Hidalg et al. 2003; Zavala-Hidalgo et al. 2006).

Regarding the deep circulation in the Gulf, a basin scale cyclonic circulation has been defined in the deepest layers in the GOM (DeHaan and Sturges 2005). Although the upper

layer mean flow that has been described above -when describing the LC and rings- is anticyclonic, mean flow near the edges of the GOM below 2000 m is cyclonic. The mechanism underling this cyclonic deep flow is based on deep topographic Rossby waves that are rectified by bottom friction (Mizuta and Hogg 2004). Direct observations from drifters in the intermediate depths of the GOM at 900 dbar (approximately at depths of 900 m) also show a mean cyclonic circulation along the northern and western edges of the GOM.

3.3 Coastal flow regimes

Coastal circulation in the GOM may be characterized dynamically as mostly wind and buoyancy forced on the inner and middle continental shelves. For wide shelves, coastal circulation regimes over the inner and middle shelves tend to be decoupled dynamically from flows over the continental slope and rise. Both downwelling and upwelling coastal regimes are found in the GOM, typically a seasonal phenomena due to observed regional wind fields. Many of the adjacent shelf circulation systems in the GOM interact with each other.

The mechanism of cross-shelf-slope exchange in the region is related to the presence of the LC ring and a cyclonic byproduct of its topographic interaction. This exchange, firstly reported in 1972 (Nowlin Jr 1972), is due to the onshore/offshore movement of water between the shelf and the deep GOM as induced by this type of cyclone-anticyclone pair over the continental slope (Brooks and Legeckis 1982). Pairs of sub-mesoscale cyclonic eddies with a presence on the continental slope are also a well established mechanism for moving water off the shelf system in the northern GOM (Biggs and Müller-Karger 1994; Biggs et al. 2005; Hamilton and Lee 2005). Eddy vorticity flux over the continental slope and rise is typically greater than the contribution from wind-stress curl (Ohlmann et al. 2001; Ohlmann and Niiler 2005). Obviously, circulation patterns on the continental shelf also depend on shelf geometry as well as river distribution and the nature of offshore flow and forcing (Weisberg et al. 2005).

3.4 Is there a unique mechanism for Loop Current intrusion and ring sheddings?

Resolving, understanding, and monitoring the upper ocean mesoscale field and its vertical thermal structure, including an accurate knowledge of the position LC rings and LC fronts, appear to be critical elements for a variety of applications: in tropical cyclones intensification studies and forecasts (Leipper and Volgenau 1972, Shay et al. 2000, Kaplan et al. 2009, Goni et al. 2010); in oil spill response management (Kolch et al. 1991, Kaiser and Pulsipher 2007); in navigation; in search and rescue operations; and in understanding the environmental conditions that influence distributions of the larvae of different fish species and spawning sites (Ortner et al. 1984, Richards et al. 1993, Bakun 2006). Also the detached LC rings may have a measurable impact on the heat budget of the GOM since a LC ring can extend to a maximum depth of 1000 m and the volume of a LC ring has been estimated to be as much as 7% of the total volume of the GOM (Elliot, 1982). This leads to the question: What physical processes might drive the LC intrusion, trigger the ring shedding, and set the initial state of the LC after ring separation?

The mechanism supporting LC and ring shedding has been widely studied, notably by Hurlburt and Thompson (1980) on their classic modeling paper (henceforth HT), and more recently interpreted using the "momentum imbalance paradox" idea of Pichevin and Nof (1997) (henceforth PN) (see also Nof and Pichevin, 2001; Nof, 2005). These studies showed that the ring shedding can be captured by a single layer reduced gravity (1.5) layer model without the need to consider the interaction with the variable bottom topography.

When discussing circulation features and model resolutions, it is relevant to have a clear idea of the first-mode baroclinic radius of deformation in the region. The baroclinic Rossby radius of deformation plays a fundamentally important role in large-scale ocean circulation theory, since it describes the horizontal scales of meso-scale processes and it represents an important measure of the ocean dynamics. The internal (baroclinic) Rossby radius of deformation is the ratio between the phase speeds of the long internal waves to the Coriolis parameter. Basically, it is the horizontal (length) scale at which rotation effects become as important as buoyancy (or gravity waves) effects (*e.g.*, Gill 1982); in other words it defines the length scale of baroclinic variability longer than which internal vortex stretching is more important than relative vorticity and it is intimately related to the dominant

length scale of unstable waves in a stratified shear flow. Outside near-equatorial latitudes (about $\pm$ 10° from the equator), the first baroclinic Rossby radius can be formally defined as the distance, λ_1, that first baroclinic gravity waves of speed c_1 propagate over time f^{-1} (Gill 1982):

$$\lambda_1 = \frac{c_1}{|f|} \tag{2}$$

where f is the planetary vorticity. Values of the first baroclinic Rossby radius in the ocean vary with latitude, ranging from a few kilometers at high latitudes to greater than 100 km near the equator. A standard procedure for evaluating the baroclinic Rossby radii of deformation is to use a linearized quasi-geostrophic potential vorticity equation. Employing the Wentzel-Kramers-Brillouin (WKB) method (Gill 1982; Chelton et al. 1998), the phase speed of the first baroclinic gravity wave is

$$c_1 = \pi^{-1} \int_{-H}^{0} N(z)\ dz \tag{3}$$

where N is a buoyancy frequency, computed following the procedure outlined in section d of appendix B in Chelton et al. (1998), and $H(x, y)$ is the depth of the ocean. Calculation for the GOM gives a first baroclinic Rossby of deformation of approximately 40 km (Chelton et al. 1998).

3.4.1 The Hurlburt and Thompson model

Hurlburt and Thompson (1980) (henceforth HT) pioneering work in modeling the LC and rings in the GOM is today a benchmark against which many later model experiments are measured. HT experimented with 1-layer barotropic, 1.5-layer reduced-gravity, and 2-layer models of an idealized rectangular Gulf of Mexico basin with inflow (Yucatan Channel) and outflow (Florida Straits) ports (Figure 2.6).

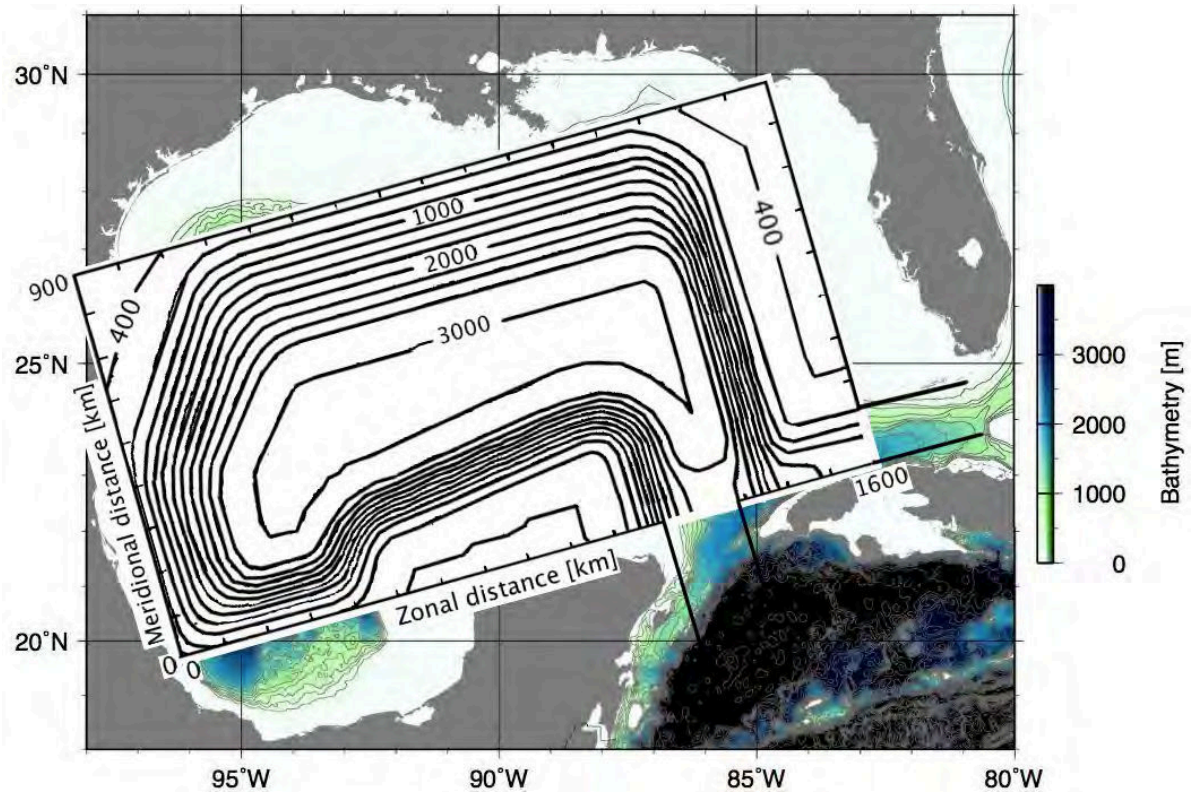

Figure 2.6. Domain of the Hurlburt and Thomson model superimposed on a map of the Gulf of Mexico. The deepest water is at 3000 m and the shallowest water is 400 m deep, with contour interval of 250 m. The locations of the inflow and outflow ports are also indicated. The model is driven by the inflow through the southern port (160 km wide, Yucatan Straits) and compensated by outflow though the eastern port (150 km wide, Florida Straits). The β-plane approximation and hence taking into account the variation of the local rotation rate is used ($f = f(y)$ only), but not the earth sphericity.

The following summarizes HT's findings regarding the modeling of the LC and ring shedding:

1. 1.5-layer model is the simplest relevant model of LC and ring shedding.
2. Shedding is caused by horizontal shear instability of the internal mode.
3. Shedding occurs despite steady inflow specified at Yucatan Channel.
4. Planetary β-effect is essential in the Loop Current's penetration into the GOM (first pointed out by Reid [1972]) and also in eddy-shedding (through westward spreading of the Loop Current and removal of eddies); the penetration time scales dictate shedding time scales. For example, when β=0, the solution evolved to steady source-sink flow with no ring shedding or westward spreading, and this held true even when inflow was augmented with a large westward component.

5. From 4., the f-plane solution is a steady source-sink flow (no shedding).
6. Nonlinearity is necessary for shedding – the linear solution (when inflow is weak, HT used 0.1 Sv) is also a steady source-sink flow.
7. In the 2-layer model, loss of energy due to baroclinic instability to the lower layer results in weaker and smaller eddies and in shorter shedding periods (*e.g.*, from 12 months for 1.5-layer model to 8 months for 2-layer with topography, and 5.4 months for 2-layer flat-bottom).
8. Eddy-shedding period is dominated by the natural period (≈ 12 months with steady inflow), though there is also some dependency on time-varying inflow.
9. Eddy-shedding period increases with Reynolds number (please see below); irregular shedding (10~14 months) can occur at a sufficiently high Reynolds number.
10. In the 2-layer model with topography, sufficiently strong (10 Sv) bottom inflow from Yucatan Channel traces a clockwise circulation around the Gulf following the f/H contours; the resulting divergence over the west Florida slope can prevent upper-layer deepening, Loop Current's westward spreading and eddy-shedding. Shedding resumes when the bottom deep inflow weakens.

A particularly interesting result is that the LC would "short-circuit" from Yucatan-port to Florida-port (*i.e.*, without penetrating into the Gulf and making a loop) when (1) the two ports are close to each other (*i.e.*, the distance L_p between the centers of the inflow, Yucatan Channel, and outflow, Florida Strait, is small); or 2) when the flow entering the GOM is strong. Although the first condition is quite intuitive, the second condition is not (see HT's experiments RG40 and RG43, listed in their Table 2). In this case, the tendency for the Loop to spread or bend westward, due to the β-effect, is balanced by northward advection of the relative vorticity, and streamlines tend to curve eastward. In all general circulation models since HT, β and L_p are fixed. The latter may us hypothesize that a port-to-port mode can occur if surface inflow from the Caribbean increases and/or deep inflow increases through the Yucatan Channel (HT 's finding 10 above).[1]

[1] Some general circulation models presently used do display this port-to port configuration (Sheng et al. 1998; Cherubin et al. 2005; Oey et al. 2005; Eden et al. 2007; Lin et al. 2010).

3.4.2 The "momentum imbalance paradox" of Pichevin and Nof

The findings of HT are significant in that an analytical treatment of the 1.5 layer model may provide valuable insights into the dynamics of LC and ring shedding. The paper by Pichevin and Nof (1997) (henceforth PN) is an important contribution in this regard (also see Nof and Pichevin 2001; Nof et al. 2004; Nof 2005). PN analyze the consequences of a northward narrow outflow, Q, (*i.e.*, width ~ Rossby radius or less situated next to a southern boundary) debouching into an open ocean (Figure 2.7).

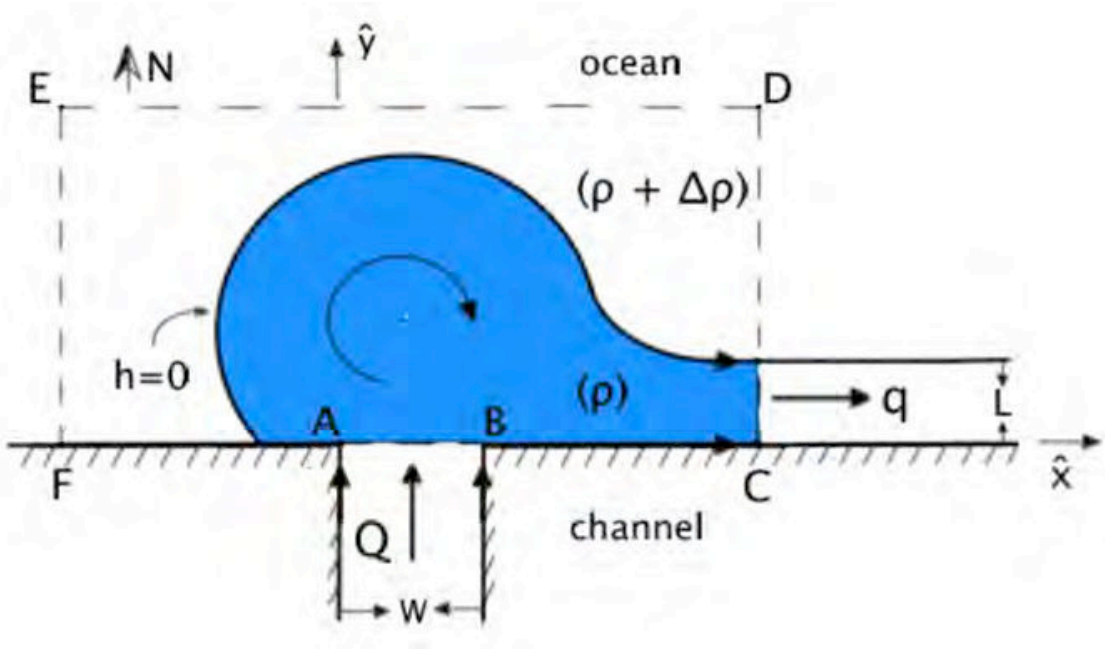

Figure 2.7. Diagram illustrating the "momentum imbalance paradox". A northward meridional channel carrying water with density ρ empties into an otherwise stagnant ocean with density $(\rho + \Delta\rho)$. Along the front it is assumed that the thickness h=0. The streamlines in the channel are assumed to remain parallel to the channel walls until the coastline is reached (*i.e.*, section AB). The hypothetical steady configuration is not possible on both a f and β-plane. In the PN scenario, a steady inviscid outflow cannot exist because the long-shore momentum flux of the downstream current is not balanced.

The traditional view of this phenomenon was that, due to Coriolis force, such an anomalous flowing current turns to the right (looking offshore) and forms a zonal boundary current that flows eastward. In this scenario, a front (corresponding to a surface interface)

separates the oceanic and the anomalous water (Figure 2.7). By integrating the x-momentum equation over a rectangular domain just outside the outflow (area FEDC of figure 2.7), PN show that the integrated momentum exerted on the domain by water exiting the rectangle on the right cannot be balanced in a steady state (it gave an unbalanced long-shore flow-force). This "momentum imbalance paradox," as the authors called it, is resolved if either (time dependent) rings are allowed to shed to the left (β-plane; Figure 2.8a) or the outflow grows forever (f-plane; Figure 2.8b). The β-effect is again a "must" for ring shedding. Thus shedding (or growing bulge) in PN is a necessary consequence of the flow's inability to keep the long-shore momentum in a steady-state balance. This new shedding mechanism explains why the LC produces loops and shed rings.

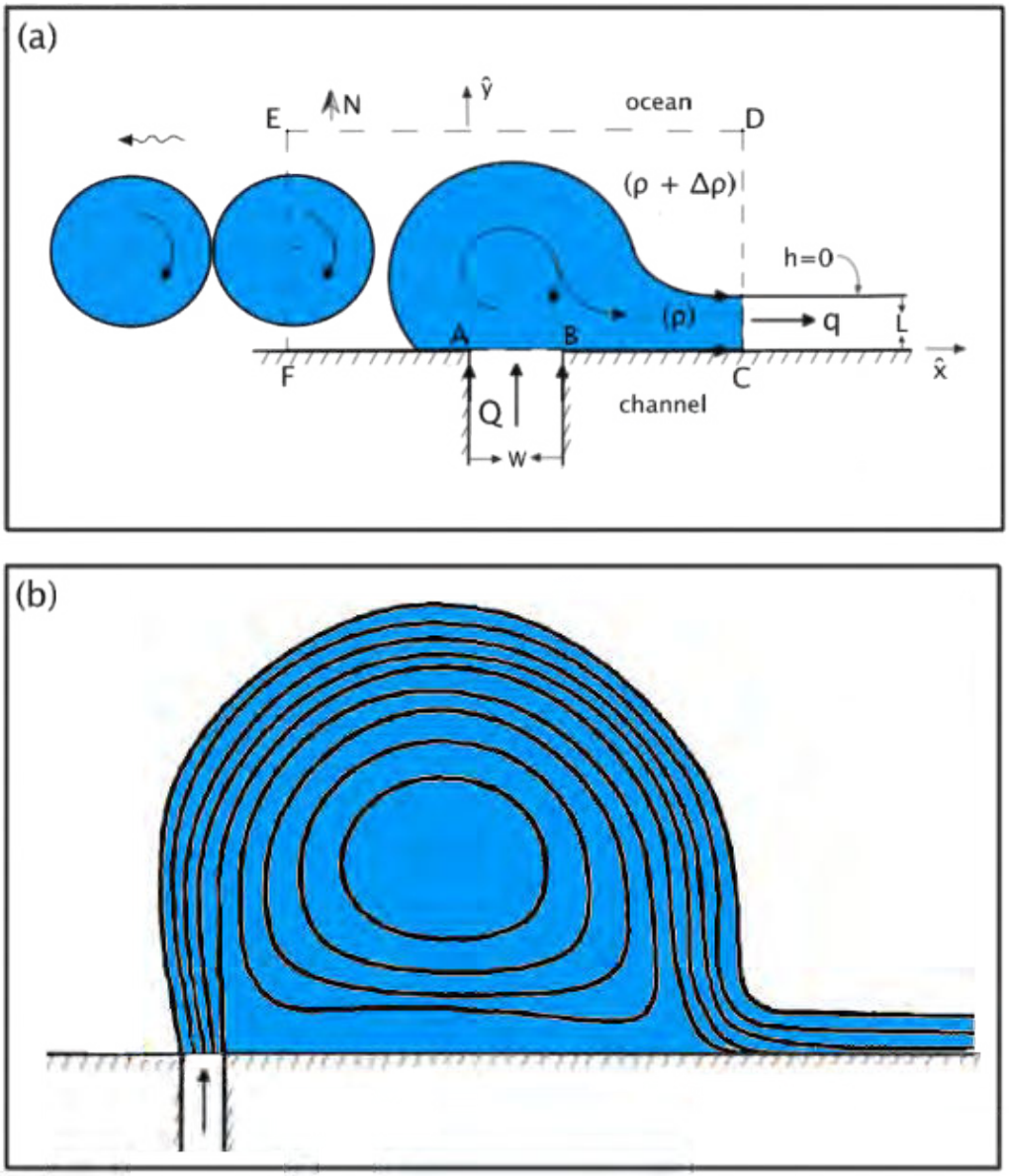

Figure 2.8. Diagrams showing the (a) PN resolution of the "momentum imbalance paradox" and (b) the depth contours of the f-plane flow. Because of the imbalance paradox sketched in Figure 2.7, the flow of the downstream current is not balanced. As a result, there are two possibilities. On a β-plane (a), the anticyclonic ring growth is ultimately arrested and, as a result, rings are periodically shed on the left-hand side (looking offshore). Through the β effect, these eddies are forced to propagate to the left. Pichevin and Nof (1997) obtained their analytical solution by equating the momentum flux through EF to the momentum flux through CD. Nof (2005) added that we should not deal with the momentum flux through CD. Instead, the integrated Coriolis force associated with the slowly growing base ring -the one that is still no detached and whose center migrates slowly offshore- is equated to the momentum flux through CD. The base ring, which is the eddy in contact with the source, should be distinguished from the already detached eddies downstream. The assumption that the eddies are "kissing" each other as they propagate westward is made in both PN and Nof 2005. (b) Conversey on a f-plane (b), the eddy grows forever and the downstream current mass flux is smaller than the incoming mass flux.

It is important, however, to remember the "narrow outflow" condition implicit in the PN analysis, in which the line integral across the outflow is zero, since u = 0 there (h is the upper-layer depth in their 1.5-layer model). This result does not contradict HT's finding 2. On the other hand, HT's outflow does not grow indefinitely when f = constant (finding 5). This apparent (but fundamental) discrepancy is puzzling; it may be due to the additional constraint that exists in HT's model: that the port at Florida fixes the magnitude and location of the outflow, *i.e.*, due to the existence of the additional length scale L_p in HT.

In summary, HT's 1.5-layer model may be simple, yet it captures remarkably well the gross characteristics of LC variability: its extension (growth), shedding of an eddy, and retraction. The periods of shedding predicted by PN (~10 months) are in agreement with the periods predicted by HT (~12 months). In addition, the PN predictions of ring size and speed are in very good agreement with observations. The model also helped to clarify the longstanding misconception that the Loop Current sheds eddies in response to quasi-annual variation in inflow through the Yucatan Channel. Similar techniques have been applied to the generation of Brazil Current (Nof and Pichevin 1996).

The real ocean works in a curiously complex manner: the observed shedding periods cover a wide range (approximately 3 to 18.5 months); the LC can extend and retract (scales ~ months and 100 km) without necessarily shedding a ring; a ring can temporarily detach then reattach to the LC (time scales ~ weeks); frontal meanders, eddies and cyclones can develop and can influence eddy shedding; Yucatan shelf/slope, deep-layer and Caribbean influences may be significant, etc. Present and future models are challenged to capture some of these complications.

3.5 Consideration of upstream conditions

The interconnectivity of the flow processes in the western tropical Atlantic Ocean is a significant aspect of the Gulf Stream System, of which the general circulation in the GOM is one component. These remote flow regimes, as well as regional and local forcing, can influence the general circulation in the CS and thence the GOM. The net inflow into the Caribbean Passages and then into the GOM is approximately 40% of South Atlantic origin

(Schmitz and Richardson 1991). This water of South Atlantic origin is in the Florida Current concentrated in two comparatively fresh water masses. There is an additional significant contribution of deeper, mostly upper Antarctic Intermediate Water (Schmitz and Richardson 1991b; Schmitz Jr 2004).

The rest of the upper ocean water entering the CS, the GOM though the LC, and then flowing to the Atlantic within the Florida Current is of North Atlantic origin. These water masses have been studied in the GOM by different authors, and it has been suggested that the it is related with the variability in the flow in Windward Passage and the Old Bahama Channel (Johns et al. 2002; Hamilton et al. 2005).

The two passageways providing the entry and exit routes for transport in and out of the GOM, flow through the Yucatan Channel between Yucatan and Cuba and flow though the Straits of Florida between Florida and Cuba, are intimately connected. Assuming incompressibility in the mass conservation law, the equation for the balance of volume in the Gulf of Mexico may be written as

$$\frac{dV_{GOM}}{dt} = T_Y + T_F + R + (P - E) \tag{4}$$

where V_{GOM} is the total volume of water in the Gulf of Mexico, T_Y is the volume transport across Yucatan Channel, T_F is the volume transport across the Florida Straits, R is the runoff and $(P - E)$ is the volume transport due to precipitation minus evaporation. Estimates of $R + (P - E)$ made by Etter [1983] show that these terms are very small, on the order of 0.1 percent of T_Y and T_F. Since altimetry derived estimates of $\frac{dV_{GOM}}{dt}$ indicate that it is a small term (Bunge et al. 2002), large terms in equation (4) (T_Y and T_F) almost balance out, the transport into the GOM through the Yucatan Current is expected to be balanced by the transport out through the Straits of Florida.

The deep flow between the Caribbean and the Gulf has been studied, finding a 3-layer flow in the waters below the sill depth (approximately of 700 to 800 m) of the Straits of Florida. First there is inflow to the Gulf from the Caribbean, through the Yucatan Channel, at depths of approximately 800 m down to 1200 m. There is also an inflow from the Caribbean in the layers just above the sill at 2000 m. What it is surprising is that there is a return flow of approximately 1 Sv at depths of 1300 to 1900 m, from the GOM into the Caribbean (Rivas et al. 2005).

Many efforts have been made in the past to connect the intrusion of the Loop Current into the GOM and the associated ring shedding with the flow structure and transport through the Yucatan Channel (Maul et al. 1985; Candela et al. 2003; Bunge et al. 2002; Oey 1996; Ezer et al. 2003). The time dependent exchange at the Yucatan Strait between the GOM and the CS, within both the upper and deep ocean, was first suggested in 1977 when co-oscillation between the Cayman Sea and the GOM were found to be connected with time dependent growth of the LC (Maul 1977, 1978). That is, the growth of the LC as it expands to the north displaces an approximately equivalent volume of Gulf water, which is observed to flow back into the CS at depths below 800 m (Bunge et al. 2002). The *Maul View* has become a key contemporary issue (Bunge et al. 2002; Candela et al. 2002, 2003; Oey et al. 2003; Oey 2004; Oey et al. 2005; Rivas et al. 2005; Chérubin et al. 2005). The intrusion of the Loop Current into the GOM is measured differently in different studies. For example, Vukovich (1995) used monthly averaged distance between the northern boundary of the Loop Current and the 30°N latitude line to study the Loop Current ring shedding frequency. Bunge et al. (2002) evaluated the variability of the Loop Current by the surface extension of the Loop Current, which was inferred from a series of radiometer images using graphic software to manually define the boundaries of the current. Ezer et al. (2003) generated a time series of variations of the Loop Current extension defined as the area averaged sea surface elevation over the region of the Loop Current (89°W to 83°W, 21°N to 27°N).

The Gulf-Caribbean connectivity is explored in Sturges (1992), who demonstrated interactions of the natural shedding frequency with the frequencies of variability of other oceanographic forcing fields, such as the Yucatan Channel inflow, the Florida Current and the North Brazil Current variability, as well as the synoptic meteorological forcing variability. Murphy et al. (1999), showed that Caribbean eddies that squeeze through the Yucatan Channel can affect the timing of Loop Current shedding. Oey et al. (2003) concluded that wind-induced transport fluctuations through the Greater Antilles Passages cause shedding at shorter periods, while Caribbean eddies (anticyclones) cause shedding at longer periods. Oey (2004) argued that the potential vorticity flux anomaly at the Yucatan Channel may serve as a determining factor.

Although previous studies consitute a big endeavor to better understand the behavior of the LC and detached ring field by exploring the upstream conditions, the variability in the LC system -including the Yucatan Current and Florida Current- associated with ring shedding remains not fully understood.

4. Marine biology and fisheries of the Gulf of Mexico

> Ichthyoplankton (from Greek: *ιχθυς*, *ikhthus*, "fish"; and *πλαγκτος*, *planktos*, "drifter") refers to fish eggs, newly hatched eggs (fry), young fish, and adults of small fish, whose sizes are from 153 μm long to 5,000 μm or longer (Froese and Pauly 2011).

Planktonic organisms -any drifting organisms (animals, plants, archaea, or bacteria) that inhabit the pelagic zone of oceans, seas, or bodies of fresh water- are typically aggregated in the vertical and horizontal dimensions on a variety of temporal and spatial scales. This aggregation is influenced by biological characteristics of these organisms and by physical features of their habitat (Ortner et al. 1978; Owen 1981; Mackas et al. 1985). The propagation of plankton, their behavior, and their buoyancy interact with the physical hydrographic structure and hydrodynamic motion of the ocean to affect aggregation.

Among the planktonic organism, ichthyoplankton is referred to the eggs and larvae of fish. Although they are typically considered inert particles, fish larvae are interactive components of the ecosystem (Cowen 2002; Fuiman 2002). Most fishes have a pelagic stage, whose duration varies between weeks to months (Brothers et al. 1983; Victor 1986). During this pelagic stage, important changes occur in short time periods. For example, most fishes increase their weight 5 orders of magnitude throughout their life and three of them occur during this pelagic stage (Werner and Gilliam 1984; Houde 1987; Miller et al. 1988). The sharp biomass increase during the short larval period evidences the importance of this stage as a recruitment modulator (Houde 1987). Thus, growth and processes that favor larval survival are crucial for recruitment success (Cushing 1975; Cowan Jr and Shaw 2002). Thus, it is important to study ichthyoplankton because the abundances of eggs and larvae of several species have been demonstrated to be good indicators of the transient spawning population size of the adults. Determining the abundance of eggs and larvae in an area is usually less expensive to do than sampling the adults. For species such as sardine and anchovy, for instance, egg and larval counts are good indicators of population size. Thus, we can use the egg and larval data to monitor trends in population abundance of the adults. We are able to tell when populations are declining, often more rapidly than we could if we were just

monitoring adults. For species that are not captured by a fishery, monitoring their population trends by monitoring their eggs or larvae can provide an indication of a healthy or stressed ecosystem. It is unlikely that we would have an idea of the abundance, growth or decrease of these species in any other way, so ichthyoplankton monitoring becomes essential.

4.1 Biological levels and limiting factors in the Gulf of Mexico

Plankton typically flow with ocean currents. While some forms are able to move independently and they can swim hundreds of meters vertically in a single day -a behavior called diel (or diurnal) vertical migration- their horizontal position is primarily determined by the surrounding currents. This is in contrast to nekton organisms that can swim against the ambient flow and control their position (*e.g.*, squid, fish, and marine mammals). Within the plankton, holoplankton spend their entire life cycle as plankton (*e.g.*, most algae, copepods, salps, and some jellyfish). By contrast, meroplankton are only planktic for part of their lives (usually the larval stage), and then graduate to either a nektic or benthic (sea floor) existence. Examples of meroplankton include the larvae of sea urchins, starfish, crustaceans, marine worms, and most fish. Planktonic organisms are primarily divided into 3 trophic level groups: phytoplankton, zooplankton, and bacterioplankton[2].

4.1.1 Phytoplankton variability in a non-oligotrophic region

Phytoplankton (from Greek *phyton*, or plant) are autotrophic, prokaryotic or eukaryotic algae that live near the water surface where there is sufficient light to support photosynthesis. Among the more important groups are the diatoms, cyanobacteria, dinoflagellates and coccolithophores. Although phytoplankton are too small to be individually seen with the unaided eye, when present in high enough numbers, they may appear as a green discoloration of the water due to the presence of chlorophyll-*a* within their cells. They are agents for

[2] Bacterioplankton refer to the bacterial component of the plankton that drifts in the water column. bacteria and archaea, which play an important role in remineralising organic material down the water column. They will not be further described in this work.

primary production, the creation of organic compounds from carbon dioxide dissolved in the water, and a process that sustains the aquatic food web (Peters and Marrasé 2000). Phytoplankton obtain energy through the process of photosynthesis and must therefore live in the euphotic zone of the ocean, account for half of all photosynthetic activity on Earth (Boyce et al. 2010).

The GOM had in the past been described as an oligotrophic system (Ortner et al. 1984). However, satellite data and *in situ* observations (Muller-Karger et al. 1991; Gilbert et al. 1996; Gilbes et al. 1996, 2002; Muller-Karger and Fuentes-Yaco 2000; Biggs and Ressler 2001; Belabbassii et al. 2005; Biggs et al. 2008) helped demonstrate that the GOM experiences intermediate to high phytoplankton concentrations both over the shelf and in certain offshore areas, and that some of these patterns are seasonal. Some changes in inshore areas are related to wind-driven coastal upwelling (Chuang et al. 1982; Schroeder et al. 1987; Yang and Weisberg 1999; Muller-Karger and Fuentes-Yaco 2000; Weisberg et al. 2000) and river plumes (Gilbes et al. 1996; Walker 1996; Del Castillo et al. 2000; Hu et al. 2003). In deeper water, variation in chlorophyll-*a* is affected by seasonal convective mixing, divergence- and convergence-associated cyclonic and anticyclonic eddies (Biggs and Muller-Karger 1994) and the off-margin entrainment dispersal of riverine outflows (Biggs et al. 2008). Using Coastal Zone Color Scanner (CZCS) images, Muller-Karger et al. (1991) found that variability in pigment concentration seaward of the shelf was synchronous throughout the Gulf of Mexico, with the highest values in winter (from December to February) and the lowest during summer (from May to July). Also using CZCS images, Gilbes et al. (1996) observed an episodic plume with high pigment concentration developed each spring extending along the West Florida Shelf from an origin region within the North Eastern GOM. This plume persisted for 1–6 weeks in a pattern that extended >250 km southward along the shelf. After the plume dissipates, low pigment concentrations are generally observed during the summer along the outer West Florida Shelf, while coastal concentrations increase as a result of higher river discharge by Florida rivers (Gilbes et al. 1996). Occasionally in summer, surface waters from the Mississippi River can be entrained either by deep water off the edge of the West Florida Shelf or by slope eddies into the eastern edge of the Loop Current, and therefore extend for hundreds of kilometers to the southeast of the delta (Hu et al. 2003, 2005). The high spatial and temporal variability of pigment concentration in the GOM increases from east to west and from south to north, due to the difference in thermal stratification across the region, the intrusion of nutrient-poor waters from the western

Caribbean, the occurrence of cold fronts and extra-tropical low pressure systems, and the nutrient distribution from the Mississippi river (Melo-González et al. 2000).

4.1.2 Zooplankton, from near-shore to central Gulf

Zooplankton (from Greek *zoon*, or animal), are small protozoans or metazoans (*e.g.*, crustaceans and other animals) that feed on other plankton and telonemia. Some of the eggs and larvae of larger animals, such as fish, crustaceans, and annelids, are included here. Zooplankton feed on bacterioplankton, phytoplankton, other zooplankton (sometimes cannibalistically), detritus (or marine snow) and even nektonic organisms. As a result, zooplankton are primarily found in surface waters where food resources (phytoplankton or other zooplankton) are abundant. Just as any species can be limited within a geographical region, so is zooplankton. However, species of zooplankton are not dispersed uniformly or randomly within a region of the ocean. Instead 'patches' of zooplankton species (this also applies to phytoplankton) exist throughout the ocean. Though few physical barriers exist above the mesopelagic[3] zone, specific species of zooplankton are strictly restricted by salinity and temperature gradients; while other species can withstand wide temperature and salinity gradients (Lalli and Parsons 1997). Zooplankton patchiness can also be influenced by biological factors, as well as other physical factors. Biological factors include breeding, predation, concentration of phytoplankton, and vertical migration (Lalli and Parsons 1997). The physical factor that influences zooplankton distribution the most is the mixing of the water column (upwelling and downwelling along the coast and in the open ocean) that affects nutrient availability and, in turn, phytoplankton production (Lalli and Parsons 1997). Through their consumption and processing of phytoplankton and other food sources, zooplankton play a role in aquatic food webs, as a resource for consumers on higher trophic levels (including fish). Thus, zooplankton are the initial prey item for almost all fish larvae as they switch from their yolk sacs to external feeding (Figure 2.9), and it is considered as the principal food of larval fish (Turner 1984; Govoni et al. 2010). Fish rely on the density and distribution of zooplankton to match that of new larvae, which can otherwise starve. Natural factors (*e.g.*, current variations) and man-made factors (*e.g.*, river dams) can strongly affect zooplankton,

[3] The mesopelagic zone limits are from 200 m to around 1000 m. Although some light penetrates this second layer, it is insufficient for photosynthesis. At about 500 m the water also becomes depleted of oxygen.

which can in turn strongly affect larval survival, and therefore breeding success.

Figure 2.9. Larval fish (*Salmo salar,* Atlantic salmon*)* egg hatching, and start of the external feeding. The Alevin (larva) has grown around the remains of the yolk sac. In about 24hrs it will be a fry without yolk sac and it will start external feeding from zooplankton. Image provided by Dr. Uwe Kils Institute of Marine and Coastal Sciences, Rutgers University.

Studies of vertical distribution of zooplankton in the eastern GOM showed that the zooplankton community is diverse, 21 genera individually exceeding 1% of the biomass in the 0 to 1000 m layer (Hopkins 1982). Grazers (herbivores, detritivores, omnivores) are 66% of the 0 to 1000 m standing stock and carnivores 34%, their biomass in the epipelagic[4] zone above the base of the thermocline (150 m) at night increasing from 46 to 57%. Zooplankton biomass available as forage for higher trophic levels is most concentrated in the upper 50 m, whereas, paradoxically, the zooplanktivorous micronekton, the myetophid fishes in particular, are centered deeper, primarily between 50 and 150 m (Hopkins 1982). Regarding the variability of zooplankton in the GOM, analysis of zooplankton community composition

[4] The epipelagic zone is the illuminated zone at the surface of the sea where there is enough light for photosynthesis. Almost all the primary production in the ocean occurs here. The epipelagic zone limits are from the surface mean sea level down to around 200 m.

and abundance in and beneath the Mississippi River outflow, and at similar depths at control stations in regions beyond the influence of the river off western Florida and in the central Gulf, showed that copepod[5] abundances were significantly higher in the nearshore regions than in the central GOM (Ortner et al. 1989).

4.1.3 Are light or nutrients conditioning phytoplankton success?

The dominant factor limiting growth of phytoplankton and zooplankton varies from region to region in the world's oceans. On a broad scale, growth of phytoplankton in the oligotrophic tropical and subtropical gyres is generally limited by nutrient supply, while light often limits phytoplankton growth in subarctic gyres. Like many other aquatic plants, photosynthetic marine organisms (*i.e.*, phytoplankton) rely upon sunlight and chlorophyll-*a* to absorb visible light from the sun as well as nitrogen (N), nearly all phosphorus (P), and silica (Si) to generate food and promote growth and reproduction. However, the amount of light penetrating the ocean surface tends to decrease with increasing water depth, therefore photosynthesis can only take place within a small band near the surface of the water (called the photic zone). In addition, nutrient availability often varies significantly from place to place. For example, in the open ocean, nutrient levels are often very poor causing primary production to be very low. In contrast, near shore waters such as estuaries and marshes are often rich in nutrients, allowing primary production to be very high. In some instances, nearshore ecosystems have an excess of nutrients due to runoff and other terrestrial sources. Excess nutrients can cause an over-stimulation of primary production, depleting oxygen levels and causing eutrophic conditions to occur in coastal habitats.

Environmental variability at multiple scales influences the nutrient and light available for phytoplankton, and as these organisms form the base of the marine food web, this variability in phytoplankton growth influences higher trophic levels. For example, at inter-annual scales phytoplankton levels temporarily plummet during El Niño periods, influencing populations of zooplankton, fishes, sea birds, and marine mammals. On broad scales, phytoplankton and zooplankton have patchiness that is consistent with the local hydrodynamic features (*i.e.*, passive response), while zooplankton shows more spatial

[5] Copepods are usually the dominant members of the zooplankton (Boxshall and Halsey 2004).

variability than phytoplankton at finer scales and some other mechanisms such as the swimming behavior (i.e. active response) must be invoked to explain zooplankton patchiness (Levin 1992). The behavioral mechanisms (Bollens and Frost 1991; Rios-Jara and Gonzalez 2000) and physical processes (Peterson et al. 1996; Yen et al. 1998) affecting the patchiness of zooplankton are likely to be species- and size-specific.

Ichthyoplankton may also be affected by those factors, although not with the same intensity since the relationship between zooplankton biomass and ichthyoplankton commonly is not straightforward (de Ciechomski and Sanchezf 1983; Cowan Jr and Shaw 1991; Flores-Coto et al. 2009). Observed heterogeneity in distribution patterns of the ichthyoplankton can be explained by different processes acting in a continuum of scaling dimensions that range from El Niño events (Yoklavich et al. 1996), circulation patterns, fronts (Cowen et al. 1993), river plumes (Govoni et al. 1989), flood and ebb tides(Raynie and Shaw 1994), physical properties of the water column (Rakocinski et al. 1996), and finer scale turbulence (Muelbert et al. 1994).

In the GOM, the depth of the mixed layer -embodying both light limitation and nutrient availability- has been suggested to be the single most important factor controlling the seasonal variation of chlorophyll-*a* concentrations in offshore waters. Since algal biomass is higher when the surface mixed layer is deeper, this is strong evidence that primary production in the region is controlled by variations in upward nutrient flux (Muller-Karger et al. 1991) There is enough illumination in the mixed layer all year round, and only in the northern GOM and during winter months light could appear as a factor to take into consideration (Rabalais et al. 2001). For example, phytoplankton growth rate limitation due to underwater light attenuation has been shown to be substantially greater than growth rate limitation due to non-optimal nutrient concentrations in the Louisiana inner shelf, but the degree of nutrient limitation increases with increasing distance from the Mississippi Delta (Bierman et al. 1994). Nutrients loadings in the GOM have increased during the last century, especially during the rapid growth of population, agriculture, and fertilizer production beginning in the 1950's (Nixon 1995). However, phytoplankton productivity in the Northern GOM region has been shown to be inorganic phosphorus limited in the spring and early summer during high runoff periods (Ammerman 1992; Dortch and Whitledge 1992; Lohrenz et al. 1999; Rabalais et al. 2007; Sylvan et al. 2006; Turner et al. 2007), and silicate limited in the spring has also been documented (Dortch and Whitledge 1992; Redalje and Fahnenstiel 1994; Lohrenz et al. 1999). Phytoplankton may also be light limited at times on the Louisiana shelf (Rowe and

Chapman 2002). It is for those reasons that it is important to monitor the ocean structures that control the upwelling and downwelling processes (Biggs and Müller-Karger 1994; Toner et al. 2003), as well as the wind field, responsible of enhancing eddy pumping of nutrients into surface (McGillicuddy et al. 1998; Falkowski et al. 1991).

4.2 Larval fish assemblages in the Gulf of Mexico

A larval fish assemblage can be defined as a suite of species whose larvae are collected in the same area at the same time (Miller 2002). Therefore, a larval assemblage is by definition transient and does not necessarily imply or require evolutionary convergence or biological interactions (*e.g.*, competition, predation). The species association within an assemblage only denotes that they have come to a similar solution for a precise stage of their lives (Miller 2002). Mortality is critical during the larval stage of a fish, because larvae have to overcome survival rates below 1% (Houde 1987; Chambers 1997). Nowadays, predation is considered as the main mortality factor influencing recruitment (Hunter 1981; Bailey and Houde 1989) , and mortality is modulated by other factors: (1) Temperature that influences physiology, metabolism, behavior, and early life growth rates (Blaxter 1991). It operates on all time and space scales (from cell level to large ocean basins); (2) Physical processes (diffusion, advection and dispersion), whose importance was already acknowledged in some recruitment hypotheses (Cushing 1975; Heath et al. 1988); (3) Large amounts of prey are associated with increased survival rates and with faster larval growth (Zenitani et al. 2007). However, turbulence can increase encounter rates in environments with low prey densities (MacKenzie et al. 1994); and (4) Nutritional condition and growth rates influence predation through larval size and growth rates (Meekan and Fortier 1996; Vigliola and Meekan 2002): “the faster you get bigger the better” (Houde 1987). Many factors influencing larval behavior and physiology are size-dependent (Hunter 1981). Thus, smaller larvae, with limited energy storage (yolk sac), are more susceptible to starvation and, consequently, to be predated. Therefore, recruitment variability is now considered to be the result of an integration of processes operating on different time and space scales acting throughout the pre-recruit fish life-stage (Figure 2.10). That is to say, recruitment success is not determined during a particular ontogenetic stage and it depends on the species, populations and environmental factors (Houde 2008).

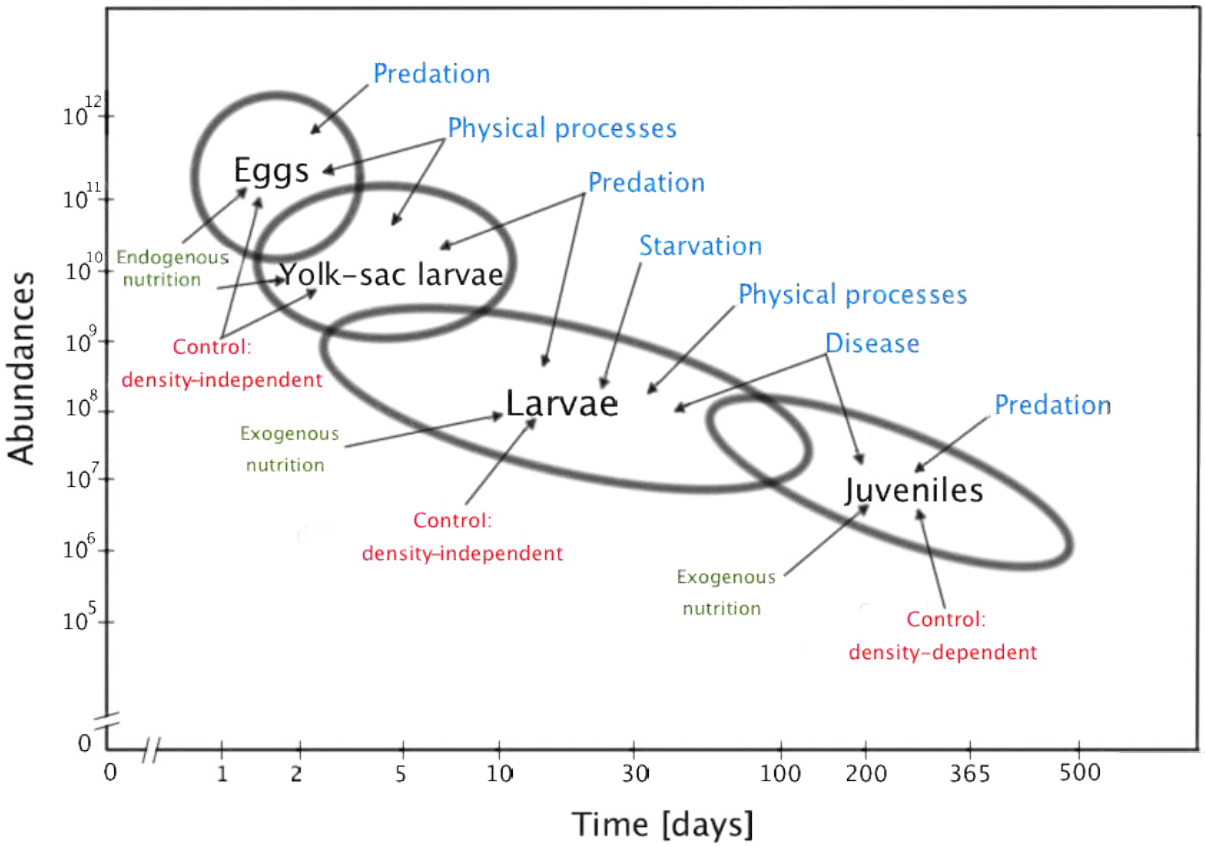

Figure 2.10. Diagram of the recruitment process during early life stages of marine fish, showing the temporal evolution of abundances of eggs, yolk-sac larvae, larvae, and juveniles. Sources of nutrition (green), probable sources of mortality (blue), and hypothesized mechanisms of control (red) are included. Reproduced from Houde 1987.

Ichthyoplankton surveys provide fisheries-independent information that is inherently "ecosystem-based"; entire larval fish assemblages are collected (*i.e.*, early stages of both exploited and unexploited finfish species) along with zooplankton predators and prey, and often with a suite of environmental observations (*e.g.*, salinity, temperature). At the ecosystem level, information on larval assemblages can be used to detect changes in marine fish community composition and abundances over time (Sherman et al. 1984). Previous studies have indicated that larval assemblages are the result of convergent spawning strategies by multiple species taking advantage of favorable environmental conditions for larval fish survival (Doyle et al. 1993; Sherman et al. 1984). The composition of larval fish assemblages varies spatially and temporally because of the behaviors of the larvae (Gray and Miskiewicz 2000; Hare and Govoni 2005) and the spawning adults (Sherman et al. 1984;

Hernández-Miranda et al. 2003), as well as oceanographic transport and mixing processes (Auth 2008; Muhling et al. 2008). Variability in any of these factors, therefore, may result in a different structure of larval fish assemblages. Because larval fish survival is closely tied with primary and secondary productivity in coastal oceans, changes in larval fish assemblage structure (over larger time scales) can be an early indicator of climate-related environmental shifts (Auth 2008; Brodeur et al. 2008).

Despite the importance of the GOM region to fisheries, seasonal variability in larval fish assemblages in the northern Gulf of Mexico has been examined in relatively few studies. Much of the previous ichthyoplankton research has focused on estuarine assemblages (Raynie and Shaw 1994; Tolan et al. 1997) or on relatively short-term interactions between assemblages and specific oceanographic features, such as the Mississippi River plume (Sogard et al. 1987; Govoni et al. 1989) or the Loop Current (Richards et al. 1993). Other studies have used ichthyoplankton survey data from the National Marine Fisheries Service's (NMFS's) gulf-wide Southeast Monitoring and Assessment Program (SEAMAP), but these studies are typically focused on a single species (Scott et al. 1993; Lyczkowski-Shultz et al. 2007). Ditty et al. (1988) summarized The available ichthyoplankton literature at the time has been summarized to provide information on larval fish seasonality for the entire northern Gulf of Mexico (Ditty et al. 1988), and more recently larval fish seasonality and distribution for the northeastern Gulf of Mexico has been reported (Lyczkowski-Shultz et al. 2004).

Although these latter studies provided information on multiple species, few analyses of larval fish assemblages and environmental variability driven by mesoscale ocean features were presented in the Gulf of Mexico. The Introduction and Discussion section of Chapter IV will summarize the recent state of the art on assemblages of specific larval fishes (*e.g.*, *Thunnus thynnus)* of in the GOM, and Results section of Chapter IV will contribute to our overall goal of understanding the oceanographic factors that maintain those larval fish assemblages.

5. Satellite remote sensing, blending physical oceanography and fisheries

Since the birth of the space age in the late 1950s, there has been a rapid expansion of satellite remote sensing for civil applications: meteorology, aviation, positioning, and communication. Satellite remote sensing has now become instrumental in ecology for environmental monitoring (*e.g.*, biogeochemistry and physical oceanography), and is a promising tool for conservation issues (Turner et al. 2003; Mumby et al. 2004). In recent decades, the ecosystem approach to fisheries management (EAFM), promoted by the Food and Agriculture Organization of the United Nations (FAO), recognizes the importance of maintaining the complexity, structure, and function of marine ecosystems and of ensuring the sustainability of the fisheries and human communities they support (Garcia and Do Chi 2003). In this context, the availability of global, daily, systematic, high resolution images obtained from satellites has been a major data source for elucidating the relationships between exploited marine organisms and their habitat (Polovina and Howell 2005; Dulvy et al. 2009). Several studies since the 1980's have investigated the linkages between oceanographic conditions derived from satellite remote sensing data and *in situ* fisheries data for large and small pelagic fish, shrimps, cephalopods, and sharks in the world ocean (Maul et al. 1984; Klimley and Butler 1988; Herron et al. 1989; Yang et al. 1995; Bigelow et al. 1999a; Valavanis et al. 2002; Fuentes-Yaco et al. 2007; Ouellet et al. 2007; Kumari and Raman 2010).

Regarding the resolution of remote sensing data, the spatial resolution specifies the nominal pixel size of the satellite image, and the temporal resolution specifies the revisiting frequency of observation for a specific location. The most common and useful relevant parameters datasets used for fisheries studies are: sea surface temperature (SST), sea surface salinity (SSS), windspeed, sea surface height (SSH), chlorophyll-*a* (Chl-*a*), and Chl-*a* derived primary production (PP) (Table 2.1).

Table 2.1. Main sensors and datasets of interest for oceanographers and fishery scientists

Parameter	Institution	Sensor	Platform	Temporal resolution	Spatial	Period
SST	NASA OBPG	MODIS	EOS AQUA	d, wk, mo, clim.	9 km, 4.5 km	07/2002-present
SST	NASA PO-DA AC	Pathfinder V5	NOAA AVHRR	d, wk, mo, season, clim.	4.5 km	01/1985-12/2005
SST	NASA PO-DA AC	Pathfinder V4, V5	NOAA AVHRR	wk, mo, clim.	9 km	01/1985-08/2003
SST	OSI-SAF	SEVIRI	MSG, GOES	3-12 h, hourly	1/10°, 1/20°	07/2004-present
SST	OSI-SAF	METOP	AVHRR	d, (2 d^{-1}: 00-12h)	1/20°	07/2007-present
SST	OSI-SAF	METOP (Level 2)	AVHRR	d, (2 d^{-1}), season	1 km	11/2009-present
SST	NASA REMSS	TRMM	TMI	d, 3-d, wk, mo, clim.	1/4°,	11/1997-present
		AQUA	AMSR-E			08/2002-present
SSS	ESA CNES	MIRAS (Level 1/2)	SMOS	10-30d	50-200 km	01/2010-present
Chl *a*	NASA OBPG	MODIS	EOS AQUA	d (1 d^{-1}), 3-d, 8d, mo, clim.	4 km	07/2002-present
Chl *a*	NASA OBPG	SeaWIFS	SeaStar	8d, mo, clim.	9 km	12/1997-present
Chl *a*	NASA OBPG	MODIS (Level 2)	EOS AQUA	d, 5 mo orbit	250 m, 500	07/2002-present
Chl *a*	ESA GLOBCOLOR	MERIS	ENVISAT	d, wk, mo	300 m, 1 km	03/2002-present
Windspeed	IFREMER CERSAT	ERS	AMI	8-d, mo, clim.	1°	08/1991-04/2002
Wind direction		Quickscat	Seawind		1/2°	12/1999-11/2009
Windspeed and direction	NASA REMSS	Quickscat	Seawind	d, 3-d, wk, mo	1/2°	12/1999-11/2009
Windspeed	NASA REMSS	SSM/1	DMSP series	d, 3-d, wk, mo	1/4°	07/1987-present
		TMI	TRMM			12/1997-present
		AMRS-E	EOS-AQUA			08/2002-present
SSH	CLS AVISO	ERS-TOPEX-JASON	-	wk (delayed time)	1/4°	10/1992-present
SHA				d (real time)		
PP	NASA OBPG	SeaWIFS	-	8-d, mo	9, 18 km	10/1997-12/2008
PP	NASA OBPG	MODIS	-	8-d, mo	9, 18 km	07/2002-12/2007

Mesoscale structures are important ecosystem features, often associated with enhanced productivity and fish aggregation (Olson et al. 1994; Bakun 2006). They were initially investigated with conductivity-temperature-depth surveys, acoustic Doppler current profiler, and ocean circulation models, then more directly and synoptically by satellite remote sensing. Several objective methods have been developed for the detection of SST frontal activity, and the two prevailing approaches are gradient-measurements (Oram et al. 2008; Belkin and O'Reilly 2009) and histogram-based methods (Cayula and Cornillon 1992; Miller 2009). However, the detection of ocean color (OC) fronts has been limited (Miller 2004; Royer et al. 2004) since Chlorophyll-*a* fronts arise from physical, chemical, and biological interactions within complex spatial patterns and features, such as blooms, which are more difficult to detect than SST fields (Belkin and O'Reilly 2009). Altimetry data provide information on sea height anomaly (SHA) and geostrophic currents and allow 1) to visually identify cyclonic and anticyclonic eddies, and 2) to derive indicators such as vorticity, stretch, shear, and deformation rate that can be computed to describe the eddy (Okubo 1970; Weiss 1991; Isern-Fontanet et al. 2003). The Soil Moisture and Ocean Salinity (SMOS) satellite launched on November 2009, which derives salinity directly from microwave radiometer

measurements (Font et al. 2010), could be helpful in detecting plume extension without using products dependent on biological processes, such as OC.

The two main ecological processes underlying the relationships between oceanographic features and marine resources in the literature are 1) prey availability, and 2) development, growth, and survival or early life-history stages. The remote sensing products introduced above are being used to improve our understanding of mesoscale ocean features such as fronts, filaments, eddies, Lagrangian coherent structures, and river plumes, all of them essential in the biological and ecological functioning of marine ecosystems.

Chapter III: Loop Current excursions and ring field detachments during 1993-2010

1. Introduction

The objectives of this chapter are 1) to monitor and describe the spatial and temporal variability of LC intrusions (northward), LC retreats (southward), and ring detachments, and 2) to explore a possible link between this variability and the changes in the upper ocean thermal structure in the GOM. In order to do that, satellite altimetry observations are used in this work to determine the dynamic structure in the region. The temporal and spatial variability of the main mesoscale features in the GOM are addressed here in terms of the northward and westward intrusion of the LC, and using a characterization of ring shedding events. A peer-reviewed paper focused on these aspects of the LC excursions and ring field detachments is under revision:

Lindo-Atichati, D., F. Bringas, and G. Goni, 2011: Loop Current excursions and ring field detachments during 1993-2010. Submitted to *Remote Sensing Letters*.

The upper ocean circulation in the Gulf of Mexico (GOM) is characterized by the fluctuations of the Loop Current (LC), which irregularly sheds anticyclonic rings that travel in a northwest direction into the GOM. The LC forms an intense anticyclonic flow, which expands northwestward in accordance to Rossby wave dynamics (Hurlburt and Thompson 1980) and can extend northward into the GOM to 28ºN, in the vicinity of the shelf break of the West Florida Shelf (WFS) at about 250 km off Mobile Point (Molinari and Mayer 1982). Although the LC intrusion tends to form more frequently in the spring, it may occur in any season and with periods varying from 6 to 17 months with an average period of 10-11 months (Maul and Vukovich 1993). The large, warm-core anticyclonic rings generally propagates westward at speeds of approximately 4 km day^{-1} with a standard deviation of 3 km day^{-1}, and have lifetimes of days to approximately a year (Vukovich 2007). These rings have radii of about 150 km, may reach depths of 800 m (Oey et al. 2005) and are generated irregularly, with an average shedding period of 11 months and a standard deviation of 4 months (Vukovich 2007). Whereas many authors have studied the frequency of LC ring shedding, the mechanism for eddy detachment remains unknown. However, it has been proposed that when

the LC grows, the westward Rossby wave speed (which is $\propto -\beta R^2$, where R is the Rossby radius based on the matured deep Loop) overcomes the growth rate, then the LC goes to an unstable configuration and it usually sheds a ring (Nof 2005).

An accurate knowledge of the position and dynamics of mesoscale ocean features, mainly LC rings and LC fronts, is critical for a variety of applications: for understanding the environmental conditions that influence habitat of marine fish larvae (Bakun 2006); oil spill response management (Kaiser and Pulsipher 2007); navigation; search and rescue operations; and hurricane forecasting (Shay et al. 2000). Moreover, northward excursions of the LC have been suggested to be anticorrelated with shoreward excursions of a resilient Cross-Shelf Transport Barrier (CSTB) on the WFS, which provide a large degree of isolation and is consequential for controlling red tides development on the southern WFS (Olascoaga 2010).

Satellite altimetry allows the measurement of mesoscale activity over the World Ocean from 1993. More than 18 years of continuous monitoring of the GOM circulation using altimetry help to understand the upper ocean dynamics and the vertical thermal structure at a spatial and temporal resolution that resolves ocean mesoscale features and fronts (Goni and Wainer 2001; Le Traon et al. 1998). Although studies using thermal satellite imagery continue to be invaluable due to the unsurpassed spatial resolution of satellite infrared data, they are limited to winter months due to the lack of thermal contrast over the GOM. In addition, clouds often obscure the thermal satellite imagery, making it difficult to locate and track dynamic mesoscale features. For this reason, satellite altimetry fields, obtained from two to three satellites, are used in this investigation for year round monitoring of the mesoscale circulation in the GOM from January 1993 to December 2009.

This chapter is organized as follows. In section 2 the data and methods used in this work are described. Section 3 presents results and analysis of the variability of the LC and anticyclonic rings in the GOM. Finally, section 4 summarizes the main findings of this work.

2. Data and methodology

The altimetry data used herein are the optimally interpolated gridded sea height anomaly (SHA) fields produced by Archiving, Validation and Interpretation of Satellite Oceanographic data (AVISO) according to an improved objective analysis method (Le Traon et al. 1998). These fields have a spatial resolution of 0.25 degrees, and temporal resolution of 1 week. The AVISO SHA fields are anomalies computed with respect to the 1993–1999 mean from the direct altimetry observations. It has been found from numerical modeling studies that SHA fields from two independent altimeters are needed for adequate spatial and temporal coverage to properly position mesoscale features and (Goni and Wainer 2001; Le Traon et al. 1998). For example JASON-1 altimeter, which measures the sea height anomaly (SHA) along satellite ground tracks that are approximately separated by 3 degrees zonally and repeats its tracks every 9.91 days, does not allow complete identification of mesoscale features, such as warm core rings (Goni et al. 2011). It has also been found from numerical modeling studies with the Real-Time Ocean Forecast System (RTOFS) that sea height anomaly fields from two independent altimeters are needed for adequate spatial and temporal coverage to properly position mesoscale features and fronts (Goni et al. 2011). The altimetric observations used here to produce gridded fields are obtained from two or three satellites throughout the period from January 1993 to December 2009.

The investigation of the dynamics of mesoscale features in the GOM is performed using sea surface height (SSH) fields derived from SHA data and a mean dynamic topography (MDT) of the ocean (Rio and Hernandez 2004) (Figure 3.1), *i.e.*:

$$SSH = SHA + MDT \tag{5}$$

where SSH, SHA, and MDT are measured in cm.

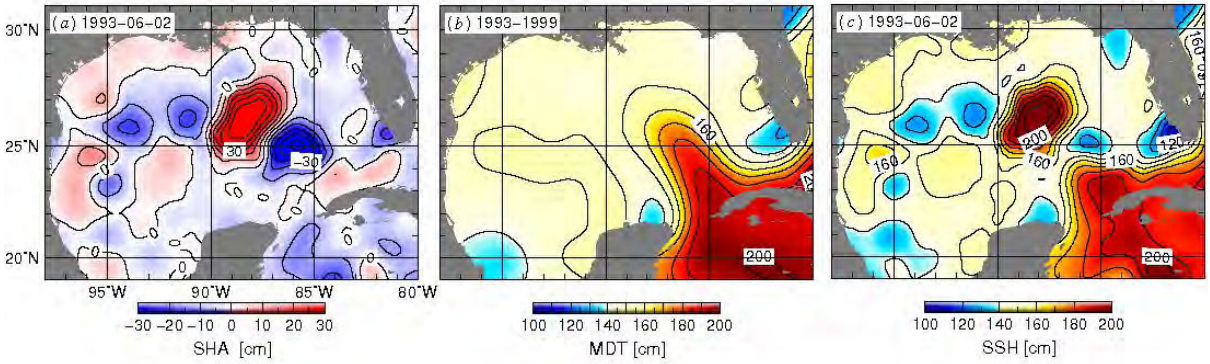

Figure 3.1. Example of general circulation through the Gulf of Mexico from satellite altimetry fields, on May 17 1995. Fields illustrate the LC and the ring shed in terms of (a) sea height anomaly (SHA) and (c) sea surface height (SSH). SSH fields are obtained by adding (b) mean dynamic topography (MDT) to (*a*) SHA fields.

The temporal and spatial variability of the main mesoscale features in the GOM is addressed herein in terms of the northward and westward intrusion of the LC, and using a characterization of ring shedding events. The LC and the ring field are characterized by their anticyclonic motion and SSH values that are larger than those of their surrounding waters (Figure 3.1(c)). Selected contours of constant SSH values are used here to objectively define the locations of the LC front and the shedding of the rings.

2.1 Location of LC front

The location of the LC front is determined as the contours of maximum horizontal gradient of SSH. Specifically, the northernmost and westernmost locations of the LC are detected by characterizing the maximum latitude and longitude of the SSH contours corresponding to the location of the maximum gradient of SSH (Figure 3.2). The methodology used herein to locate the LC front and its northernmost and westernmost locations consists of the following steps:

1) The absolute value of the SSH gradient is computed using zonal and meridional derivatives of the SSH field.

2) The SSH gradient is mapped over the corresponding SSH contour map.

3) The value of SSH contours corresponding to the location of maximum SSH gradient defines the LC front. To avoid confusion between the LC front and the boundary of a ring,

which may have maximum SSH gradients as well, the selected SSH contours belonging to a location of maximum SSH gradient must describe an opened path.

4) The northernmost latitude of these selected contours defines the LC northernmost location.

5) The westernmost longitude of these selected contours defines the LC westernmost location.

For example, for the GOM conditions on May 26, 1993 (Figure 3.2(a)), the LC northernmost location is 28°N (upper grey square) and the LC westernmost location is 89.75° W (left grey square).

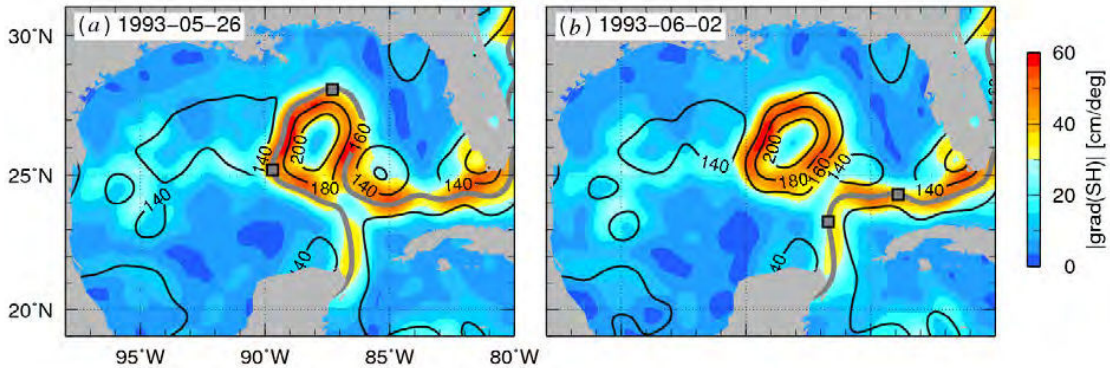

Figure 3.2. Fields of altimetry-derived SSH gradient in the GOM with contours of SSH (in cm, black lines) superimposed, for (a) May 26, 1993, and (b) June 02 1993. Fields illustrate (a) the location of the LC front, and (b) the detection of a LC ring and the LC front. The northernmost and westernmost locations of the LC are tagged with a square in both panels.

2.2 Detection of ring shedding

The LC ring shedding events are also detected using the methodology described in 2.1. A LC ring is considered to be separated from the LC at the surface when the following two conditions are satisfied: 1) when all the SSH contours belonging to the higher values of SSH gradient describe a closed path (Figure 3.2(b)), and 2) when the first condition last for a period of time longer than four weeks, which is the observed maximum period of time for a LC ring to reattach. The life span of a ring is determined herein as the period of time since the

ring is shed until the values of the enclosed dynamic height contours decrease to reach similar values to the surrounding waters, typically between 160 cm and 140 cm.

Results obtained here are compared with those obtained in previous works of the LC northward penetration (Zavala-Hidalgo et al. 2006) and ring separation (Sturges and Leben 2000; Alvera et al. 2009) that cover shorter study periods. The fact that rings identified and LC excursions studied in this work are in agreement with the findings of previous studies confirms the consistency of the novel methodology used here and complements the valuable previous studies. The results showed here are more complete, cover longer time span, and define objectively the locations of the LC front and the shedding of the rings.

3. Results and discussion

3.1 Northern and western LC excursions

Weekly time series of the northernmost and westernmost position of the LC during the period from November 1992 to December 2009 are presented in Figure 3.3. These signals are filtered using a Butterworth filter (black lines in Figure 3.3). This filter is designed with order 6 and angular cutoff frequency 1/7 rad s^{-1}, which means that the boundary in the filter response is 7 weeks and the maximum filter slope is 20 degrees $week^{-1}$.

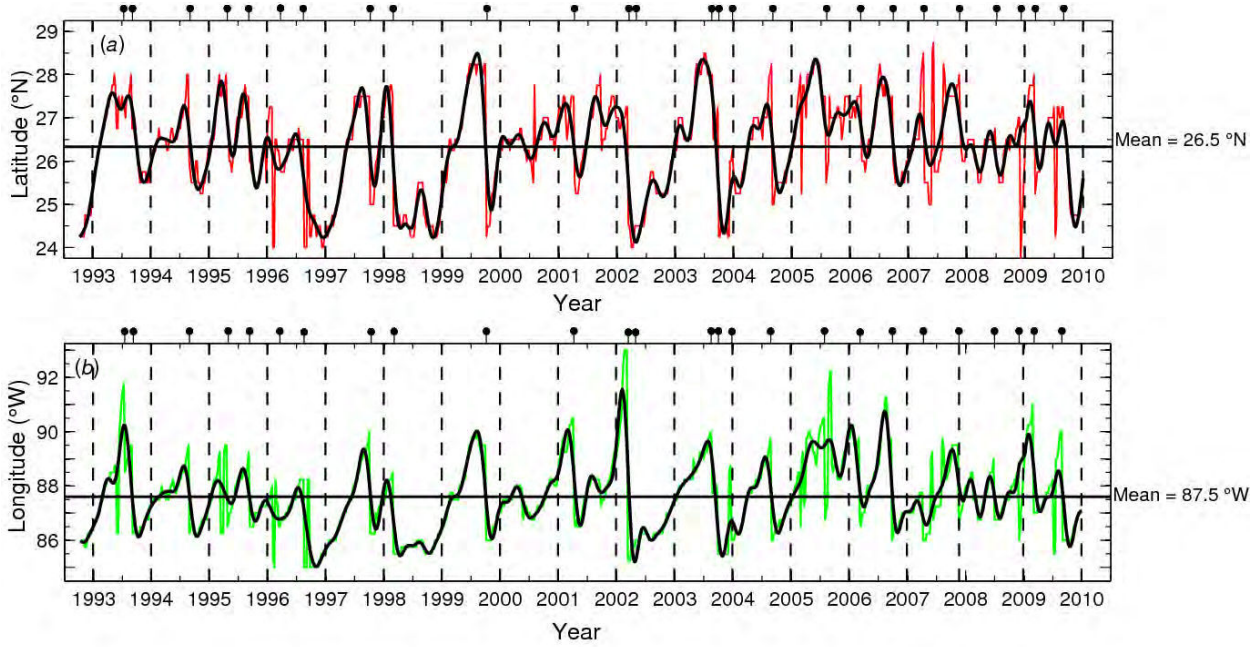

Figure 3.3. Time series of (a) LC northward penetration (red line) and (b) LC westward penetration (green line), from November 1992 to December 2009. Black circles indicate the time of separation of LC rings. The signal was filtered using a Butterworth filter of order 6 and cutoff frequency 1/7 rad/s (black line).

The northernmost location of the LC oscillates between 24ºN and 28.5ºN, with a mean value (mean $\pm$ SD) of (26.5 $\pm$ 1)ºN and marked seasonal variability (Figure 3.3(*a*)). The amplitude of the oscillations exhibits maximum values with meridional motions of 4 degrees of latitude from 1993 to 2003, and meridional motions of 2.5 degrees of latitude from 2004 to 2009.

Monthly mean values of the LC northward excursions between 1993 and 2009 indicate that the location of the LC in summer (July through August) is significantly more to the north than in the fall season, with winter and spring having values closer to the mean (Figure 3.4(a)). Similar results are found in previous studies that, using data from 47 cruises in the eastern GOM and monthly fields of temperature at 200 m from 1970 to 1976, have shown that on average the penetration of the LC into the GOM increases during the winter and spring, reaching a maximum in the early summer (Behringer et al. 1977). The northward penetration of the LC also exhibits year-to-year variability (Figure 3.4(b)), showing a mean maximum value of 27.5ºN in the annual northernmost location of the LC in 2005, a minimum value of 25ºN in the annual northernmost location of the LC in 1998, and an interannual mean of around 26.3ºN. Between 1993 and 2002 the mean location of the LC northward penetration is 26ºN, below the annual mean. Conversely, between 2003 and 2009 the mean

location of the LC northward penetration is 27ºN, above the annual mean. The link between northward excursions and ring formation will be discussed in section 3.2.

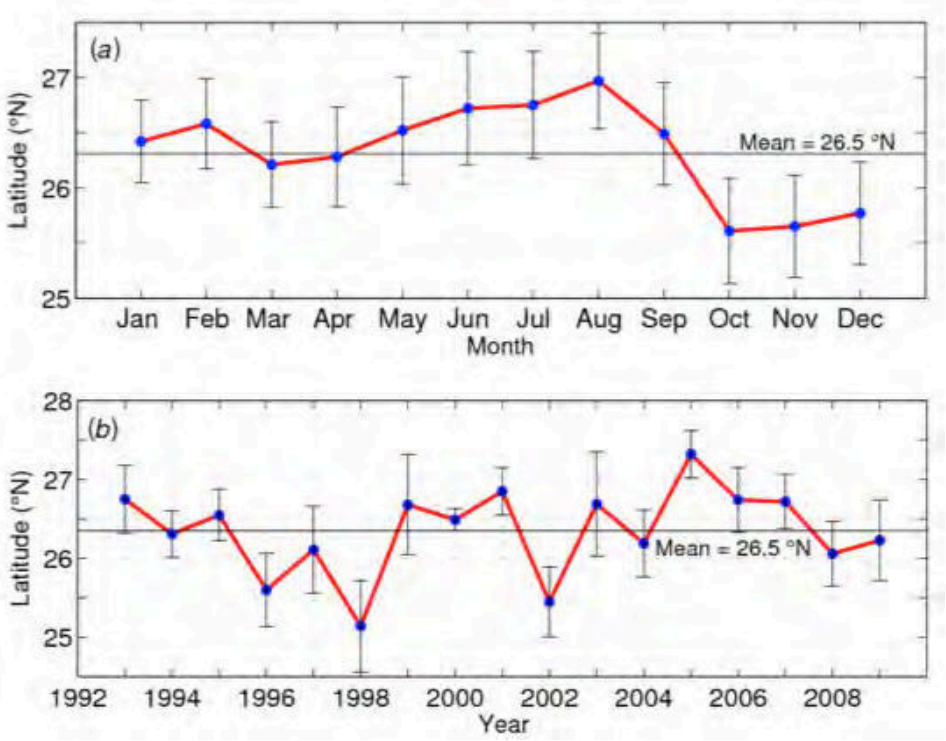

Figure 3.4. (a) Monthly Mean location of the LC northward penetration (blue circles) and (b) annual mean location of the LC northward penetration. Black bars indicate one standard deviation over the 17 years of data analyzed, from January 1993 to December 2009.

The LC westernmost location oscillates between 91ºW and 85ºW, with a mean value of 88ºW and pronounced seasonal variability (Figure 3.3(b)). The amplitude of the oscillations exhibits maximum values with zonal motions of approximately 6º degrees of longitude from 1993 to 2003, and zonal motions of 4 degrees of longitude from 2004 to 2009.

3.2 Ring shedding events

The location, lifetime, shape, size, kinetic energy, and available potential energy of LC rings can be characterized by undertaking a ring census similar to those carried out in other regions that used observations of infrared imagery (Brown et al. 1986) or a combination of climatological data, *in situ* data and satellite altimetry (Goni and Johns 2001). Following the

methodology described in section 2, all the LC ring shedding events between November 1992 and December 2009 (black circles in Figures 3.3(a) and (b)) are identified and described (Table 1).

A total of 26 rings are identified as having been shed from the LC between November 1992 and December 2009 (Table 1 and Figure 3.5). The average number of rings formed per year is 1.5, with a standard deviation of 0.7. A marked increase in ring formation is detected beginning in 2003. While from 1993 to 2002 an average number of rings formed per year of 1 ring $year^{-1}$ is observed, starting in 2003 the average number of rings formed per year is 2 ring $year^{-1}$. Thirteen out of the 26 rings identified here are shed in the 3-month period from July to September, which is in agreement with the seasonality in the timing of ring shedding suggested in a previous work that monitored ring detachment events from October 1993 to February 2006 using satellite altimetry observations and a visual methodology for ring determination (Alvera et al. 2009). September and August, which are months with LC intrusions to the north, are also the months that exhibit more ring-separation events. There were no ring-separation events identified during the months of January, May, and June from November 1992 to December 2009. The average period between consecutive LC ring detachments is approximately 9 months from 1993 to 2003 with a standard deviation of 6 months, which also is in agreement with the 8.2 months period suggested by other authors (Alvera et al. 2009). The average period between consecutive LC ring detachments and its variability are reduced from 2004 to 2009, exhibiting average periods between consecutive shedding of 6 months with standard deviation of 1 month.

Table 3.1. Compilation of ring-separation events, including dates of LC ring detachment, period that followed until the next detachment, dates of extreme LC intrusions (northward or westward), dates of extreme LC retreats (southward), and description of such extreme excursions (intrusions or retreats). Rings were identified using estimates of the gradient of SSH derived from satellite altimetry observations, from January 1993 to December 2010, using the methodology described in section 2.

Ring	Date	Life span	Extreme LC intrusion	Extreme LC retreat	Description
			Jul 7 to Jul 14 1993		LC intrudes to 92°W
1-93	1993 Jul 21	5			
2-93	1993 Sep 8	5			
3-94	1994 Aug 31	6			
4-95	1995 Apr 26	5			
5-95	1995 Sep 13	5			
6-96	1996-Mar-20	7			
7-96	1996 Aug 21	9			
				Dec 4 to Dec 25	LC retreats to 24 °N
8-97	1997 Sep 24	10			
9-98	1998 Mar 04	11			
			Jun 23 to Sep 22		LC intrudes to 28 °N
10-99	1999 Sep 29	12			
11-01	2001 Apr 11	7			
			Feb 20 to Mar 6 2002		LC intrudes to 93 °W
12-02	2002 Mar 13	1			
13-02	2002 Apr 17	11		Apr 3 to Apr 17 2002	LC retreats to 24 °N
			May 7 to Aug 13		LC intrudes to 28 °N
14-03	2003 Aug 20	4			
15-03	2003 Sep 24	10			
16-03	2003 Dec 24	8			
17-04	2004 Sep 01	11			
			Apr 13 to Jun 29		LC intrudes to 28 °N
18-05	2005 Aug 03	9			
19-06	2006 Mar 08	5			
			Aug 9 to Aug 23		LC intrudes to 91 °W
20-06	2006 Sep 27	12			
21-07	2007 Apr 11	4			
22-07	2007 Nov 14	6			
23-08	2008 Jul 2	8			
24-08	2008 Dec 3	2			
			Feb 11 to Feb 25		LC intrudes to 91 °W
25-09	2009 Mar 4	8			
26-09	2009 Sep 2	7			

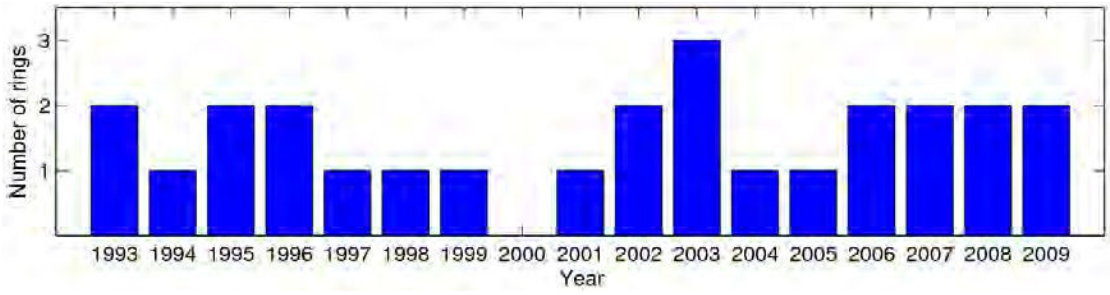

Figure 3.5. Number of LC rings shed during each year, from January 1993 to December 2009 as obtained according to the methodology described in section 2.

If the present ring census is compared to previous relevant work in the GOM region, some similarities are found in the main results discussed above. The present census shows 10 ring separation events between 1993 and 1999, the same LC ring detachments reported by a previous work (Sturges and Leben 2000). Results from November 1992 to March 2006 are compared to results from a more recent work on the compilation of ring separation events (Alvera et al. 2009). The present census shows 19 ring separation events in this period of time, and 20 LC ring detachments are reported by the previous work in the same period. The difference in the criteria that is used in both works to determine when a ring has shed is the main cause of this one ring mismatch. Specifically this difference is due to the fact that because the rings shed in September 1999 and March 2000 were not detected in our work by our methodology, and previous authors using their methods did not detect the ring shed in September 2003. Other than that, there are only slight differences in shedding dates between both studies.

When LC excursions are linked to ring formation events, it is observed that in 70% of the cases the separation of the LC rings (circles in Figure 3.3(a)) occurs when the northernmost location exceeds 27ºN (approximately 1ºN of its mean location), with separation events happening at a frequency ranging from 2 to 18 months. Conversely when the LC is located to the south for long periods of time, few or no rings are detached (Alvera et al. 2009), which is also observed in 1997, 1998, and 2002 (Figure 3.3 (a)). In 2003 the maximum number of ring separations from the LC are detected; three rings were shed after extreme northward intrusion of the LC to 28ºN during spring and summer months and after a long period of 17 months without shedding (Figure 3(a) and Figure 5).

3.3 SHA residuals and upper ocean thermal structure

Our results regarding the LC location more to the north and the marked increase in ring formation beginning in 2003 are reflected in an increase of the monthly sea height residuals (SHR) over the entire GOM, estimated as the difference between the mean SHA for each specific month and the mean SHA value for that month since November 1992. A positive linear trend in the monthly SHR is estimated (Figure 3.6). SHR are increasing at a rate of (2.8 $\pm$ 0.3) cm decade^{-1} from November 1992 to December 2009. In addition to that, 80% of negative SHR and 20% of positive SHR are observed from December 1992 to December 1999, and conversely 15% of negative SHR and 85% of positive SHR are observed from January 2000 to December 2009. It is suggested here that higher mean SHA values for the GOM starting in 2000 may be related to the increase in the mean LC northward intrusions and the increase in the number of rings shed starting in 2003 (section 3.2). The amplitude of the meridional oscillations of the LC decreased from mean meridional motions of 4 degrees of latitude from 1993 to 2003 to mean meridional motions of 2.5 degrees of latitude from 2004 to 2009 (section 3.1). This shorter amplitude of the meridional oscillations of the LC, together with a LC generally more to the north starting in 2003, may also be associated with the higher mean SHA values for the GOM from 2000 to 2009.

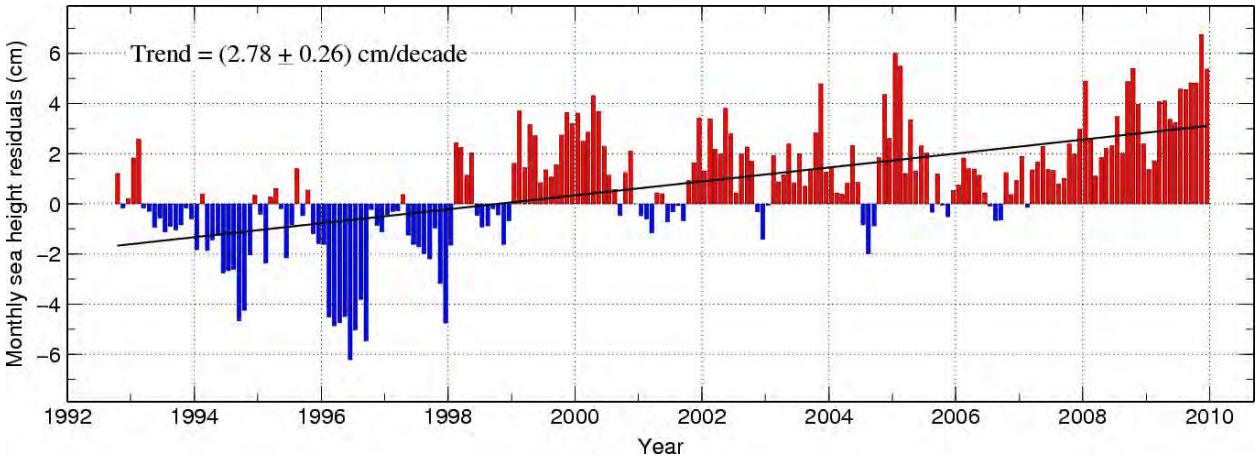

Figure 3.6. Monthly sea height residuals (SHR), estimated as the difference between the mean SHA for each specific month and the mean SHA value for that same month since November 1992. The black line indicates a mean SHR increase of 2.78 cm per decade over the 17 years of data analyzed.

Sea surface height anomalies are strongly related to the internal thermal structure of the ocean. Higher SSH corresponds to deeper layers of warmer water masses. Depending on

many factors, such as the vertical stratification and the dynamic processes involved, the relationship between selected isotherms (such as the depth of the 20°C isotherm, which usually lies within the thermocline waters in most tropical regions) and the SSH can be readily estimated from the altimeter-derived SHA, in combination with *in situ* and climatological hydrographic observations. In general, variations in the depth of the main thermocline can be associated with variations in the SHA field (Willis et al. 2004). Given the strong relationship that exists between SHA and the thermal structure of the ocean, it is hypothesized from our results that the observed increase in mean SHA in the GOM from 1992 to 2009, especially marked starting in 2000, is linked to the increase of the mesoscale activity in the region shown in this work through variations in the thermal structure of the GOM. This hypothesis may become a topic for future studies.

4. Conclusions

Satellite altimetry fields were used to identify mesoscale features in the GOM during the period 1993-2009. The key result obtained in this work is that starting in 2003, the LC is located more to the north and there is a marked increase in the number of rings that are shed from the LC (Figure 3.3 and Figure 3.5). Consequently, beginning in 2003 the mean location of the LC northward penetration is 27ºN, or 1.5 degree of latitude above the interannual mean, and approximately 2 rings are formed per year. The amplitude of the meridional oscillations of the LC exhibits maximum values with meridional motions of 4 degree of latitude from 1993 to 2003, and meridional motions of 2.5 degrees of latitude from 2004 to 2009. The amplitude of the zonal oscillations of the LC exhibits maximum values with zonal motions of approximately 6 degree degrees of longitude from 1993 to 2003, and zonal motions of 4 degree of longitude from 2004 to 2009. The higher mesoscale activity observed from 2003 to 2009 may have a measurable impact on the mean SHA in the GOM, showing positive SHR from 2000 to 2009.

On the other hand, the LC northward penetration appears to be mostly seasonal (Figure 3.4 (a)), with maximum values of 0.8 degrees of latitude above the annual mean during June, July and August, in consistence with previous studies (Behringer et al. 1977). However, the mean northward penetration of the LC is highly variable from year-to-year

(Figure 3.4 (b)). Half of the rings identified here are shed in the 3-month period from July to September. September and August are the months that exhibit the most ring-separation events, showing 7 and 4 events, respectively.

Monthly sea height residuals, estimated as the difference between the mean sea height anomaly for each specific month and the mean sea height anomaly value for that month since November 1992 exhibits a linear trend of (2.78±0.26) cm/decade during 1993-2009. It is hypothesized here that this increase in the sea height anomaly residuals is linked to the observed increase in mesoscale activity in the region for the same period.

This study provides an updated statistics of the LC and ring variability (position and number). By covering longer time span and defining objectively the locations of the LC front and the shedding of the rings, the results discussed here complements helpful previous studies that report ring detachments and LC excursions in the GOM.

Chapter IV: Effects of mesoscale variability on the GOM on larval fish distribution

1. Introduction

The objective of this paper is to assess the influence of mesoscale ocean features on the distribution of fish larvae spawned in the northern GOM in spring months from 1993 to 2007. A improved understanding of larvae assemblages in different water masses, characterized by circulation and sea surface height (SSH), will provides a benchmark for future coupled biophysical studies and habitat models in the region. A peer-reviewed paper focused on these aspects of the effects of mesoscale structures on larval fish distribution is under revision:

Lindo-Atichati, D., F. Bringas, and G. Goni, B.A. Muhling, F.E. Muller-Karger, S. Habtes 2011: Variability of mesoscale structures in the Gulf of Mexico with effects on larval fish distribution during spring months. Submitted to *Marine Ecology Progress Series* (accepted after minor revisions).

The Gulf of Mexico (GOM) is the preferred spawning habitat for several commercially-important pelagic and benthic fish species (Rabalais et al. 1999; Shipp 1999). This basin is also characterized by a complex and highly variable system of currents and eddies, which affects the physical environment where fish spawn (Teo and Block 2010). The mesoscale circulation in the GOM is dominated by the Loop Current (LC) and rings shed by this major current (Figure 4.1). The LC flows into the GOM through Yucatan Channel as the Yucatan Current, with some secondary flow reversals observed along the margins of the Yucatan Peninsula and along Cuba, as well as deep within Yucatan Channel, at depths exceeding 600-800 m below the northward-flow of the Yucatan Current (Candela et al. 2002, 2003). Upon entering the GOM, the flow of water has an intense anticyclonic flow, known as the Loop Current. This current can extend as far north as 29.1°N, within close proximity to the Mississippi River delta or the Florida Panhandle coast (Molinari and Mayer 1982). Although the LC intrusion into the northern GOM is often observed in spring, it may occur during any time of the year. The cycle of extension and contraction of the Loop Current varies from 6 to 17 months (Molinari 1980), with an average period of 10-11 months (Maul

and Vukovich 1993). The LC returns to its southern location, where water from the Yucatan Current flows more directly toward Florida Strait, after the pinching off of the northern extension of the LC. This process forms large anticyclonic rings which then propagate westward at speeds of 2-5 km day^{-1}, with a lifetime of days to approximately a year (Elliott 1982; Forristall et al. 1992; Shay et al. 1998). These anticyclonic rings have radii of approximately 150 km, swirl speeds of 1.8-2 m s^{-1}, and reach around 800 m depth (Oey et al. 2005). The average time between consecutive sheddings is 9.5 months, with a range of 3 to 21 months (Sturges and Leben 2000; Zavala-Hidalgo et al. 2006). The annual fluctuations in LC flow have been attributed to wind forcing (Sturges and Evans 1983) and to variations in the inflow of water from the Caribbean (Lee et al. 1995; Oey et al. 2003; Alvera et al. 2009).

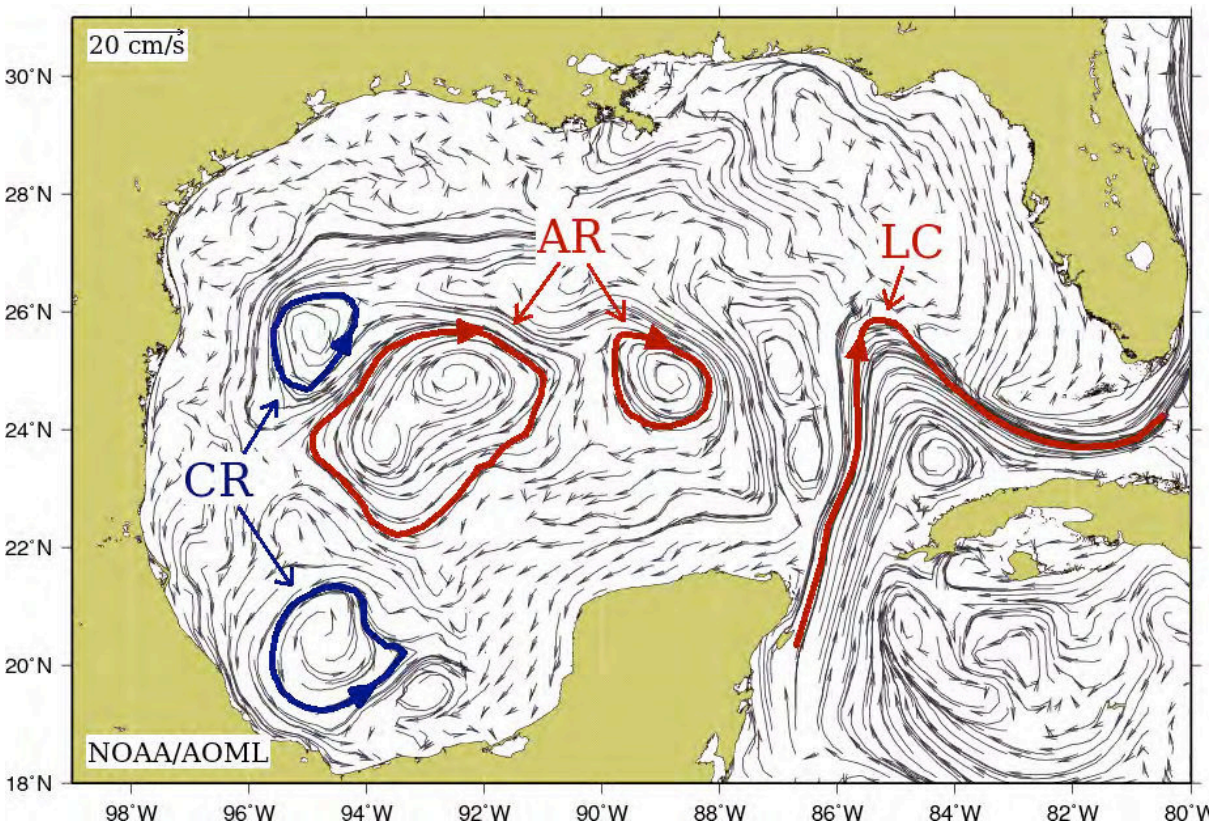

Figure 4.1. General circulation in the Gulf of Mexico on October 22, 2010. Thin arrows represent geostrophic currents derived by combining satellite altimeter observations and numerical model results. Thick arrows contour anticyclonic (Loop Current/LC and rings/AR) and cyclonic features (rings/CR).

Knowledge of the temporal and spatial variability of mesoscale structures in the GOM is fundamental for understanding the distribution of larvae of pelagic fish, their spawning

habitat, and food availability for larvae (Ortner et al. 1978, 1984; Davis and Wiebe 1985; Richards et al. 1993; Medina et al. 2002; Royer et al. 2004; Wilson et al. 2005; Bakun 2006). Both anticyclonic and cyclonic eddies have been shown to positively affect the abundance and distribution of plankton and fish larvae in other regions of the ocean (Nakata et al. 2000; Okazaki et al. 2002).

Physical and biological conditions in the GOM exhibit high spatial and temporal variability (Müller-Karger et al. 1991). The intersection of particular conditions of water temperature, salinity, chlorophyll-*a* concentration and zooplankton abundance, depth of the water, and day of the year has been associated with a higher abundance of fish larvae in particular areas of the GOM during annual surveys conducted by the NOAA National Marine Fisheries Service (NMFS) in the GOM since 1982 (Muhling et al. 2010; Richardson et al. 2010). Therefore, adult fish appear to target specific habitats or oceanographic features to spawn. The NMFS SEAMAP surveys conducted in spring 1987 showed higher displacement volumes of plankton and higher densities of fish larvae in LC frontal areas (Richards et al. 1993).

2. Materials and methods

2.1 Satellite data

Boundaries of mesoscale features in the GOM has frequently been defined using sea surface temperature (SST) and ocean color (OC) observations from satellites, and a more limited number of hydrographic observations (*e.g.*, Breaker 1981; Maul et al. 1984; Richards et al. 1989; Müller-Karger et al. 1991; Bigelow et al. 1999b; Royer et al. 2004). Satellite derived observations of sea surface height and surface height anomaly (SSH and SHA), SST and OC offer sufficient temporal and spatial resolution to study the evolution of the main surface mesoscale features in the region. Altimetry measurements have shown great utility in biophysical studies (*e.g.*, Polovina and Howell 2005; Chiswell et al. 2003; Rudorff et al. 2009), and can be used to monitor surface ocean features year-round. For example, SST, SHA, SSH, and the gradient of SSH fields clearly show the structure of the LC and an anticyclonic ring in May 1998 (Figure 4.2a, b, c, & d). Conversely, during the month of June 1998 the LC and the ring cannot be easily observed in SST data (Figure 4.2e) due to the lack of marked gradients as the surface of the GOM warmed up. These features are clearly distinguishable using altimetry observations (Figure 4.2f, g, & h).

SST fields were obtained from a number of satellite sources. Optimally-interpolated SST fields were obtained from microwave observations retrieved by the TMI and AMSR-E radiometers onboard the TRMM and Aqua satellites, respectively (http://trmm.gsfc.nasa.gov/, http://nsidc.org/data/amsre/). These daily fields have a spatial resolution of 0.25 degrees. SST observations from the Advanced Very High Resolution Radiometer (AVHRR) were available with a resolution of 2 days and 18 km equal-area grid (Ryan et al. 1996).

The altimetric observations used in this study were obtained from between two and four satellites operating during the period covered by this study. Altimetry data were the optimally interpolated according to an improved objective analysis (Le Traon et al. 1998) with a resolution of 0.25 degrees and 1 week.

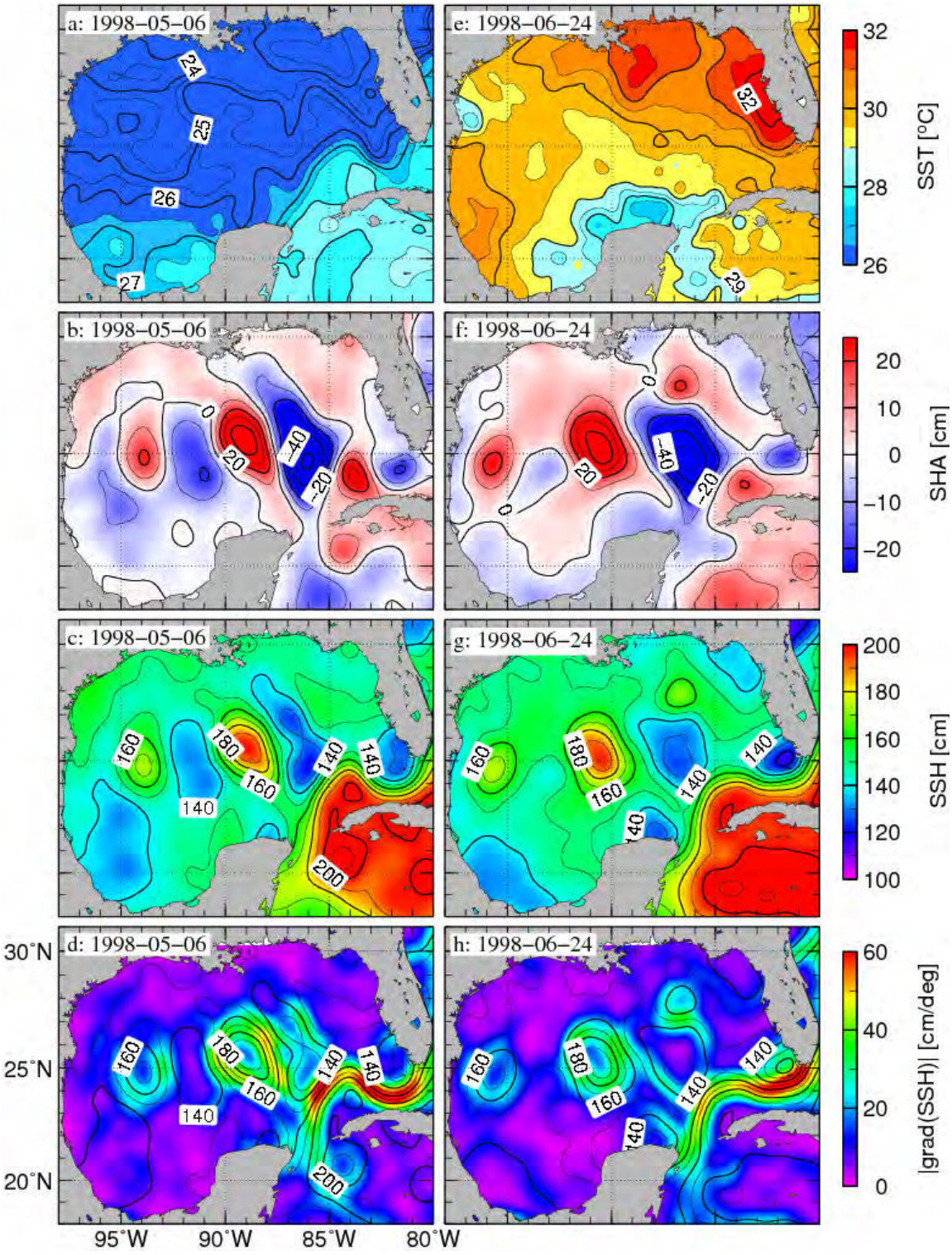

Figure 4.2. Comparison between SST and SSH satellite derived fields. Fields on the left panels illustrate a ring separation event in terms of (a) SST, (b) SHA, (c) SSH, and (d) gradient of SSH on May 6, 1998. Fields on the right panels illustrate a ring already shed by the LC in terms of (e) SST, (f) SHA, (g) SSH, and (h) gradient of SSH on June 24, 1998.

Because of uncertainties in the geoid, altimeter data are generally estimated as variations about mean sea level. To obtain an estimate of the geostrophic component of the circulation it is therefore necessary to add a mean dynamic height field to the anomalies. The absolute geostrophic velocities derived from the satellite altimeter measuring SSH were obtained from the French AVISO (Archiving, Validation and Interpretation of Satellite Oceanographic data) using the mean dynamic topography (MDT) of the ocean (Rio and Hernandez 2004), as follows:

$$SSH\ (cm) = SHA\ (cm) + MDT\ (cm) \tag{6}$$

2.2 Spatial variability of LC front and local oceanographic feature identification

The LC is characterized by a sea surface height greater than surrounding waters, and its position can be determined from the horizontal gradient of SSH. Specifically, the northernmost, westernmost, and easternmost locations of the LC were measured by obtaining the maximum latitude, maximum longitude, and minimum longitude of the SSH contours corresponding to the location of the maximum gradient of SSH (red regions in Figure 4.2d and h, for example). The spatial variability of the LC was studied in terms of northward penetration of the front using the 768 weekly fields of SSH gradient in the GOM. One-way ANOVA was employed to test the seasonal variability of the northern intrusion of the LC.

Our approach to study the distribution of larval fish in the LC included defining a region of influence (ROI hereafter) of the LC. The ROI is the area limited by the northernmost latitude, westernmost longitude and easternmost longitude of the LC front. These were compared with the weekly collections of the *in situ* fish larvae surveys from 26 April 1993 to 29 May 2007.

To identify the main mesoscale features in the GOM outside the LC ROI, we classified every grid point in the altimeter fields to have one of the following characteristics:

a) An anticyclonic region (AR):

$$SSH \geq SSH_{max} - n \cdot \sigma(SSH) \tag{7}$$

b) A cyclonic region (CR):

$$SSH \leq SSH_{min} + p \cdot \sigma(SSH) \tag{8}$$

c) An anticyclonic region boundary (AB):

$$SSH \geq m \cdot SSH_{max} \quad \text{and} \quad grad(SSH) \geq r \cdot \sigma(|grad(SSH)|) \tag{9}$$

d) A cyclonic region boundary (CB):

$$SSH \leq q \cdot SSH_{min} \quad \text{and} \quad grad(SSH) \geq r \cdot \sigma(|grad(SSH)|) \tag{10}$$

e) Common Waters (CW) if none of the previous conditions was satisfied. They are defined as the background waters in between the boundaries of mesoscale features.

Here, $\sigma(SSH)$ is the standard deviation of SSH in the region and $\sigma(|grad(SSH)|)$ is the standard deviation of the absolute value of the gradient of SSH in the region. SSH_{min} and SSH_{max} are the minimum and maximum values of SSH in the GOM for any given date. The five dimensionless parameters *m*, *n*, *p*, *q* and *r* were tuned by comparing the circulation patterns classified using the relationships above at 758 sampling stations distributed on a one-degree grid in the northern GOM during summer 2009, using the actual satellite-derived SSH fields, their geostrophic currents for this period of time, and ocean color fields. The values obtained by the tuning for these parameters were:

$$m=0.91 \qquad n=3.30 \qquad p=0.60 \qquad q=1.08 \qquad r=0.67 \tag{11}$$

An example of the results from this classification showing the five regions of circulation is shown in Figure 4.3.

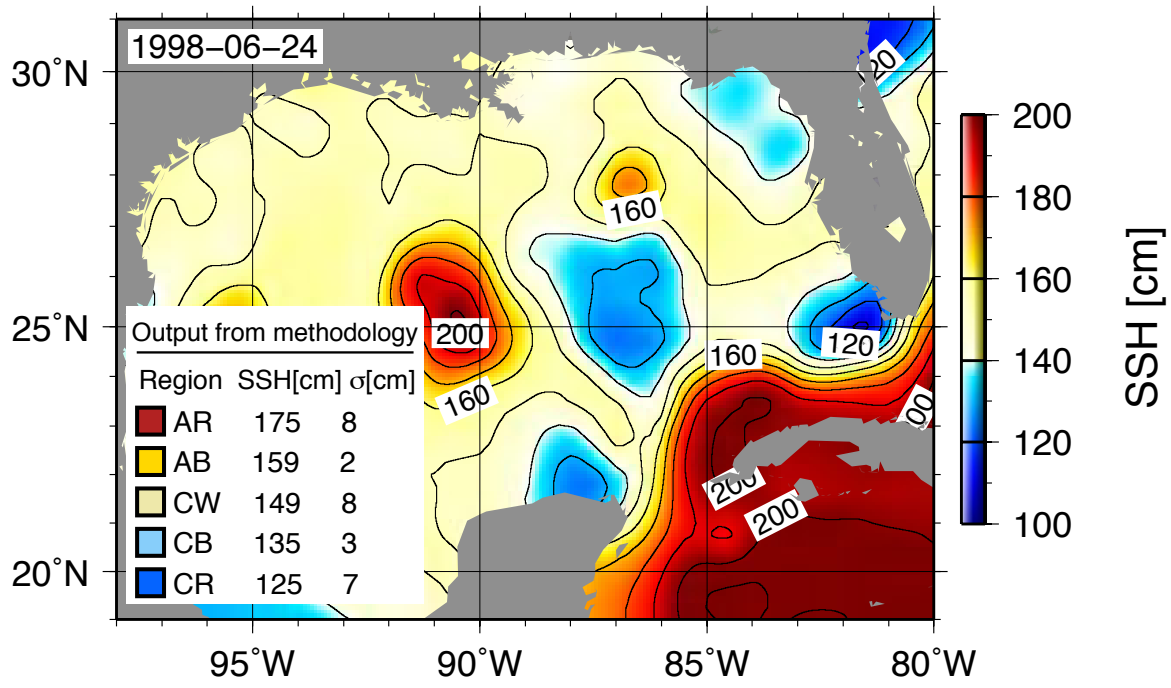

Figure 4.3. Example of the five regions of circulation and boundaries defined using the mesoscale classification algorithm for June 24, 1998. The background field is the satellite derived SSH. The legend illustrates the mean SSH and standard deviation of SSH for each region of circulation. Colors in the legend correspond to the colors of the satellite derived SSH field.

2.3 Biological data

Samples were collected in the GOM north of 24°N during spring (April to June) NMFS SEAMAP surveys between 1993 and 2007. Larval fish data were available from the National Marine Fisheries Service Southeast Area Monitoring and Assessment Program (SEAMAP) database. Cruises were divided into 2 legs and were conducted throughout the United States Exclusive Economic Zone (EEZ) in the northern GOM only. Most of the sampling effort was focused on a one-degree grid of stations, and this grid was usually completed twice each year, with the exception of 2003 and 2004 when they were completed only once. Additional stations were sampled in 1994, 1995, 2005, and 2006 (Table 4.1). Between 41 and 137 hydrographic-plankton stations were carried out each year, with an average of 86 stations per survey in the 15 years covered by this study. At each station, plankton was collected with bongo nets, and CTD casts were completed. Abundance of larvae captured was standardized to larval concentrations (number of larvae per m^2) by estimating volume filtered using a flow-meter fitted to the bongo net, and integrating to the towing depth at each station.

Table 4.1. Sampled SEAMAP stations between 1993 and 2007 across the northern GOM.

Year	Sampling dates	Region sampled	No of sampled stations with satellite data extracted (*)	Net type
1993	26 April - June 15	24°N - 30°N / 84°W - 96°W	84 (14, 38, 26, 13, 16)	Bongo
1994	28 April - 9 June	24°N - 29°N / 84°W - 96°W	137 (29, 75, 45, 25, 15)	Bongo
1995	19 April - 7 June	24°N - 30°N / 84°W - 96°W	110 (26, 61, 42, 23, 21)	Bongo
1996	17 April - 25 May	24°N - 29°N / 83.5°W - 96°W	84 (15, 17, 30, 17, 15)	Bongo
1997	17 April - 9 June	24°N - 30°N / 84°W - 96°W	84 (23, 6, 35, 9, 7)	Bongo
1998	26 April - 23 June	24°N - 29°N / 84°W - 96°W	68 (16, 44, 27, 15, 16)	Bongo
1999	24 April - 31 May	24°N - 29°N / 83.5°W - 96°W	78 (18, 39, 21, 14, 8)	Bongo
2000	20 April - 26 May	24°N - 30°N / 83.5°W - 95°W	85 (26, 56, 26, 16, 11)	Bongo
2001	18 April - 29 May	24°N - 29°N / 83.5°W - 96°W	87 (24, 45, 20, 22, 9)	Bongo
2002	19 April - 28 May	24°N - 29°N / 83.5°W - 96°W	79 (17, 46, 31, 16, 13)	Bongo
2003	13 May - 30 May	24°N - 29°N / 83.5°W - 96°W	51 (9, 38, 15, 17, 2)	Bongo
2004	13 May - 30 May	25°N - 29°N / 84°W - 96°W	41 (10, 24, 17, 12, 7)	Bongo
2005	23 April - 17 July	24°N - 30°N / 83.5°W - 96°W	118 (21, 44, 39, 31, 29)	Bongo
2006	23 April - 16 July	24°N - 30°N / 84°W - 97°W	113 (16, 70, 55, 21, 28)	Bongo
2007	17 April - 29 May	24°N - 30°N / 84°W - 96°W	66 (21, 48, 17, 19, 10)	Bongo

* stations containing *Coryphaenidae*, *Thunnus* spp., *Auxis* spp., *Thunnus thynnus*, and *Euthynnus alleteratus*

Bongo net tows were generally completed across the grid of stations in the GOM in late April and May, with sampling continuing into late June in some years. Sampling extended to July in 2005 and 2006 (Table 4.1). Bongo nets were fitted with 333 μm mesh, on two 61 cm diameter round frames, and were towed obliquely to 200 m depth or to just above the bottom at shallower stations (Richards et al. 1993). Nets were towed at 2-3 knots, and sampling took place during both day and night. Samples from bongo nets were sorted, and larvae identified to the lowest possible taxa at the Sea Fisheries Institute, Plankton Sorting and Identification Center, Gdynia and Szczecin, Poland.

2.4 Larval fish data analysis

The spring plankton surveys were originally designed to target *Thunnus thynnus* larvae (*T. thynnus* hereafter). However, larvae of more than 500 taxa were recorded over the duration of the surveys. In this study, larvae of five taxa from three commercially important families were analyzed. In many cases, larvae from closely-related species were not distinguishable

visually, and so larval groups were merged at genus or family level. Larvae of *Coryphaenidae* (*Coryphaena* spp. hereafter, likely incorporating *Coryphaena hippurus* and *Coryphaena equiselis*) were analyzed at genus level. Within the family Scombridae (tunas), *Auxis* larvae (*Auxis* spp. hereafter, likely incorporating larvae of *Auxis rochei rochei* and *Auxis thazard thazard*) were analysed at genus level, as were *Thunnus* larvae (*Thunnus* spp. hereafter, likely a mix of *Thunnus albacares* and *Thunnus atlanticus*, and not including *T. thynnus*). Larvae of both *T. thynnus* and *Euthynnus alleteratus* (*E. alleteratus* hereafter) were visually distinguishable from other tuna species, and were therefore analyzed at species level.

Larval distributions were compared to the mesoscale ocean features identified as anticyclonic locations, anticyclonic boundaries, cyclonic locations, cyclonic boundaries or common waters using the altimeter data. The statistical methods to analyze the LC seasonality and variability of larval fish relative to the mesoscale circulation features are explained below.

2.5 Probability analyses

Associations between larval catches of *T. thynnus*, *E. alleteratus*, *Thunnus* spp., *Auxis* spp., and *Coryphaena* spp., and the inner and outer regions of mesoscale features were determined by mean of a probabilistic analysis. The capture locations of each taxon were classified as one of five different categories (AR, AB, CR, CB, or CW). The probability of finding larvae of taxon *i* in an oceanic mesoscale feature *j* was calculated using the following quotient:

$$P_i(j) = \frac{\frac{c_{ij}}{e_{ij}}}{\sum_{i=1}^{j=5}\left[\frac{c_{ij}}{e_{ij}}\right]} \tag{12}$$

Where c_{ij} is the number of individuals of taxon *i* captured in feature *j*, e_{ij} is the fishing effort, the denominator is the summation of the captures divided by the fishing effort in the five regions, *i* is the taxa (*T. thynnus* (1), *E. alleteratus* (2), *Auxis* spp. (3), *Thunnus* spp. (4), and *Coryphaena* spp. (5)), and *j* is the region (AR, AB, CR, CB, and CW). The captures of taxon *i* were standardized by e_{ij}, defined as the number of times that feature *j* was sampled finding a particular taxon *i*. This was necessary because sampling effort was not equal within

all water mass classes. For example, regions defined as CW were sampled more often simply due to the location of the stations during the SEAMAP surveys.

2.6 Multivariate analyses

Permutational multivariate analysis of variance (PERMANOVA; Anderson 2001) was used to test the null hypothesis of no difference in 1) total abundances of all the five taxa among the five regions of circulation, 2) the species assemblages of the five taxa among the five regions of circulation, 3) individual abundances of each taxa among the five regions of circulation, and 4) the presence/absence (occurrence) of each taxa among the five regions of circulation. Each test was run on a fourth-root transformed Bray Curtis similarity matrix, in Primer-6 software, with 999 unique permutations to determine significance at $p<0.05$ (Clarke and Gorley 2006).

3. Results

3.1 The Loop Current and larval fish distribution

Between 1993 and 2007, 1285 stations with paired satellite and larval concentration data were available for *Coryphaena* spp., *Thunnus* spp., *Auxis* spp., *T. thynnus*, and *E. alleteratus* larvae (Table 1). These larvae were respectively found at 22%, 51%, 35%, 21%, and 16% of these stations across the northern GOM (Figure 4.4).

Weekly values of northernmost latitude, westernmost longitude, and easternmost longitude of the LC delimited the LC ROI. This fluctuated between 25°N and 28°N on its northern boundary, from 86°W to 89°W on its western boundary, and from 83°W to 85°W on its eastern boundary. From 1993 to 2007, the mean northernmost, westernmost, and easternmost locations of the ROI of the LC were 26°N, 87°W, and 84°W respectively, and the percentage of captures (mean $\pm$ SD) in the ROI of the LC were 17 $\pm$ 10 % (Figure 4.4). The larval fish collected in the ROI of the LC for each sampling period ranged from 11 larval fish in 2006 (3% of the larval fish captured) to 166 in 1998 (31% of larval fish captured; Table 4.2). The mean geostrophic current (mean $\pm$ SD) in the ROI of the LC was 57 $\pm$ 31 cm s^{-1}.

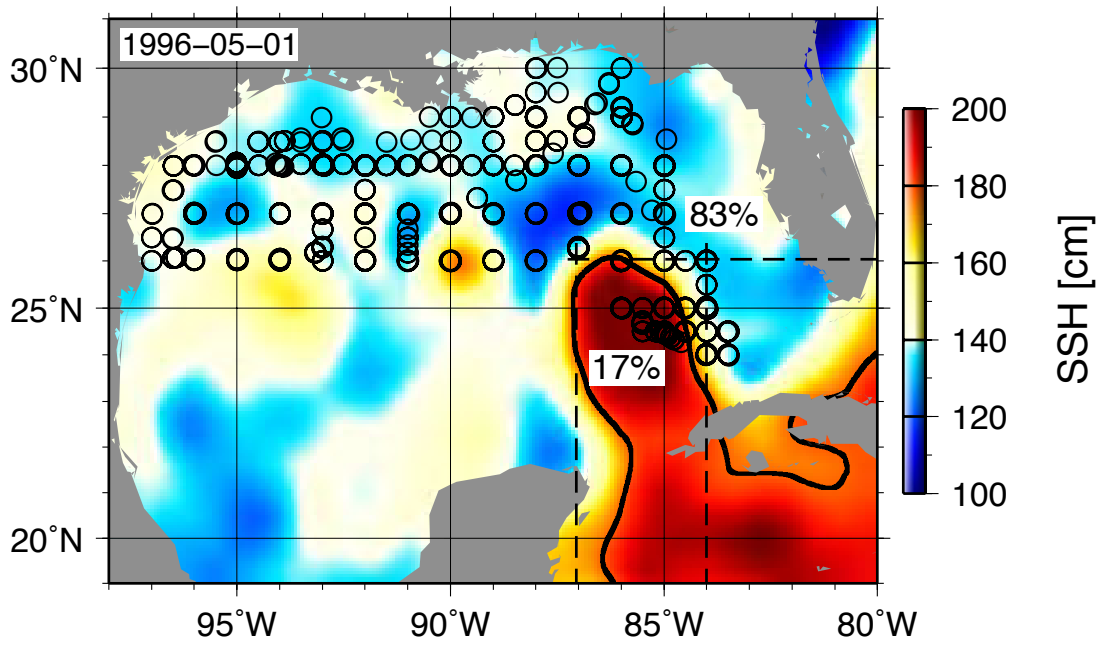

Figure 4.4. Station locations of the NOAA/SEFSC SEAMAP annual larvae survey and percentage of larval fish captured in (17%) and out (83%) of the LC ROI from 1993 to 2007. The background color is the satellite derived SSH for May 1, 1996. The black solid line represents the mean LC front. The dashed lines illustrates northernmost latitude, westernmost longitude and easternmost longitude of the LC front in the GOM north of 23°N, which were 26°N, 87°W, 84°W.

Table 4.2. Details of sampled SEAMAP stations between 1993 and 2007 across the northern GOM.

Sampling dates	No of larvae collected (*)	LC ROI [°]	No of larvae collected in LC ROI	% Larvae in LC ROI
26 April-15 June, 1993	350 (10, 111, 178, 25, 26)	28°N, 88°W, 85°W	51 (4, 17, 13, 17, 0)	15%
28 April-9 June, 1994	499 (28, 161, 232, 40, 38)	26°N, 88°W, 85°W	30 (4, 11, 14, 0, 1)	6%
19 April-7 June, 1995	424 (8, 197, 131, 53, 35)	27°N, 88°W, 84°W	128 (5, 80, 23, 4, 16)	30%
17 April-25 May, 1996	367 (5, 72, 131, 53, 35)	26°N, 87°W, 84°W	86 (2, 22, 52, 3, 7)	23%
17 April-9 June, 1997	191 (16, 6, 101, 35, 33)	25°N, 86°W, 84°W	32 (2, 0, 22, 0, 8)	17%
26 April-23 June, 1998	539 (9, 144, 289, 16, 81)	25°N, 86°W, 83°W	166 (6, 46, 57, 0, 57)	31%
24 April-31 May, 1999	190 (10, 94, 52, 29, 5)	27°N, 88°W, 85°W	40 (2, 28, 6, 4, 0)	21%
20 April-26 May, 2000	397 (17, 259, 77, 30, 14)	27°N, 88°W, 84°W	155 (7, 99, 40, 1, 8)	39%
18 April-29 May, 2001	264 (27, 108, 31, 60, 38)	25°N, 87°W, 85°W	12 (0, 10, 0, 0, 2)	5%
19 April-28 May, 2002	276 (5, 114, 84, 42, 31)	25°N, 86°W, 84°W	35 (4, 23, 7, 0, 1)	13%
13 May-30 May, 2003	145 (3, 75, 25, 38, 4)	28°N, 89°W, 85°W	27 (12, 7, 2, 6, 0)	19%
13 May-30 May, 2004	125 (4, 45, 42, 30, 4)	27°N, 88°W, 85°W	14 (0, 11, 3, 0, 0)	11%
23 April-17 July, 2005	417 (9, 130, 134, 44, 100)	28°N, 89°W, 85°W	70 (4, 39, 23, 4, 0)	17%
23 April-16 July, 2006	398 (6, 171, 117, 34, 70)	27°N, 88°W, 85°W	11 (1, 7, 2, 1, 0)	3%
17 April-29 May, 2007	253 (10, 114, 87, 34, 8)	25°N, 86°W, 84°W	18 (2, 14, 1, 1, 0)	7%

* Larval fish of *Coryphaena* spp., *Thunnus* spp., *Auxis* spp., *T. thynnus,* and *E. alleteratus*

The weekly northernmost location of the LC was determined for the survey periods and also for the rest of the year, to assess the overall cycle of penetration and eddy shedding of the LC. The northernmost location (mean ± SD) was 26.30 ± 1.06ºN, and varied from 24.25ºN to 28.50ºN (Figure 4.5). The northernmost location of the LC showed some seasonal variability, with summer (July through August) showing maximum average latitudes, and fall and winter (October through December) showing minima in extension.

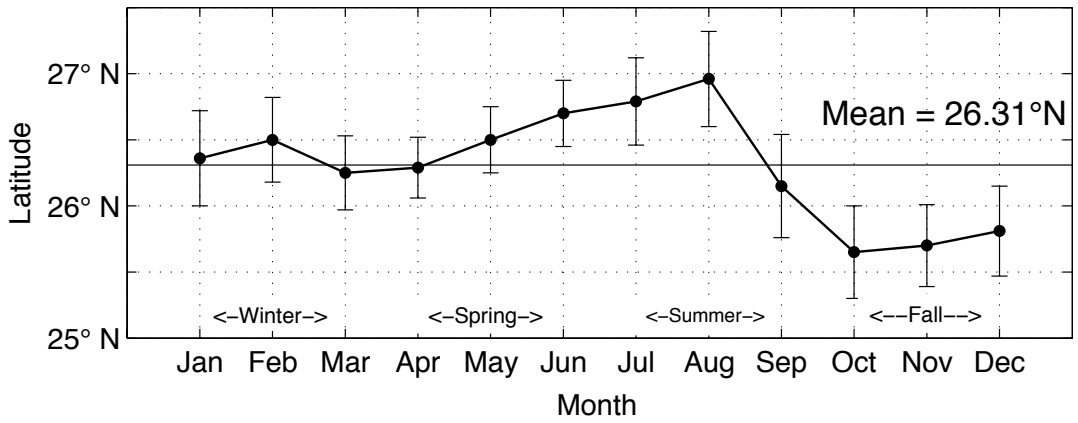

Figure 4.5. Monthly mean location of the LC northward penetration. Bars indicate one standard deviation over the 16 years of data (January 1993 to December 2008).

To further analyze the relationship between LC excursions and larval fish distribution, larval fish collections were examined within a square bin of 2° centered at 87°W and 26°N, which represents the mean northernmost latitude and westernmost longitude of the LC during spring months (Figure 4.6). A time series of deviations from the mean northernmost location of LC in spring time was also analyzed on Figure 4.6.

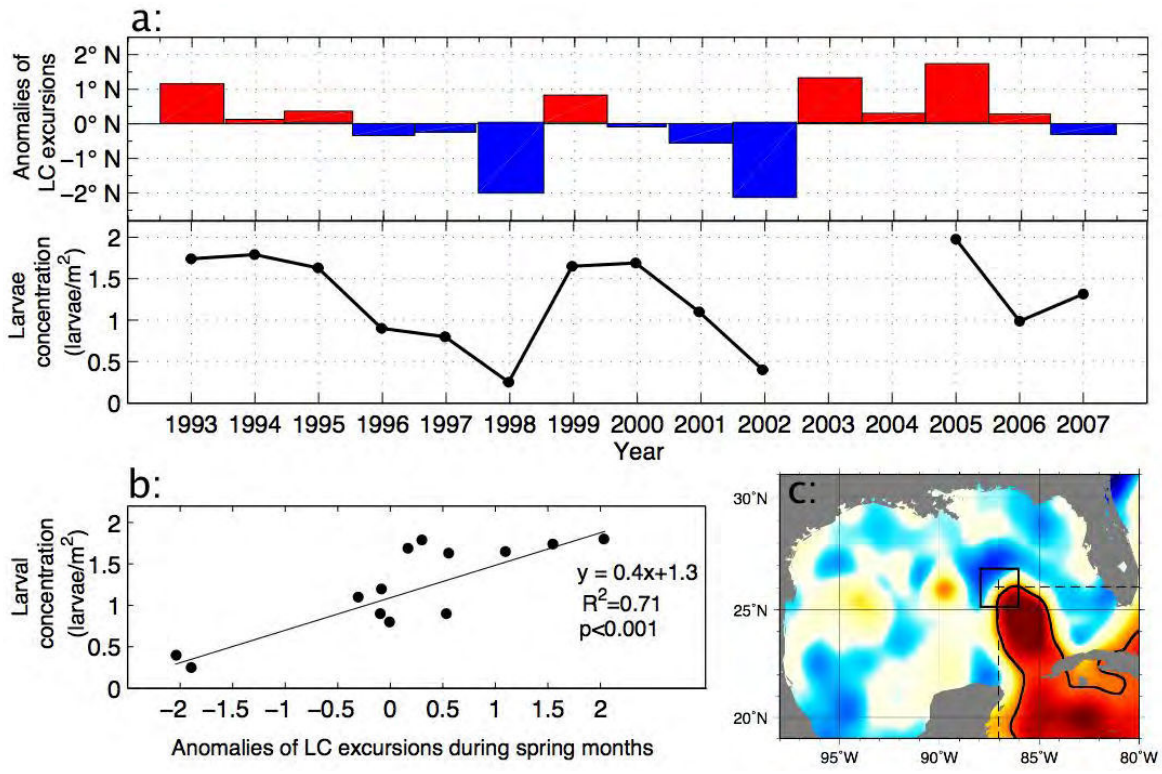

Figure 4.6. (a) Anomalies of the mean northernmost location of the LC in relation to spring larval concentration of larvae captured in a 2° box centered at 87°W and 26°N . Black line shows mean larval concentration of captures of *T. thynnus, E. alleteratus, Auxis* spp., *Thunnus* spp., and *Coryphaena* spp., from May 1993 to June 2007 with exception of 2003 and 2004. (b) Regression analysis of mean larval concentration vs. anomalies in the LC excursions. (c) Location examined represented with a black square.

During spring, the LC is usually to the north of its mean location at 26.31°N (Figure 4.5). However, the LC spring-time northward excursions exhibit a year-to-year variability. They range from a minimum mean latitude of 24.23°N in 2002 to a maximum mean latitude of 27.92°N in 2005. Similar year-to-year variability is found in the mean density of captures of fish larvae analysed herein (Figure 4.6a). A regression analysis (Figure 4.6b) showed that oscillations of the LC about its mean latitude (Figure 4.6c) were significantly correlated with larval concentrations ($r^2 = 0.71$, $p < 0.001$). Northern/southern excursions of the LC usually lead to an increase/decrease in mean larval fish densities within 86°W to 88°W, and from 25°N to 27°N. For example, in spring 2002 an extreme southern excursion of the LC translated to only 4 larvae collected within this subarea, corresponding to a mean density of 0.5 larvae m^{-2}.

3.2 Effects of mesoscale structures on larval fish distributions

Probabilities of collecting larvae of *T. thynnus*, *E. alleteratus*, *Thunnus* spp., and *Coryphaena* spp. were higher in the boundaries of anticyclonic features, and larval distributions of *Auxis* spp. were higher in common waters (Table 4.3). Probabilities (P) of finding larval-fish of all taxa together were significantly different among the five regions (PERMANOVA, p = 0.001), and this was a result of larval concentrations within CW being significantly different than AR (p = 0.001), CB (p = 0.015), and CR (p = 0.009).

Table 4.3. Captures (*c*), efforts (*e*) and probabilities (*P*) of finding larvae in anticyclonic regions (AR), anticyclonic boundaries (AB), cyclonic regions (CR), cyclonic boundaries (CB) and common waters (CW) *for T. thynnus, E. alleteratus, Auxis* spp., *Thunnus* spp., and *Coryphaena* spp. Calculated from altimetry derived fields and spring sampling using bongo tows from 1993 to 2007.

		AR	AB	CR	CB	CW
T. thynnus	*C*	26	199	26	52	301
	E	72	62	38	52	100
	P	**0.044**	**0.389**	**0.082**	**0.121**	**0.364**
E. alleteratus	*C*	19	101	2	7	299
	E	59	63	19	35	140
	P	**0.102**	**0.384**	**0.020**	**0.063**	**0.431**
***Auxis* spp.**	*C*	71	305	29	102	1015
	E	86	96	26	71	270
	P	**0.091**	**0.295**	**0.091**	**0.158**	**0.368**
***Thunnus* spp.**	*C*	287	347	56	120	501
	E	113	102	36	34	180
	P	**0.186**	**0.269**	**0.144**	**0.188**	**0.213**
***Coryphaena* spp.**	*C*	21	38	9	16	54
	E	70	69	22	52	101
	P	**0.151**	**0.299**	**0.191**	**0.157**	**0.202**

Probabilities of finding larvae of *T. thynnus* (P, p-value) were significantly higher in anticyclonic boundaries (0.389, 0.03) and common waters (0.364, 0.03), and similarly *Auxis* spp. larvae were more likely to be collected (P, p-value) in common waters (0.368, 0.001) and anticyclonic boundaries (0.295, 0.001). *Auxis* spp. larvae were more likely to be collected

within boundaries of anticyclonic features than in core regions of anticyclonic features (p = 0.04), but no significant differences were found between the inner and outer regions of cyclonic features (p = 0.2). Although *Coryphaena* spp. larvae were scarce and patchy, probability of finding larvae of *Coryphaena* spp. (P) was higher in anticyclonic boundaries (0.299), and it was marginally significant (p = 0.057). *E. alleteratus* was mostly likely collected (P) within common waters (0.431) and anticyclonic boundary regions (0.384), but this was not significant (p = 0.45). *Thunnus* spp. were frequently found in anticyclonic boundaries, but their presence was not significant either (p = 0.48).

Associations between altimetry fields and larval distribution were also investigated by relating the mean larval concentration of captures and the proportion of captures to actual values of sea level using satellite derived SSH fields from 1993 to 2007. To create a better picture of the SSH values that lie below the mesoscale features in the GOM during from 1993 to 2007, each region of circulation was characterized here by its SSH minimum, maximum, mean value, and standard deviation (Table 4.4).

Table 4.4. SSH minimum (min), maximum (max), mean, and standard deviation (SD) of cyclonic regions (CR), cyclonic boundaries (CB), common waters (CW), anticyclonic boundaries (AB) and anticyclonic regions (AR), calculated from the mean and standard deviation of the SSH and gradient of SSH fields for each of the five regions, from 1993 to 2007.

	min (cm)	**max (cm)**	**mean (cm)**	**SD (cm)**
CR	114	135	124	4.9
CB	121	147	137	5.2
CW	128	161	145	5.1
AB	138	175	153	5.3
AR	153	216	177	15.0

Larvae of *T. thynnus*, *E. alleteratus*, *Auxis* spp., *Thunnus* spp., and *Coryphaena* spp. showed both a high mean larval density and a high proportion of positive stations at SSH of 140 cm to 150 cm. Results also showed that *T. thynnus*, *E. alleteratus*, *Auxis* spp., and *Coryphaena* spp. were less abundant at high values of SSH (Figure 4.7a, b, c, e, & f).

Conversely, *Thunnus* spp. were more abundant at higher SSH than other species (Figure 4.7d).

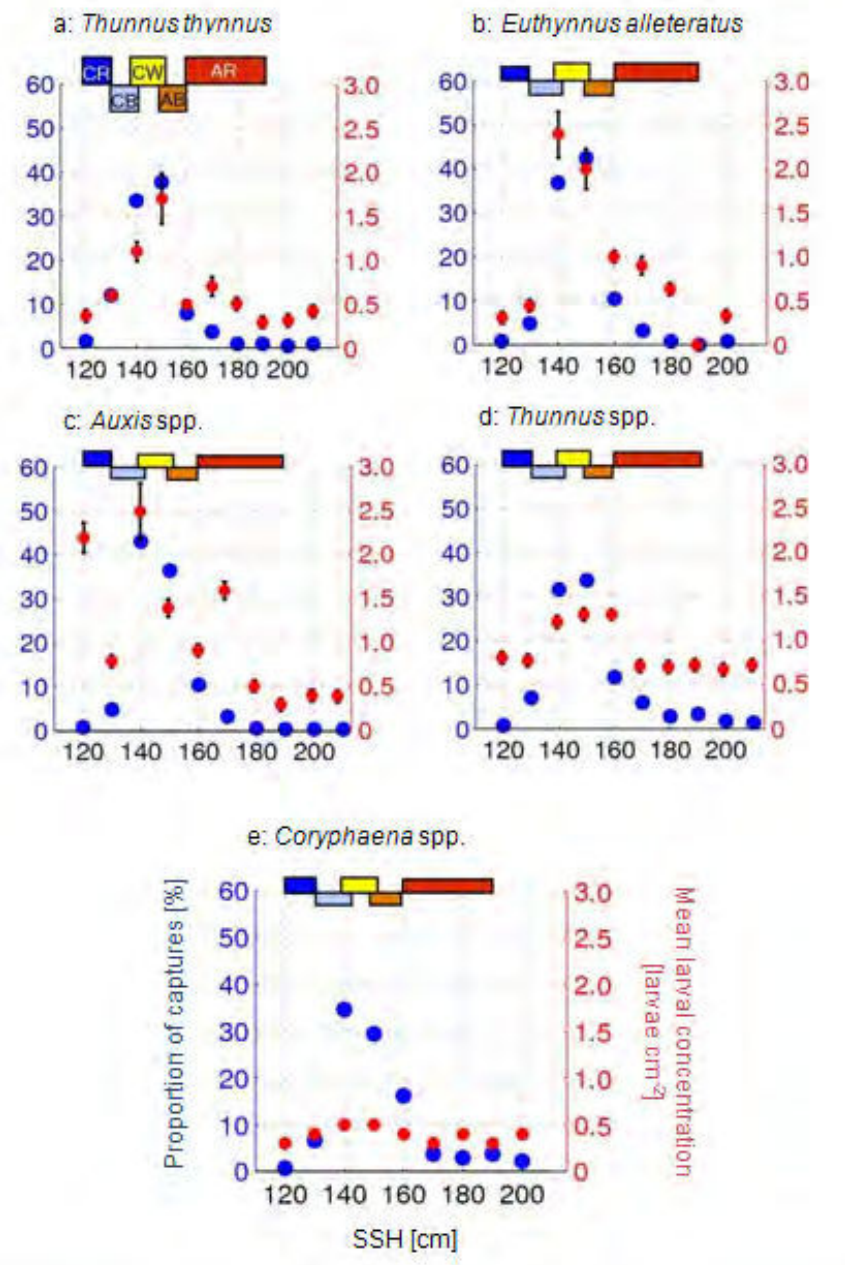

Figure 4.7. Mean larval concentration of captures (red circles) and proportion of captures (blue circles) for larvae of (a) *T. thynnus*, (b) *E. alleteratus,* (c) *Auxis* spp., (d) *Thunnus* spp., and (e) *Coryphaena* spp. in relation to satellite derived observations of sea surface height (SSH), from 1993 to 2007. SSH values were binned to 10 cm intervals. Error bars represent one standard error. Colored blocks represent SSH intervals of cyclonic regions (CR), cyclonic boundaries (CB), common waters (CW), anticyclonic boundaries (AB) and anticyclonic regions (AR), calculated from the mean and standard deviation of the SSH field for each of the 5 regions

4. Discussion

The average cycle of northward penetration of the LC showed maximum values in early summer. This is consistent with the findings of Behringer et al. (1977). While this seasonality was not statistically significant, there was a positive correlation with larval fish density, with higher mean larval concentrations in the eastern Gulf of Mexico when the Loop Current intruded farther north and vice versa. This could be due to a biological response by either adults or larvae to the LC feature, but also to purely physical mechanisms of northward displacement of larvae carried by the LC. Larvae were less abundant in the core of both cyclonic and anticyclonic mesoscale features, and more abundant near anticyclonic frontal areas (Table 4.3 and Figure 4.7). This suggested that larval concentrations within the LC frontal zone may be higher than within the main body of the current.

Larvae may be more abundant in boundaries of mesoscale features simply because these represent convergence zones where favorable prey concentrations exist (zooplankton, or fish larvae). Fish larvae eat a variety of zooplankton, and some (e.g. scombrids) may eat each other (piscivory) once they are post-flexion. Alternatively, adult fish may actively spawn in the vicinity of such frontal regions. There is indeed some indication of spatial autocorrelation in the abundance of larvae from different species of fish throughout the SEAMAP time series.

T. thynnus, *E. alleteratus*, and *Auxis* spp. larvae were most often present within the boundaries of anticyclonic features and in GOM common waters (this typically corresponds to SSH of 140 cm to 150 cm). Presence of *T. thynnus* was significantly different among zones ($p = 0.038$), as also was presence of *Auxis* spp. ($p = 0.001$). However, probabilities of finding larval-fish were not different among zones for *E. alleteratus* ($p = 0.45$), *Thunnus* spp. ($p = 0.488$), and *Coryphaena* spp. ($p = 0.057$). These results are similar to those from studies in the western Mediterranean (García et al. 2005; Alemany et al. 2010), in which tuna spawning grounds were related to anticyclonic features, and *T. thynnus* larvae were more abundant near frontal areas. Previous studies showed highest abundance of *E. alleteratus* and *Auxis* spp. eggs outside cyclonic eddies in open waters near southern Brazil (Matsuura and Sato 1981) and in the eastern Pacific (Klawe 1963). We found *Thunnus* spp. larvae to be distributed more broadly and over a wider range of SSH. This agrees with reports that that adult tropical tunas have broader habitat preferences in the GOM than *T. thynnus* (Weng et al. 2009; Teo

and Block 2010), including higher tolerances for warm features (Teo and Block 2010; Muhling et al. 2010) such as the LC and warm LC rings. SSH is proportional to integrated vertical water temperature (Willis et al. 2004), and our results therefore suggest higher tolerances for warm waters for these tropical tuna species, which also is in agreement with previous studies showing that the present *Thunnus* spp., which included mainly larvae of *Thunnus atlanticus*, were more abundant in warmer waters than other species such as *T. thynnus* (Muhling et al. 2010). Some of the variability in larval abundances in GOM common waters, may be due to smaller-scale oceanographic features which were not apparent from an analysis which used only altimetry data. For example, small cyclonic eddies generated at irregular intervals tend to travel along the LC edge (Zavala-Hidalgo et al. 2003b), and may influence larval distributions.

Larvae were typically very small, with mean lengths of approximately 4 mm in bongo net samples, and thus young age of around 7 days or less (Brothers et al. 1983; Oxenford and Hunte 1983; Macias et al. 2006; Muhling et al. 2010). They were present in waters with mean geostrophic current (mean $\pm$ SD) of 32 $\pm$ 28 cm s^{-1} in the northern GOM, and of 20 $\pm$ 18 cm s^{-1} north of 26°N and west of 87°W. This suggests that larval fish outside the ROI of the LC were captured approximately 120 km from where they were spawned (SD = 100 km). The larvae are unlikely to cross oceanographic boundaries during these early life stages. We believe that larvae outside the LC region were observed near to the spawning location in the northern GOM region.

The year-to-year variability of the LC might be reflected in adult recruitment, with possibly higher adult recruitment of *T. thynnus*, *E. alleteratus*, *Auxis* spp., *Thunnus* spp., and *Coryphaena* spp. during years of high northward penetration of the LC. Mean geostrophic currents (mean $\pm$ SD) in the ROI of the LC were ~57 $\pm$ 31 cm s^{-1}. Therefore, larvae captured in this region were transported a mean distance of 342 km from their spawning location (SD = 186 km), i.e. in the northwestern Caribbean. The largest fraction of the spawning habitat of *T. thynnus* and *Auxis* spp., however, was within the boundaries of anticyclonic eddies and in GOM common waters of the northern GOM, outside the ROI of the LC.

In conclusion, our findings based on coarse spatial resolution altimeter data show that AB regions show higher concentrations of *T. thynnus* larvae than CB, CR, or AR. Similarly to recent studies in the northern GOM (Muhling et al. 2010) (Muhling et al. 2010), the mesoscale circulation is shown to introduce significant variability into time series which rely

on plankton surveys in the region. The larval fish distributions in GOM common waters may be investigated in future research by using other sources of satellite data to overlay on the altimetry. Tracing frontal zones from SST and OC data would give more detail regarding the location of larvae relative to smaller scale features.

Chapter V: Future research

1. Introduction

Now that we have presented the main characteristics of the Physical Oceanography and Fisheries in the Gulf of Mexico (Chapter II), provided an extensive description of the long term variability of the Loop Current, associated ring field, and sea height anomaly in the GOM (Chapter III), and assessed linkages between mesoscale circulation and the spatial and temporal distribution of larval fish in the GOM (Chapter IV), this chapter will explore some potential future research resulting from this dissertation.

The results of this dissertation give us room for a wide scope of upcoming research. Three scientific questions that arise after this work are highlighted below:

1. Is there a significant atmospheric coupling between wind stress forcing and the LC migrations?
2. What may be the role of cyclonic mesoscale eddies shed by the LC on the resolution of the "momentum imbalance paradox" raised by PN (1997)?
3. How are primary producers correlated with mesoscale structures in the Gulf of Mexico?

In this chapter we will shed some light essentially on the first and second questions, which describe our planned future research directions. The third question will only be introduced broadly, to highlight that including primary production data would complement the binomial ocean mesoscale features – larval-fish distribution section of this dissertation.

2. Evidence of coupling between atmospheric pressure/wind field and LC migrations

2.1 Introduction

As it has been shown in chapter II, the findings of Hurlburt and Thomson (1980), Pichevin and Nof (1997), and Nof (2005) provide significant insights into the dynamics of the Loop Current and ring shedding. In particular, the latter explains how the LC expands with a mass influx from the Yucatan Current, and how eddies are shed from the LC when, up to a certain large size, the westward Rossby wave speed overcomes the growth rate and the LC. Their valuable works indicate that understanding mass balances in the Gulf of Mexico may hold the key to also understanding the LC and eddy dynamics.

The preliminary research presented in this section regarding the possible effects of atmospheric pressure/wind on the migrations of the Loop Current has been inspired by the recent modeling work of Chang and Oey (2010). In their paper they analyze transport balances, and study how these are modified by a local, steady westward wind blowing inside the Gulf of Mexico, intentionally excluding wind stress curl so that they can focus solely on eddy transports (Chang and Oey 2010). They hypothesize that the intensification of the prevailing zonal wind field creates an eastward transport in the central GOM, which delays the detachment of rings and strengthens them (see their Figure 3, p. 2485, and Figure 6, p. 2489). They show that this is caused by the variability in Ekman transport instead of Ekman pumping, since wind curl is excluded in their study. The modeling effort of the work of Chang and Oey (2010) on the effect of wind stress on the delay of LC ring shedding suggests that future study of atmospheric modulation of LC migrations would be beneficial. To date the atmospheric modulation of the LC migrations has not been studied from an observational approach, and this therefore represents a novel future research direction.

2.2 Atmospheric pressure variability and LC migrations

In order to explore whether variability of Ekman transport has some effect on the migrations (northward and southward) of the Loop Current, the pressure gradients between the northern and southern locations of the loop current were measured. This first approximation based on pressure gradients was assumed to be a valid estimation due to the fact that the wind field in the region is mainly zonal (westward). Future work will extend the direct analysis to the wind stress and wind curl, which drive Ekman transport and Ekman pumping, respectively.

Monthly means of surface winds computed from the FNMOC (Fleet Numerical Meteorology and Oceanography Center) 6-hourly analyzed wind fields on a 360 by 181 global spherical grid (1 degree) are calculated and posted to PFEL's (Pacific Fisheries Environmental Laboratory) Live Access Server a few days after the first of every month (Clancy 1992; Rosmond 1992). Monthly mean pressure differences between the northern and southern locations in the GOM were estimated. The northern and southern locations were located along 86.5ºW at 27.5ºN, one degree of latitude above the mean northernmost location of the LC (see Chapter III), and 21.5ºN just in the middle of the Yucatan Channel (Figure 5.1).

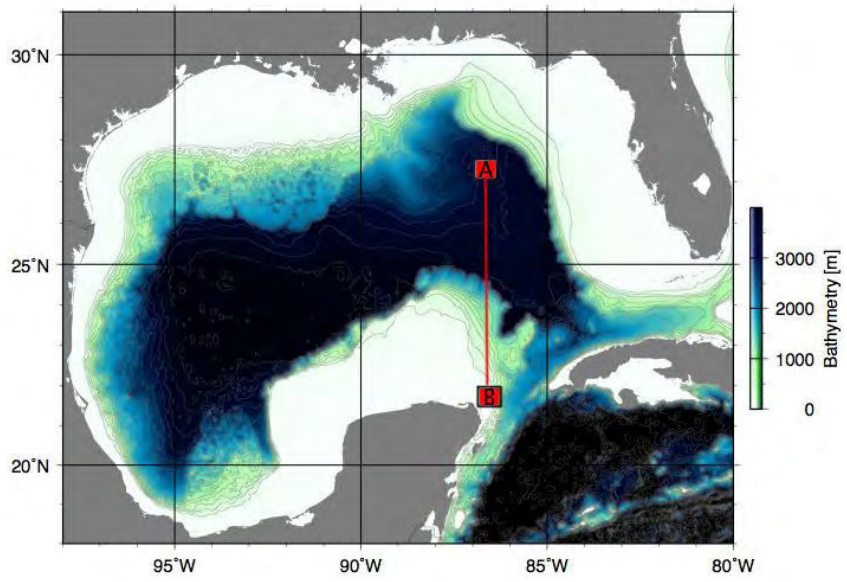

Figure 5.1. Bottom topography in the Gulf of Mexico (GOM), data retrieved from ETOPO1 1-minute Global Relief (Amante et al. 2009). The map illustrates section A-B, used to estimate the difference in the mean sea level.

The wind regime in the Caribbean (including the Yucatan basin) is determined by the North Atlantic Subtropical High (NASH). Located between Bermuda and the Azores, a high air pressure zone centered at around 30°N drives northeasterly trade winds on the southern side of its clockwise atmospheric circulation (Tomczak and Godfrey 2003). The winds over the Caribbean Sea vary owing to the northward migration of the Intertropical Convergence Zone (ITCZ) (Muñoz et al. 2008), from its southernmost position in winter (over the Amazon basin, approximately the Equator) to its northernmost position in summer (Costa Rica-Nicaragua border, ~ 11°N) (Poveda et al. 2006). Once they approach the Yucatan basin, the northeasterly trades intensify, forming the easterly Caribbean low-level jet (CLLJ) (between 12.5°– 17.5°N and 70°– 80°W) with wind speeds > 13 m s^{-1} at sea level pressures around 925 mb (Wang 2007; Wang and Lee 2007). To test the hypothesis that the wind regime affects the migrations of the Loop Current, we tested the monthly difference (or anomaly) in the sea level pressure between two locations north and south of the Loop Current, as explained above.

Time series of monthly Loop Current migrations overlaid on time series of monthly Sea Level Pressure Anomalies (SLPA) have been determined for 17 years of data, from November 1992 to December 2009, and the time of separation of LC rings has been added (Figure 5.2). Although both time series data were sampled weekly, they were merged to monthly scales to facilitate easier analysis. In general, we observe an apparent negative correlation (or anticorrelation) between the LC migrations and the monthly SLPA. This indicates that when the gradient of pressure increases (and therefore the wind stress and Ekman transport increases), the LC retreats southward. Conversely, when the gradient of pressure decreases the LC intrudes northward. For example, after a ring has been shed (vertical black line on Figure 5.2) in March 1998, the LC migrates south from March 1998 to June 1998, then moves northward from June 1998 to August 1998, and finally moves south from August 1998 to November 1998. The LC then starts a strong and continuous northward intrusion into the Gulf of Mexico from November 1998 to July 1999. For the same period – from March 1998 to July 1999– the SLPA describes an inverse oscillation to the one shown by the LC, increasing SLPA when the LC retreats southward and decreasing SLPA when the LC migrates northward into the Gulf of Mexico. Generally, the visual characterization of this apparent negative correlation is very clear, although there are some periods of time when there is no correlation, such as from 2007 to 2009.

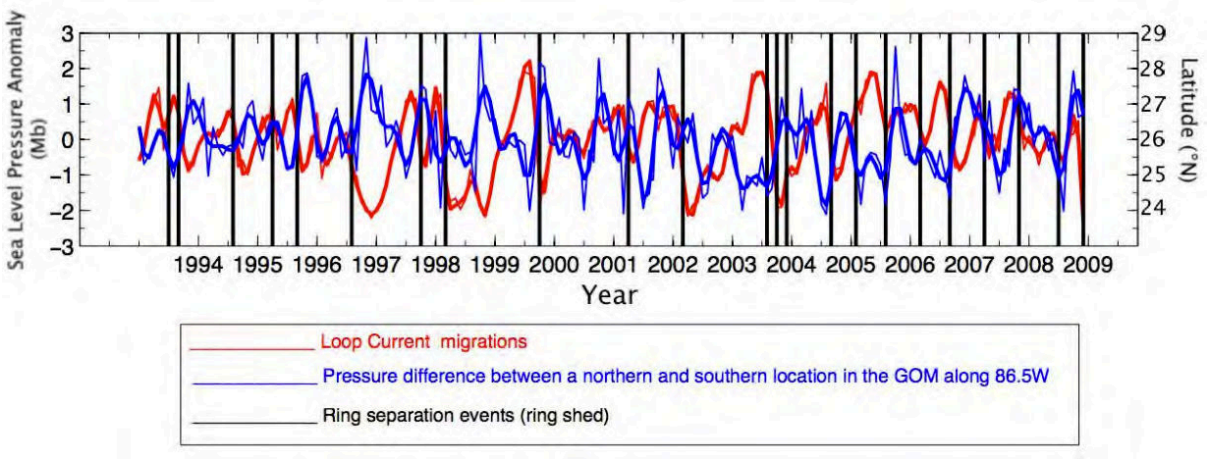

Figure 5.2. Time series of monthly Loop Current migrations (thin red line) determined from altimetry derived fields, and monthly Sea Level Pressure Anomalies (thin blue line) determined from the pressure difference between two locations north and south of the Loop Current, from November 1992 to December 2009. Vertical black lines indicate the time of separation of LC rings. The signals were filtered using a Butterworth filter of order 6 and cutoff frequency 1/7 rad/s (thick red line and thick blue line for LC migrations and pressure anomalies respectively).

Continuous wavelet transforms (CWT) of the time series presented above were used to analyze the variability of the dominant periods of the series, and a wavelet-based semblance analysis was used to correlate them (Figure 5.3). Semblance analysis allows the local phase relationships between the two datasets to be studied as a function of both scale (or wavelength) and time (Cooper and Cowan 2008). In the time series of LC migrations, the periods of 20 weeks and 12 weeks were the dominant periods (Figure 5.3b), with 20 weeks showing the highest amplitude. Similarly, in the time series of the gradient of pressure (or SLPA), there was also a clear signal in the period of 20 weeks (Figure 5.3d), although this signal was faded by the signal at 12 weeks, which in this case showed a much higher amplitude. The semblance analysis showed a negative correlation at all periods along most of the time interval (blue regions on Figure 5.3d). In particular the negative correlation between the LC migrations and the pressure gradient is higher than 80% in the 12 to 20 weeks range.

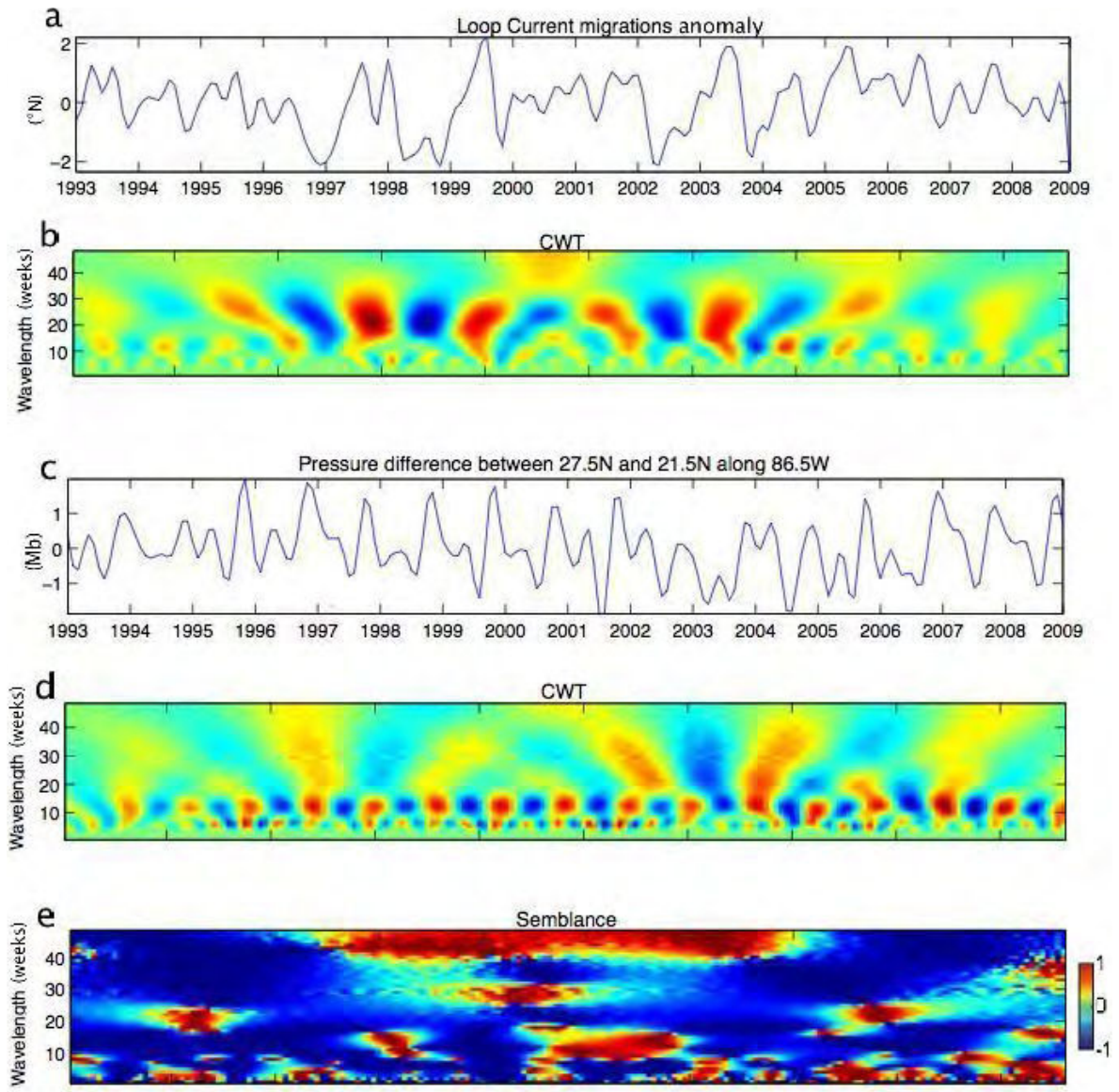

Figure 5.3. (a) Time series of monthly Loop Current migrations determined from altimetry derived fields from November 1992 to December 2009. (b) Real part of the complex CWT of dataset in (a). Bright red indicates large positive amplitude and dark blue indicates large negative amplitude. (c) Monthly Sea Level Pressure Anomalies determined from the pressure difference between two locations north and south of the Loop Current, from November 1992 to December 2009. (d) Real part of the complex CWT of dataset in (c). Bright red indicates large positive amplitude and dark blue indicates large negative amplitude. (e) Semblance S (calculated from Eq. (20), with n=1). Bright red corresponds to a semblance of +1, green to a semblance of zero, and dark blue to a semblance of −1.Wavelength ranges from zero to 48 units, which in time scale corresponds from zero to 4 years (48 months).

The main conclusion derived from the results shown in this preliminary analysis is that there is a clear negative correlation between gradients of pressure and the migrations of the Loop Current, which suggest that LC dynamics may be modulated to some extent by

atmospheric forcing. Despite the recent modeling efforts to investigate the frequency of the shedding of LC rings, which are suggested to be delayed by westward wind stress (Chang and Oey 2010), to date the atmospheric effect on the LC migrations does not appear to have been considered, either through modeling or using a observational or theoretical approach. However, we note that there could be some correlation between the delay in LC ring shedding caused by westward wind stress (Chang and Oey 2010) and the atmospheric effect on the LC migrations shown herein, which should be investigated in future studies. This preliminary analysis on the atmospheric modulation of LC dynamics will be explored in more depth in the near future.

3. Westward propagating long-lived eddies generated by the LC

3.1 Introduction

The Loop Current not only generate mesoscale anticyclonic rings, but it is also a source of mesoscale cyclonic eddies which are generated along the edge of the current. For example, on Figure 5.4 we can clearly observe three mesoscale cyclonic eddies generated by the LC, one on the eastern boundary and two on the western boundary of the LC. Although cyclonic frontal eddies have been recognized to play a crucial role in warm core ring separation (Cochrane 1972; Zavala-Hidalgo et al. 2003b; Cherubin et al. 2005; Schmitz 2005), the often rapid motion of frontal eddies of the LC -compared with the anticyclonic rings shed by the LC- and the frequent cloud cover over the GOM have historically made their study problematic on short timescales (Walker et al. 2009).

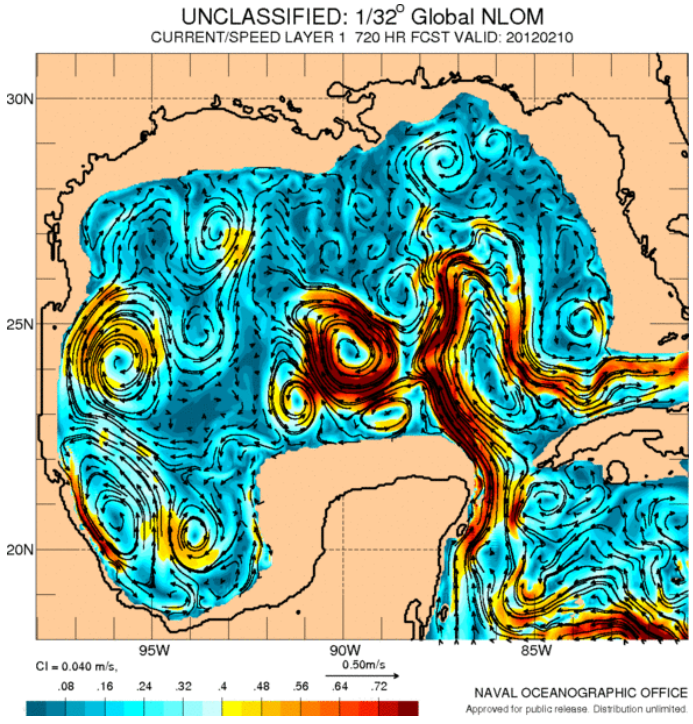

Figure 5.4. Forecasted currents in the Gulf of Mexico for February 10, 2012. Thin arrows and color scale represent current direction and magnitude, and are obtained from the operational 1/32° global NLOM (Navy Layered Ocean Model). The model presently assimilates SSH from 3 satellite altimeters (ENVISAT, JASON-1 interleaved and JASON-2) and SST from satellite infrared imagery. Three cyclonic eddies are clearly revealed, one on the eastern boundary of the Loop Current and two on the western boundary of the Loop Current.

The main goal here is to advance understanding of the role that is played by cyclonic eddies in the balance of momentum and mass when solving the "momentum imbalance paradox". The role of cyclonic eddies may be important if the number of long-lived westward propagating cyclonic eddies generated is significant. In that case, cyclonic eddies would transport mass and momentum to the west in a similar fashion to anti-cyclonic rings, and cyclones would therefore contribute to solve the momentum paradox stated by PN in their work (Pichevin and Nof 1997). As far as we know, long-lived cyclonic eddies have not been considered in the solution of the momentum paradox, which to date has only been attributed to the westward propagation of anticyclonic rings.

3.1 Westward propagating long-lived eddies generated by the LC

The first and preliminary approach we started with was to explore if the generation of long-lived cyclonic eddies to the west of the Gulf of Mexico was significant. Potential eddies were identified by applying the Okubo–Weiss parameter (W), which allows the separation of vorticity-dominated regions (Isern-Fontanet et al. 2004). The Okubo–Weiss parameter has been widely used to detect eddies in the ocean (Font et al. 2004; Isern-Fontanet et al. 2006; Chelton et al. 2007; Sangrà et al. 2009) and recently to better understand mesoscale structure of larval fish assemblages in the waters off Chile (Morales et al. 2010). This parameter is defined as

$$W = s_n^2 + s_s^2 - \omega^2 \tag{13}$$

$$s_n = \mathrm{d}u/\mathrm{d}x - \mathrm{d}v/\mathrm{d}y \tag{14}$$

$$s_s = \mathrm{d}u/\mathrm{d}y + \mathrm{d}v/\mathrm{d}x \tag{15}$$

where s_n and s_s are the normal and shear components of strain, ω is the relative vorticity, and u and v the horizontal components of geostrophic velocity fields derived from merged altimeter data. Since vortices are regions of concentrated relative vorticity in which there is a dominance of vorticity over strain, we used a threshold value (U_w) for W, where $U_w = -0.2\sigma_w\ s^{-2}$ and σ_w represents the spatial standard deviation of W. Therefore, eddies were

defined as regions with $W < U_w$. Following Isern-Fontanet et al. (2006), we obtained initial values for U_w from statistical analysis, which resulted in values of $-1 \times 10^{-11}\ s^{-2}$ and $-1.5 \times 10^{-11}\ s^{-2}$ for zones with positive and negative vorticity, respectively. For eddy tracking we followed Chelton et al. (2007), and allocated each eddy to a single point calculated as the centroid from the mean values of W at its closed contour. The criteria used to join a centroid detected at t to a trajectory at $t-1$ was based on a search radius (r), estimated from the weekly mean translation velocity of eddies. Thus, a centroid at t was merged to the closest centroid at $t-1$ with the same polarity if distances lower than the search radius separated them. Similarly to Sangrà et al. (2009), we tested the eddy detection and tracking process using several values for both r and U_w, varying r from 20 to 40 km and U_w from -0.5×10^{-11} to $-5 \times 10^{-11}\ s^{-2}$, between October 1992 and October 1993. The best results were obtained with $r = 30$ km and $U_w = -1 \times 10^{-11}\ s^{-2}$, which retrieved whole trajectories. Cyclonic and anticyclonic eddies are distinguished by the vorticity sign ($-$ or $+$, respectively) in their centers.

According to the methodology described above, westward tracks described by cyclonic eddies and anticyclonic eddies are calculated in the GOM from October 1992 to December 2010 (Figure 5.5).

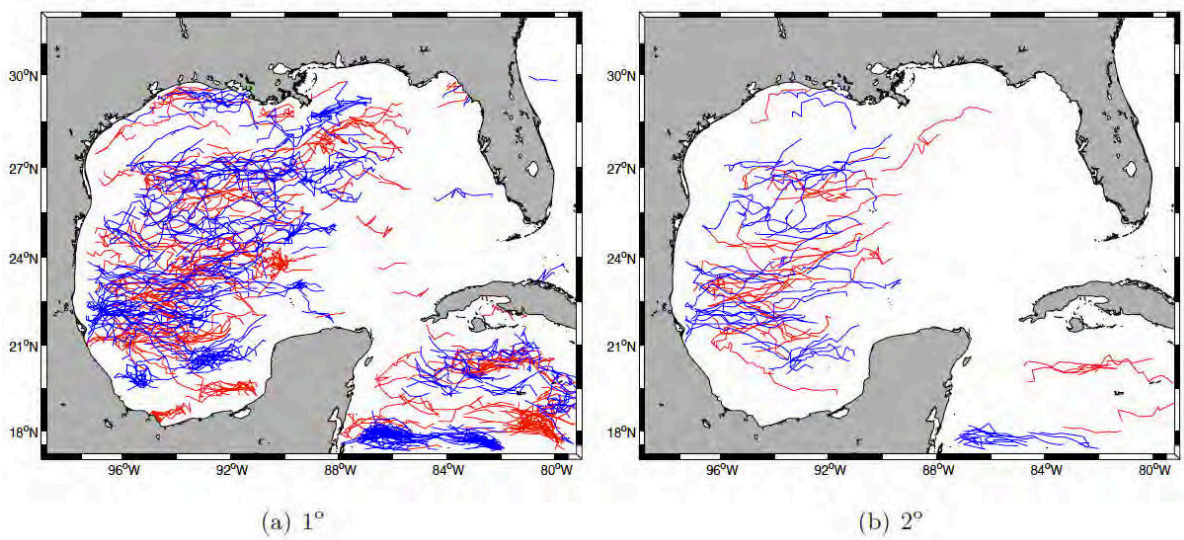

Figure 5.5. Westward tracks of cyclonic eddies (blue) and anticyclonic eddies (red) from October 1992 to December 2010, provided movement to the west of (a) at least 1°, and (b) at least 2°.

As the mean origin location of eddies coincided with the mean position of the western boundary of the LC, which is 87.5°W for the entire period (from time series shown on Figure 3.3 included in Chapter III), we concluded that the LC was the main source of westward

propagating long-lived eddies. This statement held both for cyclonic and anticyclonic eddies. However, we note that our eddy detection methodology is not refined enough yet to discriminate between mesoscale anticyclonic rings and anticyclonic eddies. Surprisingly, we found that the number of eddies (N) that moved at least 1° to the west was higher for cyclonic eddies (N=374) than for anticyclonic eddies (N=287), meaning that there were 30% more westward-propagating cyclonic eddies than anticyclonic eddies. The ratio of cyclonic eddies/anticyclonic eddies was greater than one when eddies were filtered for lifetimes greater than one, two, three, and four months, and remained balanced for eddies older than five months. The marked difference in the demography of eddies will be further explored, likely by improving the detection technique and discriminating anticyclonic rings from anticyclonic eddies, which would further increase the ratio of cyclonic/anticyclonic eddies.

The preliminary results showed here suggest that the number of westward propagating long-lived mesoscale cyclones may be crucial in rethinking the “momentum imbalance paradox”, and this will be explored further in the future. Specifically, we plan to implement the eddy tracking technique to differentiate between rings and anticyclonic eddies by means of products already developed (Figure 5.5), and *in situ* data. This will allow us to obtain an estimate of the transport of the westward momentum and mass by cyclonic eddies and rings generated by the LC.

4. Mesoscale features affecting primary productivity in the GOM

Addressing the influence of mesoscale features on primary productivity in the GOM will be a valuable complement to the present work, since it will allow us to better understand correlations between mesoscale ocean features and larval-fish assemblages.

We already know that a marked seasonality in phytoplankton concentration is present in the GOM, with maxima during winter and minima during summer (Muller-Karger et al. 1991). In addition, there is high spatial and temporal variability in pigment concentrations, which generally increase from east to west and from south to north, due to the difference in thermal stratification across the region, the intrusion of nutrient-poor waters from the western Caribbean, the occurrence of cold fronts and extra-tropical low pressure systems, and nutrient distribution from the Mississippi river (Melo-González et al. 2000). There is sufficient illumination for primary production in the GOM mixed layer all year round, and it has been suggested in previous studies that primary production in the region is controlled by variations in upward nutrient flux (Muller-Karger et al. 1991). Consequently, the preliminary hypothesis of the proposed research is that regional mesoscale ocean features, which control upwelling and downwelling processes, may have a significant effect on the distribution of phytoplankton through deepening the mixed layer and through vertical mixing in the region. The first approach that we will consider will use regional ocean color imagery overlaid on altimetry fields to study spatial and temporal variability of both mesoscale features and phytoplankton in the GOM. Chlorophyll-*a* images will be derived from the HERMES multi-sensor combined product (MODIS, MERIS, SeaWiFS) obtained from GlobColorWeb (ftp.fr-acri.com).

Chapter VI: General discussion and conclusions

1. Synthesis of results and general discussion

The central goal of this dissertation work has been to study the temporal and spatial variability of the Loop Current and rings, and the regulation of larval fish distributions of some species by mesoscale oceanic features. To this end, we developed methodology to locate LC fronts, detect the shedding of LC rings, and we addressed the seasonal and inter-annual variability of Loop Current excursion, ring field detachments and sea height anomaly trends in the Gulf of Mexico from 1993 to 2009. Once the variability of mesoscale circulation structures in the GOM was defined, we assessed linkages between circulation and the spatial and temporal distribution of larval fish.

The first part of the second section of the dissertation (Chapter III) showed four main findings. The first result was that northward penetration of the LC appeared to be seasonal, with a tendency to increase during the spring and show maximum values in the summer. In particular, the location of the LC from July through August was more to the north than in the fall season, with winter and spring having values closer to the mean. This result is based on the long time series of weekly LC migrations we derived, and it is in agreement with what previous studies -covering shorter life span and based on visual methods and *in situ* temperature sampling- had concluded. Our second finding was that starting in the 2003, the LC was located more to the north; 1.5 degree of latitude above the interannual mean. To date, this result is novel, and it may be closely related with our third result, which showed that also starting in 2003, there was an increase in the number of rings shed from the Loop Current. Finally, we determined the variability of the meridional and zonal oscillations of the LC, showing that meridional motions decreased 1.5 degrees of latitude, and that zonal motions decreased 2 degrees of longitude, from 2004 to 2009. Our proposed future research (Chapter V) is partially oriented to better understand the dynamics of the LC and shedding of rings.

The second part of second section of the dissertation (Chapter IV) proposed to combine oceanography and biology to study the variability in spring larval fish collections in the GOM from 1993 to 2009. We obtained three main findings. The first result was that generally, higher larval concentrations occurred during years of high northward penetration. A regression analysis showed that oscillations of the LC about its mean latitude were

significantly correlated with larval concentrations. This could be due to a biological response by either adults or larvae to the LC feature, but also to purely physical mechanisms of northward displacement of larvae carried by the LC. The second finding was that larvae were less abundant in the core of both cyclonic and anticyclonic mesoscale features, and more abundant near anticyclonic frontal areas. Larvae may be more abundant in boundaries of mesoscale features simply because these represent convergence zones where favorable prey concentrations exist (zooplankton, or fish larvae). Fish larvae eat a variety of zooplankton, and some (e.g. scombrids) may eat each other (piscivory) once they are post-flexion. Alternatively, adult fish may actively spawn in the vicinity of such frontal regions. The third finding is that *Thunnus thynnus* -one of the most commercially important species of our work- showed significantly higher concentrations in the boundaries of anticyclonic features than in anticyclonic features, cyclonic features, and the boundaries of cyclonic features. Our future research (Chapter V) will investigate the larval fish distributions at a higher level of detail by using ocean color to assess phytoplankton concentration in the mesoscale ocean features of the region. In particular, we will analyze a recently available larval data from a synoptic survey conducted in 2010, which has a high number of Scombridae larvae and may allow the study of larval-fish assemblages in small eddies with a higher level of detail.

2. Conclusions

The main conclusions that arise from this dissertation are:

1. Starting in 2003, the LC was located further to the north than the 1993-2009 mean, and there was a marked increase in the number of rings shed from the Loop Current.

2. The amplitude of the meridional oscillations of the Loop Current has decreased, exhibiting maximum values with meridional motions of 4 degree of latitude from 1993 to 2003, and meridional motions of 2.5 degrees of latitude from 2004 to 2009. Similarly, the amplitude of the zonal oscillations of the LC exhibited maximum values with zonal motions of approximately 6 degree degrees of

longitude from 1993 to 2003, and zonal motions of 4 degree of longitude from 2004 to 2009.

3. The Loop Current northward penetration appears to be mostly seasonal (Figure 3.4 (*a*)), with maximum values of 0.8 degrees of latitude above the annual mean during June, July and August.

4. Monthly sea height residuals, estimated as the difference between the mean sea height anomaly for each specific month and the mean sea height anomaly value for that month since November 1992, showed a positive linear trend of (2.78±0.26) cm/decade during 1993-2009. It is hypothesized here that this increase in the sea height anomaly residuals is linked to the observed increase in mesoscale activity in the region for the same period.

5. The apparent seasonality of the Loop Current northward penetration was positively correlated to larval fish density, with higher mean larval concentrations in the eastern Gulf of Mexico when the Loop Current intruded farther north and vice versa.

6. Larvae of *T. thynnus*, *E. alleteratus, Auxis* spp., *Thunnus* spp., and *Coryphaena* spp. were less abundant in the core of both cyclonic and anticyclonic mesoscale features, and more abundant near anticyclonic frontal areas of the Gulf of Mexico. Specifically, larvae of *T. thynnus*, *E. alleteratus,* and *Auxis* spp. were most often present within the boundaries of anticyclonic features, and also in common waters of the Gulf of Mexico, defined as the background waters in between the boundaries of mesoscale features.

7. The distributions of *T. thynnus* larvae in the Gulf of Mexico were similar to the distributions of *T. thynnus* larvae in the western Mediterranean, in which tuna spawning grounds were related to anticyclonic features, and *T. thynnus* larvae were more abundant near frontal areas.

8. *Thunnus* spp. larvae were distributed more broadly and over a wider range of sea surface height than *T. thynnus,* which confirms reports that adult tropical tunas have broader habitat preferences in the GOM than *T. thynnus.*

9. Analysis of geostrophic currents in the mesoscale features of the Gulf of Mexico and larvae size and age indicate that larvae outside the Loop Current region were likely to be near to the spawning location in the northern GOM region.

10. The mesoscale circulation was shown to introduce significant variability into time series that rely on plankton surveys in the region.

11. Preliminary investigations show a clear negative correlation between gradients of pressure and the migrations of the Loop Current, suggesting that the Loop Current dynamics might be modulated at some extent by atmospheric forcing.

Preliminary investigations on westward propagating long-lived mesoscale eddies indicate that the number of westward propagating cyclonic eddies, likely originated in the Loop Current western boundary, is higher than the number of westward propagating anticyclonic eddies. This might be crucial in rethinking the “momentum imbalance paradox”

Chapter VII: Resumen en español (Spanish summary)

1. Introducción

El resumen en español se organiza de la siguiente manera. La sección 2 presenta las principales metas y objetivos de la tesis. La sección 3 describe las principales características de la oceanografía física y de los ecosistemas del Golfo de México (GDM): por un lado haciendo especial hincapié en la dinámica de la Corriente de Lazo (CL) y el desprendimiento de anillos, y por otro resaltando los niveles biológicos y sus factores limitantes en el GDM. El planteamiento adoptado y la metodología utilizada en este trabajo de tesis se describe en la sección 4. Los principales resultados y una discusión general de las aportaciones originales de los capítulos centrales (Capítulos III y IV) se presenta en la sección 5. Las futuras líneas de investigación se exponen y discuten en la sección 6. Finalmente, la sección 7 concluye con un resumen de las principales conclusiones.

2. Objetivos de la investigación

El objetivo general de este estudio es investigar la conexión entre las primeras fases de desarrollo de los peces, usualmente denominado ictioplancton, y la variabilidad de las estructuras de mesoescala en el Golfo de México. Este vínculo se explora en esta tesis mediante el uso de observaciones satelitales y muestreos biológicos *in situ*. Hay muchos ejemplos en la literatura de correlaciones entre los cambios de los parámetros físicos del océano y cambios en los recursos pesqueros (Ortner et al. 1984; Mann 1993; Bakun 2006). Comúnmente, estas correlaciones se mantienen vigentes durante unos años para luego dejar de serlo. Sin embargo esto no significa que la correlación fuera invalida, sino que requiere un mejor entendimiento del mecanismo de interacción en el complejo sistema entre la física y la biología antes de que podamos entender la dependencia temporal de dichas correlaciones.

El Golfo de México es un mar semi-cerrado bordeado por los Estados Unidos, México y Cuba. El sustento de las economías de esta comunidad internacional depende de los bienes y servicios que ofrece el GMD; siendo las pescaderías uno de los servicios más importantes. Considerado como una joya entre los recursos naturales del hemisferio oeste, los pantanos del GDM son fuente de una importante industria de marisco, y sus aguas cercanas a la costa sostienen ricas pescaderías comerciales y recreacionales, siendo la zona de desove y hábitat de especies de peces pelágicos de relevancia comercial (Shipp 1999; Rabalais et al. 1999). No obstante, el GDM es susceptible al cambio climático y presiones antropogénicas, como demuestra el hecho que años de intenso desarrollo y explotación han resultado en cambios significativos de los recursos pesqueros. Los serios problemas que está afrontando el GDM, incluyendo modificación de hábitat, contaminación marina y sobre-explotación, están generando impactos que todavía no están determinados en el gran ecosistema marino que constituye el GDM.

La región se caracteriza por una compleja y altamente variable circulación oceánica, con una intensa actividad de mesoescala que está dominada por dos estructuras principales: la Corriente de Lazo (CL) y los anillos desprendidos por la CL. Estas poderosas estructuras oceánicas transportan anomalías en las propiedades físicas, biológicas y químicas de la región, y afectan –ya sea directamente como indirectamente a través de estructuras secundarias- prácticamente a cada aspecto de la oceanografía del Golfo. Es por estos motivos que la investigación propuesta se enfoca en la monitorización satelital de la variabilidad

espacio-temporal de la CL y anillos, así como en la regulación de las distribuciones de larvas de algunas especies llevada a cabo por estructuras oceánicas de mesoescala.

Varios estudios muestran que las condiciones físicas y biológicas tanto para las larvas como para los peces adultos en el GDM exhiben una elevada variabilidad espacial y temporal (Müller-Karger et al. 1991), la cual está probablemente ligada a los patrones de desove (Ortner et al. 1984; Bakun 2006). La variabilidad en las abundancia larvarias de algunas especies pelágicas ha sido ligada en recientes estudios a parámetros ambientales –tales como la temperatura del agua, la salinidad, la profundidad del agua, y la duración de la luz del día- y la distribución de plancton en la región del GDM (Muhling et al. 2010; Richardson et al. 2010). Dado que algunos ecosistemas son susceptibles a ser altamente afectados por cambios en las condiciones ambientales y en la distribución del plancton (Teo and Block 2010), la variabilidad de las propiedades oceánicas y las estructuras de mesoescala en el GDM se espera que tengan un efecto directo en los ecosistemas de esta región. En particular, recientes estudios muestran que un conocimiento detallado de la variabilidad temporal y espacial de las estructuras oceánicas de mesoescala al este del GDM es fundamental para entender las condiciones ambientales que influyen en las distribuciones de larvas de diversas especies de peces, sus lugares de desove, crecimiento larvario y consecuente variabilidad en la supervivencia larvaria y juvenil (Richards et al. 1993; Bakun 2006). Sin embargo, parece que existe una falta de información sobre cómo los ecosistemas responden a patrones de variabilidad a corto y largo plazo en la regiones, lo cual puede ayudar adaptarse a posibles presiones de cambio climático en el GDM.

De acuerdo con todo lo expuesto, el principal objetivo de esta tesis es investigar, evaluar y analizar la conexión entre los recursos pesqueros y la variabilidad temporal y espacial de las propiedades oceánicas asociadas a la actividad de mesoescala en el GDM. A este respecto, este trabajo proporciona una mejor descripción de la dinámica de mesoescala de la CL y el campo de anillos asociado, y arroja luz sobre la regulación física de la distribución de algunas especies de larvas en el GDM.

3. Oceanografía física y ecosistemas marinos en el Golfo de México

3.1 Introducción

Las primeras descripciones de la circulación oceánica en el Golfo de México se remontan a los primeros años de las exploraciones europeas de las Américas, con unos primeros mapas de circulación a gran escala ya en 1578 (Peterson et al. 1996). Similarmente a estas primeras descripciones, el estudio de las distribuciones de peces en la región también comenzó durante la exploración de las Américas con la creación de diagramas de los peces nativos del este y oeste de la Florida (Romans and Concise 1775).

Actualmente, en el GDM están censadas 3.302 especies (Galtsoff 1954), de las cuales 986 están listadas como especies de peces distribuidas en 197 familias (Froese and Pauly 2011). Esta biodiversidad se apoya en los procesos físicos oceanográficos que modulan la fisiología, metabolismo, comportamiento y tasas crecimiento de la vida marina (Blaxter 1991). Por tanto es crucial conocer los procesos oceanográficos que dominan en la región para explorar la regulación física de recursos pesqueros en el GDM.

Extensos estudios de campo y de modelización han examinado el GDM durante los últimos 50 años (Amante et al. 2009). Lo que principalmente ha llamado la atención han sido la caliente Corriente de Lazo y los grandes anillos anticiclónicos que repetidamente se desprenden de dicha corriente (Vukovich et al. 1979; Vukovich and Maul 1985; Yukovich 1986; Maul and Vukovich 1993; Elliott 1982; Lewis and Kirwan Jr 1987; Forristall et al. 1992; Sturges and Leben 2000; Nof 2005; Zavala-Hidalgo et al. 2006; Lugo-Fernández 2007; Alvera et al. 2009; Lugo-Fernández and Leben 2010). Sin embargo, comparado con el conocimiento que se ha acumulado sobre los procesos físicos en el GDM, poco se conoce sobre la oceanografía biológica de la región y la mayoría de estudios biológicos en el GDM se han restringido a determinadas zonas del Golfo (*e.g.*, Ortner et al. 1984; Biggs et al. 1984, 1988).

El área de estudio de este trabajo es la región comprendida entre 20°N y 31°N, y entre 80°W a 97°W. No obstante, el GDM es una región geográfica que, junto con el Mar Caribe, el Estrecho de la Florida y la adyacente región del Atlántico Norte oeste, conforman el Mar Mediterráneo Americano (Sverdrup et al. 1942) o el Mar Intra-Americano (Figura 7.1).

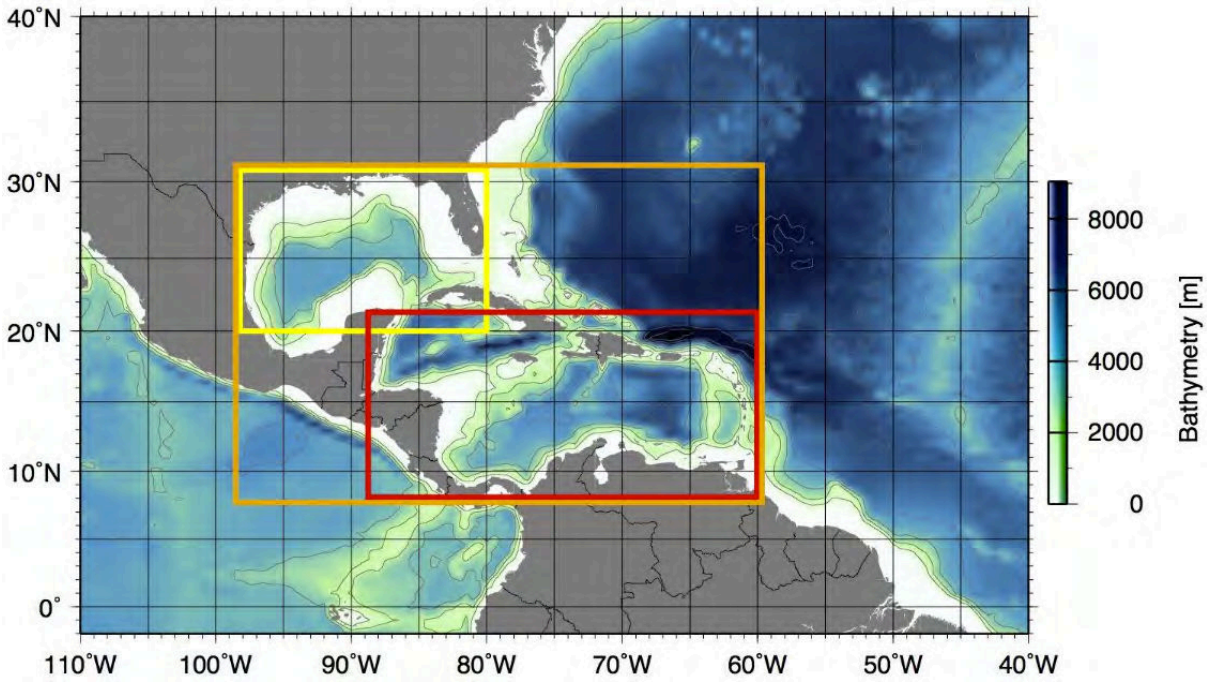

Figura 7.1. Mar Intra-Americano (rectángulo naranja) abarcando el Mar Caribe (rectángulo rojo) y el Golfo de México (rectángulo amarillo y región de estudio aquí). Los datos batimétricos fueron obtenidos de ETOPO1 (Amante et al. 2009), y los contornos en gris indican isóbatas desde 500 a 8000 m con intervalos de contorno de 1000 m.

En los siguientes apartados se va a mostrar una descripción general de la circulación del Mar Intra-Americano y detallada el Golfo de México, desde su topografía hasta los posibles mecanismos para explicar la variabilidad de la Corriente de Lazo y el campo de anillos. Esto dará lugar a explorar las bases de la biología marina y pescaderías de la región, desde los más bajos niveles biológicos hasta las comunidades de larvas de peces. Finalmente, se resumirá el estado del arte de la teledetección y también su importancia como una herramienta apropiada para estudiar acopladamente la física y la biología de los océanos.

3.2 Circulación en el Mar Intra-Americano

Con el fin de entender la circulación del Mar Intra-Americano (Figura 7.2), el principal foco aquí será el Mar del Caribe, el cual es también importante para entender la circulación en el GDM. El Mar del Caribe está caracterizado por cuencas profundas y por una compleja batimetría y geometría. Al sur y al oeste está limitado por América del Sur y América Central, al norte está limitado por Cuba, La Española, Puerto Rico y las Islas Vírgenes (Antillas Mayores), y al este por la cadena de islas de las Antillas Menores. El Mar del Caribe está compuesto por numerosas masas de agua de diferentes orígenes que entran a través de los diferentes pasajes entre islas (Wüst and Gordon 1964; Metcalf 1976; Morrison and Nowlin Jr 1982). Algunas de estas aguas se originan en el Atlántico Norte, mientras que otras lo hacen en el Atlántico Sur con orígenes mucho más lejanos (*e.g.*, el Océano Indico). La circulación está también influida por los influjos de agua dulce del Amazonas, Orinoco y río Magdalena (Froelich et al. 1978; Restrepo and Kjerfve 2000; Hellweger and Gordon 2002; Muller-Karger and Castro February; Corredor et al. 2004).

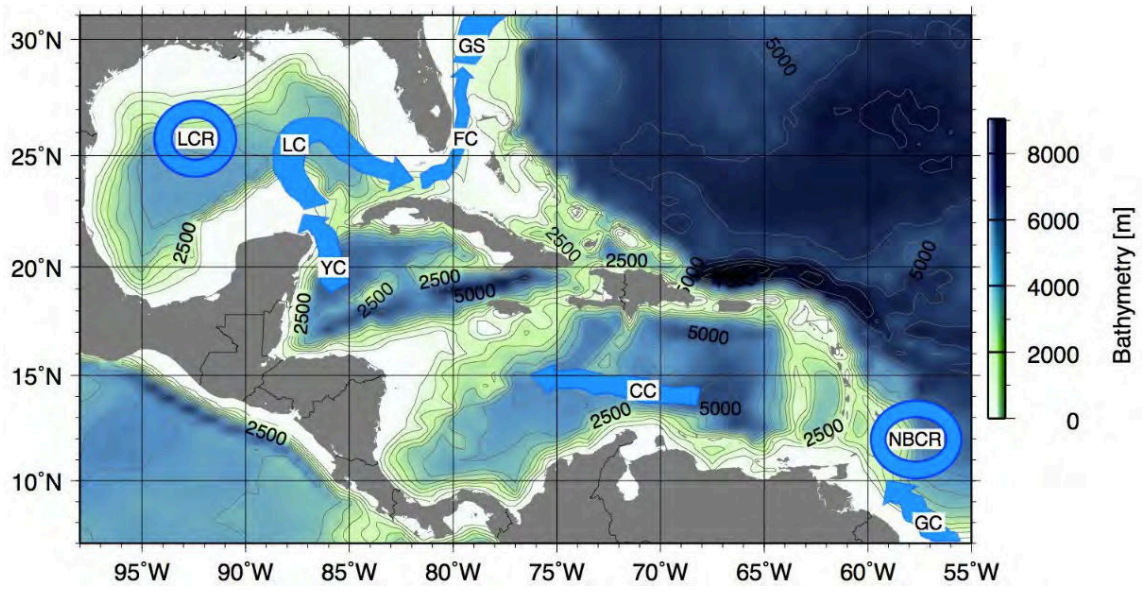

Figura 7.2. Principales estructuras oceanográficas del Mar Intra-Americano, abarcando el Golfo de México y el Mar Caribe, con dibujos esquemáticos de la Corriente de Guyana (GC), el anillo de la Corriente Norte de Brasil (NBCR), la Corriente del Caribe (CC), la Corriente de Yucatán (YC), la Corriente de Lazo (LC en la figura), el anillo de la Corriente de Lazo (LCR), la Corriente de la Florida (FC), y la Corriente del Golfo (GS). Los datos batimétricos fueron obtenidos de ETOPO1 (Amante et al. 2009), y los contornos en gris indican isóbatas desde 500 a 8000 m con intervalos de contorno de 500 m.

El flujo mas energético en el Mar del Caribe se encuentra en el tercio más al sur de la región y se denomina Corriente del Caribe (CC), la principal circulación superficial del Mar del Caribe (Wüst and Gordon 1964; Hernández-Guerra and Joyce 2000). En el Caribe central, la CC parece tomar la forma de dos chorros centrados cerca de 13°N y 15°N, separados por un débil flujo hacia el este. La Corriente del Caribe vuelve a confluir hacia el noroeste del Caribe y pasa a denominarse la Corriente de Yucatán (YC). La YC fluye a través del canal del Yucatán, el cual conecta el Mar del Caribe con el Golfo de México y forma la Corriente de Lazo, la cual sale del GDM al sur de la Florida para convertirse en la Corriente de Florida, o la que es considerada como el inicio de la Corriente del Golfo. Una clara descripción de la distribución de los influjos medios en los pasajes que conectan el Océano Atlántico con el Mar del Caribe, y luego con el Golfo de México se muestran en la Figura 7.3 (datos de Johns et al. 2002).

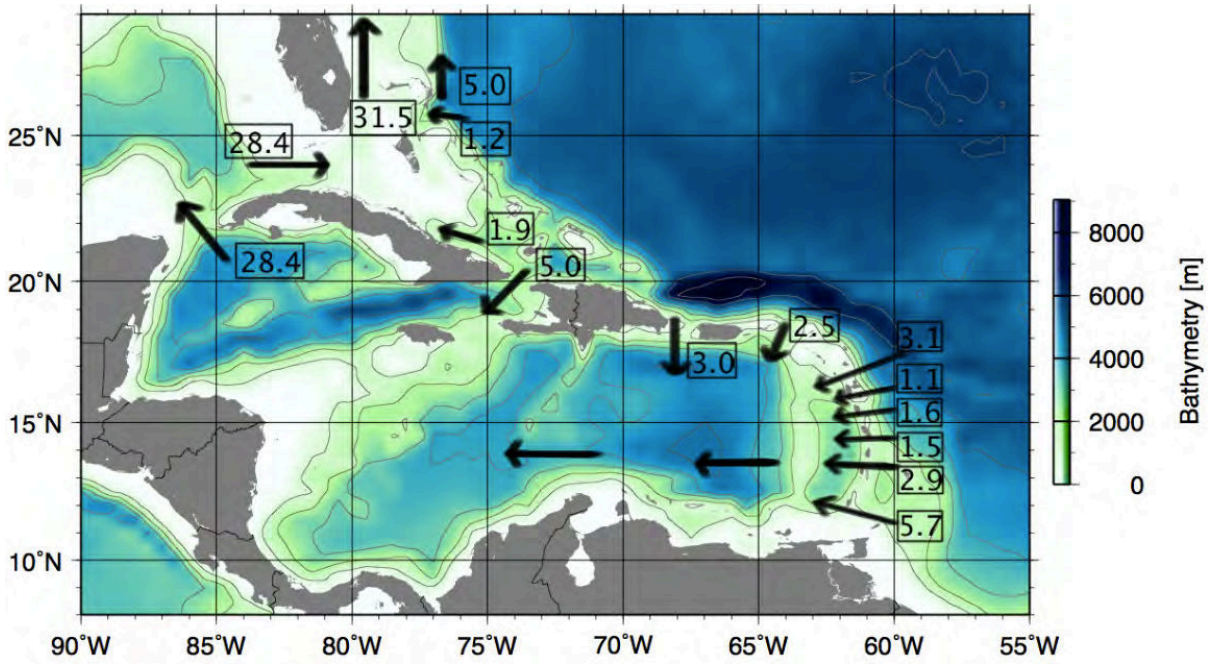

Figura 7.3. Transportes medios (Sv) a través de los principales pasajes en el Mar Intra-Americano a partir de combinar simulaciones numéricas con forzamientos de vientos con observaciones de transportes (Johns et al. 2002; Smith 2010). Los datos batimétricos fueron obtenidos de ETOPO1 (Amante et al. 2009), y los contornos en gris indican isóbatas cada 1000 m.

Con respecto a su dinámica, la circulación del Caribe se encuentra bajo la constante influencia de los vientos alisios del Atlántico Tropical, que varían en función de la migración al norte de la zona de convergencia intertropical (ITZC), desde su punto más al sur en invierno (aproximadamente en el Ecuador) a su posición más al norte en verano (aproximadamente alrededor de 11°N). El forzamiento atmosférico en forma de ciclones tropicales y huracanes también juega un papel significativo en dar forma a la circulación oceánica. Con respecto a la circulación en el Caribe en el rango de la mesoescala, la más reciente explicación de la variabilidad de mesoescala incluye los anillos del norte de Brasil (Goni and Johns 2001), y relaciona la variabilidad de mesoescala con olas de remolinos, que ocurren cuando anillos anticiclónicos de la corriente de Brasil colisionan con los pasajes de las Bajas Antillas (Andrade et al. 2000).

Los remolinos del Caribe pueden afectar significativamente a la intrusión de la Corriente de Lazo y al compotamiento de desprendimiento de anillos anticiclónicos (Oey et al. 2003). Una primera explicación potencial es que el desprendimiento de anillos de la CL exhibe correlación con el flujo de vorticidad a traves del canal de Yucatán (Candela et al. 2003). Este flujo de vorticidad potencial es transportado por remolinos y meandros en el Mar del Caribe. Sin embargo, el efecto de los remolinos del Caribe en la circulación del Caribe y del Golfo de México no se comprende completamente.

3.3 Oceanografía del Golfo de México

Aquí se resume el estado del arte de 1) la topografía local del Golfo de México, 2) la circulación general del GDM, 3) los flujos costeros en sus márgenes continentales, 4) los mecanismos físicos que conducen las migraciones de la Corriente de Lazo y disparan lasseparaciones de anillos, y 5) las condiciones de las aguas arriba que definen la circulación a gran escala de sus aguas circundantes. Esta sinopsis posee una naturaleza básicamente descriptiva con el propósito de asentar las bases para llevar a cabo una monitorización a largo plazo de las estructuras de mesoescala en el GDM y poder integrar los resultados de dicha monitorización para comprender mejor los procesos que regulan las distribuciones de larvas en la región.

3.3.1 Topografía

El Golfo de México yace aproximadamente entre los límites del oeste de la Florida; el estado de Texas y la costa este Mexicana; y las costas de Luisiana, Alabama y Misisipi al norte. Ocupando una cuenca tipo mediterránea conectada con el Caribe por el estrecho del Yucatán y con el Océano Atlántico por el estrecho de la Florida, el GDM ocupa una superficie de 564.200 km^2, con una dimensión máxima este-oeste de 1.575 Km y una dimensión máxima norte-sur de aproximadamente 900 km.

La topografía del fondo marino del GDM se ilustra en la Figura 7.4. Una plataforma continental estrecha en algunas zonas y amplia en otras (~0-200 m de profundidad), se encuentra localizada en los límites del GDM y constituye aproximadamente el 35% de su área. Casi la mitad de la cuenca es de escasa profundidad y solamente una cuarta parte del GDM es muy profunda (~3.000 m). La zona más profunda, el Sigsbee Deep, tiene aproximadamente 3.850 m de profundidad.

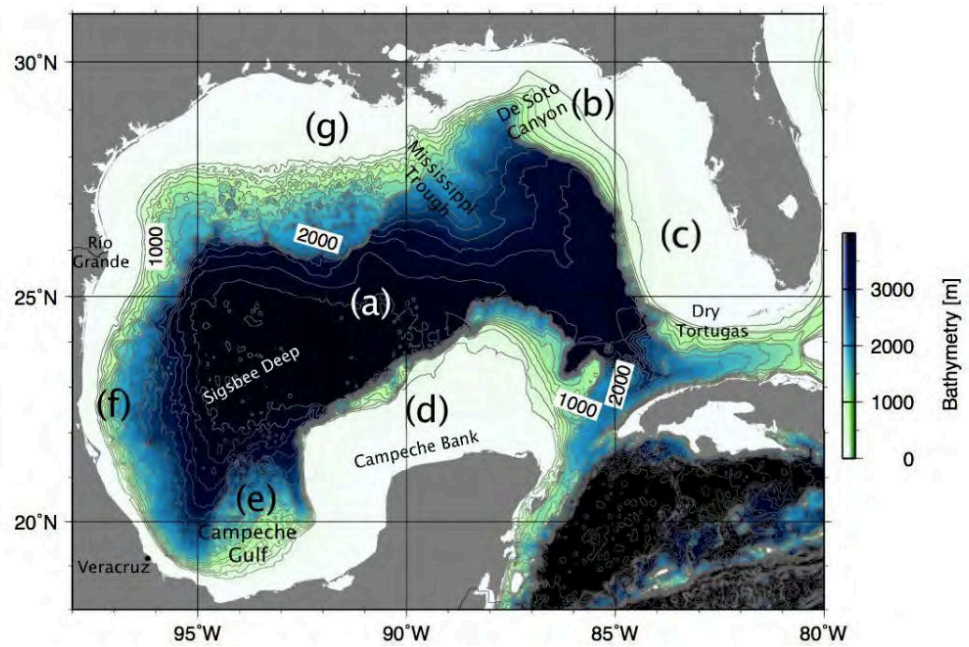

Figura 7.4. Topografía del fondo del Golfo de México (GDM), datos batimétricos obtenidos de ETOPO1 (Amante et al. 2009) y los contornos en gris indican isóbatas desde 500 a 8000 m con intervalos de contorno de 1000 m.. El mapa ilustra las siete regiones geográficas en las que se divide el GDM: (a) Cuenca del GDM, (b) Noreste del GDM, (c) Plataforma continental del Sur de la Florida, (d) Banco de Campeche, (e) Bahía de Campeche, (f) Plataforma continental del este del GDM, y (g) Norte del GDM.

3.3.2 Circulación general

La componente más prominente y energética de la circulación general del GDM es la Corriente de Lazo, los remolinos de mesoescala, y los anillos que se han desprendido de la corriente. Estos tres componentes y la formación de un anillo anticiclónico por el estrangulamiento de la CL se pueden observar claramente en la Figura 7.5.

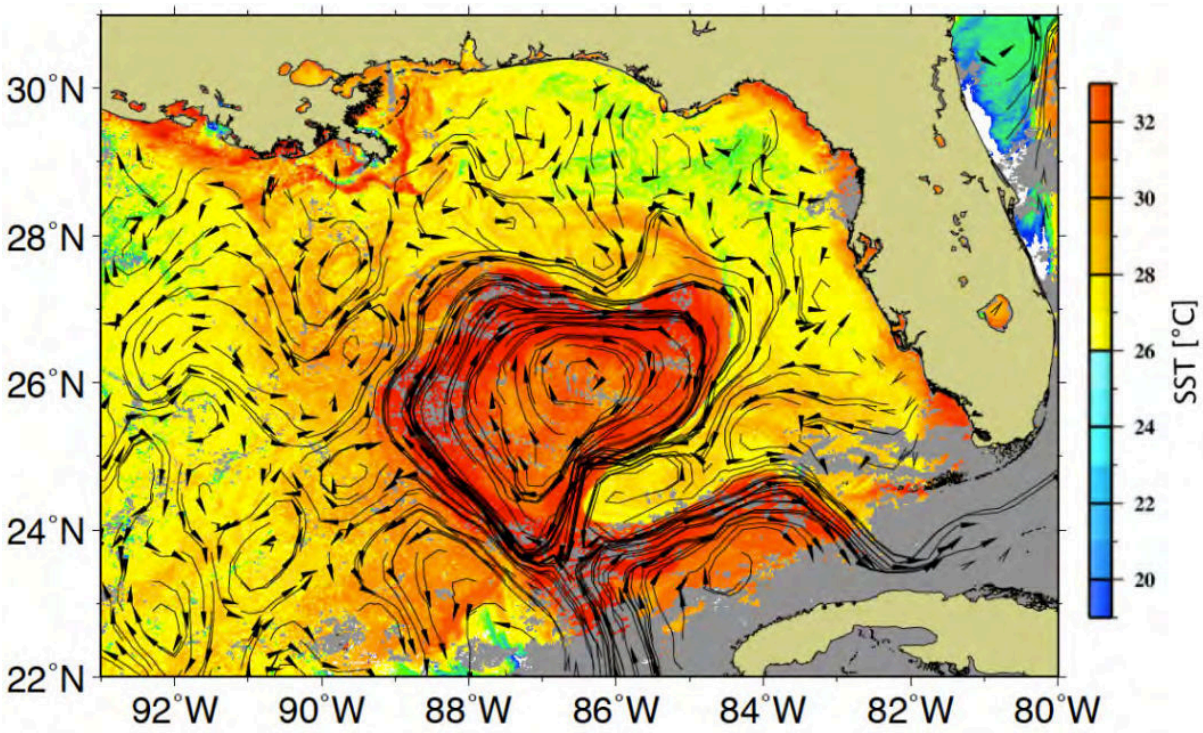

Figure 7.5. Temperatura superficial del mar (SST) el 25 de abril de 2011, mostrando la Corriente de Lazo (CL) extendida en el Golfo, y un caliente anillo anticiclónico formándose a partir de la estrangulación de la corriente. Nótese la aparición de remolinos ciclónicos a lo largo de los márgenes exteriores de la CL, en particular dos ciclones localizados en el "cuello de botella" de la corriente (aproximadamente centrados en 23°N, 88°W y 24.5°N, 85.5°W). Los datos fueron obtenidos del Advanced Very High Resolution Radiometer (AVHRR), disponible con una resolución de 2 días en una malla de 18 km. Las flechas negras en el fondo de la imagen representan corrientes geostróficas derivadas de datos satelitales.

Anillos anticiclónicos se desprenden de la CL en el este del GDM a intervalos irregulares (Vukovich 1988a; Sturges and Leben 2000; Leben 2005) en el rango de 4 a 18 meses (Sturges and Leben 2000). Llegados a este punto se debe distinguir bien entre remolinos de mesoescala y anillos. Aunque normalmente hallamos en la literatura que a los

anillos de la CL se les denomina indistintamente anillos o remolinos, es conveniente especificar que remolinos y anillos son estructuras diferentes. Justo después de su formación, estas estructuras son anillos, con poca o ninguna vorticidad relativa en su centro, mientras que más tarde el centro gana suficiente velocidad angular (a través de difusión radial del anillo) como para hablar propiamente de un remolino (Auladell et al. 2010). El anillo de la CL normalmente representa una fracción que se ha separado de la corriente principal tras describir un bucle o lazo, y es por ello que durante sus estadios iniciales –antes de que la difusión tenga lugar– el anillo está compuesto de una región frontal que retiene la intensa corriente del lazo en sus bordes, y una región central en su núcleo donde las aguas están estancadas. Por otro lado, mientras los remolinos de mesoescala muestran radios comparables al radio de deformación Rossby (~40 km, (Chelton et al. 1998)), el radio de los anillos es mucho más grande (~150 km, (Oey et al. 2005)). Un modelo simple de difusión y advección con un coeficiente de difusión efectivo (Sangrà et al. 2007) es apropiado para simular aproximadamente la evolución temporal de la velocidad angular de remolinos que comienzan con una tipo de rotación de sólido rígido (Auladell et al. 2010). La ecuación de difusión y advección para estudiar la evolución de la velocidad angular, que se deriva de las ecuaciones de momento en coordenadas cilíndricas bajo las aproximaciones del plano-f y simetría axial, es la siguiente:

$$\frac{\partial \omega}{\partial t} + u_r \frac{\partial \omega}{\partial t} = \frac{1}{r} \frac{\partial^2 (Kr\omega)}{\partial r^2} \tag{16}$$

donde ω es la velocidad angular, $u_r$es la velocidad radial, K es un coeficiente de difusión horizontal, t es el tiempo, y r la posición radial.

En base a lo expuesto anteriormente y a la naturaleza de su generación, rotación, robustez y su larga vida (Fuglister 1971; Olson 1991), los anillos anticiclónicos de la CL serán llamados anillos en esta tesis, y no remolinos. Estos grandes anillos desprendidos por la CL tienen radios de aproximadamente 150 km, velocidades de giro de 1.8-2 m s^{-1}, alrededor de 800 m de profundidad (similarmente a la CL), se trasladan hacia el oeste en el GDM en una escala de cien a mil kilómetros y tienen un periodo de vida que puede variar de meses a años (Oey et al. 2005). En su trayecto hacia el oeste, los anillos transportan anomalías en las propiedades físicas, biológicas y químicas, afectando así a cada aspecto de la circulación del GDM. Una vez los anillos se están propagando hacia el oeste, estructuras ciclónicas pueden ocasionalmente partir los anillos dividiéndolos en remolinos más pequeños (Biggs et al. 1996).

El proceso de desprendimiento puede tomar entre días y varias semanas y a menudo, después de que el anillo se ha separado, se vuelve a unir a la CL (Sturges et al. 1993). La frecuencia de separación de anillos ha sido estudiada por varios autores (Maul and Vukovich 1993; Sturges and Leben 2000; Leben 2005), y se ha establecido que el intervalo de tiempo entre desprendimiento de anillos varia de 6 a 17 meses (Molinari, 1980), con periodos primarios de 6 a 11 meses (Sturges and Leben 2000).

Varios procesos participan en el mecanismo de desprendimiento de anillos. Un mecanismo generalizado de desprendimiento, parcial o completo, también puede ser explicado mediante el rol que juegan pares de remolinos ciclónicos uno a cada lado de la CL juegan un papel clave. El desprendimiento puede ocurrir después de que una extendida CL sea estrangulada por remolinos ciclónicos, aunque no todo estrangulamiento está seguido por un desprendimiento (Schmitz et al. 2005). La primera descripción observacional fue publicada hace 40 años cuando se observaron ciclones periféricos en los límites de la CL (Cochrane 1972). A esto se le denominó el *primer modo de desprendimiento*. Otra visión del desprendimiento se observa cuendo la CL adquiere una orientación este-oeste en su extremo más superior (Schmitz et al. 2005). Este proceso tiende a ocurrir después de un primer desprendimiento y se le llama *segundo modo de desprendimiento*. Una combinación de estos dos modos también puede ocurrir, englobando ambos modos de desprendimiento al mismo tiempo (Schmitz 2005). Una lista exaustiva de estudios previos muy relevantes con respecto a los elementos que participan en el proceso de desprendimiento de anillos de la CL puede encontrarse en las referencias y están descritos en mayor detalle en el Capítulo II de esta tesis (Cochrane 1972; Elliott 1982; Fratantoni et al. 1998; Molinari et al. 1978; Sturges and Leben 2000; Sturges et al. 1993; Vukovich 1988; Vukovich and Maul 1985; Zavala-Hidalgo et al. 2003; Zavala-Hidalgo et al. 2006).

3.3.2 ¿Hay un único mecanismo para las intrusiones de la Corriente de Lazo y los desprendimientos de anillos?

En esta sección se muestran los mecanismos físicos que pueden liderar las intrusiones de la CL, disparar el desprendimiento de anillos, y establecer el estado inicial después de una separación de anillo.

Cuando discutimos las estructuras de circulación oceánica es relevante tener clara la idea del radio de deformación de Rossby baroclínico (o interno), el cual juega un papel importante en la teoría de la circulación oceánica a gran escala puesto que describe las escalas horizontales de los procesos de mesoescala y representa una medida importante de la dinámica oceánica. El radio de deformación de Rossby baroclínico es el ratio entre las velocidades de fase de las ondas internas con respecto al parámetro de Coriolis, y fundamentalmente indica la escala horizontal (longitud) a la que los efectos de rotación llegan a ser tan importantes como las ondas de gravedad (flotabilidad). Los cálculos para el GDM dan un primer radio de deformación de Rossby baroclínico de aproximadamente 40 km (Chelton et al. 1998).

El mecanismo que explica el comportamiento de la CL y el desprendimiento de anillos ha sido ampliamente estudiado, especialmente por Hurlburt y Thompson (1980) en su clásico artículo de modelización (de ahora en adelante HT), y más recientemente ha sido interpretado utilizando la idea del "*momentum imbalance paradox*" de Pichevin y Nof (1997)[6] (de ahora en adelante PN) (ver también Nof y Pichevin, 2001; Nof 2005). Dichos estudios muestran que el desprendimiento de anillos puede ser capturado por un modelo de gravedad reducida de 1.5 capas sin necesidad de considerar la interacción con la topografía del fondo marino. En particular, el artículo de PN tiene un especial interés ya que analiza las consecuencias de un flujo Q que se mueve hacia el norte por un canal estrecho (*i.e.*, de una anchura comparable al radio Rossby o inferior) y que desemboca en un océano abierto (Figura 7.6).

[6] ver también (Nof y Pichevin, 2001) y (Nof, 2005)

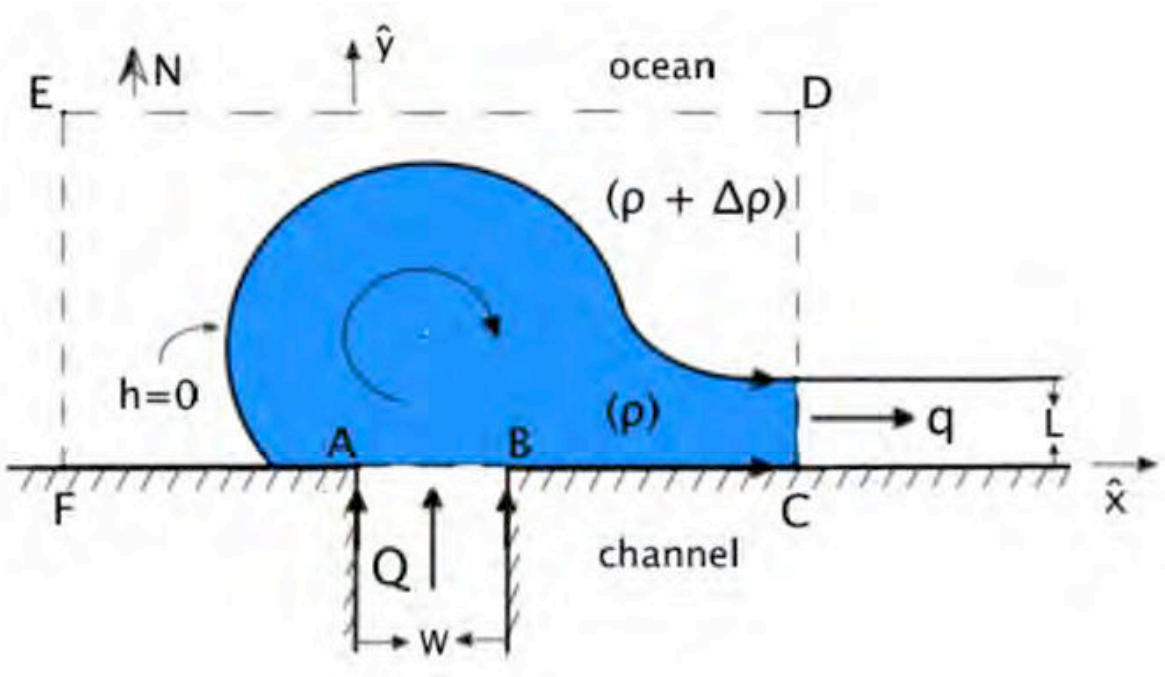

Figura 7.6. Diagrama que ilustra el "*momentum imbalance paradox*". Un canal abierto hacia el norte por el que fluye agua de densidad ρ se vacía en un océano estanco con densidad $(\rho + \Delta\rho)$. A lo largo del frente se asume que el espesor es h=0. Se asume que las líneas de corriente en el canal permanecen paralelas a las paredes del canal hasta que se alcanza la línea horizontal de la desembocadura (i.e., sección AB). La hipotética configuración de estado estacionario no es posible en plano-f ni el plano-β. En el escenario de PN un flujo continuo no puede existir debido a que el momento del flujo de corriente no está en equilibrio.

La visión tradicional de este fenómeno era que, debido a la fuerza de Coriolis, una corriente entrante como la mostrada gira hacia la derecha (mirando hacia fuera de la costa o canal) y forma una corriente de frontera (o limítrofe) occidental que fluye hacia el este. En este escenario, un frente (correspondiente a la interfase superficial) separa las aguas oceánicas y las aguas anómalas (las entrantes) (Figura 7.6). Al integrar la ecuación del momento en el eje x sobre un dominio rectangular exterior al flujo (área FEDC en la Figura 7.6), PN muestran que el momento integrado que se ejerce en el dominio por el aguan que sale del dominio a la derecha no puede ser equilibrada en un estado estacionario (lo que da una fuerza de flujo a lo largo de la costa no equilibrada). Esta paradoja en el balance del momento, "*momentum imbalance paradox*" como la llamaron los autores, puede resolverse si se permite que anillos se vayan desprendiendo hacia la izquierda (plano-β, Figura 7.7a) o bien si el flujo crece ininterrumpidamente (plano-f, Figura 7.7b).

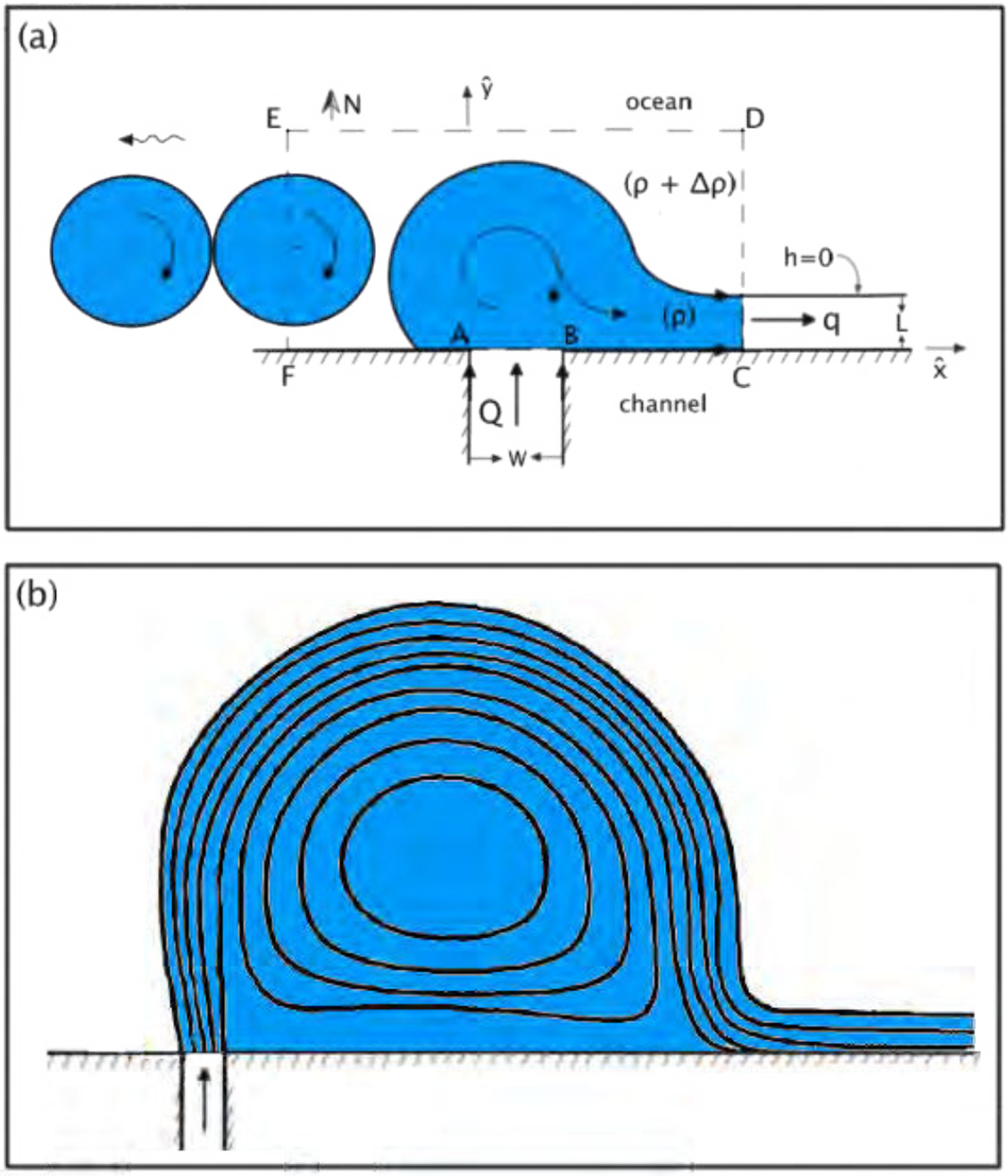

Figura 7.7. Diagramas que muestran (a) la resolución de PN del "momentum imbalance paradox" y (b) los contornos flujo del plano-f. A causa de la paradoja esbozada en la Figura 7.6, el flujo de la corriente entrante no está en equilibrio. Como resultado, hay dos posibilidades. En un plano-β (a), el crecimiento del anillo anticiclónico es finalmente detenido y, consecuentemente, se desprenden anillos periódicamente hacia la izquierda. A través del efecto β, estos remolinos se ven forzados a propagarse hacia la izquierda. Pichevin y Nof (1997) obtienen su solución analítica mediante la identificación del momento del flujo a través de EF con el momento del flujo a través de CD. (b) Por el contrario, en un plano-f), el remolino crece eternamente y el flujo de masa de corriente que sale es menor que el flujo de masa de corriente entrante.

En resumen, el modelo de HT puede ser simple pero captura remarcablemente bien las características generales de la variabilidad de la CL: su extensión (crecimiento), el desprendimiento de los anillos, y las retiradas de la CL. Los periodos de desprendimientos predichos por PN (~10 meses) están en concordancia con los periodos predichos por HT (~12 meses). Además, las predicciones de PN con respecto al tamaño del anillo y la velocidad están de muy de acuerdo con las observaciones. El modelo también ayuda a desmentir duradera idea falsa de que la CL desprende remolinos en respuesta a una casi anual variación del flujo entrante a través del canal de Yucatán.

El océano real funciona de una manera curiosa y compleja: los periodos de anillos observados cubren un rango de tiempo más extenso (de 3 a 18.5 meses); la CL puede extenderse y retirarse (escalas de ~ meses y 100 km) sin necesariamente desprender anillo alguno; un anillo puede temporalmente desprenderse para luego volverse a unir a la CL (escalas de tiempo de ~ semanas); meandros frontales y remolinos pueden desarrollarse e influir en el desprendimiento de los anillos; la plataforma y la vertiente del Yucatán, la capa profunda y las influencias del Caribe pueden ser significativas, etc. Los modelos presentes y futuros tienen el reto de capturar algunas de estas complicaciones.

3.3.3 Consideraciones aguas arriba

El flujo neto que entra en el GDM es de origen del Atlántico Sur en aproximadamente un 40% (Schmitz and Richardson 1991b), y existe también una contribución considerable de agua profunda, mayoritariamente aguas intermedias Antárticas (Schmitz and Richardson 1991b; Schmitz Jr 2004). El otro componente importante de aguas entrantes en el Mar del Caribe y luego en el GDM a través de la Corriente de Lazo tiene su origen en el Atlántico Norte (Johns et al. 2002; Hamilton et al. 2005).

Los dos pasajes que dan entrada y salida al transporte de masa en el GDM son el canal de Yucatán (entre Yucatán y Cuba) y el estrecho de la Florida (entre Cuba y la Florida). Asumiendo incompresibilidad en la ley de conservación de la masa, la ecuación del balance de volumen en el GDM puede escribirse como

$$\frac{dV_{GOM}}{dt} = T_Y + T_F + R + (P - E) \quad (17)$$

donde V_{GOM}es el volumen total de agua en el GDM, T_Y es el volumen transportado a través del canal de Yucatán, T_F es el volumen transportado a través del estrecho de la Florida, R es la descarga de los ríos y $(P - E)$ es el volumen transportado debido a la precipitación menos evaporación. Estimaciones de $R + (P - E)$ por Etter (1983) muestran que el término es un 0.1% de T_Y y T_F, mientras que estimaciones satelitales muestran que $\frac{dV_{GOM}}{dt}$ también es un término pequeño (Bunge et al. 2002) con lo que los grandes términos en la ecuación (17) (T_Y y T_F) están prácticamente en equilibrio. Esto significa que el transporte hacia el GDM a través de la Corriente de Yucatán está en equilibrio con el transporte a través del estrecho de la Florida.

3.4 Biología marina y pescaderías en el Golfo de México

Los organismos planctónicos son cualquier organismo errante (sea animal, plantas, arqueas o bacterias) que habita en la zona pelágica de los océanos, mares, o aguas dulces. Estas agregaciones se encuentran influidas por las características biológicas de dichos organismos y por las características físicas de su hábitat (Ortner et al. 1978; Owen 1981; Mackas et al. 1985).

Entre los organismos planctónicos, el ictioplancton se refiere a los huevos y larvas de peces. Aunque normalmente son considerados partículas inertes, las larvas de peces son componentes interactivos del ecosistema (Cowen 2002; Fuiman 2002). La mayoría de los peces tienen un estadio pelágico, el cual varia de semanas a meses (Brothers et al. 1983; Victor 1986) y durante el cual importantes cambios ocurren en cortos intervalos de tiempo, como por ejemplo un importante aumento de la biomasa, con un aumento de hasta 5 órdenes de magnitud (Werner and Gilliam 1984; Houde 1987; Miller et al. 1988). Este incremento de masa durante el periodo larvario evidencia la importancia de este estadio como un modulador del reclutamiento (Houde 1987). De esta manera, es importante estudiar el ictioplancton ya que las abundancias de huevos y la supervivencia de larvas es un indicador del tamaño de la población de adultos. Al ser usualmente más económico muestrear huevos y larvas que adultos, determinar la abundancia de ictioplancton deviene esencial.

3.4.1 Niveles biológicos y factores limitantes en el Golfo de México

Mientras que algunas formas de plancton son capaces de moverse independientemente y pueden nadar cientos de metros verticalmente en un día –un comportamiento llamado migración vertical diurna– su posición horizontal está principalmente determinada por las corrientes secundarias. Los organismos planctónicos se dividen principalmente en tres grupos tróficos: fitoplancton, zooplancton y bacterioplancton.

El fitoplancton está compuesto por organismos autótrofos, algas procariotas o eucariotas que viven cerca de la superficie del agua donde hay suficientemente luz como para permitir la fotosíntesis. Aunque el fitoplancton es demasiado pequeño para ser observado a simple vista, cuando se presenta en número suficientemente elevado puede aparecer como una decoloración del agua debido a la presencia de clorofila en las células del fitoplancton. Son responsables de la producción primaria la creación de compuestos orgánicos a partir del dióxido de carbono disuelto en el agua, y son parte de un proceso que sostiene la cadena alimenticia acuática (Peters and Marrasé 2000).

El Golfo de México ha sido habitualmente descrito como un sistema oligotrófico (Ortner et al. 1984). Sin embargo la combinación de datos satelitales con observaciones *in situ* (Muller-Karger et al. 1991; Gilbert et al. 1996; Gilbes et al. 1996, 2002; Muller-Karger and Fuentes-Yaco 2000; Biggs and Ressler 2001; Belabbassii et al. 2005; Biggs et al. 2008) han ayudado a demostrar que el GDM experimenta de intermedias a altas concentraciones de fitoplancton tanto en la plataforma como en ciertas zonas no costeras. En las zonas costeras la variabilidad en el fitoplancton del GDM está relacionada con afloramientos derivados del viento (Chuang et al. 1982; Schroeder et al. 1987; Yang and Weisberg 1999; Muller-Karger and Fuentes-Yaco 2000; Weisberg et al. 2000) y plumas de río (Gilbes et al. 1996; Walker 1996; Del Castillo et al. 2000; Hu et al. 2003). En aguas más profundas, las variaciones de clorofila-*a* están afectadas por la mezcla convectiva estacional, la divergencia y convergencia asociada a remolinos ciclónicos y anticiclónicos (Biggs and Muller-Karger 1994) y la incorporación de aguas dispersadas de efluentes de ríos (Biggs et al. 2008). La elevada variabilidad espacial de concentración de pigmentos en el GDM aumenta de este a oeste y de sur a norte debido a la diferencia en la estratificación térmica en la región, la intrusión de aguas pobres en nutrientes desde el Mar del Caribe occidental, los acontecimientos de frentes

frios y sistemas tropicales de baja presión, y la distribución de nutrientes del río Misisipi (Melo-González et al. 2000).

El zooplancton está compuesto por pequeños protozoos o metazoos que se alimentan de bacterioplancton, fitoplancton, otro zooplancton e incluso detritus. Como resultado, encontramos zooplancton en aguas superficiales donde hay recursos alimenticios en abundancia. Como ocurre con cualquier especie, también pueden estar limitados geográficamente. El factor físicos que influye principalmente en la distribución del zooplancton es básicamente la mezcla en la columna de agua (surgencia y contrasurgencia) a lo largo de la costa y en el océano profundo que afectan tanto a la disponibilidad de nutrientes como a la producción de fitoplancton (Lalli and Parsons 1997). A través del consumo y procesamiento de fitoplancton y otros recursos, el zooplancton juega un papel muy importante en la redes acuáticas de alimentos, como un recurso para consumidores de niveles tróficos superiores, incluyendo los peces. Así, el zooplancton es la presa inicial para casi todas las larvas de peces tan pronto cambian su saco vitelino por la alimentación externa, y es considerado como el principal alimento de las larvas de peces (Turner 1984; Govoni et al. 2010). Estudios de la distribución vertical de zooplancton en el este del Golfo de México revelan que la comunidad de zooplancton es diversa, 21 géneros que exceden el 1% de la biomasa de la capa de 0 a 1.000 m (Hopkins 1982). Con referencia a la variabilidad de zooplancton en el GDM, varios análisis de la composición de la comunidad de zooplancton y de la abundancia en la desembocadura del río Misisipi y en similares profundidades fuera de la influencia fluvial al oeste de la Florida y en el Golfo central, muestran que las abundancias de copépodos son significativamente más elevadas en zonas cercanas a la costa que en zonas centrales del GDM (Ortner et al. 1989).

Como se observa en esta sección, el fitoplancton es determinante para varios niveles biológicos. Ahora cabe preguntarnos, cuál es el factor limitante del éxito del fitoplancton? El factor dominante en la limitación del crecimiento del fitoplancton y zooplancton varía de región en región en los océanos. A escala global, el crecimiento de fitoplancton en los oligotróficos giros tropicales y subtropicales está generalmente limitado por el aporte de nutrientes, mientras que la luz a menudo limita el crecimiento de fitoplancton en giros subárticos. La fotosíntesis depende tanto de la disponibilidad de luz (en la zona fótica) como de la disponibilidad de nitrógeno (N), y de casi todo el fósforo (P) y silicio (Si) para generar alimento y promover el crecimiento y reproducción. En el GDM, la profundidad de la capa de mezcla –que comprende la limitación de luz y la disponibilidad de nutrientes- se ha sugerido

como el factor más importante que controla la variación estacional de clorofila en aguas no costeras. En el GDM hay suficiente iluminación en la capa de mezcla durante todo el año, y únicamente en el norte del GDM y durante los meses de invierno la luz podría aparecer como un factor limitante a considerar (Rabalais et al. 2001). La limitación del crecimiento del fitoplancton debido a la atenuación de luz en la capa fótica se ha demostrado que es superior a la limitación del crecimiento debido a la concentración de nutrientes en la plataforma interior de Luisiana, pero el grado de limitación por nutrientes crece al aumentar la distancia del Delta del Misisipi (Bierman et al. 1994). Debido a la escasa información en numerosas regiones del GDM con respecto a los factores limitantes del fitoplancton, se hace una vez más imprescindible entender mejor las estructuras oceánicas que crean procesos de surgencia en el GDM (Biggs and Muller-Karger 1994; Toner et al. 2003).

3.4.2 Comunidades de larvas de peces en el Golfo de México

Una comunidad de peces puede ser definida como una serie de especies cuyas larvas son colectadas en una misma área a la vez (Miller 2002). Por lo tanto, la asociación de especies en una comunidad principalmente denota que han llegado a una solución similar para un determinado estadio de sus vidas (Miller 2002). La mortalidad es crítica es estos estadios (Houde 1987; Chambers 1997), y hoy en día se considera la depredación como el primer factor de mortalidad que afecta el reclutamiento (Hunter 1981; Bailey and Houde 1989). Dicha mortalidad está regulada por los siguientes factores: (1) la temperatura, que influye en la fisiología, metabolismo, comportamiento, y velocidades de crecimiento en los primeros estadios de vida (Blaxter 1991); (2) los procesos físicos (difusión, advección y dispersión), cuya importancia ya fue reconocida en alguna hipótesis de reclutamiento (Cushing 1975; Heath et al. 1988); (3) la presa, cuya cantidad está relacionada con las tasas de supervivencia y con crecimientos larvarios más rápidos (Zenitani et al. 2007) y; (4) las condiciones nutricionales y tasas de crecimiento influyen la depredación (Meekan and Fortier 1996; Vigliola and Meekan 2002): "*the faster you get bigger the better*"(Houde 1987). La variabilidad en el reclutamiento, por tanto, está considerada como una integración de procesos que actúan en diferentes escalas de tiempo y espacio (Figura 7.8), con lo que el reclutamiento depende de la especie, población y factores ambientales (Houde 2008).

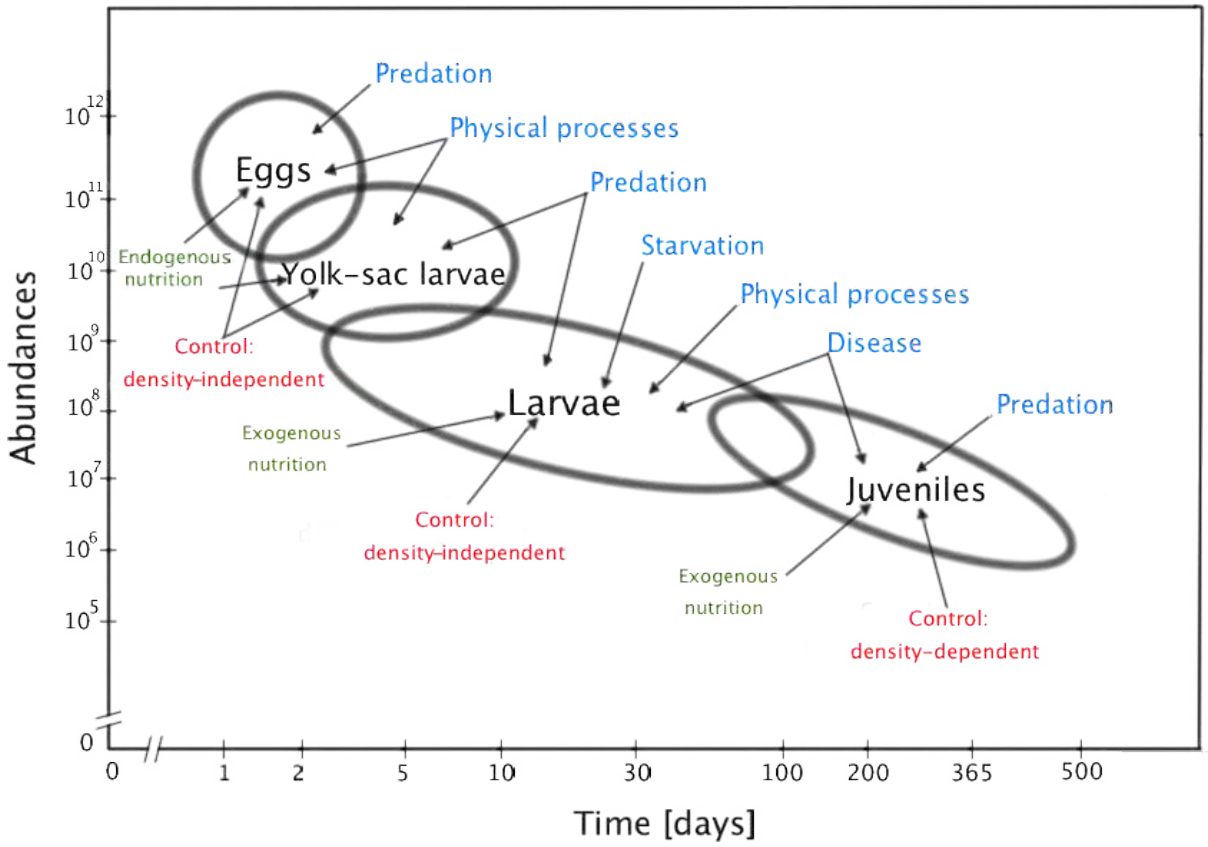

Figura 7.8. Diagrama del proceso de reclutamiento durante los primeros estadios de vida de los peces marinos, mostrando la evolución temporal de las abundancias de huevos, larvas con saco vitelino, larvas, y juveniles. Se incluyen las fuentes de nutrición (verde), las fuentes probables de mortalidad (azul), y el hipotético mecanismo de control (rojo). Figura reproducida de Houde 1987.

A pesar de la importancia del Golfo de México para las pescaderías, la variabilidad estacional de las comunidades larvarias en el norte del GDM ha sido estudiada en pocos estudios. Numerosas investigaciones previas acerca del ictioplancton se han enfocado en comunidades en estuarios (Raynie and Shaw 1994; Tolan et al. 1997) o interacciones en relativamente cortos periodos de tiempo y estructuras oceánicas específicas, como la pluma del río Misisipi (Sogard et al. 1987; Govoni et al. 1989) o la Corriente de Lazo (Richards et al. 1993). La literatura reciente disponible sobre ictioplancton en el GDM se encuentra recapitulada por Lyczkowski-Shultz et al. (2004).

4. Planteamiento y metodología

Un conocimiento adecuado de la posición y dinámica de las estructuras oceánicas de mesoescala, principalmente el frente de la Corriente de Lazo y los anillos que de ella se desprenden, es clave para varias aplicaciones: para la gestión de los potenciales derrames de hidrocarburos (Kaiser and Pulsipher 2007); navegación; operaciones de búsqueda y rescate; previsión de huracanes (Shay et al. 2000); y como planteamos en esta tesis, es importante para entender las condiciones ambientales que influyen en el hábitat de las larvas de peces marinos (Bakun 2006).

Las observaciones satelitales de las que hacemos uso en este trabajo nos permiten estudiar la actividad de mesoescala en el Golfo de México. Entre dichas observaciones, la altimetría nos proporciona mas de 18 años de continua monitorización del GDM y nos ayuda a entender mejor la dinámica de la superficie del océano con una resolución espacial y temporal que nos permite resolver estructuras oceánicas de mesoescala y frentes (Goni and Wainer 2001; Le Traon et al. 1998). Aunque los estudios usando imágenes satélites de temperatura continúan siendo incalculables debido a su inigualada resolución espacial (e.g. Figure 7.9a), están limitados en este estudio a los meses de invierno debido a la falta de contraste térmico en el GDM (e.g. Figure 7.9b). En el presente trabajo los campos de altimetría de anomalía superficial del mar (SHA) (e.g. Figure 7.9b y f)., altura superficial del mar (SSH) (e.g. Figure 7.9c y g) y gradiente de la altura superficial del mar (grad(SSH)) (*e.g.*, Figure 7.9d y h) nos facilitarán información sobre transporte de anomalías en las propiedades del agua, identificación de estructuras oceánicas y localización de dichas estructuras respectivamente.

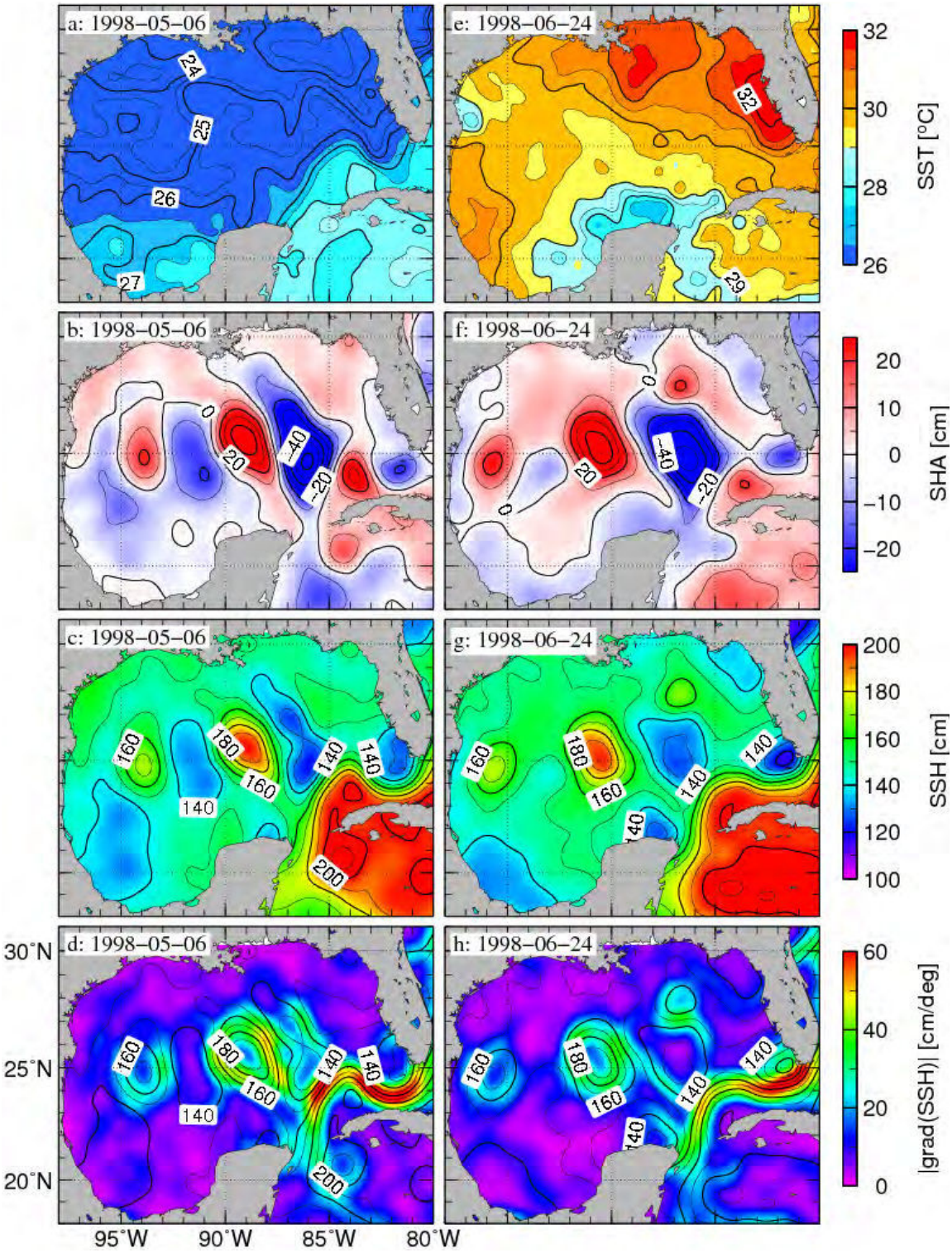

Figura 7.9. Comparación entre campos satelitales de SST y SSH. Los campos en los paneles de la izquierda ilustran eventos de separación de anillos en términos de (a) SST, (b) SHA, (c) SSH, y (d) gradiente de SSH a 6 de mayo de 1998. Los campos en los paneles de la derecha ilustran un anillo desprendido de la Corriente de Lazo en términos de (e) SST, (f) SHA, (g) SSH, y (h) gradiente de SSH a 24 de junio de 1998.

Por otro lado, la presencia de nubes a menudo oscurece las imágenes térmicas, haciendo difícil la localización y seguimiento de estructuras de mesoescala. A ello se le une que los datos de las campañas oceanográficas de pesquería que vamos a utilizar, aun cubriendo más de 20 años, son realizadas durante los meses de primavera e inicio de verano cuando el GDM comienza a tener una temperatura alta y uniforme en todas sus regiones. Los datos de dichas campañas, llevadas a cabo por la NOAA National Marine Fisheries Service, han sugerido que unas condiciones determinadas de temperatura superficial del mar, la concentración de clorofila, la abundancia de zooplancton, el día del año y la profundidad en ciertas zonas se asocian a altas abundancias de larvas de peces en la región del GDM (Muhling et al. 2010; Richardson et al. 2010). Por lo tanto, todo parece indicar que los adultos podrían estar buscando hábitats específicos o estructuras oceánicas donde desovar. A continuación, se resume la metodología empleada tanto para describir la variabilidad de la CL y el desprendimiento de anillos, como para identificar diferentes masas de agua y evaluar su influencia en la distribución de larvas en el GDM.

4.1 Localización del frente del la Corriente de Lazo

La localización del frente de la Corriente de Lazo está determinada por los contornos de máximo gradiente horizontal de altura superficial del mar (SSH). Específicamente, las posiciones más al norte y más al oeste de la Corriente de Lazo se detectan caracterizando la máxima latitud y longitud de los contornos de SSH correspondientes a una localización de máximo gradiente de SSH (Figura 7.10).

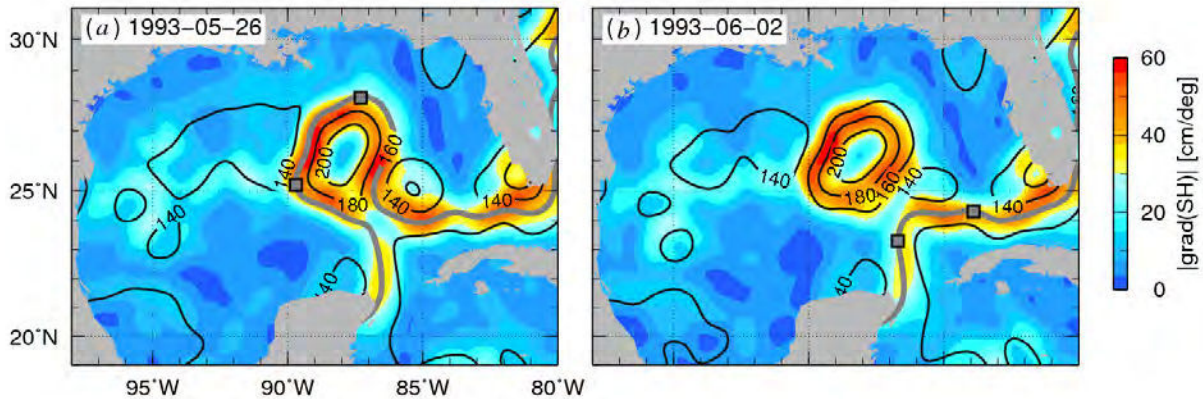

Figura 7.10. Campos de gradiente de SSH derivados de altimetría en el GDM con contornos de SSH superpuestos (en cm, líneas negras), para *(a)* 26 de mayo de 1993, y *(b)* 02 de junio de 1993. Los campos ilustran *(a)* la posición del frente de la CL, y *(b)* la detección del anillo de la CL y el frente de la CL. Las posiciones más al norte y más al oeste están marcadas con un cuadrado en ambos paneles.

Los pasos seguidos en esta metodología son los siguientes:

1) El valor absoluto del gradiente de SSH es calculado utilizando derivadas zonales y meridionales del campo de SSH.

2) El gradiente de SSH se mapea sobre el correspondiente mapa de contornos de SSH.

3) El valor de los contornos de SSH correspondientes a las posiciones del máximo gradiente de SSH definen el frente de la CL. Para evitar confusión entre el frente de la CL y un anillo, el cual podría tener también máximos gradientes, el contorno seleccionado de SSH perteneciente a una localización de máximo gradiente de SSH debe describir una trayectoria abierta.

4) La latitud más al norte de los contornos seleccionados define la posición más al norte de la CL.

5) La longitud más al oeste de los contornos seleccionados define la posición más occidental de la CL.

Siguiendo esta metodología se han analizado 768 campos de semanales de SSH durante el periodo comprendido entre 1993 y 2009, y se han derivado series temporales de intrusiones al norte y al oeste del la CL.

4.2 Detección del desprendimiento del anillo y periodo de vida

Los desprendimientos de anillos también se detectan con la metodología descrita en 4.1 y los siguientes criterios. Un anillo se considera que se ha separado de la CL en la superficie cuando 1) todos los contornos de SSH que pertenecen a los valores máximos del gradiente de SSH describen una trayectoria cerrada (Figura 7.10b) y 2) cuando la primera condición dura un tiempo superior a cuatro semanas, el cual es el máximo periodo de tiempo observado que toma un anillo de la CL en volverse a unir. El periodo de vida de un anillo se determina aquí como el periodo de tiempo desde que el anillo se desprende hasta que los valores de las alturas dinámicas del anillo alzan valores similares al de las aguas que lo rodean, típicamente entre 160 cm y 140 cm.

Los resultados que se obtuvieron aquí fueron comparados con los trabajos previos de la intrusión al norte de la CL (Zavala-Hidalgo et al. 2006) y separación de anillos (Sturges and Leben 2000; Alvera et al. 2009), los cuales cubren periodos de estudio más cortos. El hecho que los anillos identificados y las migraciones de la CL estudiadas en este trabajo estén en acuerdo con los hallazgos de los estudios previos confirman la consistencia de esta novedosa metodología y complementan los valiosos estudios previos. La metodología descrita permite unos resultados más completos, que cubren un periodo de tiempo más largos, y definen objetivamente las posiciones de la CL y los anillos.

Siguiendo esta metodología se han analizado 768 campos semanales de SSH durante el periodo comprendido entre 1993 y 2009, y se han derivado un censo de anillos.

4.3 Identificación de estructuras oceanográficas locales

El enfoque utilizado para estudiar la distribución de peces de larvas en la Corriente de Lazo ha consistido en definir previamente una región de influencia (ROI) de la CL. La ROI es el área limitada por la latitud mas al norte, la longitud más al oeste y la longitud más al este del frente de la CL. Estas regiones fueron comparadas con los datos *in situ* de las capturas semanales de larvas desde el 26 de abril de 1993 hasta el 29 de mayo de 2007.

Para identificar las principales estructuras de mesoescala fuera de la ROI de la CL, diseñamos un algoritmo que clasifica cada punto de malla de los campos de altimetría como perteneciente a una de las siguientes regiones:

a) Una región anticiclónica (AR):

$$SSH \geq SSH_{max} - n \cdot \sigma(SSH) \tag{18}$$

b) Una región ciclónica (CR):

$$SSH \leq SSH_{min} + p \cdot \sigma(SSH) \tag{19}$$

c) La frontera de una región anticiclónica (AB):

$$SSH \geq m \cdot SSH_{max} \quad \text{y} \quad grad(SSH) \geq r \cdot \sigma(|grad(SSH)|) \tag{20}$$

d) La frontera de una región ciclónica (CB):

$$SSH \leq q \cdot SSH_{min} \quad \text{and} \quad grad(SSH) \geq r \cdot \sigma(|grad(SSH)|) \tag{21}$$

e) Aguas comunes (CW) si ninguna de las condiciones previas es satisfecha. En este trabajo definimos las aguas comunes como aguas entre fronteras de estructuras de mesoescala.

Donde $\sigma(SSH)$ es la desviación estándar de SSH en la región del GDM y $\sigma(|grad(SSH)|)$ es la la desviación estándar del valor absoluto del gradiente de SSH en la región. SSH_{min} y SSH_{max} son los valores máximo y mínimo de SSH en el GDM para un día determinado. Los cinco parámetros adimensionales *m*, *n*, *p*, *q* y *r* fueron afinados mediante la comparación de los patrones de circulación descritos anteriormente en las 758 estaciones distribuidas en una malla de un grado en el norte del GDM durante el verano de 2009, usando los valores de los campos de SSH y sus corrientes geostróficas para ese periodo de tiempo. Los valores obtenidos por tras el afinamiento fueron:

$$m=0.91 \quad n=3.30 \quad p=0.60 \quad q=1.08 \quad r=0.67 \tag{22}$$

La Figura 7.11 constituye un ejemplo de los resultados de esta clasificación que muestra cinco regiones de circulación.

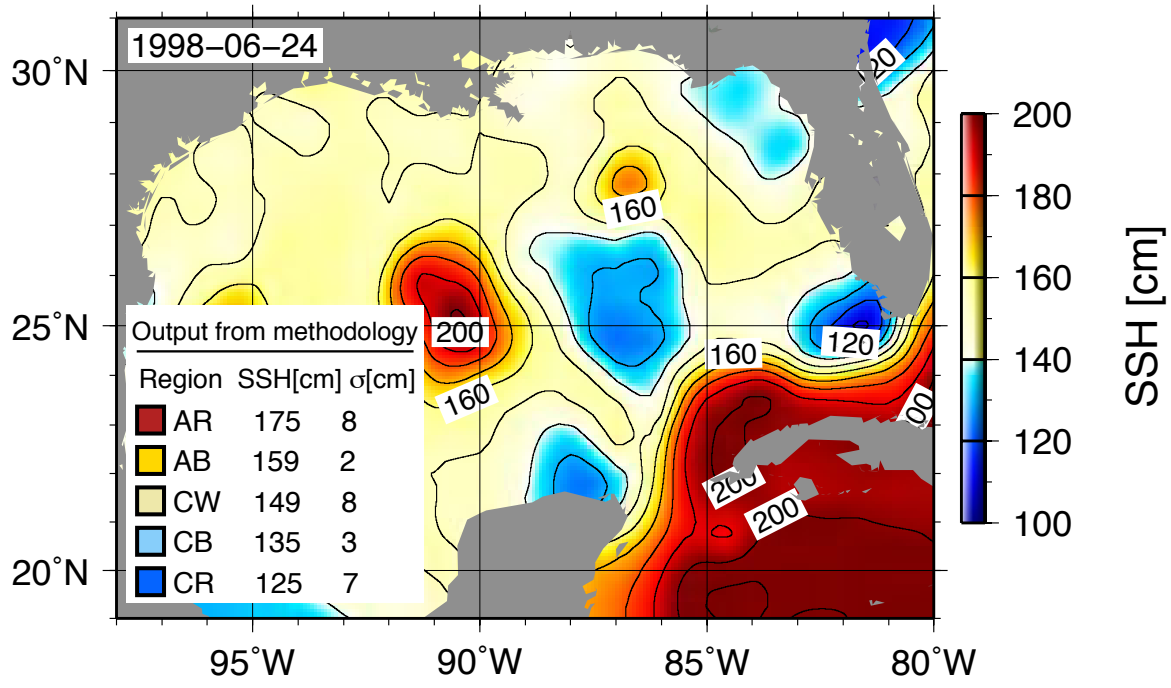

Figura 7.11. Ejemplo de las cinco regiones de circulación y sus fronteras definidas usando un algoritmo de clasificación de las estructuras de mesoescala para el 24 de junio de 1998. El campo de fondo es la SSH satelital. La leyenda ilustra la SSH media y la desviación estándar de la SSH para cada región de circulación. Los colores de la leyenda se corresponden aproximadamente con los colores del campo de SSH para cada región identificada.

4.4 Muestreo de larvas y análisis de datos

Las muestran fueron recogidas en el Golfo de México al norte de 24°N aproximadamente durante la primavera (de abril a junio) y entre 1993 y 2007 en el marco del programa *Southeast Area Monitoring and Assessment Program* de la NOAA. Cada campaña se dividió en dos partes y fueron llevadas a cabo en la zona económica exclusiva de los Estados Unidos. La mayoría del esfuerzo de muestreo se concentró en una malla de estaciones separadas un grado y esta malla fue completada dos veces al año, con la excepción

de 2003 y 2004 cuando se completaron solamente una vez. Estaciones adicionales fueron muestreadas en 1994, 1995, 2005 y 2006 (Tabla 7.1). Entre 41 y 137 estaciones hidrográficas y de plancton fueron llevadas a cabo cada año, con un promedio de 86 estaciones por crucero en los 15 años cubiertos por este estudio. En cada estación, el plancton fue recogido con redes bongo y se completaron perfiles CTD. Las abundancias de las larvas fueros estandarizadas a concentraciones larvarias (larvas por m^2) estimando el volumen filtrado utilizando un caudalímetro incorporado a la red bongo e integrando la profundidad a la que la red fue recogida en cada estación.

Tabla 7.1. Estaciones SEAMAP muestreadas entre 1993 y 2007 a lo largo del norte del Golfo de México.

Year	Sampling dates	Region sampled	No of sampled stations with satellite data extracted (*)	Net type
1993	26 April - June 15	24°N - 30°N / 84°W - 96°W	84 (14, 38, 26, 13, 16)	Bongo
1994	28 April - 9 June	24°N - 29°N / 84°W - 96°W	137 (29, 75, 45, 25, 15)	Bongo
1995	19 April - 7 June	24°N - 30°N / 84°W - 96°W	110 (26, 61, 42, 23, 21)	Bongo
1996	17 April - 25 May	24°N - 29°N / 83.5°W - 96°W	84 (15, 17, 30, 17, 15)	Bongo
1997	17 April - 9 June	24°N - 30°N / 84°W - 96°W	84 (23, 6, 35, 9, 7)	Bongo
1998	26 April - 23 June	24°N - 29°N / 84°W - 96°W	68 (16, 44, 27, 15, 16)	Bongo
1999	24 April - 31 May	24°N - 29°N / 83.5°W - 96°W	78 (18, 39, 21, 14, 8)	Bongo
2000	20 April - 26 May	24°N - 30°N / 83.5°W - 95°W	85 (26, 56, 26, 16, 11)	Bongo
2001	18 April - 29 May	24°N - 29°N / 83.5°W - 96°W	87 (24, 45, 20, 22, 9)	Bongo
2002	19 April - 28 May	24°N - 29°N / 83.5°W - 96°W	79 (17, 46, 31, 16, 13)	Bongo
2003	13 May - 30 May	24°N - 29°N / 83.5°W - 96°W	51 (9, 38, 15, 17, 2)	Bongo
2004	13 May - 30 May	25°N - 29°N / 84°W - 96°W	41 (10, 24, 17, 12, 7)	Bongo
2005	23 April - 17 July	24°N - 30°N / 83.5°W - 96°W	118 (21, 44, 39, 31, 29)	Bongo
2006	23 April - 16 July	24°N - 30°N / 84°W - 97°W	113 (16, 70, 55, 21, 28)	Bongo
2007	17 April - 29 May	24°N - 30°N / 84°W - 96°W	66 (21, 48, 17, 19, 10)	Bongo

* stations containing *Coryphaenidae*, *Thunnus* spp., *Auxis* spp., *Thunnus thynnus*, and *Euthynnus alleteratus*

Las muestras con las redes bongo se extendieron hasta junio en algunos años y excepcionalmente hasta julio en 2005 y 2006 (Tabla 7.1). Las redes estaban compuestas de una mala de 333 µm en dos ventanas de 61 cm de diámetro, y fueros remolcadas oblicuamente hasta 200 m de profundidad o justo en la superficie en estaciones muy someras (Richards et al. 1993). Las redes se remolcaron a 2-3 nudos y el muestreo se tomó tanto de día como de noche. Las muestras de las redes bongo fueros ordenadas y las larvas fuern identificadas hasta el mínimo taxón posible en el *Sea Fisheries Institute, Plankton Sorting and Identification Center, Gdynia and Szczecin* de Polonia.

Las campañas de plancton fueron originalmente diseñadas con el objetivo de estudiar el hábitat de larvas de *Thunnus thynnus* (*T. thynnus* de aquí en adelante). Sin embargo, larvas de peces de más de 500 taxones fueron registradas durante la duración de las campañas. En esta tesis las larvas de 5 taxones de tres familias comercialmente importantes fueron analizadas. En muchos casos, las larvas de especies estrechamente relacionadas no fueron distinguibles visualmente y por tanto los grupos fueron fusionados a nivel de género o familia. Las larvas de *Coryphaenidae* (*Coryphaena* spp. de aquí en adelante, probablemente incorporando *Coryphaena hippurus* and *Coryphaena equiselis*) fueron analizadas a nivel de género. En las familias de las Scombridae (atunes), las larvas de *Auxis* (*Auxis* spp. de aquí en adelante, incorporaban probablemente larvas de *Auxis rochei rochei* y *Auxis thazard thazard*) y fueron analizadas a nivel de género, de la misma manera que las larvas de *Thunnus* (*Thunnus* spp. de aquí en adelante, probablemente una mezcla de *Thunnus albacares* and *Thunnus atlanticus*, y no incluyendo *T. Thynnus*). Finalmente, las larvas tanto de *T. thynnus* como de *Euthynnus alleteratus* (*E. Alleteratus* de aquí en adelante) fueron identificables visualmente de otras especies de atunes, y por tanto fueron analizadas a nivel de especie.

Las distribuciones de larvas fueron comparadas con las estructuras oceánicas de mesoescala identificadas como regiones anticiclónicas, fronteras anticiclónicas, regiones ciclónicas, fronteras ciclónicas y aguas comunes identificadas con el algoritmo que ha sido diseñado (ver apartado 4.3) y que se basa en altimetría.

4.5 Análisis de probabilidades

Las asociaciones entre capturas de larvas de *T. thynnus*, *E. alleteratus*, *Thunnus* spp., *Auxis* spp., y *Coryphaena* spp., y las zonas interiores (regiones) y exteriores (fronteras) de estructuras oceánicas de mesoescala fueron determinadas a partir de análisis de probabilidad. Las ubicaciones de las capturas de cada taxón fueron clasificadas como pertenecientes a una de las cinco diferentes categorías (AR, AB, CR, CB, o CW). La probabilidad de encontrar larvas de un taxón *i* en una estructura de mesoescala *j* fue calculada utilizando el siguiente cociente:

$$P_i(j) = \frac{\frac{c_{ij}}{e_{ij}}}{\sum_{i=1}^{j=5}\left[\frac{c_{ij}}{e_{ij}}\right]} \quad (23)$$

Donde c_{ij}es el número de individuos de un taxón *i* capturado en una estructura *j*, e_{ij} es el esfuerzo de pesca, el denominador es el sumatorio de las capturas dividido por el esfuerzo de pesca en las cinco regiones, *i* es el taxón (*T. thynnus* (1), *E. alleteratus* (2), *Auxis* spp. (3), *Thunnus* spp. (4), y *Coryphaena* spp. (5)), y *j* es la región (AR, AB, CR, CB, y CW). Las capturas del taxón *i* fueron estandarizadas por e_{ij}, definido como el número de veces que una estructura *j* es muestreada encontrando un taxón *i*. Esta estandarización fue necesaria debido a que el esfuerzo de muestreo no era igual entre todas las clasificaciones de estructuras. Por ejemplo, las regiones definidas como CW fueron muestreadas más a menudo que las otras regiones y fronteras simplemente por la localización delas estaciones durante las campañas SEAMAP.

4.6 Análisis multivariado

Un análisis permutacional multivariado de la varianza (PERMANOVA; Anderson 2001) fue utilizado para testar la hipótesis nula de no diferencia en 1) las abundancias totales de todos los cinco taxones entre las cinco regiones de circulación, 2) las comunidades de especies de los cinco taxones entre las cinco regiones de circulación, 3) las abundancias individuales de cada taxón entre las cinco regiones de circulación, y 4) la presencia/ausencia (ocurrencia) de cada taxón entre las cinco regiones de circulación. Cada test fue realizado sobre matriz de similaridad transformada de Bray Curtis de la raíz cuarta, utilizando el software Primer-6, con 999 permutaciones únicas para determinar la significancia a $p<0.05$ (Clarke and Gorley 2006).

5. Síntesis de resultados

5.1 Las excursiones hacia el norte y hacia el oeste de la Corriente de Lazo

Series temporales semanales de las localizaciones más al norte y más al oeste de la Corriente de Lazo durante el periodo comprendido entre noviembre de 1992 y Diciembre de 2009 se presentan en la Figura 7.12. Las señales están filtradas con un filtro Butterworth (líneas negras en la Figura 7.12).

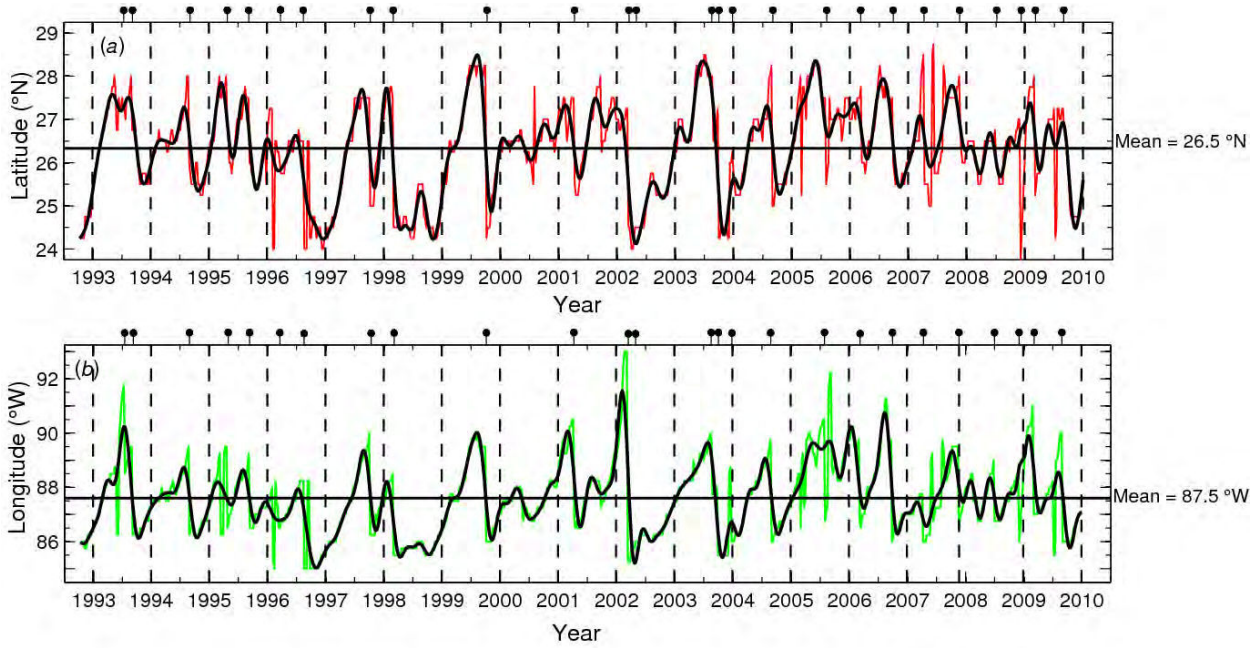

Figure 7.12. Series temporales de (a) la penetración hacia el norte de la Corriente de Lazo (línea roja) y (b) la penetración hacia el oeste de la Corriente de Lazo (línea verde), desde noviembre 1992 hasta diciembre 2009. Los círculos negros indican el momento de separación de los anillos de la CL. La señal fue filtrada con un filtro Butterworth de orden 6 y frecuencia de corte 1/7 rad/s (línea negra).

La ubicación del punto más al norte de la CL oscila entre 24ºN y 28.5ºN, con un valor medio de (media $\pm$ SD) de (26.5 $\pm$ 1)ºN y una marcada variabilidad estacional (Figura 7.12a). La amplitud de las oscilaciones exhibe valores máximos de movimientos meridionales de 4 grados de latitud entre 1993 y 2003, y movimientos meridionales de 2.5 grados de latitud entre 2004 y 2009.

Valores medios mensuales de las excursiones al norte de la CL entre 1993 y 2009 indican que la posición de la CL en verano (de julio a agosto) está significativamente más hacia el norte que en otoño, con invierno y primavera mostrando valores cercanos a la media (Figura 7.13a). La penetración hacia el norte de la CL también exhibe una variabilidad interanual (Figura 7.13b), mostrando un valor medio de 27.5ºN en la posición anual del la ubicación más al norte de la CL en 2005, un valor mínimo de 25ºN en 1998, y una media interanual alrededor de 26.3ºN. Ente 1993 y 2002 la posición media de las excursiones al norte de la CL es 26ºN, por debajo de la media interanual. Por el contrario, entre 2003 y 2009 la posición media de las excursiones al norte de la CL es 27ºN, por encima de la media anual.

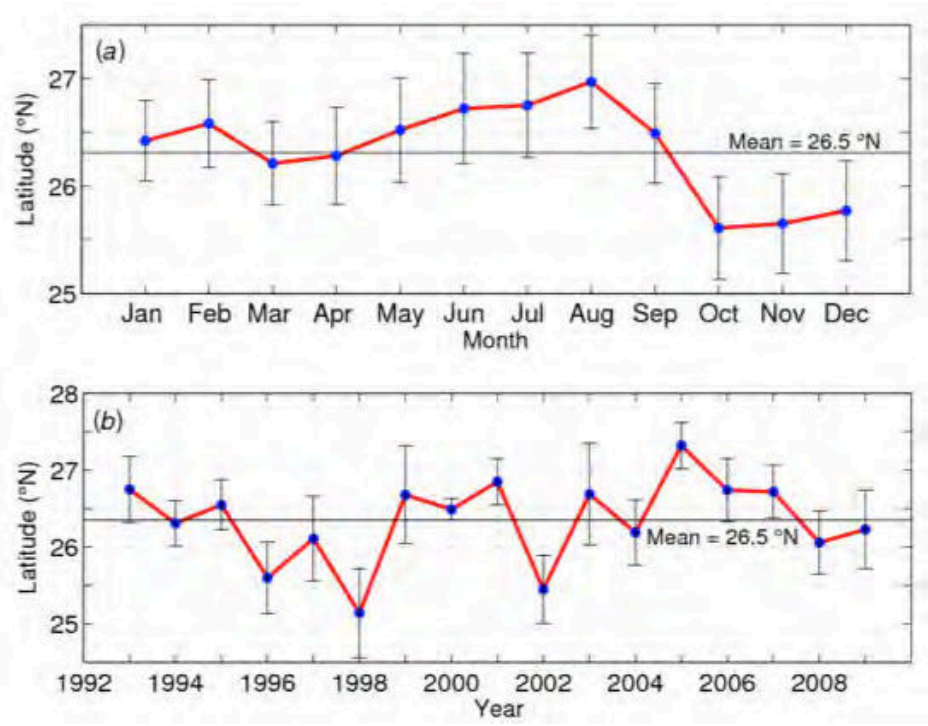

Figura 7.13 (a) Ubicación media mensual de la posición más al norte de la CL (círculos azules) y (b) posición media anual de la posición más al norte de la CL (círculos azules). Las barras negras ndican una desviación estándar sobre 17 años de datos analizados, desde enero de 1993 hasta diciembre de 2009.

La ubicación del punto más al oeste de la CL oscila entre 91ºW y 85ºW, con un valor medio de 88ºW y una pronunciada variabilidad estacional (Figura 7.12b). La amplitud de las oscilaciones exhibe valores máximos con movimientos zonales de aproximadamente 6 grados de longitud desde 1993 hasta 2003, y movimientos zonales de 4 grados de longitud desde 2004 hasta 2009.

5.2 Eventos de desprendimientos de anillos

Siguiendo la metodología descrita en el apartado 4.3 de esta sección, todos los desprendimientos de anillos entre noviembre de 1992 y diciembre de 2009 (círculos negros en la figura 7.12) son identificados y descritos en función de su vida y la ubicación de la Corriente de Lazo en el momento del desprendimiento (Tabla 7.2.)

Un total de 26 anillos han sido identificados como desprendidos de la Corriente de Lazo entre noviembre de 1992 y diciembre de 2009 (Tabla 7.2 y Figura 7.14). El promedio de anillos formados por año es de 1.5, con una desviación estándar de 0.7. Trece de los 26 anillos identificados en este trabajo se han desprendido en el periodo de 3 meses desde julio a septiembre. Septiembre y agosto, que son los meses en los que se producen las intrusiones al norte de la CL son también los meses que exhiben mas eventos de separación de anillos. Por el contrario, no se producen desprendimientos de anillos en los meses de enero, mayo y junio en el periodo analizado desde Octubre 1992 hasta Diciembre 2009. El periodo promedio entre desprendimientos de anillos consecutivos es de aproximadamente 9 meses desde 1993 a 2003 con una desviación estándar de 6 meses. El periodo promedio entre desprendimientos de anillos consecutivos es de aproximadamente 6 meses desde 2004 a 2009 con una desviación estándar de 1 mes.

Tabla 7.2. Compilación de eventos de separación de anillos, incluyendo as fechas de separación, periodo que pasa entre separaciones consecutivas, fechas de intrusiones extremas de la Corriente de Lazo (hacia el norte o hacia el oeste), fechas de retiros extremos de la Corriente de Lazo (hacia el sur), y descripción de los retiros al sur. Los anillos fueron identificados usando estimados de gradiente de altura superficial del mar, derivados de datos de altimetría, de enero de 1993 a diciembre de 2010, usando la metodología descrita en el apartado 4.3 de esta sección.

Ring	Date	Life span	Extreme LC intrusion	Extreme LC retreat	Description
			Jul 7 to Jul 14 1993		LC intrudes to 92°W
1-93	1993 Jul 21	5			
2-93	1993 Sep 8	5			
3-94	1994 Aug 31	6			
4-95	1995 Apr 26	5			
5-95	1995 Sep 13	5			
6-96	1996-Mar-20	7			
7-96	1996 Aug 21	9			
				Dec 4 to Dec 25	LC retreats to 24 °N
8-97	1997 Sep 24	10			
9-98	1998 Mar 04	11			
			Jun 23 to Sep 22		LC intrudes to 28 °N
10-99	1999 Sep 29	12			
11-01	2001 Apr 11	7			
			Feb 20 to Mar 6 2002		LC intrudes to 93 °W
12-02	2002 Mar 13	1			
13-02	2002 Apr 17	11		Apr 3 to Apr 17 2002	LC retreats to 24 °N
			May 7 to Aug 13		LC intrudes to 28 °N
14-03	2003 Aug 20	4			
15-03	2003 Sep 24	10			
16-03	2003 Dec 24	8			
17-04	2004 Sep 01	11			
			Apr 13 to Jun 29		LC intrudes to 28 °N
18-05	2005 Aug 03	9			
19-06	2006 Mar 08	5			
			Aug 9 to Aug 23		LC intrudes to 91 °W
20-06	2006 Sep 27	12			
21-07	2007 Apr 11	4			
22-07	2007 Nov 14	6			
23-08	2008 Jul 2	8			
24-08	2008 Dec 3	2			
			Feb 11 to Feb 25		LC intrudes to 91 °W
25-09	2009 Mar 4	8			
26-09	2009 Sep 2	7			

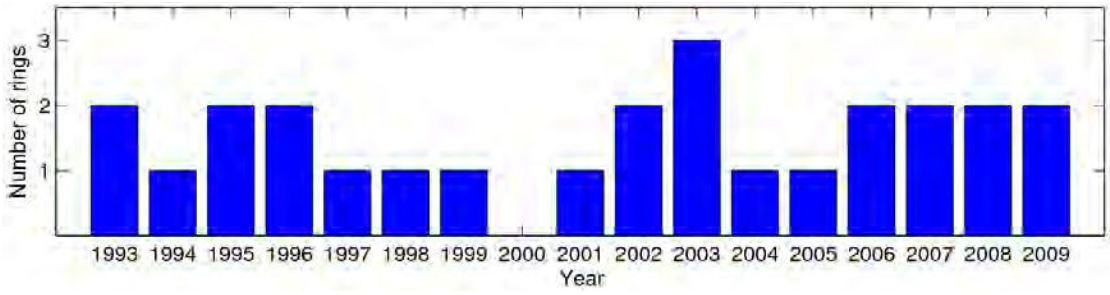

Figura 7.14. Número de anillos desprendidos durante cada año, de enero de 1993 a diciembre de 2009, obtenidos de acorde a la metodología descrita en el apartado 4.3 de esta sección.

5.3 Residuos de la anomalía de la altura superficial del mar

Los residuos de la anomalía de la altura superficial del mar (SHR) para toda la cuenca del Golfo de México se han estimado como la diferencia entre la anomalía de la superficie del mar (SHA) media para cada mes específico y la media del valor de SHA desde el mes de inicio de los datos de los altímetros (noviembre de 1992). De esta manera se ha estimado una tendencia positiva del SHR de (2.8 ± 0.3) cm decada^{-1} desde Noviembre de 1992 hasta Diciembre de 2009 mensual (Figura 7.15). Además de ello, se observa una inversión en las SHR aproximadamente en el año 2000, es decir, se observan un 80% de SHR negativas y un 20% de SHR positivas desde diciembre de 1992 a Diciembre de 1999 y, en cambio, se observa un 15% de SHR negativas y un 85% de SHR positivas entre enero del 2000 y diciembre de 2009.

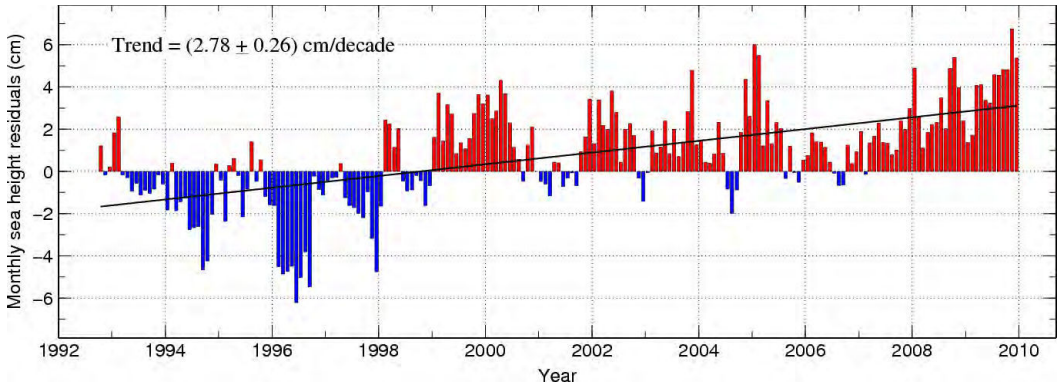

Figura 7.15. Residuos mensuales de la anomalía de la altura superficial del mar (SHR), estimados como la diferencia entre la SHA media mensual y la SHA media para ese determinado mes desde Noviembre de 1992. La línea negra indica la línea de tendencia, que muestra un incremento de 2.78 cm por década.

5.4 La Corriente de Lazo y las distribuciones de larvas

Entre 1993 y 2007, hemos analizado 1285 estaciones con datos emparejados de origen satelital y concentración de larvas de *Coryphaena* spp., *Thunnus* spp., *Auxis* spp., *T. thynnus*, y *E. Alleteratus*. Estas larvas fueron encontradas respectivamente en el 22%, 51%, 35%, 21%, y 16% de las estaciones en el norte del GDM (Figura 7.16).

Los valores semanales de la latitud más al norte, longitud más al oeste y longitud más al este de la Corriente de Lazo nos han permitido obtener una serie temporal de los límites aproximados de la región de influencia (ROI) de la CL. Ésta fluctúa entre 25°N y 28°N en su frente norte y entre 83°W y 85°W en su frente oeste. De 1993 a 2007 la posición media de las ubicaciones norte, oeste y este de la ROI de la CL fueron respectivamente 26°N, 87°W, y 84°W, y el porcentaje de capturas (media $\pm$ SD) la ROI de la CL fue de 17 $\pm$ 10 % (Figura 7.16). Las larvas recogidas en la ROI de la CL para cada periodo de muestreo variaron desde 11 larvas de peces en 2006 (3% de las larvas capturadas) a 166 en 1998 (31% de las larvas capturadas, Tabla 7.3). La velocidad geostrófica media (media $\pm$ SD) de la ROI de la CL fue de 57 $\pm$ 31 cm s^{-1}.

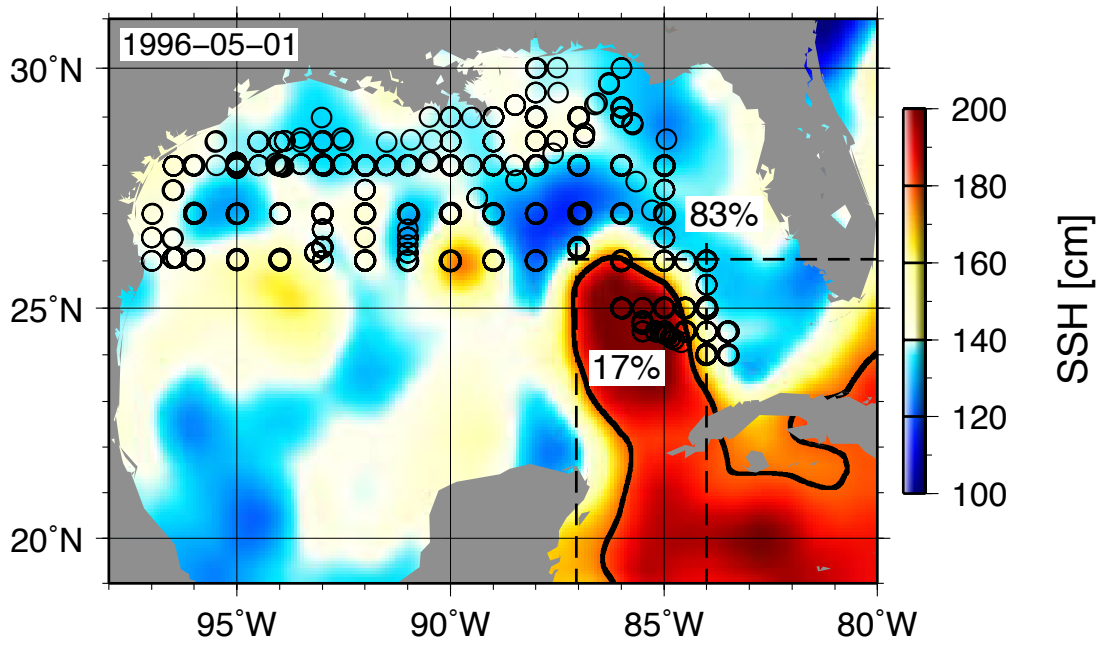

Figure 7.16. Localización de las estaciones de las campañas anuales del programa NOAA/SEFSC SEAMAP y porcentaje de larvas de peces capturados dentro (17%) y fuera (83%) de la región de influencia de la Corriente de Lazo de 1993 a 2007. El color de fondo es la altura superficial del mar para 1 de mayo de 1996. Los líneas sólidas negras representan el frente medio de la CL. Las líneas discontinuas ilustran la latitud más al norte, la longitud más al oeste y la longitud más al este del frente de la CL en el norte del Golfo de México al norte de 23°N, que son respectivamente 26°N, 87°W, 84°W.

Tabla 7.3. Detalles of de las estaciones SEAMAP muestreadas entre 1993 y 2007 a lo largo del norte del GDM.

Sampling dates	No of larvae collected (*)	LC ROI [°]	No of larvae collected in LC ROI	% Larvae in LC ROI
26 April-15 June, 1993	350 (10, 111, 178, 25, 26)	28°N, 88°W, 85°W	51 (4, 17, 13, 17, 0)	15%
28 April-9 June, 1994	499 (28, 161, 232, 40, 38)	26°N, 88°W, 85°W	30 (4, 11, 14, 0, 1)	6%
19 April-7 June, 1995	424 (8, 197, 131, 53, 35)	27°N, 88°W, 84°W	128 (5, 80, 23, 4, 16)	30%
17 April-25 May, 1996	367 (5, 72, 131, 53, 35)	26°N, 87°W, 84°W	86 (2, 22, 52, 3, 7)	23%
17 April-9 June, 1997	191 (16, 6, 101, 35, 33)	25°N, 86°W, 84°W	32 (2, 0, 22, 0, 8)	17%
26 April-23 June, 1998	539 (9, 144, 289, 16, 81)	25°N, 86°W, 83°W	166 (6, 46, 57, 0, 57)	31%
24 April-31 May, 1999	190 (10, 94, 52, 29, 5)	27°N, 88°W, 85°W	40 (2, 28, 6, 4, 0)	21%
20 April-26 May, 2000	397 (17, 259, 77, 30, 14)	27°N, 88°W, 84°W	155 (7, 99, 40, 1, 8)	39%
18 April-29 May, 2001	264 (27, 108, 31, 60, 38)	25°N, 87°W, 85°W	12 (0, 10, 0, 0, 2)	5%
19 April-28 May, 2002	276 (5, 114, 84, 42, 31)	25°N, 86°W, 84°W	35 (4, 23, 7, 0, 1)	13%
13 May-30 May, 2003	145 (3, 75, 25, 38, 4)	28°N, 89°W, 85°W	27 (12, 7, 2, 6, 0)	19%
13 May-30 May, 2004	125 (4, 45, 42, 30, 4)	27°N, 88°W, 85°W	14 (0, 11, 3, 0, 0)	11%
23 April-17 July, 2005	417 (9, 130, 134, 44, 100)	28°N, 89°W, 85°W	70 (4, 39, 23, 4, 0)	17%
23 April-16 July, 2006	398 (6, 171, 117, 34, 70)	27°N, 88°W, 85°W	11 (1, 7, 2, 1, 0)	3%
17 April-29 May, 2007	253 (10, 114, 87, 34, 8)	25°N, 86°W, 84°W	18 (2, 14, 1, 1, 0)	7%

* Larval fish of *Coryphaena* spp., *Thunnus* spp., *Auxis* spp., *T. thynnus,* and *E. alleteratus*

Con el objetivo de analizar en más profundidad las relaciones entre las excursiones de la CL y las distribuciones de larvas de peces, las capturas de larvas fueron examinadas dentro de un cubo cuadrado de 2° y centrado en 26°N y 87°W, coordenadas que representan la latitud y longitud media de la localización más al norte y la localización más al oeste de la CL. Una serie temporal de las desviaciones de latitud media de la CL durante primavera y las capturas en el cubo también fueron analizadas (Figura 7.17).

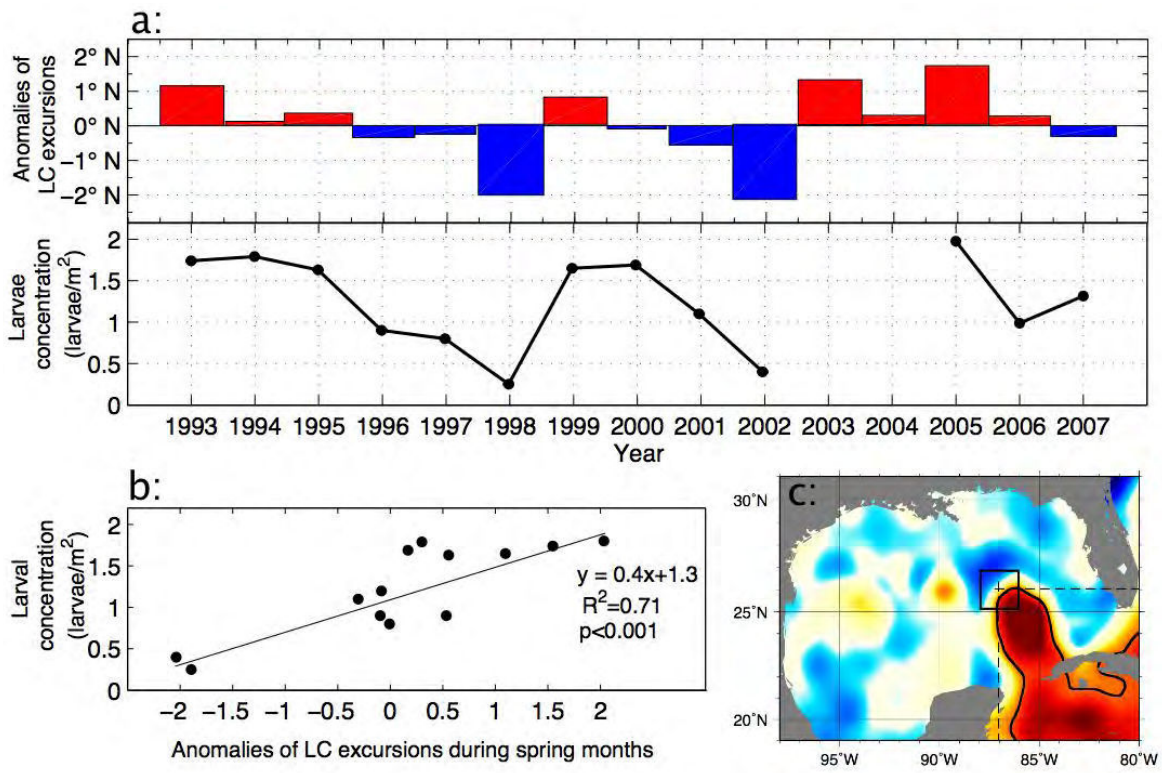

Figura 7.17. (a) Anomalías de latitud media del la Corriente de Lazo en relación con concentraciones de larvas capturadas en una región simbolizada por una caja de 2° centrada en 87°W y 26°N. La línea negra muestra la concentración media de las capturas de *T. thynnus, E. alleteratus, Auxis* spp., *Thunnus* spp., y *Coryphaena* spp., de mayo 1993 a junio 2007 con excepción de 2003 y 2004. (b) Análisis de regresión de la concentración media de larvas vs. las anomalías anomalías en las intrusiones de la CL. (c) La región examinada, simbolizada por un cuadrado negro.

Durante primavera, la CL está ubicada usualmente al norte de su posición media en 26.31°N. Sin embargo, las excursiones de primavera de la CL exhiben una variabilidad interanual. Varían entre una latitud media mínima de 24.23°N en 2002 a una latitud media máxima de 27.92°N en 2005 (Figura 7.17a). Similar variabilidad interanual se encuentra en la

concentración media de las capturas de las larvas analizadas aquí (Figura 7.17a). Un análisis de regresión (Figura 7.17b) muestra que las oscilaciones de la CL alrededor de su latitud media (Figura 7.17c) estaban significativamente correladas con las concentraciones de larvas (r^2 = 0.71, p < 0.001). Excursiones de la CL al norte/sur llevaban a un incremento/disminución delas concentraciones larvarias medias entre 86°W y 88°W, y entre 25°N y 27°N.

5.5 Efectos de las estructuras de mesoescala en las distribuciones de larvas

Las probabilidades de capturar larvas de *T. thynnus*, *E. alleteratus*, *Thunnus* spp., y *Coryphaena* spp. fueron más altas en las fronteras de estructuras anticiclónicas y las distribuciones de larvas de *Auxis* spp. fueron más altas en las regiones clasificadas como aguas comunes (Tabla 7.4). Las probabilidades (P) de encontrar larvas de peces de todos los taxones juntos fueron significativamente diferentes entre regiones (PERMANOVA, p = 0.001), y este resultado fue causado porque las concentraciones en CW fueron significativamente diferentes a las de AR (p = 0.001), CB (p = 0.015), y CR (p = 0.009).

Tabla 7.4. Capturas (*c*), esfuerzos (*e*) y probabilidades (*P*) de encontrar larvas en regiones anticiclónicas (AR), fronteras anticiclónicas (AB), regiones ciclónicas (CR), fronteras ciclónicas (CB) y aguas comunes (CW) para *T. thynnus, E. alleteratus, Auxis* spp., *Thunnus* spp., y *Coryphaena* spp.

		AR	**AB**	**CR**	**CB**	**CW**
T. thynnus	*C*	26	199	26	52	301
	E	72	62	38	52	100
	P	**0.044**	**0.389**	**0.082**	**0.121**	**0.364**
E. alleteratus	*C*	19	101	2	7	299
	E	59	63	19	35	140
	P	**0.102**	**0.384**	**0.020**	**0.063**	**0.431**
***Auxis* spp.**	*C*	71	305	29	102	1015
	E	86	96	26	71	270
	P	**0.091**	**0.295**	**0.091**	**0.158**	**0.368**
***Thunnus* spp.**	*C*	287	347	56	120	501
	E	113	102	36	34	180
	P	**0.186**	**0.269**	**0.144**	**0.188**	**0.213**
***Coryphaena* spp.**	*C*	21	38	9	16	54
	E	70	69	22	52	101
	P	**0.151**	**0.299**	**0.191**	**0.157**	**0.202**

Las probabilidades de encontrar larvas de *T. thynnus* (P, p-value) fueron significativamente más elevadas en fronteras anticiclónicas (0.389, 0.03) y aguas comunes (0.364, 0.03), y de manera similar las larvas comprendidas en *Auxis* spp. mostraron más probabilidades de ser encontradas (P, p-value) en aguas comunes (0.368, 0.001) y fronteras anticiclónicas (0.295, 0.001). *Auxis* spp. también mostraron una probabilidad más alta de ser encontradas en las fronteras de estructuras anticiclónicas (p = 0.04), pero no se encontraron diferencias significativas entre las zonas interiores y exteriores de estructuras ciclónicas (p = 0.04). Aunque las larvas de *Coryphaena* spp. son escasas e irregulares, las probabilidades de encontrar larvas de *Coryphaena* spp. (P) fueron más altas en fronteras anticiclónicas (0.299), y esto fue marginalmente significativo (p = 0.057). *E. Alleteratus* mostraba una probabilidad más alta de ser capturado (P) en aguas comunes (0.431) y fronteras de regiones anticiclónicas (0.384), pero esto no fue significativo (p = 0.45). *Thunnus* spp. se encontraron más frecuentemente en fronteras anticiclónicas, pero su presencia tampoco fue significativa (p = 0.48).

También se han estudiado asociaciones entre campos de altimetría y distribuciones de larvas relacionando las concentraciones medias de las larvas capturadas y la proporción de las capturas con valores de altura del mar utilizando campos de altimetría desde 1993 a 2007. Para facilitar que el lector tenga una mejor idea de los valores de SSH que yacen bajo las estructuras de mesoescala en el GDM desde 1993 a 2007, cada región de circulación fue caracterizada por su mínimo, máximo, valor medio y desviación estándar (Tabla 7.5).

Tabla 7.5. SSH mínima (min), máxima (max), media, y desviación estándar (SD) de regiones ciclónicas (CR), frentes ciclónicos (CB), aguas comunes (CW), frentes anticiclónicos (AB) y regiones anticiclónicas (AR), calculadas a partir de la media y desviación estándar de la SSH y del gradiente de la SSH para casa una de las regiones, desde 1993 a 2007.

	min (cm)	**max (cm)**	**mean (cm)**	**SD (cm)**
CR	114	135	124	4.9
CB	121	147	137	5.2
CW	128	161	145	5.1
AB	138	175	153	5.3
AR	153	216	177	15.0

Con respecto a las asociaciones entre campos de altimetría, concentraciones de larvas y proporción de capturas que acabamos de anunciar, se encontró que la distribución de larvas de *T. thynnus*, *E. alleteratus*, *Auxis* spp., *Thunnus* spp., y *Coryphaena* spp mostraron tanto altas concentraciones como elevadas proporciones de capturas en valores de SSH comprendidos entre los 140 cm y los 150 cm. Los resultados también mostraron que *T. thynnus*, *E. alleteratus*, *Auxis* spp., y *Coryphaena* spp. fueron menos abundantes en elevados valores de SSH (Figure 7.18a, b, c, e, y f). Por el contrario, *Thunnus* spp. fueron más abundantes en altas SSH que en otras especies (Figure 7.18d).

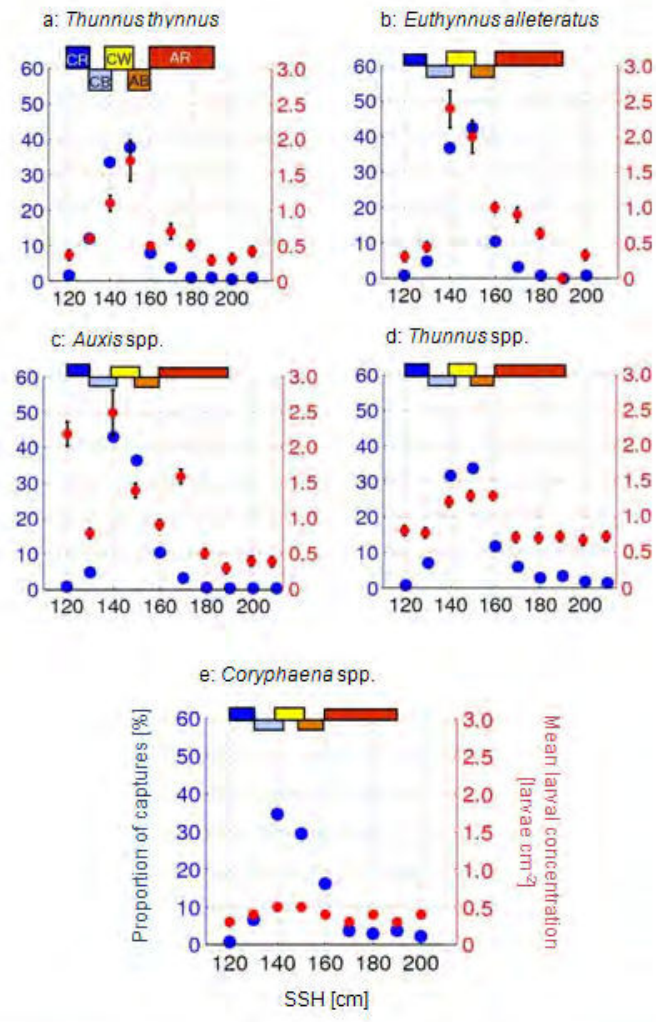

Figura 7.18. Concentraciones medias de capturas (círculos rojos) y proporción de capturas (círculos azules) (a) *T. thynnus*, (b) *E. alleteratus*, (c) *Auxis* spp., (d) *Thunnus* spp., y (e) *Coryphaena* spp en relación con observaciones satelitales de SSH, de 1993 a 2007. Los rectángulos coloreados representan los intervalos de SSH de regiones ciclónicas (CR), frentes ciclónicos (CB), aguas comunes (CW), frentes anticiclónicos (AB) y regiones anticiclónicas (AR), calculadas a partir de la media y desviación estándar del campo de SSH para cada una de las 5 regiones.

6. Futuras líneas de investigación

Una vez presentadas 1) las características principales de la Oceanografía Física del Golfo de México, 2) provisto de una descripción completa de la variabilidad a largo plazo de la Corriente de Lazo, el campo de anillos asociados, y la evolución de la anomalías en la altura superficial del mar, y 3) evaluados los vínculos entre la circulación de mesoescala y la distribución espacio-temporal de larvas de peces en el GDM, en este apartado exploraremos brevemente algunos de las investigaciones futuras que resultan de esta tesis.

Los resultados de esta tesis dan lugar a un amplio abanico de futuras investigaciones, algunas de ellas ya en curso. Tres cuestiones científicas se erigen de este trabajo:

1. ¿Existe un acoplamiento atmosférico significativo entre el forzamiento de la tensión del viento y las migraciones de la Corriente de Lazo?
2. ¿Cuál puede ser el rol de los remolinos ciclónicos de mesoescala que se desprenden de la Corriente de Lazo en la resolución de la paradoja "*momentum imbalance paradox*" formulada por Pichevin y Nof (1997)?
3. ¿Cómo los productores primarios se correlacionan con las estructuras de mesoescala en el Golfo de México?

En este apartado vamos a arrojar luz sobre la primera y la segunda pregunta, en base a los resultados preliminares que se han obtenido.

6.1 Evidencias de un acoplamiento ente el campo de presiones/viento y las migraciones de la Corriente de Lazo

La investigación que se está llevando a cabo con referencia a los posibles efectos de la presión atmosférica sobre las migraciones de la Corriente de Lazo están inspirados por el reciente trabajo de modelización de Chang y Oey (2010). Mientras que dichos autores plantean la hipótesis de que la intensificación del viento zonal puede demorar el desprendimiento de anillos, en este trabajo se plantea que el la variabilidad del transporte de Ekman tiene efectos en las migraciones de la CL.

Para explorar nuestra hipótesis, como primera aproximación se han medido los gradientes de presiones entre ubicaciones al norte y al sur de la CL. Se ha determinado la serie temporal de las anomalías mensuales de la presión superficial del nivel del mar (SLPA) y se ha comparado con la serie temporal de las migraciones mensuales de la CL (Figura 7.19). En general se observa una aparente correlación negativa entre SLPA y migraciones al norte de la CL, *i.e.*, cuando el gradiente de presiones aumenta (y por tanto también lo hace la tensión del viento y el transporte de Ekman), la CL se retira al sur y viceversa.

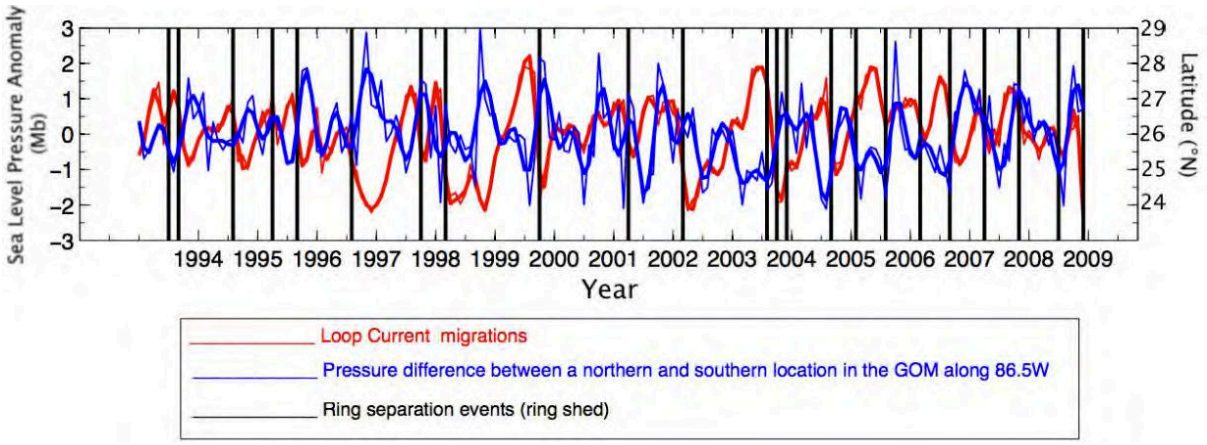

Figura 7.19. Series temporales de las migraciones mensuales de la Corriente de Lazo (línea roja fina) determinadas mediante campos de altimetría, y anomalías mensuales de la presión de la superficie del mar (línea azul delgada) determinadas a partir de ubicaciones al norte y sur de la Corriente de Lazo, de noviembre de 1992 a diciembre 2009. Las líneas verticales negras indican el momento de separaciones de anillos de la Corriente de Lazo. Las señales fueron filtradas utilizando un filtro Butterworth de orden 6 y frecuencia de corte 1/7 rad/s (línea roja gruesa y línea azul gruesa para migraciones de la Corriente de Lazo y anomalías de presión respectivamente).

La variabilidad de los periodos dominantes de las series temporales presentadas arriba ha sido analizada mediante un análisis de *semblance* (Cooper and Cowan 2008). El análisis y su discusión pueden encontrarse en la versión en ingles de esta tesis (Chapter V, sección 2.2). La conclusión preliminar que se extrae de dicho análisis es que la correlación negativa es clara para diversos periodos dominantes.

A pesar de los esfuerzos por investigar el efecto del viento hacia el oeste en la demora de los desprendimientos de anillos de la CL (Chang and Oey 2010), el efecto atmosférico parece con las migraciones de la CL parece no haber sido considerado hasta el momento.

6.2 Remolinos generados por la Corriente de Lazo que se propagan hacia el oeste

El objetivo principal aquí es proporcionar conocimiento sobre el papel que juegan los remolinos ciclónicos en el balance de momento y masa en para resolver la paradoja del "*momentum imbalance paradox*".

El primer enfoque de esta investigación preliminar ha sido explorar si la generación de remolinos ciclónicos longevos que se propagan hacia el oeste es significativa. Para ello los remolinos potenciales han sido identificados aplicando el parámetro Okubo–Weiss (W), el cual permite distinguir entre zonas dominadas por la vorticidad (Isern-Fontanet et al. 2004, Sangrà et al. 2009). De acuerdo a la citada técnica de detección, se han trazado las trayectorias hacia el oeste de anillos ciclónicos y anticiclónicos desde octubre de 1992 hasta diciembre de 2010 (Figura 7.20).

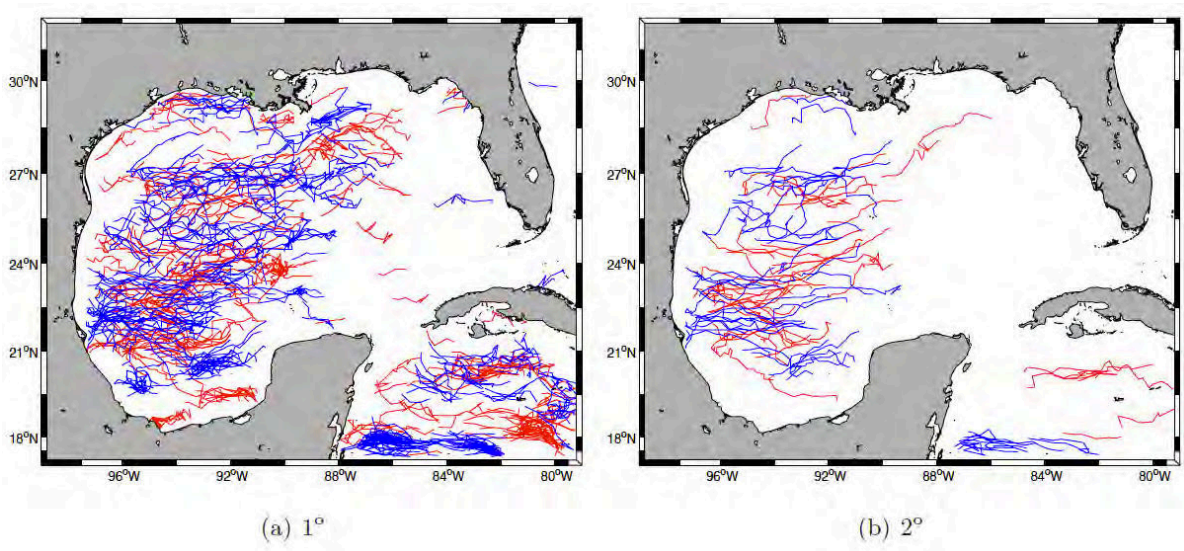

Figura 7.20. Trayectorias hacia el oeste de los remolinos ciclónicos (azul) y anticiclónicos (rojo) de octubre 1992 a diciembre 2010, bajo la condición de que el movimiento hacia el oeste sea de (a) al menos 1°, y (b) al menos 2°.

Aunque la técnica de detección para esta región todavía ha de ser refinada, preliminarmente encontramos que el número de remolinos (N) que se propagan hacia el oeste al menos 1° es mas alto para los remolinos ciclónicos (N=374) que para los remolinos anticiclónicos (N=287), lo que significa un 30% más de remolinos ciclónicos que de remolinos anticiclónicos que se propagan hacia el oeste. Este resultado podría ser crucial para

repensar el "*momentum imbalance paradox*", y va a ser explorado en el futuro. En particular, se planea implementar una técnica de seguimiento de remolinos que diferencie entre anillos y remolinos estimados del transporte hacia el oeste de momento y masa llevado a término por remolinos ciclónicos y anillos generados por la Corriente de Lazo.

7. Discusión

El objetivo central de esta tesis ha sido el estudio de la variabilidad temporal y espacial de la Corriente de Lazo y anillos, y la regulación de las distribuciones de larvas de algunas especies por parte de las estructuras oceánicas de mesoescala. Para lograr este fin, se ha desarrollado una metodología para localizar los frentes de la CL, detectar desprendimientos de anillos, y hemos explorado la variabilidad estacional e interanual de las excursiones de la CL, separación de anillos y tendencias de las anomalías de la altura superficial del mar en el Golfo de México desde 1993 a 2009. Una vez la variabilidad de la circulación de las principales estructuras de mesoescala ha sido definida, se han tratado los posibles enlaces entre la circulación y la distribución espacial y temporal de larvas de peces en el GDM.

Las secciones 5.1, 5.2 y 5.3 del presente capítulo muestran cuatro hallazgos principales. El primer resultado es que la penetración de la CL parecía ser estacional, con una tendencia a aumentar durante la primavera y mostrando valores máximos en verano. En particular, la posición de la CL entre julio y agosto era mas hacia el norte que en otoño, con valores en invierno y primavera cercanos a la media. Este resultado se basa en una larga serie temporal de migraciones semanales de la CL que fueron derivadas en esta tesis, y están en acuerdo con lo que estudios previos –que cubren menores periodos de tiempo y basados en métodos visuales y muestreos *in situ* de temperatura- han concluido. El segundo descubrimiento es que, empezando en 2003, la CL estaba localizada más hacia el norte; 1.5 grados por encima de la media interanual. Hasta la fecha este resultado es novedoso, y puede relacionarse con nuestro tercer resultado, el cual muestra que también a partir de 2003, hubo un incremento de los anillos que se desprenden de la Corriente de Lazo. Finalmente, determinamos la variabilidad de las oscilaciones meridionales y zonales de la CL, y mostramos que los movimientos meridionales disminuyeron 1.5 grados de latitud y que los movimientos zonales de la CL disminuyeron 2 grados de longitud, de 2004 a 2009. La futura investigación que proponemos está orientada parcialmente a entender mejor la dinámica de la CL y el desprendimiento de anillos.

Las secciones 5.4 y 5.5 proponen combinar la oceanografía con la biología para estudiar la variabilidad en primavera de capturas de larvas en el GDM desde 1993 a 2009. Obtuvimos 3 hallazgos principales. El primero fue que generalmente, ocurrían concentraciones de larvas más altas durante años de altas incursiones de la CL en el GDM. Un análisis de regresión mostró que las oscilaciones de la CL alrededor de su latitud media estaban correlacionadas significativamente con las concentraciones de larvas. Esto podría ser debido a la respuesta biológica por parte de los adultos o por parte de las larvas a la estructura de la CL, pero también puramente a mecanismos físicos de desplazamiento hacia el norte de las larvas, llevadas por la CL. El segundo resultado relevante fue que las larvas eran menos abundantes en regiones de estructuras ciclónicas y anticiclónicas de mesoescala, y más abundantes en zonas frontales anticiclónicas. Las larvas podrían ser más abundantes en las fronteras de las estructuras de mesoescala simplemente porque estas representan zonas de convergencia donde concentraciones favorables de presas existen (zooplancton, u otras larvas de peces). Las larvas de peces se alimentan básicamente de zooplancton y algunas (*e.g.*, los escómbridos) podían comerse los unos a los otros (piscivoría) una vez ya adquieren postflexión. Alternativamente, también se podría plantear la hipótesis de que los adultos nadaran activamente hacia las inmediaciones de tales estructuras frontales. El tercer hallazgo es que las larvas de *Thunnus thynnus* –una de las especies con más importancia comercial de nuestro trabajo- mostró concentraciones significativamente más elevadas en las fronteras de estructuras anticiclónicas que en regiones anticiclónicas, ciclónicas, y que en las fronteras de regiones ciclónicas. Nuestra futura investigación, examinará las distribuciones de larvas a un nivel de detalle más alto mediante el uso de color del océano para evaluar la concentración de fitoplancton en las estructuras oceánicas de mesoescala de la región. En particular, vamos a analizar los datos de una reciente campaña llevada a cabo en 2010 con un muy elevado numero de escómbridos y que podría permitir el estudio de larvas en pequeños remolinos con un nivel de detalle más elevado.

8. Conclusiones

Las principales conclusiones obtenidas en esta tesis son las siguientes:

1. A partir de 2003, la Corriente de Lazo ha estado situada más hacia el norte que durante el periodo 1993-2009, y ha habido un marcado aumento de los anillos desprendidos por la Corriente de Lazo.

2. La amplitud de las oscilaciones meridionales de la Corriente de Lazo ha disminuido, exhibiendo máximos valores de movimientos meridionales de 4 grados de latitud de 1993 a 2003, y movimientos meridionales de 2.5 grados de latitud desde 2004 a 2009. Similarmente, la amplitud de las oscilaciones zonales de la CL ha exhibido movimientos zonales de aproximadamente 6 grados de longitud de 1993 a 2003, y movimientos zonales de 4 grados de longitud de 2004 a 2009.

3. Las penetraciones hacia el norte de la Corriente de Lazo se han presentado como estacionales, con valores máximos de 0.8 grados de latitud por encima de la media anual durante los meses de junio, julio y agosto.

4. Los residuos de altura del mar (SHR), calculados como la diferencia entre la anomalía de la altura de mar (SHA) para cada mes específico y el valor medio de la SHA para dicho mes desde Noviembre de 1992, ha mostrado una tendencia positiva de (2.78±0.26) cm/década durante 1993-2009. Se ha planteado la hipótesis de que el aumento en el SHR en el Golfo de México puede estar ligado al incremento observado en la actividad de mesoescala en la región para el mismo periodo.

5. La aparente estacionalidad de la penetración al norte de la CL ha estado correlacionada con la concentración de larvas de peces, con más altas concentraciones medias de larvas en el este del Golfo de México cuando la CL migra más hacia el norte de la media interanual y viceversa.

6. Las larvas de *T. thynnus*, *E. alleteratus, Auxis* spp., *Thunnus* spp., y *Coryphaena* spp. han sido menos abundantes en el interior de estructuras de mesoescala ciclónicas y anticiclónicas, y por el contrario más abundantes cerca de las fronteras de regiones anticiclónicas del Golfo de México. Específicamente, las larvas de *T. thynnus*, *E. alleteratus,* y *Auxis* spp. estuvieron más presentes en las fronteras de regiones anticiclónicas y en aguas comunes del GDM, definidas como las aguas intermedias entre zonas frontales de estructuras de mesoescala.

7. La distribución de larvas de *T. Thynnus* en el Golfo de México fueron similares a las distribuciones de *T. Thynnus* en el Mediterráneo occidental, en el cual las zonas de desove han sido recientemente relacionadas con estructuras anticiclónicas de mesoescala, y las larvas de *T. Thynnus* fueron mas abundantes cerca de zonas frontales.

8. Las larvas de *Thunnus* spp. estuvieron distribuidas más ampliamente y sobre un rango más extenso de SSH que las de *T. Thynnus*, lo cual confirma reportes sobre las preferencias mas amplias de los atunes tropicales por un hábitat determinado en el GDM que las larvas de *T. Thynnus*.

9. Análisis de corrientes geostróficas en las estructuras oceánicas de mesoescala en el GDM junto al tamaño y la edad de las larvas indican que dichas larvas fueron encontradas posiblemente cerca de las zonas de desove en el GDM, siempre y cuando se encuentren fuera de la región de influencia (ROI) de la CL.

10. La circulación de mesoescala se ha mostrado que introduce variabilidad significativa en las series temporales derivadas de campañas de plancton en la región.

11. Investigaciones preliminares muestran una clara correlación negativa entre gradientes de presión y las migraciones de la CL, sugiriendo que la dinámica de la CL podría estar modulada en alguna extensión por el forzamiento atmosférico.

12. Investigaciones preliminares sobre longevos remolinos de mesoescala indican que el número de remolinos ciclónicos que se propagan hacia el oeste, probablemente originados del frente oeste de la CL, es mas alta que el número de remolinos anticiclónicos que se propagan hacia el oeste. Esto podría ser crucial para repensar el "*momentum imbalance paradox*".

Nomenclature

AOML	Atlantic Oceanographic and Atmospheric Laboratory
AVHRR	Advanced Very High Resolution Radiometer
CC	Caribbean Current
CS	Caribbean Sea
CZCS	Coastal Zone Color Scanner
EAFM	Ecosystem Approach to Fisheries Management (EAFM)
FAO	Food and Agriculture Organization
FC	Florida Current
GC	Guiana Current
GS	Gulf Stream
HT	Hurlburt and Thompson
IAS	Intra-Americas Sea
ITCZ	Inter-tropical Convergence Zone
GOM	Gulf of Mexico
LC	Loop Current
MDT	Mean Dynamic Topography
MOC	Meridional Overturning Circulation
NASH	North Atlantic Subtropical High
NBC	North Brazil Current
NBCR	North Brazil Current Ring

NMFS	National Marine Fisheries Service
NOAA	National Oceanic and Atmospheric Administration
OC	Ocean Color
PN	Pichevin and Nof
RTOFS	Real-Time Ocean Forecast System
SEAMAP	Southeast Monitoring and Assessment Program
SHA	Sea Height Anomaly
SLPA	Sea Level Pressure Anomalies
SMOS	Soil Moisture and Ocean Salinity
SSH	Sea Surface Height
SST	Sea Surface Temperature
YC	Yucatan Current

References

Alemany, F. and L. Quintanilla, P. Vélez-Belch, A. García, D. Cortés, JM. Rodríguez, M. L. Fernández de Puelles, C. González-Pola, and J. L. López-Jurado. 2010: Characterization of the spawning habitat of Atlantic bluefin tuna and related species in the Balearic Sea (western Mediterranean). *Progress in Oceanography*, **86**, 21–38.

Alvera, A., A. Barth, and R. H. Weisberg, 2009: The Surface Circulation of the Caribbean Sea and the Gulf of Mexico as Inferred from Satellite Altimetry. *Journal of Physical Oceanography*, **39**, 640-657.

Amante, C., B. W. Eakins, and N. G. D. Center, 2009: *ETOPO1 1 arc-minute global relief model: procedures, data sources and analysis*. US Dept. of Commerce, National Oceanic and Atmospheric Administration, National Environmental Satellite, Data, and Information Service, National Geophysical Data Center, Marine Geology and Geophysics Division.

Ammerman, J. W., 1992: Seasonal variation in phosphate turnover in the Mississippi River plume and the inner Gulf Shelf: Rapid summer turnover. *Proceedings of the Nutrient Enhanced Coastal Ocean Productivity Workshop. Publication Number TAMU-SG-92-109, Sea Grant College Program, Texas A&M University, College Station, Texas*, 69–75.

Andrade, C. A., E. D. Barton, and others, 2000: Eddy development and motion in the Caribbean Sea. *Journal of Geophysical Research*, **105**, 26191-26201.

Antoine, J., 1972: Structure of the Gulf of Mexico. In: Rezak, R. and V.J. Henry (eds.) Texas A&M University Oceanographic Studies, Volume 3: Contributions on the geological

and geophysical oceanography of the Gulf of Mexico. Gulf Publishing Company, Houston. 303 p.

Antoine, J., and J. Ewing, 1963: Seismic refraction measurements on the margins of the Gulf of Mexico. *Journal of Geophysical Research*, **68**, 1975–1996.

Auer, S. J., Five-Year Climatological Survey of the Gulf Stream System and Its Associated Rings. *Journal of Geophysical Research*, **92**, 11709–11726.

Auladell, M. and Coauthors, 2010: Modelling the early evolution of a Loop Current ring. *Journal of Marine Systems*, **80**, 160–171.

Auth, T. D., 2008: Distribution and community structure of ichthyoplankton from the northern and central California Current in May 2004–06. *Fisheries Oceanography*, **17**, 316–331.

Bailey, K., and E. Houde, 1989: Predation on eggs and larvae of marine fishes and the recruitment problem. *Advances in Marine Biology*, **25**, 1–83.

Bakun, A., 2006: Fronts and eddies as key structures in the habitat of marine fish larvae: opportunity, adaptive response and competitive advantage. *Scientia Marina*, **70,** 105-122.

Behringer, D. W., R. L. Molinari, and J. F. Festa, 1977: The variability of anticyclonic current patterns in the Gulf of Mexico. *Journal of Geophysical Research*, **82**, 5469–5476.

Belabbassii, L., P. Chapman, W. Nowlin, A. Jochens, and D. Biggs, 2005: Summertime nutrient supply to near-surface waters of the northeastern Gulf of Mexico: 1998, 1999, and 2000. *Gulf of Mexico Science*, **23**, 137.

Belkin, I. M., and J. E. O'Reilly, 2009: An algorithm for oceanic front detection in chlorophyll and SST satellite imagery. *Journal of Marine Systems*, **78**, 319–326.

Bierman, V. J., S. C. Hinz, D.-W. Zhu, W. J. Wiseman, N. N. Rabalais, and R. E. Turner, 1994: A Preliminary Mass Balance Model of Primary Productivity and Dissolved Oxygen in the Mississippi River Plume/Inner Gulf Shelf Region. *Estuaries*, **17**, 886.

Bigelow, K. A., C. H. Boggs, and X. He, 1999a: Environmental effects on swordfish and blue shark catch rates in the US North Pacific longline fishery. *Fisheries Oceanography*, **8**, 178–198.

Bigelow, K. A., C. H. Boggs, and X. He, 1999b: Environmental effects on swordfish and blue shark catch rates in the US North Pacific longline fishery. *Fisheries Oceanography*, **8**, 178–198.

Biggs, D., D. Smith, R. Bidigare, and M. Johnson, 1984: In situ estimation of the population density of gelatinous planktivores in Gulf of Mexico surface waters. *Memorial University of Newfoundland Occasional Papers in Biology*, **9**, 17–34.

Biggs, D., A. Vastano, R. Ossinger, A. Gil-Zurita, and A. Pérez-Franco, 1988: Multidisciplinary study of warm and cold-core rings in the Gulf of Mexico. *Mem. Soc. Cien. Nat. La Salle*, **48**, 11–32.

Biggs, D., G. Fargion, P. Hamilton, and R. Leben, 1996: Cleavage of a Gulf of Mexico Loop Current eddy by a deep water cyclone. *Journal of geophysical research*, **101**, 20629–20641.

Biggs, D. C., and F. E. Müller-Karger, 1994: Ship and satellite observations of chlorophyll stocks in interacting cyclone-anticyclone eddy pairs in the western Gulf of Mexico. *Journal of Geophysical Research*, **99**, 7371–7384.

Biggs, D. C., and P. H. Ressler, 2001: Distribution and abundance of phytoplankton, zooplankton, ichthyoplankton, and micronekton in the deepwater Gulf of Mexico. *Gulf of Mexico Science*, **19**, 7–29.

Biggs, D. C., and F. E. Müller-Karger, Ship and satellite observations of chlorophyll stocks in interacting cyclone-anticyclone eddy pairs in the western Gulf of Mexico. *Journal of Geophysical Research*, **99**, 7371–7384.

Biggs, D. C., A. E. Jochens, M. K. Howard, S. F. DiMarco, K. D. Mullin, R. R. Leben, F. E. Muller-Karger, and C. Hu, 2005: Eddy forced variations in on-and off-margin summertime circulation along the 1000-m isobath of the northern Gulf of Mexico, 2000-2003, and links with sperm whale distributions along the middle slope. *Geophysical Monograph-American Geophysical Union*, **161**, 71.

Biggs, D. C., C. Hu, and F. E. Müller-Karger, 2008: Remotely sensed sea-surface chlorophyll and POC flux at Deep Gulf of Mexico Benthos sampling stations. *Deep Sea Research Part II: Topical Studies in Oceanography*, **55**, 2555–2562.

Blaxter, J., 1991: The effect of temperature on larval fishes. *Netherlands Journal of Zoology*, **2**, 336–357.

Bollens, S. M., and B. W. Frost, 1991: Diel vertical migration in zooplankton: rapid individual response to predators. *Journal of Plankton Research*, **13**, 1359.

Borstad, G., 1982: The influence of the meandering Guiana Current and Amazon River discharge on surface salinity near Barbados. *Journal of Marine Research*, **40**, 421–433.

Bosch, W., G. Acuna, and R. Kaniuth, 2002: Caribbean sea level variability from TOPEX/Poseidon altimetry. *Proceedings of the IAG Symposium on Vertical Reference Systems, Cartagena, Colombia, IAG Symposia*, **124**, 249–254.

Boxshall, G. A., and S. H. Halsey, 2004: An introduction to copepod diversity. *The Ray Society Series.* Ray Society: London. 966 pp.

Boyce, D., M. Lewis, and B. Worm, 2010: Global phytoplankton decline over the past century. *Nature*, **466**, 591-596.

Breaker, L., 1981: The application of satellite remote sensing to west coast fisheries. *Journal of Marine Technology Society*, **15**, 32–40.

Brodeur, R. D., W. T. Peterson, T. D. Auth, H. L. Soulen, M. M. Parnel, and A. A. Emerson, 2008: Abundance and diversity of coastal fish larvae as indicators of recent changes in ocean and climate conditions in the Oregon upwelling zone. *Marine Ecology Progress Series*, **366**, 187–202.

Brooks, D. A., and R. V. Legeckis, 1982: A ship and satellite view of hydrographic features in the western Gulf of Mexico. *Journal of Geophysical Research*, **87**, 4195–4206.

Brothers, E., D. M. B. Williams, and P. Sale, 1983: Length of larval life in twelve families of fishes at "One Tree Lagoon", Great Barrier Reef, Australia. *Marine Biology*, **76**, 319–324.

Brown, O. B., P. C. Cornillon, S. R. Emmerson, and H. M. Carle, 1986: Gulf Stream warm rings: a statistical study of their behavior. *Deep Sea Research Part A. Oceanographic Research Papers*, **33**, 1459–1473.

Bryant, W. R., J. Antoine, M. Ewing, and B. Jones, 1968: Structure of Mexican continental shelf and slope, Gulf of Mexico: Am. *Assoc. Petroleum Geologists Bull*, **52**, 1204–1228.

Bunge, L., J. Ochoa, A. Badan, J. Candela, and J. Sheinbaum, 2002: Deep flows in the Yucatan Channel and their relation to changes in the Loop Current extension. *Journal of Geophysical Research*, **107**.

Candela, J., J. Sheinbaum, J. Ochoa, A. Badan, and R. Leben, 2002: The potential vorticity flux through the Yucatan Channel and the Loop Current in the Gulf of Mexico. *Geophysical Research Letters*, **29**, 16–1.

Candela, J., S. Tanahara, M. Crepon, B. Barnier, J. Sheinbaum, and others, 2003: Yucatan Channel flow: Observations versus CLIPPER ATL6 and MERCATOR PAM models. *Journal of Geophysical Research*, **108**.

Del Castillo, C. E., F. Gilbes, P. G. Coble, and F. E. Muller-Karger, 2000: On the dispersal of riverine colored dissolved organic matter over the West Florida Shelf. *Limnology and Oceanography*, 1425–1432.

Cayula, J. F., and P. Cornillon, 1992: Edge Detection Algorithm for SST Images. *Journal of Atmospheric and Oceanic Technology*, **9**, 67–80.

Chambers, R. C., 1997: Environmental influences on egg and propagule sizes in marine fishes. *Fish and Fisheries Series*, **21**, 63–102.

Chang, Y. -L., and L. -Y. Oey, 2010: Why Can Wind Delay the Shedding of Loop Current Eddies? *Journal of Physical Oceanography*, **40**, 2481–2495.

Chelton, D. B., R. A. deSzoeke, M. G. Schlax, K. El Naggar, and N. Siwertz, 1998: Geographical Variability of the First Baroclinic Rossby Radius of Deformation. *Journal of Physical Oceanography*, **28**, 433–460.

Chelton, D. B., M. C. Schlax, R. M. Samelson, and R. A. de Szoeke, 2007: Global observations of large oceanic eddies. *Geophysical Research Letters*, **34**, L15606.

Cherubin, L., Y. Morel, and E. Chassignet, 2005: The role of cyclones and topography in the Loop Current ring shedding. *Journal of Physical Oceanography*, **31**, 569–591.

Chérubin, L. M., W. Sturges, and E. P. Chassignet, 2005: Deep flow variability in the vicinity of the Yucatan Straits from a high-resolution numerical simulation. *Journal of Geophysical Research-Part C-Oceans*, **110**, C04009.

Chiswell, S. M., J. Wilkin, J. D. Booth, and B. Stanton, 2003: Trans-Tasman Sea larval transport: Is Australia a source for New Zealand rock lobsters? *Marine Ecology Progress Series*, **247**, 173–182.

Chuang, W., W. W. Schroeder, and W. J. Wiseman Jr, 1982: Summer current observations off the Alabama coast. *Contributions in Marine Science*, **25**, 121–131.

de Ciechomski, J., and R. Sanchezf, 1983: Relationship Between Ichthyoplankton Abundance and Associated Zooplankton Biomass in the Shelf Waters off Argentina. *Biological oceanography*, **3**, 77.

Clancy, R., 1992: Operational modeling: ocean modeling at the Fleet Numerical Oceanography Center. *Oceanography*, **5**, 31–35.

Clarke, K., and R. Gorley, 2006: PRIMER v6. User manual/tutorial. Plymouth routine in mulitvariate ecological research. *Plymouth Marine Laboratory*.

Cochrane, J. D., 1972: Separation of an anticyclone and subsequent developments in the Loop Current (1969). *Contributions on the Physical Oceanography of the Gulf of Mexico*, **2**, 91–106.

Condie, S. A., 1991: Separation and recirculation of the North Brazil Current. *Journal of marine research*, **49**, 1–19.

Cooper, G. R. J., and D. R. Cowan, 2008: Comparing time series using wavelet-based semblance analysis☆. *Computers & Geosciences*, **34**, 95–102.

Corredor, J. E., J. M. Morell, J. Lopez, J. Capella, and R. Armstrong, 2004: Cyclonic eddy entrains Orinoco River plume in eastern Caribbean. *Eos*, **85**, 201–202.

Cowan Jr, J., and R. Shaw, 1991: Ichthyoplankton off West Louisiana in winter 1981-1982 and its relationship with zooplankton biomass. *Contributions in Marine Science*, **32**, 103–121.

Cowan Jr, J., and R. Shaw, 2002: Recruitment. *Fishery Science: The Unique Contribution of Early Life Stages. Blackwell Science, Oxford, UK*, 88–111.

Cowen, R. K., 2002: Larval Dispersal and Retention and Consequences for Population Conectivity. *Coral reef fishes: dynamics and diversity in a complex ecosystem*, 149.

Cowen, R. K., J. A. Hare, and M. P. Fahay, 1993: Beyond hydrography: can physical processes explain larval fish assemblages within the Middle Atlantic Bight? *Bulletin of Marine Science*, **53**, 567–587.

Csanady, G., 1990: Retroflection and leakage in the North Brazil Current: Critical point analysis. *Journal of Marine Research*, **48**, 701–728.

Cushing, D., 1975: *Marine ecology and fisheries*. Cambridge University Press (Cambridge and New York).

Davis, C. S., and P. H. Wiebe, 1985: Macrozooplankton biomass in a warm-core Gulf Stream ring: Time series changes in size structure, taxonomic composition, and vertical distribution. *Journal of geophysical research*, **90**, 8871–8884.

DeHaan, C. J., and W. Sturges, 2005: Deep Cyclonic Circulation in the Gulf of Mexico. *Journal of Physical Oceanography*, **35**, 1801–1812.

Ditty, J. G., G. G. Zieske, and R. F. Shaw, 1988: Seasonality and depth distribution of larval fishes in the northern Gulf of Mexico above latitude 26 degree 00'N. *Fishery Bulletin*, **86**, 811–823.

Dortch, Q., and T. E. Whitledge, 1992: Does nitrogen or silicon limit phytoplankton production in the Mississippi River plume and nearby regions? *Continental Shelf Research*, **12**, 1293–1309.

Doyle, M. J., W. W. Morse, J. Kendall, and W. Arthur, 1993: A comparison of larval fish assemblages in the temperate zone of the northeast Pacific and northwest Atlantic oceans. *Bulletin of Marine Science*, **53**, 588–644.

Dulvy, N., E. Chassot, J. Hyemans, K. Hyde, D. Pauly, and others, 2009: Climate change, ecosystem variability and fisheries productivity. *Remote Sensing in Fisheries and Aquaculture: The Societal Benefits, IOCCG report*, 11–28.

Eden, C., R. J. Greatbatch, and J. Willebrand, 2007: A diagnosis of thickness fluxes in an eddy-resolving model. *Journal of physical oceanography*, **37**, 727–742.

Elliott, B. A., 1982: Anticyclonic rings in the Gulf of Mexico. *J. Phys. Oceanogr*, **12**, 1292–1309.

Ewing, J., M. Ewing, and R. Leyden, 1966: Seismic profiler survey of Blake Plateau. *Association of Petroleum Geologists Bulletin*, **50**, 1948–1971.

Ewing, M., D. B. Ericson, and B. C. Heezen, 1958: Sediments and topography of the Gulf of Mexico. *Habitat of oil: American Association of Petroleum Geologists*, 995–1053.

Falkowski, P. G., D. Ziemann, Z. Kolber, and P. K. Bienfang, 1991: Role of eddy pumping in enhancing primary production in the ocean. *Nature*, **352**, 55-58.

Flagg, C. N., R. L. Gordon, and S. McDowell, 1986: Hydrographic and current observations on the continental slope and shelf of the western equatorial Atlantic. *Journal of physical oceanography*, **16**, 1412–1429.

Flores-Coto, C., M. L. Espinosa Fuentes, F. Zavala García, and L. Sanvicente Añorve, 2009: Ictioplancton del sur del Golfo de México: Un compendio. *Hidrobiológica*, **19**, 49–76.

Font, J., J. Isern-Fontanet, and J. De Jesus Salas, 2004: Tracking a big anticyclonic eddy in the western Mediterranean Sea. *Scientia Marina*, **68**, 331–342.

Font, J. and A. Camps, A. Borges, M. Martin-Neira, J. Boutin, N. Reul, Y. H. Kerr, A. Hahne, and S. Mecklenburg, 2010: SMOS: The challenging sea surface salinity measurement from space. *Proceedings of the IEEE*, **98**, 649–665.

Forristall, G. Z., K. J. Schaudt, and C. K. Cooper, 1992: Evolution and kinematics of a Loop Current eddy in the Gulf of Mexico during 1985. *Journal of Geophysical Research*, **97**, 2173–2184.

Fratantoni, P. S., T. N. Lee, G. P. Podesta, and F. E. Muller-Karger, 1998: The influence of Loop Current perturbations on the formation and evolution of Tortugas eddies in the southern Straits of Florida. *Journal of Geophysical Research-Oceans*, **103**, 24759.

Froelich, P. N., D. K. Atwood, G. S. Giese, and others, 1978: Influence of Amazon River discharge on surface salinity and dissolved silicate concentration in the Caribbean Sea. *Deep Sea Research*, **25**, 735–744.

Froese, R., and D. Pauly, 2011: 2011.FishBase.World Wide Web electronic publication. www.fishbase.org, version (10/2011).

Fuentes-Yaco, C., P. Koeller, S. Sathyendranath, and T. Platt, 2007: Shrimp (Pandalus borealis) growth and timing of the spring phytoplankton bloom on the Newfoundland-Labrador Shelf. *Fisheries oceanography*, **16**, 116–129.

Fuglister, F., 1971: Cyclonic rings formed by the Gulf Stream 1965-66. *Studies in physical oceanography. Gordon & Breach*, 137–168.

Fuglister, F. C., 1951: Annual variations in current speeds in the Gulf Stream system. *Journal of Marine Research*, **10**, 119–127.

Fuiman, L., 2002: Special considerations of fish eggs and larvae. *Fishery Science. The Unique Contributions of Early Life Stages*, 1–32.

Galtsoff, P. S., 1954: Gulf of Mexico. Its origin, waters, and marine life. *United States. Department of the Interior. Fish and Wildlife Service,* **89.**

García, A. and Coauthors, 2005: Characterization of the bluefin tuna spawning habitat off the Balearic Archipelago in relation to key hydrographic features and associated environmental conditions. *Col. Vol. Sci. Pap. ICCAT*, **58**, 535–549.

Garcia, S., and T. L. Do Chi, 2003: The ecosystem approach to fisheries: issues, terminology, principles, institutional foundations, implementation and outlook. *FAO, Fisheries Technical Paper*, **443**.

Gilbert, P. S., T. N. Lee, and G. P. Podesta, 1996: Transport of anomalous low-salinity waters from the Mississippi River flood of 1993 to the Straits of Florida. *Continental Shelf Research*, **16**, 1065–1085.

Gilbes, F., C. Tomas, J. J. Walsh, and F. E. Müller-Karger, 1996: An episodic chlorophyll plume on the West Florida Shelf. *Continental Shelf Research*, **16**, 1201–1207.

Gilbes, F., F. E. Müller-Karger, and C. E. Del Castillo, 2002: New evidence for the West Florida Shelf plume. *Continental shelf research*, **22**, 2479–2496.

Gill, A. E., 1982: *Atmosphere-ocean dynamics*. New York, Academic Press (International Geophysics Series), **30**.

Goni, G. J., and W. E. Johns, 2001: A census of North Brazil Current rings observed from TOPEX/POSEIDON altimetry: 1992–1998. *Geophysical Research. Letters*, **28**, 1–4.

Goni, G. J., and I. Wainer, 2001: Investigation of the Brazil Current front variability from altimeter data. *Journal of Geophysical Research*, **106**, 31117–31131.

Goni, G. J. and Coauthors, 2011: Observed low frequency variability of the Brazil Current front. *Journal of Geophysical Research*, **116**, C10037.

González, N. M., F. E. Müler-Karger, S. C. Estrada, R. P. de los Reyes, I. V. del Río, P. C. Pérez, and I. M. Arenal, 2000a: Near-surface phytoplankton distribution in the western Intra-Americas Sea: The influence of El Niño and weather events. *Journal of Geophysical Research*, **105**, 14029–14044.

González, N. M., F. E. Muller-Karger, S. C. Estrada, R. P. de los Reyes, I. V. Del Rio, P. C. Perez, and I. M. Arenal, 2000b: Near-surface phytoplankton distribution in the western Intra-Americas Sea: The influence of El Nino and weather events. *Journal of Geophysical Research-Oceans*, **105**, 14029.

Govoni, J., J. Hare, E. Davenport, M. Chen, and K. Marancik, 2010: Mesoscale, cyclonic eddies as larval fish habitat along the southeast United States shelf: a Lagrangian

description of the zooplankton community. *ICES Journal of Marine Science: Journal du Conseil*, **67**, 403–411.

Govoni, J. J., D. E. Hoss, and D. R. Colby, 1989: The spatial distribution of larval fishes about the Mississippi River plume. *Limnology and Oceanography*, **34**, 178–187.

Grade, H. G., 1961: *On some oceanographic observations in the southeastern Caribbean Sea and the adjacent Atlantic Ocean with special reference to the influence of the Orinoco River*. Universidad de Oriente, Instituto Oceanográfico.

Gray, C., and A. Miskiewicz, 2000: Larval fish assemblages in south-east Australian coastal waters: seasonal and spatial structure. *Estuarine, Coastal and Shelf Science*, **50**, 549–570.

Halbouty, M. T., 1979: Salt Domes Gulf Region, United States and Mexico. *Gulf Publishing Co., Houston, Texas*, **561**, 150.

Hamilton, P., and T. N. Lee, 2005: Eddies and jets over the slope of the northeast Gulf of Mexico. *Geophysical Monograph-American Geophysical Union*, **161**, 123.

Hamilton, P., J. C. Larsen, K. D. Leaman, T. N. Lee, and E. Waddell, 2005: Transports through the Straits of Florida. *Journal of physical oceanography*, **35**, 308–322.

Hare, J. A., and J. J. Govoni, 2005: Comparison of average larval fish vertical distributions among species exhibiting different transport pathways on the southeast United States continental shelf. *Fishery Buletin-National Oceanic and Atmospheric Administration*, **103**, 728.

Haury, L., J. McGowan, P. Wiebe, and J. Steele, 1978: Patterns and processes in the time-space scales of plankton distributions. *Collected Reprints. Woods Hole. Dec. 1979*,.

Heath, M., E. Henderson, and D. Baird, 1988: Vertical distribution of herring larvae in relation to physical mixing and illumination. *Marine ecology progress series. Oldendorf*, **47**, 211–228.

Hellweger, F. L., and A. L. Gordon, 2002: Tracing Amazon River water into the Caribbean Sea. *Journal of Marine Research*, **60**, 537–549.

Hernández-Guerra, A., and T. M. Joyce, 2000: Water masses and circulation in the surface layers of the Caribbean at 66 W. *Geophysical research letters*, **27**, 3497–3500.

Hernández-Miranda, E., A. Palma, and F. Ojeda, 2003: Larval fish assemblages in nearshore coastal waters off central Chile: temporal and spatial patterns. *Estuarine, Coastal and Shelf Science*, **56**, 1075–1092.

Herron, R. C., T. D. Leming, and J. Li, 1989: Satellite-detected fronts and butterfish aggregations in the northeastern Gulf of Mexico. *Continental Shelf Research*, **9**, 569–588.

Hetland, R. D., Y. Hsueh, R. R. Leben, and P. P. Niiler, 1999: A Loop Current-induced jet along the edge of the West Florida Shelf. *Geophysical Research Letters*, **26**, 2239–2242.

Hopkins, T. L., 1982: The vertical distribution of zooplankton in the eastern Gulf of Mexico. *Deep Sea Research Part A. Oceanographic Research Papers*, **29**, 1069–1083.

Houde, E., 1987: Fish early life dynamics and recruitment variability. *American Fisheries Society Symposium*, Vol. 2 of, 17–29.

Houde, E. D., 2008: Emerging from Hjort's shadow. *Journal of Northwest Atlantic Fishery Science*, **41**, 53–70.

Hu, C., F. E. Muller-Karger, D. C. Biggs, K. L. Carder, B. Nababan, D. Nadeau, and J. Vanderbloemen, 2003: Comparison of ship and satellite bio-optical measurements on the continental margin of the NE Gulf of Mexico. *International Journal of Remote Sensing*, **24**, 2597–2612.

Hu, C., J. R. Nelson, E. Johns, Z. Chen, R. H. Weisberg, and F. E. Müller-Karger, 2005: Mississippi River water in the Florida Straits and in the Gulf Stream off Georgia in summer 2004. *Geophysical Research Letters*, **32**, L14606.

Huh, O. K., W. Wiseman Jr, and L. J. Rouse Jr, 1981: Intrusion of Loop Current waters onto the West Florida continental shelf. *Journal of Geophysical Research*, **86**, 4186–4192.

Hunter, J. R., 1981: Feeding ecology and predation of marine fish larvae. *Marine fish larvae (University of Washington Press)*, 33–77.

Hurlburt, H., and J. D. Thompson, 1980: A Numerical Study of Loop Current Intrusions and Eddy Shedding. *Journal of Physical Oceanography*, **10**, 1611–1651.

Isern-Fontanet, J., E. García-Ladona, and J. Font, 2003: Identification of marine eddies from altimetric maps. *Journal of Atmospheric and Oceanic Technology*, **20**, 772–778.

Isern-Fontanet, J., J. Font, E. García-Ladona, M. Emelianov, C. Millot, and I. Taupier-Letage, 2004: Spatial structure of anticyclonic eddies in the Algerian basin (Mediterranean Sea) analyzed using the Okubo-Weiss parameter. *Deep Sea Research Part II: Topical Studies in Oceanography*, **51**, 3009–3028.

Isern-Fontanet, J., E. García-Ladona, and J. Font, 2006: Vortices of the Mediterranean Sea: An altimetric perspective. *Journal of physical oceanography*, **36**, 87–103.

Johns, W. E., T. N. Lee, F. A. Schott, R. J. Zantopp, and R. H. Evans, 1990: The North Brazil Current retroflection: Seasonal structure and eddy variability. *Journal of Geophysical Research*, **95**, 22103–22122.

Johns, W. E., T. L. Townsend, D. M. Fratantoni, and W. D. Wilson, 2002: On the Atlantic inflow to the Caribbean Sea. *Deep Sea Research Part I: Oceanographic Research Papers*, **49**, 211–243.

Kaiser, M. J., and A. G. Pulsipher, 2007: The impact of weather and ocean forecasting on hydrocarbon production and pollution management in the Gulf of Mexico. *Energy policy*, **35**, 966–983.

Kinder, T. H., 1983: Shallow currents in the Caribbean Sea and Gulf of Mexico as observed with satellite-tracked drifters. *Bulletin of Marine Science*, **33**, 239–246.

Klawe, W. L., 1963: Observations on the spawning of four species on tuna (Neothunnus macropterus, Katsuwonus pelamis, Auxis thazard and Euthynnus lineatus) in the Eastern Pacific Ocean, based on the distribution of their larvae and juveniles. *Inter-American Tropical Tuna Commission Bulletin*, **6**, 447–540.

Klimley, A., and S. Butler, 1988: Immigration and emigration of a pelagic fish assemblage to seamounts in the Gulf of California related to water mass movements using satellite imagery. *Marine ecology progress series. Oldendorf*, **49**, 11–20.

Kumari, B., and M. Raman, 2010: Whale shark habitat assessments in the northeastern Arabian Sea using satellite remote sensing. *International Journal of Remote Sensing*, **31**, 379–389.

Lalli, C. M., and T. R. Parsons, 1997: Biological oceanography: an introduction. *Elsevier Science Ltd.*

Leben, R. R., 2005: Altimeter-derived loop current metrics. *Circulation of the Gulf of México: observations and models*, **161**, 181–202.

Lee, T. N., F. A. Schott, and R. Zantopp, 1985: Florida Current: low-frequency variability as observed with moored current meters during April 1982 to June 1983. *Science*, **227**, 298.

Lee, T. N., K. Leaman, E. Williams, T. Berger, and L. Atkinson, 1995: Florida Current meanders and gyre formation in the southern Straits of Florida. *Journal of geophysical research*, **100**, 8607–8620.

Levin, S. A., 1992: The problem of pattern and scale in ecology: the Robert H. MacArthur award lecture. *Ecology*, **73**, 1943–1967.

Lewis, J. K., and A. Kirwan Jr, 1987: Genesis of a Gulf of Mexico ring as determined from kinematic analyses. *Journal of Geophysical Research*, **92**, 11727–11.

Lin, Y., R. J. Greatbatch, and J. Sheng, 2010: The influence of Gulf of Mexico Loop Current intrusion on the transport of the Florida Current. *Ocean Dynamics*, **60**, 1075–1084.

Lohrenz, S. E., G. L. Fahnenstiel, D. G. Redalje, G. A. Lang, M. J. Dagg, T. E. Whitledge, and Q. Dortch, 1999: Nutrients, irradiance, and mixing as factors regulating primary production in coastal waters impacted by the Mississippi River plume. *Continental Shelf Research*, **19**, 1113–1141.

Lugo-Fernández, A., 2007: Is the loop current a chaotic oscillator? *Journal of physical oceanography*, **37**, 1455–1469.

Lugo-Fernández, A., and R. R. Leben, 2010: On the linear relationship between Loop Current retreat latitude and eddy separation period. *Journal of Physical Oceanography*, **40**, 2778-2784.

Lyczkowski-Shultz, J., and G. Ingram, 2003: Preliminary Guide to the Identification of the Early Life History Stages of Tetraodontid Fishes of the Western Central North Atlantic. *Pascagoula, MS. NOAA Technical Memorandum NMFS-SEFSC-494*, 9 p.

Lyczkowski-Shultz, J., D. Hanisko, K. Sulak, and G. Dennis III, 2004: Characterization of ichthyoplankton within the US Geological Survey's northeastern Gulf of Mexico study area: based on analysis of Southeast Area Monitoring and Assessment Program (SEAMAP) sampling surveys, 1982–1999. *US Geological Survey, USGS SIR-2004-5059*.

Lyczkowski-Shultz, J., D. S. Hanisko, W. Patterson, J. H. J. Cowan, G. Fitzhugh, and D. Nieland, 2007: A Time Series of Observations on Red Snapper Larvae from

SEAMAP Surveys, 1982-2003: Seasonal Occurrence, Distribution, Abundance, and Size. *American Fisheries Society Symposium*.

Muller-Karger, F. E., J. J. Walsh, R. H. Evans, and M. B. Meyers, 1991: On the seasonal phytoplankton concentration and sea surface temperature cycles of the Gulf of Mexico as determined by satellites. *Journal of Geophysical Research*, **96**, 12645–12.

Macias, D., L. Lema, M. Gómez-Vives, J. Ortiz de Urbina, and J. De La Serna, 2006: Some biological aspects of small tunas (Euthynnus alletteratus, Sarda sarda & Auxis rochei) from the south western Spanish Mediterranean traps. *Collect. Vol. Sci. Pap. ICCAT*, **59**, 579–589.

Mackas, D. L., K. L. Denman, and M. R. Abbott, 1985: Plankton patchiness: biology in the physical vernacular. *Bulletin of Marine Science*, **37**, 652–674.

MacKenzie, B. R., T. J. Miller, S. Cyr, and W. C. Leggett, 1994: Evidence for a dome-shaped relationship between turbulence and larval fish ingestion rates. *Limnology and Oceanography*, 1790–1799.

Mann, K. H., 1993: Physical oceanography, food chains, and fish stocks: a review. *ICES Journal of Marine Science: Journal du Conseil*, **50**, 105–119.

Matsuura, Y., and G. Sato, 1981: Distribution and Abundance of Scombrid Larvae in Southern Brazilian Waters. *Bulletin of Marine Science*, **31**, 824–832.

Maul, G., 1978: The 1972-1973 cycle of the Gulf Loop current. Part II: Mass and salt balances of the basin. *FAO Fisheries Reports*.

Maul, G., F. Williams, M. Roffer, and F. Sousa, 1984: Remotely sensed oceanographic patterns and variability of bluefin tuna catch in the Gulf of Mexico. *Oceanologica acta*, **7**, 469–479.

Maul, G. A., 1977: The Annual Cycle of the Gulf Loop Current: Part 1: Observations During a One-year Time Series. *Journal of Marine Research*, **35**, 29– 47.

Maul, G. A., and F. M. Vukovich, 1993: The relationship between variations in the Gulf of Mexico Loop Current and Straits of Florida volume transport. *Journal of physical oceanography*, **23**, 785–785.

McGillicuddy, D. and Coauthors, 1998: Influence of mesoscale eddies on new production in the Sargasso Sea. *Nature*, **394**, 263–266.

Medina, A., F. Abascal, C. Megina, and A. Garcia, 2002: Stereological assessment of the reproductive status of female Atlantic northern bluefin tuna during migration to Mediterranean spawning grounds through the Strait of Gibraltar. *Journal of Fish Biology*, **60**, 203–217.

Meekan, M. G., and L. Fortier, 1996: Selection for fast growth during the larval life of Atlantic cod Gadus morhua on the Scotian Shelf. *Marine Ecology Progress Series*, **137**, 25–37.

Mémery, L., M. Arhan, X. Alvarez-Salgado, M. J. Messias, H. Mercier, C. Castro, and A. Rios, 2000: The water masses along the western boundary of the south and equatorial Atlantic. *Progress in Oceanography*, **47**, 69–98.

Metcalf, W. G., 1976: Caribbean-Atlantic water exchange through the Anegada-Jungfern passage. *Journal of Geophysical Research*, **81**, 6401–6409.

Miller, P., 2004: Multi-spectral front maps for automatic detection of ocean colour features from SeaWiFS. *International Journal of Remote Sensing*, **25**, 1437–1442.

Miller, P., 2009: Composite front maps for improved visibility of dynamic sea-surface features on cloudy SeaWiFS and AVHRR data. *Journal of Marine Systems*, **78**, 327–336.

Miller, T. J., 2002: Assemblages, communities, and species interactions. *Fishery Science. The unique contributions of early life stages (LE Fuimann & RG Werner, eds.). Blackwell Publishing, Oxford*, 183–205.

Miller, T. J., L. B. Crowder, J. A. Rice, and E. A. Marschall, 1988: Larval size and recruitment mechanisms in fishes: toward a conceptual framework. *Canadian Journal of Fisheries and Aquatic Sciences*, **45**, 1657–1670.

Mizuta, G., and N. G. Hogg, 2004: Structure of the Circulation Induced by a Shoaling Topographic Wave. *Journal of physical oceanography*, **34**, 1793–1810.

Molinari, R. L., 1980: Current variability and its relation to sea-surface topography in the Caribbean Sea and Gulf of Mexico. *Marine Geodesy*, **3**, 409–436.

Molinari, R. L., and J. F. Festa, 1978: *Ocean thermal and velocity characteristics of the Gulf of Mexico relative to the placement of a moored OTEC plant*. NOAA Technical Memorandum ERL AOML.

Molinari, R. L., and D. A. Mayer, 1982: Current meter observations on the continental slope at two sites in the eastern Gulf of Mexico. *Journal of Physical Oceanography*, **12**, 1480-1492.

Molinari, R. L., W. D. Wilson, and K. Leaman, 1985: Volume and heat transports of the Florida Current: April 1982 through August 1983. *Science*, **227**, 295-297.

Morales, C. E., M. Loreto Torreblanca, S. Hormazabal, M. Correa-Ramírez, S. Nuņez, and P. Hidalgo, 2010: Mesoscale structure of copepod assemblages in the coastal transition zone and oceanic waters off central-southern Chile. *Progress in Oceanography*, **84**, 158–173.

Morrison, J. M., and W. D. Nowlin Jr, 1982: General distribution of water masses within the eastern Caribbean Sea during the winter of 1972 and fall of 1973. *Journal of Geophysical Research*, **87**, 4207–4229.

Muelbert, J. H., M. R. Lewis, and D. E. Kelley, 1994: The importance of small-scale turbulence in the feeding of herring larvae. *Journal of plankton research*, **16**, 927-944.

Muhling, B., L. Beckley, J. Koslow, and A. Pearce, 2008: Larval fish assemblages and water mass structure off the oligotrophic south-western Australian coast. *Fisheries Oceanography*, **17**, 16–31.

Muhling, B. A., J. T. Lamkin, and M. A. Roffer, 2010: Predicting the occurrence of Atlantic bluefin tuna (Thunnus thynnus) larvae in the northern Gulf of Mexico: building a classification model from archival data. *Fisheries Oceanography*, **19**, 526–539.

Muller-Karger, F., and C. Fuentes-Yaco, 2000: Characteristics of Wind-Generated Rings in the Eastern Tropical Pacific Ocean. *Journal of Geophysical Research - Oceans*, 1271–1284.

Muller-Karger, F. E., and R. A. Castro, 1994: Mesoscale processes affecting phytoplankton abundance in the southern Caribbean Sea. *Continental Shelf Research*, **14**, 199–221.

Muller-Karger, F. E., C. R. McClain, and P. L. Richardson, 1988: The dispersal of the Amazon's water. *Nature*, **333**, 56–59.

Muller-Karger, F. E., J. J. Walsh, R. H. Evans, and M. B. Meyers, 1991: On the seasonal phytoplankton concentration and sea surface temperature cycles of the Gulf of Mexico as determined by satellites. *Journal of Geophysical Research*, **96**, 12645–12665.

Mumby, P. J., W. Skirving, A. E. Strong, J. T. Hardy, E. F. LeDrew, E. J. Hochberg, R. P. Stumpf, and L. T. David, 2004: Remote sensing of coral reefs and their physical environment. *Marine Pollution Bulletin*, **48**, 219–228.

Muñoz, E., A. J. Busalacchi, S. Nigam, and A. Ruiz-Barradas, 2008: Winter and summer structure of the Caribbean low-level jet. *Journal of Climate*, **21**, 1260–1276.

Nakata, H., S. Kimura, Y. Okazaki, and A. Kasai, 2000: Implications of meso-scale eddies caused by frontal disturbances of the Kuroshio Current for anchovy recruitment. *ICES Journal of Marine Science: Journal du Conseil*, **57**, 143-152.

Nixon, S., 1995: Coastal marine eutrophication: a definition, social causes, and future concerns. *Ophelia*, **41**, 199–219.

Nof, D., 2005: The Momentum Imbalance Paradox Revisited. *Journal of Physical Oceanography*, **35**, 1928-1939.

Nof, D., and T. Pichevin, 1996: The Retroflection Paradox. *Journal of Physical Oceanography*, **26**, 2344–2358.

Nof, D., and T. Pichevin, 2001: The ballooning of outflows. *Journal of Physical oceanography*, **31**, 3045–3058.

Nof, D., S. Van Gorder, and T. Pichevin, 2004: A Different Outflow Length Scale? *Journal of Physical Oceanography*, **34**, 793–804.

Nowlin Jr, W. D., 1972: Winter circulation patterns and property distributions. *Contributions on the Physical Oceanography of the Gulf of Mexico*, **2**, 3–52.

Nowlin, W. D., 1971: Water masses and general circulation of the Gulf of Mexico. *Ocoanology,* **6***,* 28-33.

Oey, L., T. Ezer, and H. Lee, 2005: Loop Current, rings and related circulation in the Gulf of Mexico: A review of numerical models and future challenges. *Geophysical Monograph-American Geophysical Union*, **161**, 31-56.

Oey, L. Y., 2004: Vorticity flux through the Yucatan Channel and Loop Current variability in the Gulf of México. *Journal of Geophysical Research*, **109**, 10–1029.

Oey, L. Y., H. C. Lee, and W. J. Schmitz Jr, 2003: Effects of winds and Caribbean eddies on the frequency of Loop Current eddy shedding: A numerical model study. *Journal of geophysical research*, **108**, C10, 3324.

Ohlmann, J. C., and P. P. Niiler, 2005: Circulation over the continental shelf in the northern Gulf of Mexico. *Progress in Oceanography*, **64**, 45–81.

Ohlmann, J. C., P. P. Niiler, C. A. Fox, and R. R. Leben, 2001: Eddy energy and shelf interactions in the Gulf of Mexico. *Journal of geophysical research*, **106**, 2605–2620.

Okazaki, Y., H. Nakata, and S. Kimura, 2002: Effects of frontal eddies on the distribution and food availability of anchovy larvae in the Kuroshio Extension. *Marine and freshwater research*, **53**, 403–410.

Okubo, A., 1970: Horizontal dispersion of floatable particles in the vicinity of velocity singularities such as convergences. *Deep Sea Research and Oceanographic Abstracts*, **17**, 445–454.

Olascoaga, M., 2010: Isolation on the West Florida Shelf with implications for red tides and pollutant dispersal in the Gulf of Mexico. *Nonlinear Processes in Geophysics*, **17**, 685–696.

Olson, D., 1991: Rings in the Ocean. *Annual Review of Earth and Planetary Sciences*, **19**, 283–311.

Olson, D., G. Hitchcock, A. Mariano, C. Ashjian, G. Peng, R. Nero, and G. Podesta, 1994: Life on the edge: marine life and fronts. *Oceanography*, **7**, 52–60.

Oram, J. J., J. C. McWilliams, and K. D. Stolzenbach, 2008: Gradient-based edge detection and feature classification of sea-surface images of the Southern California Bight. *Remote Sensing of Environment*, **112**, 2397–2415.

Ordonez, E., 1936: Principal physiographic provinces of Mexico. *AAPG Bull*, **20**, 1277–1307.

Ortner, P., R. Ferguson, S. Piotrowicz, L. Chesal, G. Berberian, and A. Palumbo, 1984: Biological consequences of hydrographic and atmospheric advection within the Gulf Loop Intrusion. *Deep Sea Research Part A. Oceanographic Research Papers*, **31**, 1101–1120.

Ortner, P. B., P. H. Wiebe, L. Haury, and S. Boyd, 1978: Variability in zooplankton biomass distribution in the northern Sargasso Sea: the contribution of Gulf Stream cold core rings. *Fisheries Bulletin*, **76**, 323–334.

Ortner, P. B., L. C. Hill, and S. R. Cummings, 1989: Zooplankton community structure and copepod species composition in the northern Gulf of Mexico. *Continental Shelf Research*, **9**, 387–402.

Ouellet, P., L. Savard, and P. Larouche, 2007: Spring oceanographic conditions and northern shrimp Pandalus borealis recruitment success in the north-western Gulf of St. Lawrence. *Marine Ecology Progress Series*, **339**, 229–241.

Owen, R. W., and others, Fronts and eddies in the sea: mechanisms, interactions and biological effects. *Analysis od Marine Ecosystems*, 197-233

Oxenford, H., and W. Hunte, 1983: Age and growth of dolphin, Coryphaena hippurus, as determined by growth rings in otoliths. *Fisheries Bulletin*, **81**, 906–909.

Peters, F., and C. Marrasé, 2000: Effects of turbulence on plankton: an overview of experimental evidence and some theoretical considerations. *Marine Ecology Progress Series*, **205**, 291–306.

Peterson, R., L. Stramma, and G. Kortum, 1996: Early concepts and charts of ocean circulation. *Progress in Oceanography*, **37**, 1–115.

Pichevin, T., and D. Nof, 1997: The momentum imbalance paradox. *Tellus A*, **49**, 298–319.

Polovina, J. J., and E. A. Howell, 2005: Ecosystem indicators derived from satellite remotely sensed oceanographic data for the North Pacific. *ICES Journal of Marine Science: Journal du Conseil*, **62**, 319–327.

Poveda, G., P. R. Waylen, and R. S. Pulwarty, 2006: Annual and inter-annual variability of the present climate in northern South America and southern Mesoamerica. *Palaeogeography, Palaeoclimatology, Palaeoecology*, **234**, 3–27.

Rabalais, N., R. Carney, and E. Escobar-Briones, 1999: Overview of continental shelf benthic communities of the Gulf of Mexico. *The Gulf of Mexico large marine ecosystem. Assessment, sustainability and management*, 171–195.

Rabalais, N., R. Turner, and W. Wiseman, 2001: Hypoxia in the Gulf of Mexico. *Journal of Environmental Quality*, **30**, 320-329.

Rabalais, N., R. Turner, B. Sen Gupta, D. Boesch, P. Chapman, and M. Murrell, 2007: Hypoxia in the northern Gulf of Mexico: Does the science support the plan to reduce, mitigate, and control hypoxia? *Estuaries and Coasts*, **30**, 753–772.

Rakocinski, C. F., J. Lyczkowski-Shultz, and S. L. Richardson, 1996: Ichthyoplankton assemblage structure in Mississippi Sound as revealed by canonical correspondence analysis. *Estuarine, Coastal and Shelf Science*, **43**, 237–257.

Raynie, R. C., and R. F. Shaw, 1994: Ichthyoplankton abundance along a recruitment corridor from offshore spawning to estuarine nursery ground. *Estuarine, Coastal and Shelf Science*, **39**, 421–450.

Redalje, D. G., and G. L. Fahnenstiel, 1994: The relationship between primary production and the vertical export of particulate organic matter in a river-impacted coastal ecosystem. *Estuaries and Coasts*, **17**, 829–838.

Restrepo, J., and B. Kjerfve, 2000: Magdalena river: interannual variability (1975-1995) and revised water discharge and sediment load estimates. *Journal of hydrology*, **235**, 137–149.

Richards, W., T. Leming, M. McGowan, J. Lamkin, and S. Kelley-Fraga, 1989: Distribution of fish larvae in relation to hydrographic features of the Loop Current boundary in the Gulf of Mexico. *I C E S Marine Science Symposia.*

Richards, W., M. McGowan, T. Leming, J. Lamkin, and S. Kelley, 1993: Larval fish assemblages at the Loop Current boundary in the Gulf of Mexico. *Bulletin of Marine Science*, **53**, 475–537.

Richardson, D. E., J. K. Llopiz, C. M. Guigand, and R. K. Cowen, 2010: Larval assemblages of large and medium-sized pelagic species in the Straits of Florida. *Progress in Oceanography*, **86**, 8–20.

Rio, M. H., and F. Hernandez, 2004: A mean dynamic topography computed over the world ocean from altimetry, in situ measurements, and a geoid model. *Journal of Geophysical Research*, **109**, C12032.

Rios-Jara, E., and J. G. Gonzalez, 2000: Effects of lunar periodicity on the emergence behavior of the demersal copepod Pseudodiaptomus cokeri in Phosphorescent Bay, Puerto Rico. *Bulletin of marine science*, **67**, 887–901.

Rivas, D., A. Badan, and J. Ochoa, 2005: The ventilation of the deep Gulf of Mexico. *Journal of physical oceanography*, **35**, 1763–1781.

Romans, B., and A. Concise, 1775: Natural History of East and West Florida. *Aitken Press (New York)*, 107.

Rosmond, T. E., 1992: A prototype fully coupled ocean-atmosphere prediction system. *Oceanography*, **5**, 25–30.

Rowe, G., and P. Chapman, 2002: Continental shelf hypoxia: some nagging questions. *Gulf of Mexico Science*, **20**, 153–160.

Royer, F., J. M. Fromentin, and P. Gaspar, 2004: Association between bluefin tuna schools and oceanic features in the western Mediterranean. *Marine Ecology Progress Series*, **269**, 249–263.

Rudorff, C. A. G., J. A. Lorenzzetti, D. F. M. Gherardi, and J. E. Lins-Oliveira, 2009: Modeling spiny lobster larval dispersion in the Tropical Atlantic. *Fisheries Research*, **96**, 206–215.

Ryan, E. H., A. Mariano, D. B. Olson, and R. H. Evans, 1996: Global Sea Surface Temperature and Currents. *EOS Transactions American Geophysical Union* 77:46.

Sangrà, P. and Coauthors, 2007: On the nature of oceanic eddies shed by the Island of Gran Canaria. *Deep Sea Research Part I: Oceanographic Research Papers*, **54**, 687–709.

Sangrà, P. and Coauthors, 2009: The Canary Eddy Corridor: A major pathway for long-lived eddies in the subtropical North Atlantic. *Deep Sea Research Part I: Oceanographic Research Papers*, **56**, 2100–2114.

Schmitz Jr, W., 2004: On the circulation in and around the Gulf of Mexico: Volume I-A Review of the Deep Water Circulation. *Online publication, Texas A&M Corpus Christi http://www. cbi. tamucc. edu/gomcirculation/default. html*.

Schmitz, W., 2005: Cyclones and westward propagation in the shedding of anticyclonic rings from the Loop Current. *Circulation in the Gulf of Mexico: observations and models*, **161**, 241–262.

Schmitz, W., and P. Richardson, 1991: On the sources of the Florida Current. *Deep-sea research. Part A. Oceanographic research papers*, **38**, S379–S409.

Schmitz, W., D. Biggs, A. Lugo-Fernandez, L. Oey, and W. Sturges, 2005: A Synopsis of the Circulation in the Gulf of Mexico and on its Continental Margins. *Circulation in the Gulf of Mexico: observations and models*, **161**, 11–30.

Schott, F. A., J. Fischer, and L. Stramma, 1998: Transports and pathways of the upper-layer circulation in the western tropical Atlantic. *Journal of Physical Oceanography*, **28**, 1904–1928.

Schroeder, W. W., S. P. Dinnel, W. J. Wiseman, W. J. Merrell, and others, 1987: Circulation patterns inferred from the movement of detached buoys in the eastern Gulf of Mexico. *Continental Shelf Research*, **7**, 883–894.

Scott, G. P., S. C. Turner, G. B. Churchill, W. J. Richards, and E. B. Brothers, 1993: Indices of larval bluefin tuna, Thunnus thynnus, abundance in the Gulf of Mexico; modelling variability in growth, mortality, and gear selectivity. *Bulletin of marine science*, **53**, 912–929.

Shay, L. K., A. J. Mariano, S. D. Jacob, and E. H. Ryan, 1998: Mean and near-inertial ocean current response to Hurricane Gilbert. *Journal of physical oceanography*, **28**, 858–889.

Shay, L. K., G. J. Goni, and P. G. Black, 2000: Effects of a warm oceanic feature on Hurricane Opal. *Monthly Weather Review*, **128**, 1366–1383.

Sheng, J., D. G. Wright, R. J. Greatbatch, and D. E. Dietrich, 1998: CANDIE: A new version of the DieCAST ocean circulation model. *Journal of Atmospheric and Oceanic Technology*, **15**, 1414–1432.

Sheridan, R., C. Drake, J. Nafe, and J. Hennion, 1966: Seismic-refraction study of continental margin east of Florida. *Assoc. Petroleum Geologists Bull*, **50**, 1972–1991.

Sherman, K., 2003: Physical, biological and human forcing of biomass yields in large marine ecosystems. *ICES CM 2003 P12*.

Sherman, K., W. Smith, W. Morse, M. Berman, J. Green, and L. Ejsymont, 1984: Spawning strategies of fishes in relation to circulation, phytoplankton production, and pulses in zooplankton off the northeastern United States. *Marine ecology progress series. Oldendorf*, **18**, 1–19.

Shipp, R., 1999: Status of exploited fish species in the Gulf of Mexico. *The Gulf of Mexico Large Marine Ecosystem: Assessment, Sustainability and Management. Malden, Massachusetts: Blackwell Science,* 196-204.

Smith, R. H., 2010: Atlantic-Caribbean Exchange through Windward Passage. *Masters Thesis, University of Miami, Coral Gables*, 130p.

Sogard, S., D. Hoss, and J. Govoni, 1987: Density and depth distribution of larval gulf menhaden, Brevoortia patronus, Atlantic croaker, Micropogonias undulatus, and spot, Leiostomus xanthurus, in the northern Gulf of Mexico. *Fishery Bulletin*, **85**, 601–609.

Sturges, W., and J. Evans, 1983: On the variability of the Loop Current in the Gulf of Mexico. *Journal of marine research*, **41**, 639–653.

Sturges, W., and R. Leben, 2000: Frequency of ring separations from the Loop Current in the Gulf of Mexico: A revised estimate. *Journal of Physical Oceanography*, **30**, 1814–1819.

Sturges, W., J. Evans, S. Welsh, and W. Holland, 1993: Separation of warm-core rings in the Gulf of Mexico. *Journal of physical oceanography*, **23**, 250–268.

Sverdrup, H. U., M. W. Johnson, and R. H. Fleming, 1942: *The oceans: their physics, chemistry, and general biology*. Prentice-Hall New York.

Sylvan, J. B., Q. Dortch, D. M. Nelson, A. F. M. Brown, W. Morrison, and J. W. Ammerman, 2006: Phosphorus limits phytoplankton growth on the Louisiana shelf during the period of hypoxia formation. *Environmental science & technology*, **40**, 7548–7553.

Tang, L., J. Sheng, B. G. Hatcher, and P. F. Sale, 2006: Numerical study of circulation, dispersion, and hydrodynamic connectivity of surface waters on the Belize shelf. *Journal of Geophysical Research*, **111**, C01003.

Teo, S. L. H., and B. A. Block, 2010: Comparative influence of ocean conditions on yellowfin and Atlantic bluefin tuna catch from longlines in the Gulf of Mexico. *PLoS One*, **5**, e10756.

Tolan, J. M., S. A. Holt, and C. P. Onuf, 1997: Distribution and community structure of ichthyoplankton in Laguna Madre seagrass meadows: potential impact of seagrass species change. *Estuaries and Coasts*, **20**, 450–464.

Tomczak, M., and J. S. Godfrey, 2003: Regional oceanography: an introduction. *Pergamon, Oxford.*

Toner, M., A. Kirwan, A. Poje, L. Kantha, F. Müller-Karger, and C. Jones, 2003: Chlorophyll dispersal by eddy-eddy interactions in the Gulf of Mexico. *Journal of Geophysical Research (Oceans)*, **108**, 2–1.

Le Traon, P. Y., F. Nadal, and N. Ducet, 1998: An Improved Mapping Method of Multisatellite Altimeter Data. *Journal of Atmospheric and Oceanic Technology*, **15**, 522–534.

Turner, J. T., 1984: The feeding ecology of some zooplankters that are important prey items of larval fish. *U.S. Dept. of Commerce, National Oceanic and Atmospheric Administration, National Marine Fisheries Service, Washington, DC*.

Turner, R., N. Rabalais, R. Alexander, G. McIsaac, and R. Howarth, 2007: Characterization of nutrient, organic carbon, and sediment loads and concentrations from the Mississippi River into the Northern Gulf of Mexico. *Estuaries and Coasts*, **30**, 773–790.

Turner, W., S. Spector, N. Gardiner, M. Fladeland, E. Sterling, and M. Steininger, 2003: Remote sensing for biodiversity science and conservation. *Trends in Ecology & Evolution*, **18**, 306–314.

Valavanis, V. D., S. Georgakarakos, D. Koutsoubas, C. Arvanitidis, and J. Haralabous, 2002: Development of a marine information system for cephalopod fisheries in eastern Mediterranean. *Bulletin of Marine Science*, **71**, 867–882.

Victor, B., 1986: Duration of the planktonic larval stage of one hundred species of Pacific and Atlantic wrasses (family Labridae). *Marine Biology*, **90**, 317–326.

Vigliola, L., and M. G. Meekan, 2002: Size at hatching and planktonic growth determine post-settlement survivorship of a coral reef fish. *Oecologia*, **131**, 89–93.

Vukovich, F. M., 1988a: On the formation of elongated cold perturbations off the Dry Tortugas. *Journal of physical oceanography*, **18**, 1051–1059.

Vukovich, F. M., 1988b: Loop Current boundary variations. *Journal of Geophysical Research*, **93**, 15585–15.

Vukovich, F. M., 2007: Climatology of ocean features in the Gulf of Mexico using satellite remote sensing data. *Journal of physical oceanography*, **37**, 689–707.

Vukovich, F. M., and G. A. Maul, 1985: Cyclonic eddies in the eastern Gulf of Mexico. *Journal of physical Oceanography*, **15**, 105–117.

Vukovich, F. M., B. W. Crissman, M. Bushnell, and W. J. King, 1979: Some aspects of the oceanography of the Gulf of Mexico using satellite and in situ data. *Journal of Geophysical Research*, **84**, 7749–7768.

Walker, N., R. Leben, S. Anderson, A. Haag, and C. Pilley, 2009: High Frequency Satellite Surveillance of Gulf of Mexico Loop Current Frontal Eddy Cyclones. *OCEANS 2009, MTS/IEEE Biloxi-Marine Technology for Our Future: Global and Local Challenges*, 1–9.

Walker, N. D., 1996: Satellite assessment of Mississippi River plume variability: causes and predictability. *Remote Sensing of Environment*, **58**, 21–35.

Wang, C., 2007: Variability of the Caribbean low-level jet and its relations to climate. *Climate dynamics*, **29**, 411–422.

Wang, C., and D. B. Enfield, 2001: The tropical Western Hemisphere warm pool. *Geophysical Research Letters*, **28**, 1635–1638.

Wang, C., and S. Lee, 2007: Atlantic warm pool, Caribbean low-level jet, and their potential impact on Atlantic hurricanes. *Geophysical research letters*, **34**, 2703.

Weisberg, R. H., B. D. Black, and Z. Li, 2000: An upwelling case study on Florida's west coast. *Journal of Geophysical Research-Oceans*, **105**, 11459.

Weisberg, R. H., R. He, Y. Liu, and J. I. Virmani, 2005: West Florida Shelf Circulation on Synoptic, Seasonal, and Interannual Time Scales. *Circulation in the Gulf of Mexico: observations and models*, *American Geophysical Union*, 325.

Weiss, J., 1991: The dynamics of enstrophy transfer in two-dimensional hydrodynamics. *Physica D: Nonlinear Phenomena*, **48**, 273–294.

Weng, K., M. Stokesbury, A. Boustany, A. Seitz, S. Teo, S. Miller, and B. Block, 2009: Habitat and behaviour of yellowfin tuna Thunnus albacares in the Gulf of Mexico determined using pop-up satellite archival tags. *Journal of Fish Biology*, **74**, 1434–1449.

Werner, E. E., and J. F. Gilliam, 1984: The ontogenetic niche and species interactions in size-structured populations. *Annual review of ecology and systematics*, **15**, 393–425.

Willis, J. K., D. Roemmich, and B. Cornuelle, 2004: Interannual variability in upper ocean heat content, temperature, and thermosteric expansion on global scales. *Journal of Geophysical Research*, **109**, 2003.

Wilson, S., M. Lutcavage, R. Brill, M. Genovese, A. Cooper, and A. Everly, 2005: Movements of bluefin tuna (Thunnus thynnus) in the northwestern Atlantic Ocean recorded by pop-up satellite archival tags. *Marine biology*, **146**, 409–423.

Wiseman Jr, W. J., and S. Dinnel, 1988: Shelf currents near the mouth of the Mississippi River. *Journal of physical oceanography*, **18**, 1287–1291.

Wunsch, C., 1981: Low-frequency variability of the sea. *Evolution of physical oceanography*, 342–374.

Wüst, G., and A. Gordon, 1964: *Stratification and circulation in the Antillean-Caribbean basins*. Columbia University Press New York,.

Yang, H., and R. H. Weisberg, 1999: Response of the West Florida Shelf circulation to climatological wind stress forcing. *Journal of Geophysical Research-Oceans*, **104**, 5301.

Yang, J., C. Gu, L. Li, J. Li, C. Gao, and W. Li, 1995: Satellite remote sensing prediction of Japanese pilchard fishing ground in the Huanghai Sea and the East China Sea. *Science in China Series B. Chemistry, Life Sciences & Earth Sciences*, **38**, 336–344.

Yen, J., M. J. Weissburg, and M. H. Doall, 1998: The fluid physics of signal perception by mate-tracking copepods. *Philosophical Transactions of the Royal Society of London. Series B: Biological Sciences*, **353**, 787–804.

Yoklavich, M., V. Loeb, M. Nishimoto, and B. Daly, 1996: Nearshore assemblages of larval rockfishes and their physical environment off Central California during an extended El Nino event, 1991-1993. *Fishery Bulletin*, **94**, 766–782.

Yukovich, F. M., 1986: Aspects of the behavior of cold perturbations in the eastern Gulf of Mexico: a case study. *Journal of physical oceanography*, **16**, 175–188.

Zavala-Hidalgo, J., S. L. Morey, and J. J. O'Brien, 2003a: Cyclonic eddies northeast of the Campeche Bank from altimetry data. *Journal of physical oceanography*, **33**, 623–629.

Zavala-Hidalgo, J., S. L. Morey, and J. J. O'Brien, 2003b: Cyclonic eddies northeast of the Campeche Bank from altimetry data. *Journal of physical oceanography*, **33**, 623–629.

Zavala-Hidalgo, J., S. Morey, J. O'Brien, and L. Zamudio, 2006: On the Loop Current eddy shedding variability. *Atmósfera*, **19**, 41–48.

Zenitani, H., N. Kono, and Y. Tsukamoto, 2007: Relationship between daily survival rates of larval Japanese anchovy (Engraulis japonicus) and concentrations of copepod nauplii in the Seto Inland Sea, Japan. *Fisheries Oceanography*, **16**, 473–478.